

ggs(1)

The EMEFS Model Evaluation: An Interim Report

- | | |
|------------------------|-------------------------|
| W. R. Barchet | K. Puckett |
| R. L. Dennis | D. Byun |
| S. K. Seilkop | J. N. McHenry |
| C. M. Banic | P. Karamchandani |
| D. Davies | A. Venkatram |
| R. M. Hoff | C. Fung |
| A. M. Macdonald | P. K. Misra |
| R. E. Mickle | D. A. Hansen |
| J. Padro | J. S. Chang |
-

December 1991

Prepared for the
Electric Power Research Institute
Palo Alto, California
Contract EPRI RP1630-40

and for the
U.S. Environmental Protection Agency
Research Triangle Park, NC
IAG DW89933040-01-07

Pacific Northwest Laboratory
Operated for the U.S. Department of Energy
by Battelle Memorial Institute



PNL-7914

DISCLAIMER

This report was prepared as an account of work sponsored by an agency of the United States Government. Neither the United States Government nor any agency thereof, nor Battelle Memorial Institute, nor any of their employees, makes **any warranty, expressed or implied, or assumes any legal liability or responsibility for the accuracy, completeness, or usefulness of any information, apparatus, product, or process disclosed, or represents that its use would not infringe privately owned rights.** Reference herein to any specific commercial product, process, or service by trade name, trademark, manufacturer, or otherwise does not necessarily constitute or imply its endorsement, recommendation, or favoring by the United States Government or any agency thereof, or Battelle Memorial Institute. The views and opinions of authors expressed herein do not necessarily state or reflect those of the United States Government or any agency thereof.

PACIFIC NORTHWEST LABORATORY
operated by
BATTELLE MEMORIAL INSTITUTE
for the
UNITED STATES DEPARTMENT OF ENERGY
under Contract DE-AC06-76RLO 1830

Printed in the United States of America

Available to DOE and DOE contractors from the
Office of Scientific and Technical Information, P.O. Box 62, Oak Ridge, TN 37831;
prices available from (615) 576-8401. FTS 626-8401.

Available to the public from the National Technical Information Service,
U.S. Department of Commerce, 5285 Port Royal Rd., Springfield, VA 22161.

THE EMEFS MODEL EVALUATION:
AN INTERIM REPORT

W. R. Barchet
Pacific Northwest Laboratory

R. L. Dennis
U.S. Environmental Protection
Agency

S. K. Seilkop
Analytical Sciences Incorporated

C. M. Banic

D. Davies

R. M. Hoff

A. M. Macdonald

R. E. Mickle

J. Padro

K. Puckett
Atmospheric Environment Service,
Canada

D. Byun

J. N. McHenry
Computer Sciences Corporation

P. Karamchandani

A. Venkatram
ENSR Consulting and Engineering

C. Fung

P. K. Misra
Ontario Ministry of the Environment

D. A. Hansen

Electric Power Research Institute

J. S. Chang

State University of New York at
Albany

DECEMBER 1991

Prepared for the
Electric Power Research Institute
Palo Alto, California 94304
Contract EPRI RP1630-40

and for the
U.S. Environmental Protection Agency
Research Triangle Park, NC 27711
IAG DW89933040-01-07

Pacific Northwest Laboratory
Richland, Washington 99352

MASTER

DISTRIBUTION OF THIS DOCUMENT IS UNLIMITED *ga*

ABSTRACT

The binational Eulerian Model Evaluation Field Study (EMEFS) consisted of several coordinated data gathering and model evaluation activities. In the EMEFS, data were collected by five air and precipitation monitoring networks between June 1988 and June 1990. Model evaluation is continuing. This interim report summarizes the progress made in the evaluation of the Regional Acid Deposition Model (RADM) and the Acid Deposition and Oxidant Model (ADOM) through the December 1990 completion of a State of Science and Technology report on model evaluation for the National Acid Precipitation Assessment Program (NAPAP). Because various assessment applications of RADM had to be evaluated for NAPAP, the report emphasizes the RADM component of the evaluation.

A protocol for the evaluation was developed by the model evaluation team and defined the observed and predicted values to be used and the methods by which the observed and predicted values were to be compared. Scatter plots and time series of predicted and observed values were used to present the comparisons graphically. Difference statistics and correlations were used to quantify model performance. Model predictions for RADM2.1, RADM2.5 (6- and 15-layer versions), and ADOM2Bf, along with EMEFS surface and upper-air observations for the 33-day period from 25 August through 27 September 1988, formed the data set for the first evaluation period.

The major finding of the evaluation was that both RADM and ADOM underpredicted $\text{SO}_4^{=}$ aerosol concentrations at the surface. The consistency of this underprediction over various geographical regions within the RADM and ADOM modeling domains suggested that the models were neglecting some significant mechanism by which $\text{SO}_4^{=}$ aerosol is produced. Subsequent model development has focused on including $\text{SO}_4^{=}$ aerosol production by nonprecipitating clouds.

Other biases indicated by the evaluation included overprediction of SO_2 and HNO_3 . These biases appear to relate to incommensurability between model predictions for a grid cell and measurements at specific locations. Subgrid-scale variations in air concentrations can be neither adequately simulated by the models nor represented by the measurements. The horizontal coarseness of the modeling grid causes unrealistic spatial smoothing of pollutant emissions by the models. The vertical coarseness of the grid makes it impossible for a measurement near the surface to represent the lowest layer being simulated by the models.

Based on the preliminary results of the evaluation, the model evaluation team concluded that the biases shown by RADM were not sufficient to invalidate its use in its main NAPAP assessment applications: source attribution and estimation of deposition changes in response to changes in emissions. However, the models are being modified to eliminate the biases, and further analyses of model performance are being made to improve understanding of the sources of those biases and their implications to the various applications of the models.

CONTENTS

ABSTRACT	iii
ACRONYMS	xiii
ACKNOWLEDGMENTS	xv
1 INTRODUCTION	1
2 APPROACH	5
2.1 EVALUATION PROTOCOL	5
2.2 DATA NEEDED FOR EVALUATION	5
2.2.1 Meteorological Data	6
2.2.2 Emissions	6
2.2.3 Observed Values of Air Concentrations and Precipitation Chemistry	8
2.3 MODEL PREDICTIONS	13
2.4 COMPARISON MEASURES	13
3 FINDINGS	15
3.1 AIR CONCENTRATIONS	15
3.1.1 Evaluation Period Averages	15
3.1.2 Time Series	20
3.1.3 Regional Distributions	20
3.1.4 Surface Gradients	26
3.1.5 Daytime and Nighttime Performance	30
3.1.6 Upper-Air Concentrations	30
3.2 PRECIPITATION CONCENTRATIONS AND DEPOSITION	32
4 MEASUREMENT AND MODEL INCOMMENSURABILITY	37
5 PRELIMINARY INTERPRETIVE STUDIES AND ANALYSES	41
5.1 ADOM-RELATED STUDIES	41
5.1.1 Fog Frequency and ADOM2Bf Underprediction of $\text{SO}_4^=$ Aerosol	41
5.1.2 Dry-Deposition Velocities in ADOM2Bf	41
5.1.3 Comparison of ADOM2Bf-Predicted and Observed Vertical Profiles of Ozone	43
5.1.4 Comparison of ADOM2Bf to Observations at High- and Low-Elevation Sites	44
5.1.5 Comparison of ADOM-Predicted and Canadian Aircraft-Measured Profiles	49
5.2 RADM-RELATED STUDIES	55

5.2.1	Regional Distributions Aloft	55
5.2.2	Frontal Passage	56
5.2.3	High-Resolution Box	56
6	MODIFICATIONS TO MODELS ARISING FROM FINDINGS	59
6.1	ADOM NONPRECIPITATING STRATUS CLOUDS	59
6.2	RADM BOUNDARY-LAYER PARAMETERIZATIONS	60
6.3	RADM NONPRECIPITATING CLOUDS	67
7	DISCUSSION AND CONCLUSIONS	71
8	DIRECTION OF THE EMEFS EVALUATION	73
9	REFERENCES	75
	APPENDIX A - DETAIL EVALUATION RESULTS	A.1

FIGURES

1	Location of EMEFS Sites Active during the 25 August to 27 September 1988 Evaluation Period and Regional Groupings of RADM and ADOM Grid Cells Containing Active Sites	10
2	The Relationship between the 33-Day Average Surface Concentration of SO ₂ , SO ₄ ⁼ Aerosol, NO ₂ , and T-NO ₃ Predicted by RADM2.1 Versus the Observed Grid Cell Average	16
3	The Relationship between the 33-Day Average Surface Concentration of SO ₂ , SO ₄ ⁼ Aerosol, NO ₂ , and T-NO ₃ Predicted by RADM2.5/6 Versus the Observed Grid Cell Average	17
4	The Relationship between the 33-Day Average Surface Concentration of SO ₂ , SO ₄ ⁼ Aerosol, NO ₂ , and T-NO ₃ Predicted by ADOM2Bf Versus the Observed Grid Cell Average	18
5	The Daily Variation in the Regional Average RADM2.1-Predicted and EMEFS-Observed Concentration of SO ₂ and SO ₄ ⁼ Aerosol in Regions 3 and 5	21
6	The Daily Variation in the Regional Average RADM2.5/6-Predicted and EMEFS-Observed Concentration of SO ₂ and SO ₄ ⁼ Aerosol in Regions 3 and 5	22
7	The Daily Variation in the Regional Average ADOM2Bf-Predicted and EMEFS-Observed Concentration of SO ₂ and SO ₄ ⁼ Aerosol in Regions 3 and 5	23
8	Linear Temporal Correlation Coefficients between the Model-Predicted and EMEFS-Observed Daily Regional Average SO ₂ , SO ₄ ⁼ Aerosol, T-NO ₃ , and Maximum O ₃ Concentrations	24
9	The Daily Variation in the Regional Average RADM2.1- and ADOM2Bf-Predicted and EMEFS-Observed Maximum O ₃ Concentrations in Regions 3 and 5	25
10	Residual Daily Regionally Averaged Maximum-Hourly and Minimum-Hourly O ₃ Concentrations for All Regions and Days in the Model Evaluation Period	26
11	RADM2.1-Predicted and EMEFS-Observed Regional Distribution of the 33-Day Average SO ₂ Concentration Based on Grid Cells with Valid Long-Term Averages	27

12	Distribution of EMEFS-Observed and RADM21-Predicted 33-Day Average Concentrations of SO ₂ and SO ₄ ⁼ Aerosol along a Transect That Extends from the Southwestern Corner of Pennsylvania to the Northeastern Corner of New York	28
13	Distribution of EMEFS-Observed and ADOM2Bf-Predicted 33-Day Average Concentrations of SO ₂ and SO ₄ ⁼ Aerosol along a Transect That Extends from the Southwestern Corner of Pennsylvania to the Northeastern Corner of New York	29
14	The Relationship between the Median and Inner Quartiles of the RADM2.1-Predicted Concentrations of SO ₂ , SO ₄ ⁼ Aerosol, O ₃ , and H ₂ O ₂ and the Concentrations Observed in the Mixed Layer from the Gulfstream-1 Aircraft on Flights Made during the Model Evaluation Period	31
15	The Relationship between the 33-Day Total Precipitation Prescribed by the Meteorological Drivers for RADM and the EMEFS-Observed Grid Cell Average for the Evaluation Period	33
16	The Relationship between the 33-Day Precipitation-Weighted Average SO ₄ ⁼ and NO ₃ ⁻ Ion Concentrations and Their Wet Deposition Predicted by RADM2.1 Versus the EMEFS-Observed Grid Cell Average	34
17	The Relationship between the 33-Day Precipitation-Weighted Average SO ₄ ⁼ and NO ₃ ⁻ Ion Concentrations and Their Wet Deposition Predicted by RADM2.5/6 Versus the EMEFS-Observed Grid Cell Average	35
18	The Relationship between the 33-Day Precipitation-Weighted Average SO ₄ ⁼ and NO ₃ ⁻ Ion Concentrations and Their Wet Deposition Predicted by ADOM2Bf Versus the EMEFS-Observed Grid Cell Average	36
19	Half-Hourly Variation of Modeled and Observed O ₃ Dry-Deposition Velocity for Borden Forest on 3 and 4 August 1988	42
20	Original and Improved Modeled and Observed Average Diurnal Variation of the O ₃ Dry-Deposition Velocity for the Period 7 July through 30 August 1988	42
21	Comparison of DIAL, Aircraft, Ozonesonde, and ADOM2Bf Model Profiles of O ₃ Concentrations over Egbert, Ontario, for 3 August 1988	44
22	Time-Height Cross Sections of O ₃ Concentrations Predicted by ADOM2Bf and Measured by Ozonesondes in the Period 29 July to 6 August 1988	45

23	Time-Height Cross Sections of O ₃ Concentrations Predicted by ADOM2Bf and Measured by Ozonesondes in the Period 25 August to 1 September 1988	46
24	Daily Averages of the ADOM2Bf Modeled and CHEF-Observed O ₃ Concentration for the Period 28 July through 7 August 1988 at Roundtop and Mont Tremblant	48
25	Relationship between ADOM2Bf-Modeled and Twin Otter-Observed O ₃ Concentrations	51
26	Relationship between ADOM2Bf-Modeled and Twin Otter-Observed H ₂ O ₂ Concentrations	52
27	Relationship between ADOM2Bf-Modeled and Twin Otter-Observed SO ₂ Concentrations	53
28	Relationship between ADOM2Bf-Modeled and Twin Otter-Observed NO ₂ Concentrations	54
29	Average Aircraft-Observed and Modeled Pollutant Concentrations within the Mixed Layer along Flight Track for 2 September, 6 September, and 8 September 1988	57
30	Comparison of Event-Averaged, Layer 1 Sulfur Species Concentrations for ADOM with and without Nonprecipitating Stratus Clouds for the 25 August to 5 September 1988 Event	61
31	Comparison of Friction Velocity and Planetary Boundary Layer Height Estimated by M12 and M14 Meteorological Preprocessors for RADM for the Grid Cells Containing Pennsylvania State University and New York City from 28 August to 1 September 1988	64
32	Comparison of Dry-Deposition Velocities of O ₃ and SO ₂ Calculated by M12 and M14 Meteorological Preprocessors for RADM for the Grid Cells Containing Pennsylvania State University and New York City from 28 August to 1 September 1988	65
33	Comparison of O ₃ and SO ₂ Concentrations for RADM Layer 1 as Calculated by RADM2.1 and RADM2.6 for the Grid Cells Containing Pennsylvania State University and New York City from 28 August to 1 September 1988	66
34	Comparison of Estimated Annual Average Layer 1 SO ₄ ⁼ Aerosol Concentrations for RADM2.1 with and without Nonprecipitating Clouds	69

TABLES

1	Key Events in the History of the EMEFS Model Evaluation	3
2	Chemical Species and Other Variables Measured by the Surface Networks of the Eulerian Model Evaluation Field Study	9
3	Chemical Species Measured by Aircraft during the Summer 1988 EMEFS Intensive Measurement Campaign	11
4	Features of the Comprehensive Regional Eulerian Acid Deposition Models Examined in This Phase of the EMEFS Model Evaluation	14
5	ADOM2Bf-Predicted and CHEF-Observed Average Ozone Concentration for 28 July through 7 August 1988	47
6	Characteristics of the Twin Otter Flights Used in the Comparison to ADOM2Bf Predictions	49

ACRONYMS AND DEFINITIONS

ADOM	Acid Deposition and Oxidant Model
AES	Atmospheric Environment Service, Canada
AGL	above ground level
APIOS	Acid Precipitation in Ontario Study
CAPMoN	Canadian Air Pollution Monitoring Network
CH	cumulus humilis (clouds)
CHEF	Chemistry of High Elevation Fog
DIAL	differential infrared absorption lidar
EMEFS	Eulerian Model Evaluation Field Study
EMBSC	Eulerian Model Bi-lateral Steering Committee
EPA	U.S. Environmental Protection Agency
EPRI	Electric Power Research Institute
ERP	External Review Panel
FADMP	Florida Acid Deposition Monitoring Program
FCG	Florida Coordinating Group
GMT	Greenwich mean time
GRAD	gradient network
MET	Model Evaluation Team
MM4	mesoscale meteorological model, version 4
MT	Mont Tremblant
NAPAP	National Acid Precipitation Assessment Program
NDDN	National Dry Deposition Network
NP	nonprecipitating (clouds)
NOAA	National Oceanic and Atmospheric Administration
NY	New York City
OEN	Operational Evaluation Network operated by EPRI
OME	Ontario Ministry of the Environment
PAN	peroxyacetyl nitrate
PBL	planetary boundary layer
PMG	Project Management Group
PSU	Pennsylvania State University
QAMC	Quality Assurance Management Committee
RADM	Regional Acid Deposition Model
RT	Roundtop mountain
SOS/T	State of Science and Technology
VAR	variability cluster
VOC	volatile organic compounds

ACKNOWLEDGEMENTS

Funding for the preparation of this report was provided by the Electric Power Research Institute under Contract EPRI RP1630-40 to Battelle, Pacific Northwest Laboratories, and by the U.S. Environmental Protection Agency through interagency agreement DW89933040-01-07 with the U.S. Department of Energy under Contract DE-AC06-76RLO 1830 to the Pacific Northwest Laboratory, which is operated for the U.S. Department of Energy by Battelle Memorial Institute.

1 INTRODUCTION

The Eulerian Model Evaluation Field Study (EMEFS) is a binational program for evaluating comprehensive Eulerian acid-deposition models that have been developed for use by agencies in the United States and in Canada for assessing strategies for mitigating acid rain. The Regional Acid Deposition Model (RADM) (Chang *et al.*, 1987) was developed for and used by the U.S. Environmental Protection Agency (EPA) to determine how acid deposition would respond to various strategies for controlling SO₂ emissions and to establish patterns of source attribution for major emissions source regions and ecologically important receptor regions in eastern North America. This determination was made for the final assessment of acid deposition by the National Acid Precipitation Assessment Program (NAPAP). The Acid Deposition and Oxidant Model (ADOM) (Venkatram *et al.*, 1988) was developed for use by Canadian and German agencies for the analysis of acidic deposition and oxidant episodes.

When the Eulerian Model Bi-lateral Steering Committee (EMBSC) was organized in 1984, work on ADOM and RADM had already been under way for more than a year. However, design of a field study to support the evaluation of the Eulerian models being developed in the United States and Canada did not begin until May 1985. Four workshops between November 1985 and June 1986 (Barchet, 1987) provided the basis for the final design of the EMEFS (Hansen, 1988; Hansen *et al.*, 1991). After the fourth workshop (on quality assurance), representatives of the networks participating in the field study organized the Quality Assurance Management Committee (QAMC) to oversee and coordinate quality assurance activities among the networks. Later, with the approval of the EMBSC, the QAMC was renamed the Project Management Group (PMG) and reorganized into four teams to oversee the final design and operation of the EMEFS:

- The Model Evaluation Team designed a protocol for using the EMEFS data in the evaluation, implemented the protocol, and interpreted the evaluation results.
- The Operational Measurements Team collected air quality and wet deposition data from several collaborating monitoring networks in the eastern United States and Canada:
 - The Canadian Air and Precipitation Monitoring Network (CAPMoN)
 - The Acid Precipitation in Ontario Study (APIOS) network
 - The EPA Model Evaluation (ME-35) network
 - The EPRI Operational Evaluation Network (OEN)
 - The Florida Acid Deposition Monitoring Program (FADMP) network

- The Diagnostic Measurements Team collected air quality data and coordinated the collection of data at enhanced chemistry sites operated by cooperating agencies and from aircraft during periods of intensive measurements in 1988 and 1990:
 - 15 July to 31 August 1988 (Canada) and
15 August to 27 September 1988 (United States)
 - 1 March to 15 April 1990 (Canada) and
15 March to 30 April 1990 (United States)

- The Emissions Inventory Team obtained highly time-resolved emissions rates for SO_x and NO_x from the largest point sources and integrated these with the latest national emissions inventories for use in the Eulerian models.

The Model Evaluation Team (MET) was organized to give a multiagency focus to the evaluation of ADOM and RADM. This team recognized the need for independent peer review of its model evaluation activities and called together an External Review Panel (ERP) consisting of 10 eminent scientists whose expertise spanned all aspects of Eulerian models and their evaluation. Workshops on diagnostic evaluation (Roth, 1988) and on various statistical measures of model performance (Seilkop, 1988) supported the development of the evaluation protocol. Because final definition of the evaluation protocol (Barchet and Dennis, 1990) occurred after the field data collection program was under way, the protocol was constrained by what measurements could actually be afforded within the available EMEFS budget.

The NAPAP plan for completing its assessment of acid rain was finalized during 1988 (NAPAP, 1989). The schedule for NAPAP assessment applications and model evaluation required that various aspects of model development, evaluation, and application take place at the same time. Model development, guided by the preliminary results from the evaluation, continued as both the NAPAP assessment and EMEFS evaluation were occurring. For example, even before it had the full benefit of a comprehensive evaluation, a version of the RADM model, called RADM2.1 here, was adopted as the version to be used for all NAPAP assessment applications. A chronology of key events in the history of the EMEFS model evaluation is given in Table 1.

Completion of the State of Science and Technology (SOS/T) Report 5 on model evaluation for NAPAP (Dennis *et al.*, 1990) marked the completion of the first phase of the model evaluation. This paper presents an overview of the model evaluation developed by the MET, summarizes the results of evaluations of RADM and ADOM, and shows how various operational and diagnostic evaluation results led to improvements in the models. Although a two-year data collection effort was part of the EMEFS, the evaluation results presented here,

Table 1. Key Events in the History of the EMEFS Model Evaluation

Year	Month	Event
1984	Oct	EMBSC officially organized
1985	May	Technical committee workshop on field study plan
	Jun	RADM1 operating
	Aug	ADOM1 operating
	Sep	NAPAP Task Group C peer review of model evaluation plan
	Nov	EPRI Operation Evaluation Network workshop
1986	Feb	Workshop on model evaluation protocol
	Mar	Workshop on field study design
	Jun	Workshop on quality assurance
	Aug	QAMC organized
	Oct	Methods reconciliation workshop
1987	May	NAPAP peer review of RADM "Major Partners" coordination meeting
	Jul	QAMC first meeting
	Aug	Workshop on diagnostic evaluation using aircraft
	Oct	QAMC name changed to PMG; teams organized
	Nov	Model evaluation protocol design initiated
	Dec	MET first meeting
1988	Mar	EMEFS design completed
	Apr	ERP membership selected by MET
	May	NAPAP model evaluation peer review
	Jun	EMEFS field data collection begins
	Jul	ADOM2 operational Canadian aircraft intensive starts 15 July and ends 31 August
	Aug	RADM2 operational Measures and interpretation workshop U.S. aircraft intensive starts 15 August and ends 27 September
	Oct	First meeting of ERP with MET to review protocol design
	1989	Aug
1989	Aug	Model evaluation protocol completed
	Nov	First MET interpretation workshop: RADM2.1 & ADOM2Bf Initial hypotheses for SO ₄ ⁼ underprediction and other biases
	Dec	Second meeting of ERP and MET to review preliminary evaluation results
1990	Feb	NAPAP SOS/T review of preliminary model evaluation results
	Mar	Second EMEFS aircraft intensive: Canadian from 1 March to 30 April; U.S. from 15 March to 30 May
	Jun	EMEFS field data collection ends Second MET interpretation workshop: RADM2.1 & ADOM2Bf Refined hypotheses for SO ₄ ⁼ underprediction and other biases
	Aug	NAPAP SOS/T 5 report on preliminary model evaluation completed
1991	May	ADOM2Bg version frozen for evaluation
	Jun	RADM2.6 version frozen for evaluation
	Jul	Third MET interpretation workshop: RADM2.6 & ADOM2Bg

as Phase 1 of the evaluation, apply only to data collected in 1988 and focus on the period during which intensive measurements were taken using aircraft in the United States. This period, from 25 August through 28 September 1988, will be referred to here as the first model evaluation period. Furthermore, evaluation results are given only for those versions of RADM and ADOM that were available at the time of the NAPAP assessment. Improvements have been made in both models subsequently. The newer versions are currently being evaluated.

2 APPROACH

The subsections that follow describe various aspects of the EMEFS model evaluation: the protocol around which the evaluation was structured, the emissions and meteorological data needed by the models, the surface and upper-air data obtained in the EMEFS, and the comparison measures used to quantify the performance of the models.

2.1 EVALUATION PROTOCOL

Evaluation of RADM and ADOM has followed the protocol developed by Barchet and Dennis (1990) for comprehensive Eulerian acid deposition models. The protocol is oriented toward evaluating the use of the models for their principal NAPAP assessment applications: source-receptor analysis and deposition response to emissions change. Unfortunately, there are no field data that can be used directly to evaluate a model in either of these applications. Therefore, emphasis is given to tests of the models' ability to simulate specific spatial and temporal patterns of air concentrations and wet deposition, such as

- time-averaged ambient concentrations over the modeling domain
- spatial gradients in time-averaged ambient concentrations
- regional time series of primary and secondary pollutant concentrations
- time-averaged wet deposition and ion concentrations in precipitation.

Several statistical and graphical measures (Fox, 1981; Seilkop, 1988; Dennis *et al.*, 1990) are used to quantify model performance.

2.2 DATA NEEDED FOR EVALUATION

Four types of data are needed for the evaluation: geophysical, meteorological, emissions, and ambient air quality data. Geophysical data consisting of gridded fields of such characteristics as terrain elevation and land use are routinely produced by the modeling teams and require no further elaboration. The other kinds of data specifically obtained in the EMEFS are described more fully, though still briefly, below.

2.2.1 Meteorological Data

The meteorological data required by RADM and ADOM are produced by very different procedures. The meteorological data used by RADM were generated by running a prognostic mesoscale meteorological model (Anthes *et al.*, 1987) with four-dimensional data assimilation (Staufer and Seaman, 1990).

For ADOM, the Canadian Meteorological Centre's spectral model is used to dynamically interpolate in time between objectively analyzed fields at the mandatory pressure levels at 6-h intervals (Scholtz *et al.*, 1986). Additional near-surface vertical detail is added through the use of a one-dimensional boundary-layer model. Cloud cover and precipitation type and amount are based on both observations and numerical predictions.

2.2.2 Emissions

The Emissions Inventory Team prepared emission inventories for the evaluation period specifically for each model. Hourly estimates of anthropogenic emissions of SO₂, primary SO₄⁼ aerosol, NO_x, NH₃, and several classes of volatile organic compounds (VOC) were based on the 1985 NAPAP emissions inventory (EPA, 1989), which was supplemented during the intensive measurement periods of the EMEFS with real-time estimates of the emissions of SO₂ and NO_x and source characteristics from about 100 of the largest point sources in the United States and Canada. Plume rise from point sources was calculated from source characteristics in the emissions inventory and the hourly meteorological data. The area and mobile source components of the 1985 NAPAP emissions inventory provided area-source emissions. Mobile-source emissions were adjusted to account for the daily average temperature and the daily temperature range. Natural emissions of organic compounds and NO_x were based on the type of surface land cover and the hourly meteorological data using the methods of Lamb *et al.* (1987) and Gay (1987).

Although the inventories submitted to the modeling teams were as similar as possible, each modeling group discovered problems with the inventories that they fixed in ways that were not necessarily the same. Some of the more significant differences that resulted are listed below:

- For some major point sources, most but not all in Illinois, in the 1985 NAPAP inventory, erroneous temporal emissions factors resulted in a whole week's emissions apparently being released in one hour on Saturday morning. The Emissions Inventory Team resolved this problem for RADM by correcting the temporal emissions factors according to data in the NAPAP inventory. Without access to those data, the ADOM modeling team calculated an average for the hours immediately before and after the

time of the spurious emissions and distributed the excess emissions uniformly over all of the hours in the week.

- An examination of the 1985 NAPAP inventory by the ADOM modeling team showed that many point sources in Texas and North Dakota, which were identified as coal burning from their NO/NO₂ emissions ratios, in fact emitted no primary SO₄⁼ aerosol, only SO₂. Several other major U.S. point sources were also found to emit only SO₂. Furthermore, because of an oversight in the inventory provided to NAPAP by Canada, no point sources in Ontario or Quebec were reported as emitting primary SO₄⁼ aerosol. The ADOM team compensated for the lack of primary SO₄⁼ aerosol emissions by transferring 0.67% of the inventoried SO₂ emissions from the affected U.S. sources and 3.5% from the Canadian sources to the category of primary SO₄⁼ aerosol emissions. On the other hand, no adjustment of primary SO₄⁼ aerosol emissions from the U.S. point sources was made in the inventory used in RADM. However, the missing Canadian primary SO₄⁼ aerosol emissions were apparently corrected by the Emissions Inventory Team in the RADM inventory.
- The ADOM modeling team found numerous grid cells in the ADOM inventory, including those cells containing New York City, Toronto, and Chicago, for which mobile source emissions were zero for the 24th hour of the day. This was corrected by assigning the emissions for the 23rd hour to the 24th hour as well. No similar problem was found in the RADM inventory.
- In producing the 1985 NAPAP inventory, certain Canadian point-source emissions were treated as area sources to maintain confidentiality. For the RADM inventory, those sources were removed from the area-source totals and treated as minor point sources. As a result, about 9% of Canadian SO₂ and primary SO₄⁼ aerosol emissions and 1.3% of Canadian NO and NO₂ emissions were shifted from the area-source inventory to the minor-point-source inventory.
- In the RADM inventory, certain real-time U.S. point sources for June to September 1988 had zero emissions at midnight local time. This problem was corrected in the RADM inventory by averaging the emissions at 11:00 pm and 1:00 am local time. The ADOM inventory did not have this problem.
- In the RADM inventory, it was necessary to correct the latitude and longitude of nine point sources in Massachusetts. In ADOM, these sources were considered minor point sources and were added to the area source inventory.

- The ADOM supplementary dust emissions inventory, which provides Mn^{+2} and Fe^{+3} data, incorrectly had zero values over Canada; this shortcoming has since been corrected. By contrast, RADM merely used postulated background values of Mn^{+2} and Fe^{+3} concentrations, which are not related to any emissions.
- All minor point sources are injected according to seasonal, hourly source characteristics into the first four RADM layers and into the first model layer in ADOM. Also, since the RADM domain was used to define which major point sources were included in the real-time inventory, any point sources outside of the RADM domain that are nonetheless in the ADOM domain were treated as minor point sources in the ADOM inventory.

Several other anomalies in the emissions inventories have been noted for which no corrective action has as yet been taken. Perhaps the most important of these is the day-specific mobile-source emissions of NO_x for summer 1988 being about 15% lower than the typical daily NO_x emissions from the 1985 NAPAP summer inventory and 12% lower than those for fall 1985. Thus, in the model evaluation simulations, NO_x emissions from mobile sources jump 12% in going from 31 August to 1 September 1988. Day-specific mobile-source emissions for the summer of 1988 were generated using data on motor vehicles from 1986. Day-specific emissions of some VOC categories exhibit similar disparities. Mobile-source emissions include small amounts of primary $\text{SO}_4^{=}$ aerosol and NH_3 in Canada but not in the United States. Non-mobile, area sources in the 1985 NAPAP inventory exhibit peculiar minima in $\text{SO}_4^{=}$ aerosol emissions in the United States and in NH_3 emissions in Canada, at around 11 or 12Z. Open-source emissions were not included in either the 1985 NAPAP inventory or the 1988 supplemental real-time major-point-source inventory.

2.2.3 Observed Values of Air Concentrations and Precipitation Chemistry

The EMEFS field program has been extensively described elsewhere (Hansen, 1989; Hansen *et al.*, 1991). Surface air and precipitation chemistry variables measured at sites in the EMEFS networks are given in Table 2, together with their time resolution. The locations of EMEFS sites active during the 25 August to 27 September 1988 period are shown in Figure 1.

The intensive measurement campaigns carried out in the summer of 1988 included aircraft flights in the United States and Canada for two six-week periods that overlapped by two weeks. Each country used aircraft to measure upper-air concentrations of the chemical species listed in Table 3. The U.S. flights were designed to obtain regional distributions in cloud-free air (Spicer *et al.*, 1991) with the Gulfstream 1 and Hawker-Siddeley 125 aircraft; the King Air aircraft was used to obtain boundary layer and in-cloud measurements. The

Table 2. Chemical Species and Other Variables Measured by the Surface Networks of the Eulerian Model Evaluation Field Study

Observable	Averaging Time (hours)	Network							
		EPA				EPRI	OME	AES	FCG
		ME-35	GRAD	VAR	OTHER	OEN	APIOS	CAPMoN	FADMP
Number of stations able to measure variable									
Gaseous									
SO ₂	24	36	14	11	7	25	11	10	2
NH ₃ ^(a)	24	36	14	11	7	25	-	-	2
HNO ₃ ^(a)	24	36	14	11	7	25	11	10	2
NO ₂	24	36	14	11	7	-	-	-	-
NO ₂	1	-	-	-	-	24	-	-	2
NO _x	1	-	-	-	-	-	1	-	-
O ₃	1	-	14	11	-	24	4	9	2
Aerosol									
SO ₄ ⁻	24	36	14	11	7	25	11	10	2
NO ₃ ^{- (b)}	24	36	14	11	7	25	11	10	2
NH ₄ ^{+ (b)}	24	36	-	11	-	25	-	-	2
Precipitation									
Chemistry ^(c)	24	36	14	11	7	25	19	11	4
S(IV)	24	-	8	-	1	-	-	-	-
Depth	1	36	14	11	7	25	19	11	4
Meteorology ^(d) (at 10 m)	3	36	-	-	-	24	-	-	-
Total Stations		36	14	11	7	25	29	11	4

(a) Not compensated for gain from NH₄NO₃ volatilization.

(b) Not compensated for loss from NH₄NO₃ volatilization.

(c) pH, conductivity, SO₄⁻, NO₃⁻, Cl⁻, NH₄⁺, Na⁺, K⁺, Ca⁺², Mg⁺².

(d) Wind speed, wind direction, temperature, relative humidity, barometric pressure, insolation (EPA only).

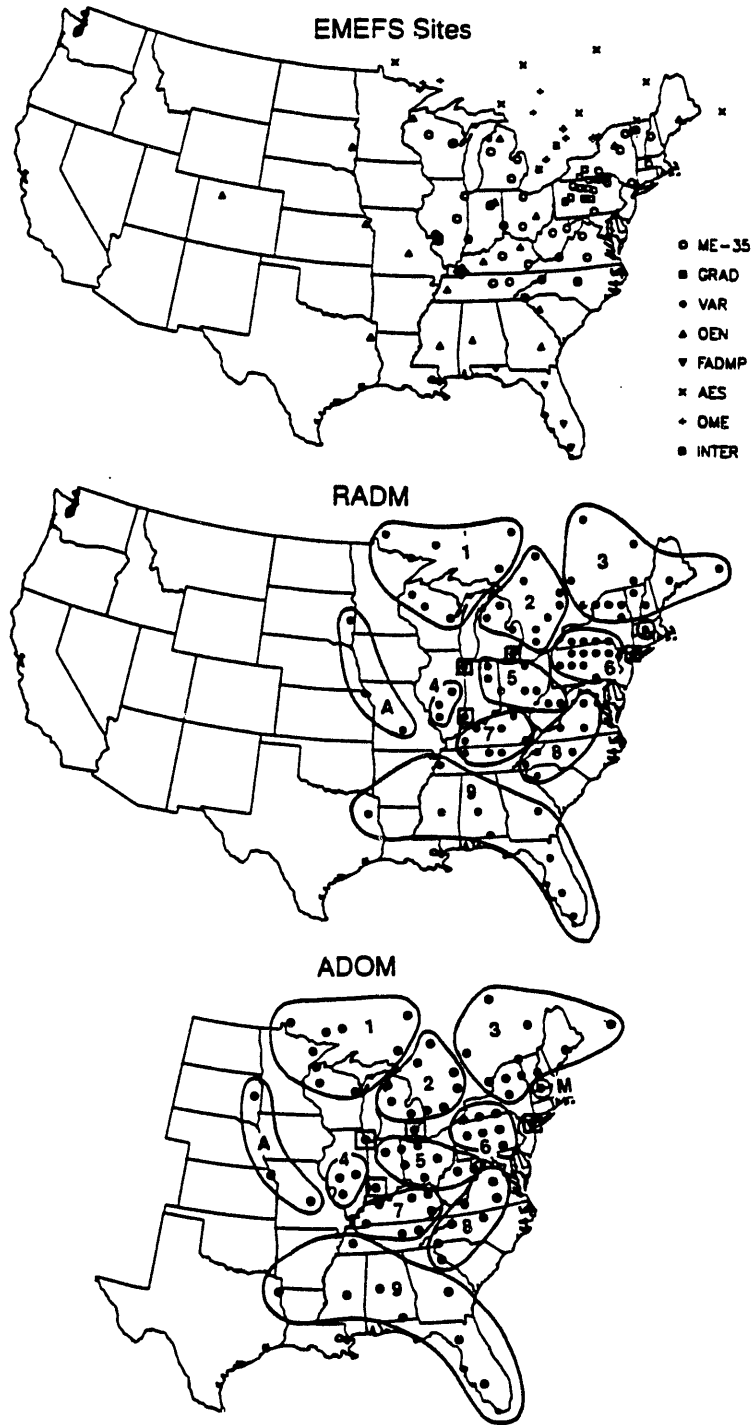


Figure 1. Location of EMEFS Sites Active during the 25 August to 27 September 1988 Evaluation Period and Regional Groupings of RADM and ADOM Grid Cells Containing Active Sites. Squares denote cells in the urban group.

Table 3. Chemical Species Measured by Aircraft during the Summer 1988 EMEFS Intensive Measurement Campaign

Variable	Aircraft				
	United States			Canada	
	G-1	HS-125	KA	TO	DC-3
Continuous					
O ₃	Yes	Yes	Yes	Yes	Yes
SO ₂	Yes	Yes	Yes	Yes	Yes
NO _y	Yes	Yes	Yes	Yes	Yes
NO	Yes	Yes	Yes	Yes	Yes
NO ₂	Yes	Yes	No	Yes	Yes
CO	Yes	Yes	No	No	No
Total Peroxide	Yes	Yes	No	Yes	Yes
H ₂ O ₂	Yes	Yes	Yes	Yes	Yes
Time Integrated					
PAN	Yes	Yes	No	No	Yes
Filter Sample					
SO ₂	No	No	No	Yes	Yes
SO ₄ ⁼ Aerosol	Yes	Yes	No	Yes	Yes
NO ₃ ⁻ Aerosol	Yes	Yes	No	Yes	Yes
NH ₄ ⁺ Aerosol	Yes	Yes	No	Yes	Yes
HNO ₃	Yes	Yes	No	Yes	Yes
NH ₃	Yes	Yes	No	Yes	Yes
Canister Sample					
VOC	Yes	Yes	No	Yes	Yes

Aircraft: G-1 Gulfstream 1 TO Twin Otter
 HS-125 Hawker Siddeley 125 DC-3 DC-3
 KA King Air

PAN = peroxyacetyl nitrate

VOC = volatile organic carbon

NO_y = NO + NO₂ + PAN + HNO₃

Canadian flights with the Twin Otter and DC-3 aircraft focused much more on measuring vertical profiles that included some in-cloud measurements (Hansen *et al.*, 1991).

Following the recommendations of Seilkop (1988), the air concentrations, precipitation chemistry, and wet deposition measured at a site were assigned as the observed values for the grid cell in which the site was located. For grid cells containing more than one active site, an arithmetical average was calculated over all sites in the cell from the valid daily air concentrations for each species. The spatial distribution of 120 air-chemistry and 136 precipitation-chemistry sites in the EMEFS networks was such that 81 and 75 grid cells for RADM contained active EMEFS air-chemistry and precipitation-chemistry sites, respectively. For ADOM, with its coarser grid, the corresponding numbers were 74 and 69 grid cells.

For tests involving the time-averaged quantities, a 33-day average of the ambient concentrations was calculated for each cell and each pollutant for which at least 22 valid daily concentrations were available in the first model evaluation period, 25 August through 27 September 1988. The 33-day average over the first model evaluation period will be referred to hereafter as the "period mean." Precipitation-weighted period mean ion concentrations were calculated for those cells with at least 90% of the total precipitation for the period being in valid samples.

To reduce the confidence interval on the observed evaluation period mean ambient concentrations for SO_2 , $\text{SO}_4^{=}$ aerosol, and T- NO_3 (total nitrate = HNO_3 + NO_3^- aerosol), a second tier of spatial aggregation was used (Dennis *et al.*, 1990). Cells were assigned to regional groups, as shown in Figure 1, according to their geographic proximity, the similarity of their day-to-day variations in the observed concentrations of SO_2 and $\text{SO}_4^{=}$ aerosol, and the similarity of their geographical location relative to major emissions source regions. For each day, the regional mean was calculated as the geometric mean of the concentrations in grid cells with valid observations. The period mean was calculated for the region as it was for each grid cell. Two clusters of relatively nearby sites, one of five sites in western Kentucky and the other of four sites in northeastern Pennsylvania, were used to estimate the 95% confidence interval around the observed daily regional mean ambient concentration.

Upper-air data collected during the 1988 aircraft intensive (Hansen *et al.*, 1991; Spicer *et al.*, 1991) had to be made comparable to the model predictions described below. Following the suggestions of Seilkop (1988) and using the technique of Hales and Pennell (1988), real-time aircraft measurements were averaged over the time interval that the aircraft was in a given grid cell, as determined from the aircraft's position and altitude. This processing of the aircraft data resulted in grid cell averages that could be related in space and time to each hour of model simulation.

2.3 MODEL PREDICTIONS

Three versions of RADM (RADM2.1, RADM2.5/6 and RADM2.5/15) and one version of ADOM (ADOM2Bf) have been used to simulate air concentrations and wet deposition during the first evaluation period. Table 4 lists the pertinent features of these models. Because of its importance to the NAPAP assessment, RADM2.1 received the most attention in the evaluation. Both 6- and 15-layer versions of the most current research version of RADM (RADM2.5) were also evaluated to determine whether their departures from the assessment version, including increased vertical resolution, would improve the simulation. The concurrent evaluation of RADM and ADOM gave an opportunity to see how models with considerable differences in how they produce their meteorological data, some differences in the mechanisms for gas-phase chemistry (Stockwell and Lurmann, 1989), grid-cell size, and large differences in the cloud and scavenging modules (Walcek *et al.*, 1991) would differ in performance.

The temporal resolution of the model output, nominally 1 h, was reduced to a daily average. The air concentrations were arithmetically averaged over the 24-h daily period. Wet deposition and precipitation amounts were summed over the 24-h period and daily precipitation-weighted concentrations were calculated from daily total wet deposition and precipitation amounts. Additional temporal and spatial averaging, as described for the observations, was applied to the model predictions to produce 33-day mean predicted ambient concentrations for each grid cell, and 33-day regional mean ambient concentrations for SO₂, SO₄⁼ aerosol, and T-NO₃.

2.4 COMPARISON MEASURES

Many statistical measures for evaluating model performance have been proposed (Fox, 1981; Anthes *et al.*, 1989; Clark *et al.*, 1989; Dennis *et al.*, 1990). The model evaluation protocol by Barchet and Dennis (1990) focuses on graphical displays that illustrate scatter and bias, and uses only a few difference statistics for bias and scatter and temporal correlation as quantitative measures of model performance. As recommended by Seilkop (1988), the difference statistics are based on the comparison of the prediction for a grid cell and the observed value for that grid cell. The observed value for the cell could be for either a single site within the cell or the average over all of the sites in the cell having valid observations.

Table 4. Features of the Comprehensive Regional Eulerian Acid Deposition Models Examined in This Phase of the EMEFS Model Evaluation

Model Version	Features
RADM2.1	<p>Eulerian grid, 35 W-E by 33 S-N cells, 80 km on side, Lambert conformal projection</p> <p>σ-coordinates, 6 layers, surface to 100 hPa</p> <p>Boundary layer (Blackadar, 1979)</p> <p>Advection (Smolarkiewicz, 1984)</p> <p>Walcek cloud scavenging (Chang <i>et al.</i>, 1987)</p> <p>Updated Stockwell (1986) gas-phase chemistry</p> <p>Plume rise (Briggs, 1975)</p>
RADM2.5/6	<p>Same as RADM2.1 except:</p> <p>Less vigorous and shallower mixed layer</p> <p>Less nighttime production of HNO₃ from N₂O₅</p> <p>Point source emissions into layer 2 or higher</p>
RADM2.5/15	<p>Same as RADM2.5/6 except 15 σ-layers</p>
ADOM2Bf	<p>Eulerian grid, 33 W-E by 33 S-N cells, 127-km sides at 60°N, polar stereographic projection</p> <p>z-coordinates, 12 layers, surface to 10 km</p> <p>Boundary layer provided by meteorology driver (Scholtz <i>et al.</i>, 1986)</p> <p>Flux advection (Yamartino and Scire, 1984) based on modified Blackman and Tukey (1958) cubic spline interpolation</p> <p>Stratus cloud (Karamchandani <i>et al.</i>, 1985)</p> <p>Convective cloud (Venkatram and Karamchandani, 1989)</p> <p>Gas-phase chemistry (Lurmann <i>et al.</i>, 1986)</p> <p>Aqueous-phase chemistry (Young and Lurmann, 1984)</p> <p>Plume rise (Weil and Brower, 1984)</p>

3 FINDINGS

This section describes the performance of the models based on the tests outlined in the model evaluation protocol. Findings pertain to the performance of the models as assessed from operational and integrated-diagnostic perspectives. Operational evaluation addresses the ability of a model to simulate quantities observed over regional spatial and monthly (or longer) temporal scales that would be consistent with the planned applications of the model (Barchet, 1987; Barchet and Dennis, 1990; Dennis *et al.*, 1990). Closer examination of model performance to determine whether individual process simulations are correct is called "diagnostic evaluation." A full diagnostic evaluation would, however, require measurements at the process level that were unavailable during most of the EMEFS. Nevertheless, some surface observations (namely the hourly O₃ and NO₂ concentrations) and the upper-air concentrations measured during the aircraft intensives, provide sufficient process-level detail to permit an initial integrated-diagnostic evaluation. "Integrated" here means that the observations and simulations represent the combined effects of many processes but with sufficient detail that shortcomings in the simulation of one or more of them should be readily apparent. From the perspective of model simulations, integrated refers to those simulations made with the full model rather than with just some subset of its modules. Section 5 summarizes several interpretive analyses that have been part of the ongoing integrated-diagnostic evaluation of the models.

3.1 AIR CONCENTRATIONS

The key findings based on the comparison of RADM simulations to EMEFS observations have been reported in a NAPAP State of Science and Technology report (Dennis *et al.*, 1990) and elsewhere (Barchet *et al.*, 1991). Those findings for RADM and similar findings for ADOM (Fung *et al.*, 1990, 1991) are summarized here. The comparisons of predicted and observed mean values of the ambient surface concentrations and precipitation chemistry for the evaluation period address mainly operational evaluation issues, as do comparisons of estimated annual and seasonal means. Integrated-diagnostic information is obtained from analyses of daily and hourly time series of surface concentrations and of the upper-air data collected during the intensive aircraft measurement campaigns.

3.1.1 Evaluation Period (33-day) Averages

Scatter plots of the predicted and observed evaluation period average ambient surface concentrations of SO₂, SO₄⁼ aerosol, NO₂, and HNO₃ for RADM2.1, RADM2.5/6, and ADOM2Bf (Figures 2 to 4) show that all three models

RADM 2.1 PREDICTIONS VERSUS OBSERVATIONS
AVERAGE OF DAILY VALUES FROM 8/25/88-9/27/88

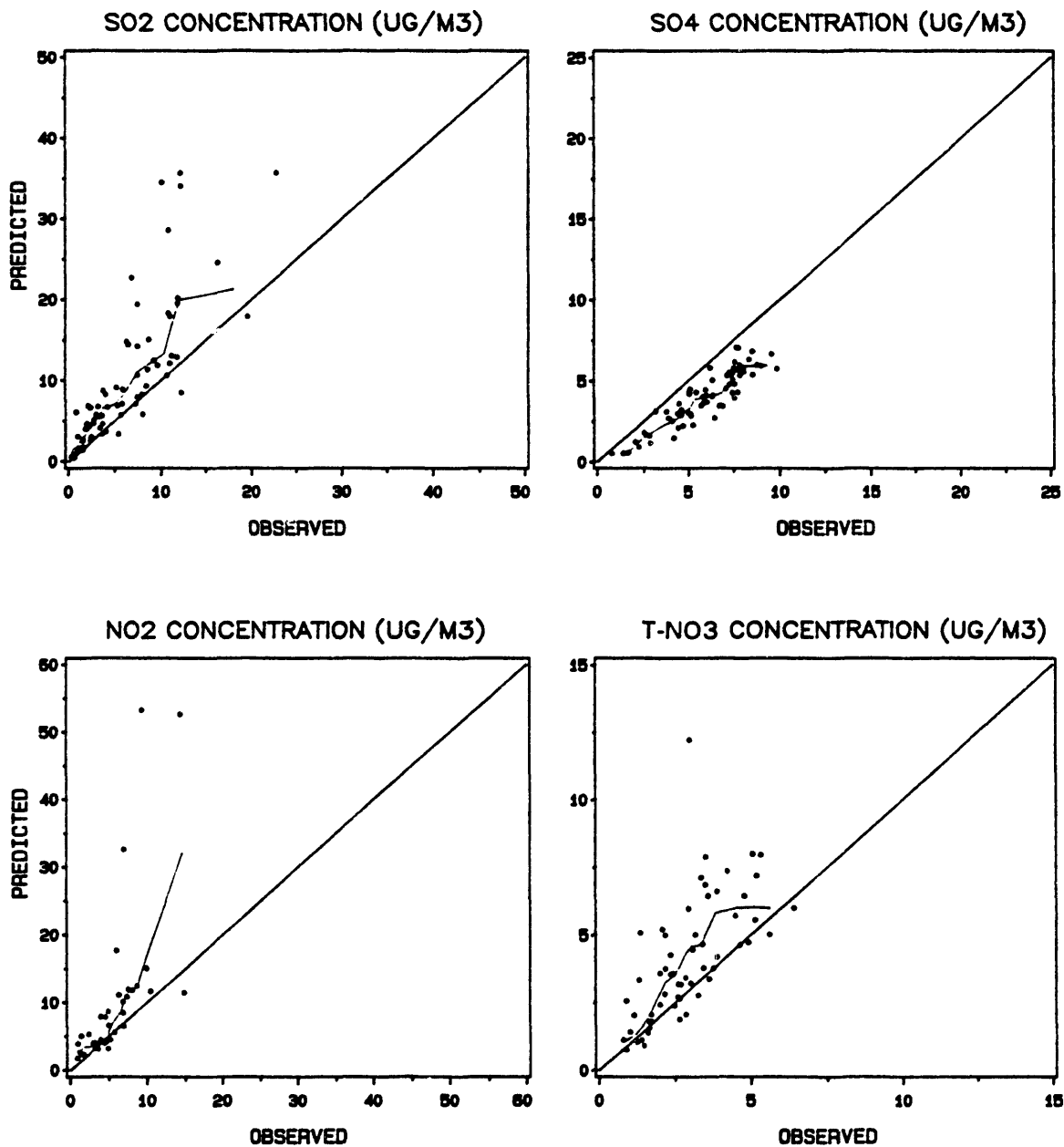


Figure 2. The Relationship between the 33-Day Average Surface Concentration of SO₂, SO₄⁼ Aerosol, NO₂, and T-NO₃ Predicted by RADM2.1 Versus the Observed Grid Cell Average

RADM 2.5/6L PREDICTIONS VERSUS OBSERVATIONS
AVERAGE OF DAILY VALUES FROM 8/25/88-9/27/88

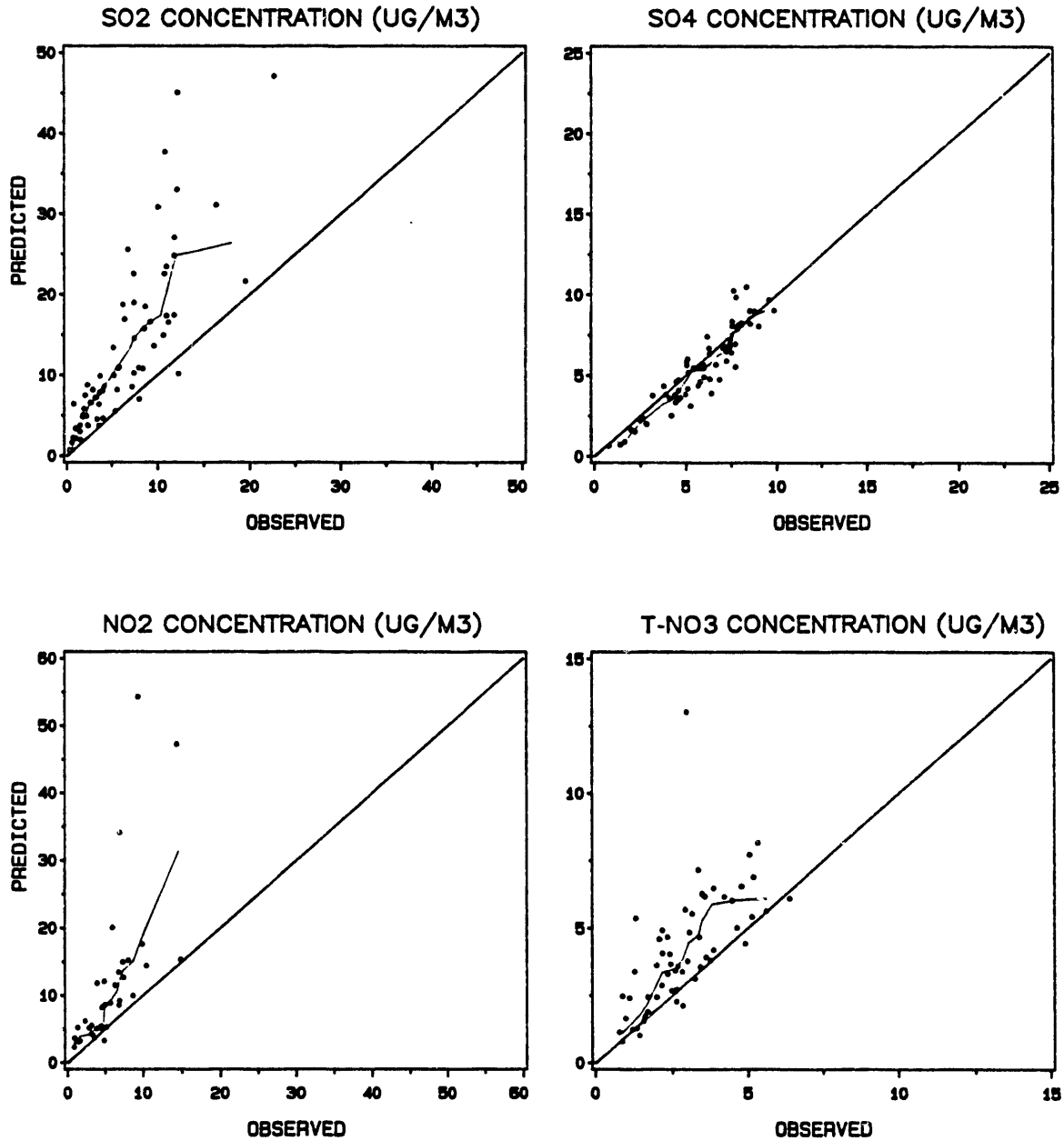


Figure 3. The Relationship between the 33-Day Average Surface Concentration of SO₂, SO₄⁼ Aerosol, NO₂, and T-NO₃ Predicted by RADM2.5/6 Versus the Observed Grid Cell Average

ADOM2BF PREDICTIONS VERSUS OBSERVATIONS
AVERAGE OF DAILY VALUES FROM 8/25/88-9/27/88

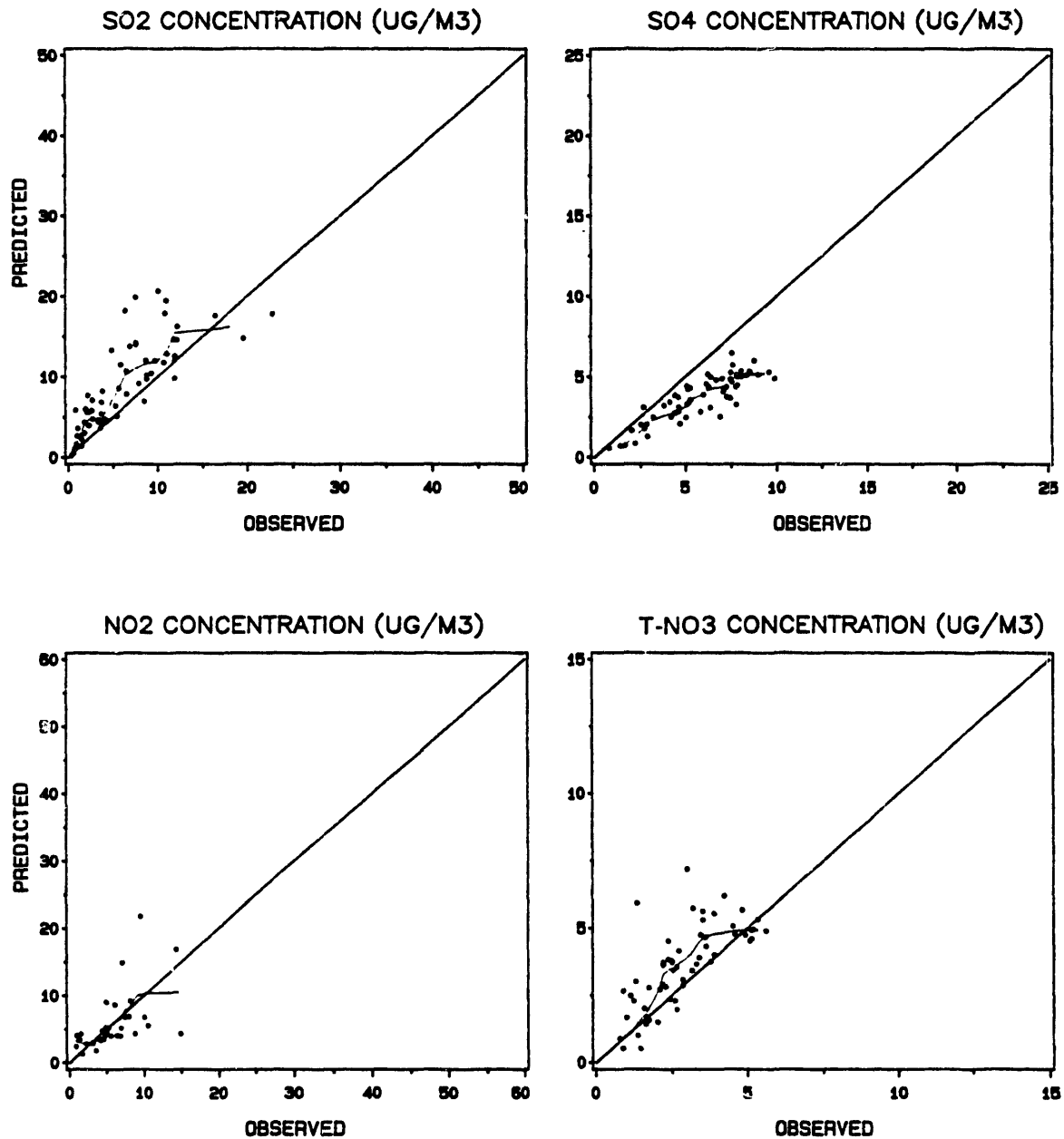


Figure 4. The Relationship between the 33-Day Average Surface Concentration of SO₂, SO₄⁻ Aerosol, NO₂, and T-NO₃ Predicted by ADOM2Bf Versus the Observed Grid Cell Average

- overpredict SO₂
- underpredict SO₄⁼ aerosol and consequently also the ratio of SO₄⁼ aerosol to total S (SO₂ + SO₄⁼ aerosol)
- overpredict T-NO₃.

Although RADM also overpredicts total S, ADOM does not. The solid line in Figures 2 to 4 traces the smoothed median of the predictions as a function of the observation (Tukey, 1977). The degree of over- and underprediction varied with model, species, and observed concentration. Tables A.1 to A.3 in Appendix A give the bias and other statistics for the period mean predicted and observed surface concentrations of SO₂, SO₄⁼ aerosol, NO₂, and T-NO₃ for RADM2.1, RADM2.5, and ADOM2Bf as a function of the observed concentration. Observed values were ranked from least to greatest and divided into five categories each containing approximately the same number of observations. For each category, the average observed and predicted values, the average percentage bias

$$\overline{Bias} = 100 \times \frac{1}{N} \sum_1^N \frac{(Prediction - Observation)}{Observation}$$

and the standard deviation of the percentage bias

$$\sigma_{Bias} = \sqrt{\frac{1}{N} \sum_1^N \left[\frac{100(Prediction - Observation)}{Observation} - \overline{Bias} \right]^2}$$

were calculated. The average bias (the difference between the average prediction and observation) tended to increase with observed concentration. For SO₂ and NO₂, the percentage bias is least for the middle of the range of observations and increases toward either extreme of the range. For T-NO₃, the average percentage bias is largest for the smallest range of observed concentration. But for SO₄⁼ aerosol, the percentage bias is fairly uniform over the entire range of observed concentrations.

Period mean average concentrations predicted by RADM2.5 tended to be slightly higher than those predicted by RADM2.1. For all species examined, the 15-layer version of RADM2.5 tended to predict slightly higher surface concentrations than the 6-layer version.

3.1.2 Time Series

Time series of the daily regional mean predicted and observed concentrations demonstrate that all of the models successfully track the day-to-day changes in ambient surface concentrations. Example time series comparisons are given in Figures 5 to 7 for SO₂ and SO₄⁼ aerosol in Regions 3 and 5 for RADM2.1, RADM2.5/6, and ADOM2Bf. The vertical bars give an estimate of the 95% confidence interval about the observed regional mean. Region 3 is relatively distant from major emissions source areas, whereas Region 5 includes the major North American SO₂ source region. Figure 8 shows considerable variability in the temporal correlation coefficient between predicted and observed daily values (Table A.7) among regions for a given model and between models for a given region. In general, correlations were highest for Regions 2 and 3 and lowest for Regions 7 and 9. Correlations appear to be weakest for the primary pollutants SO₂ and NO₂ and strongest for SO₄⁼ aerosol.

Additional time series analyses were possible with the hourly O₃ observations and predictions. Figure 9 shows the time series of daily regional mean maximum O₃ concentrations in Regions 3 and 5 for RADM2.1 and ADOM2Bf. This figure and the correlations shown for maximum O₃ concentrations in Figure 8 show that, although the models successfully tracked the day-to-day variations in O₃ concentrations, there were some pronounced biases. Figure 10 illustrates RADM2.1 performance in predicting the daily maximum and minimum hourly O₃ concentration over all regions. This figure shows that RADM2.1

- underpredicts the highest daily maximum O₃ concentrations
- overpredicts the lowest daily maximum O₃ concentrations
- consistently overpredicts the daily minimum O₃ concentrations.

3.1.3 Regional Distributions

Monthly average surface concentrations were used to determine the ability of the models to reproduce the regional distribution of ambient concentrations. As expected given the biases discussed above, spatial patterns of the predicted regional distributions differ from those that

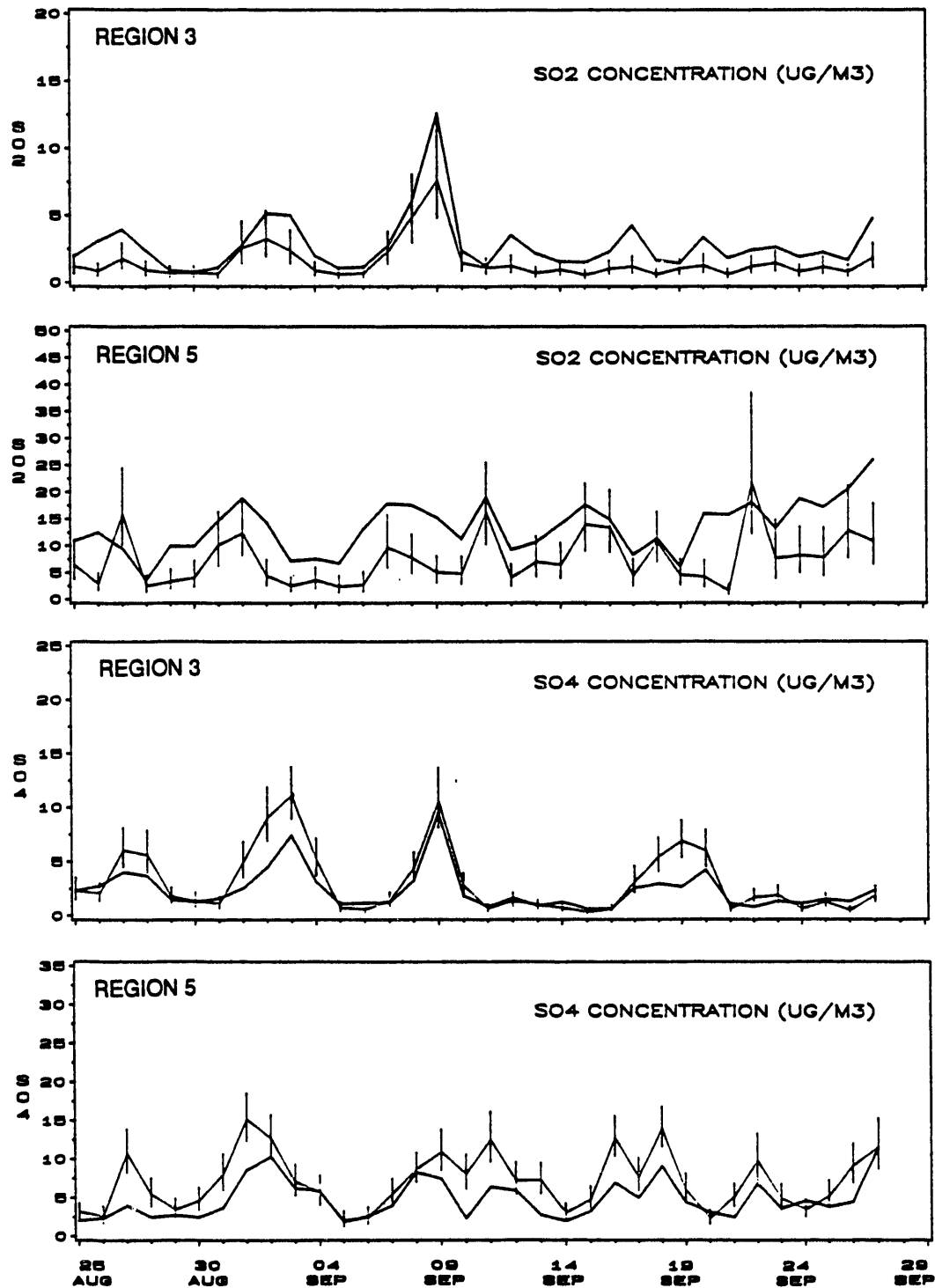


Figure 5. The Daily Variation in the Regional Average RADM2.1-Predicted (heavy line) and EMEFS-Observed (thin line) Concentration of SO₂ and SO₄⁼ Aerosol in Regions 3 and 5. Vertical Bars Show the 95% Confidence Interval for the Observations.

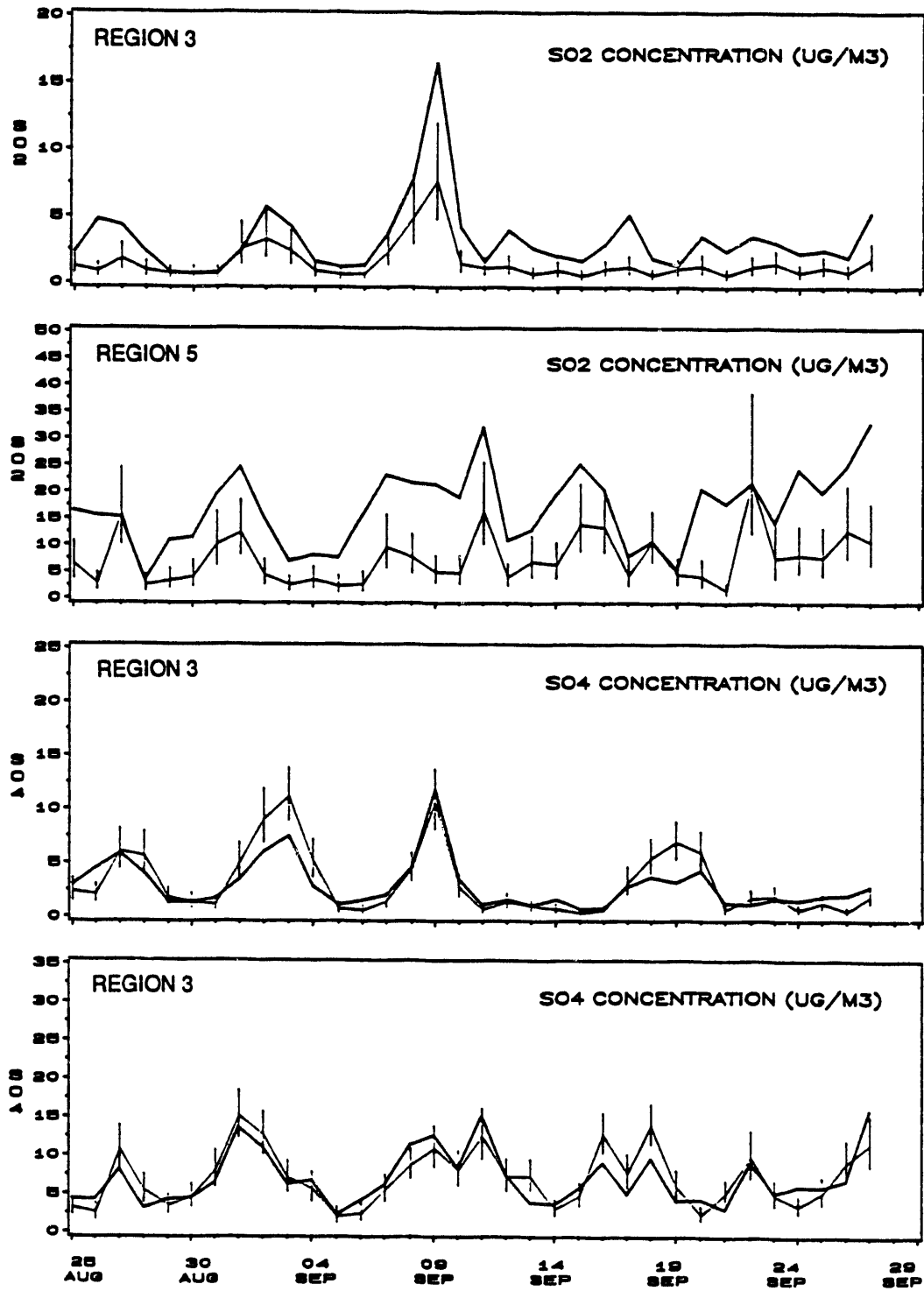


Figure 6. The Daily Variation in the Regional Average RADM2.5/6-Predicted (heavy line) and EMEFS-Observed (thin line) Concentration of SO_2 and $\text{SO}_4^{=}$ Aerosol in Regions 3 and 5. Vertical Bars Show the 95% Confidence Interval for the Observations.

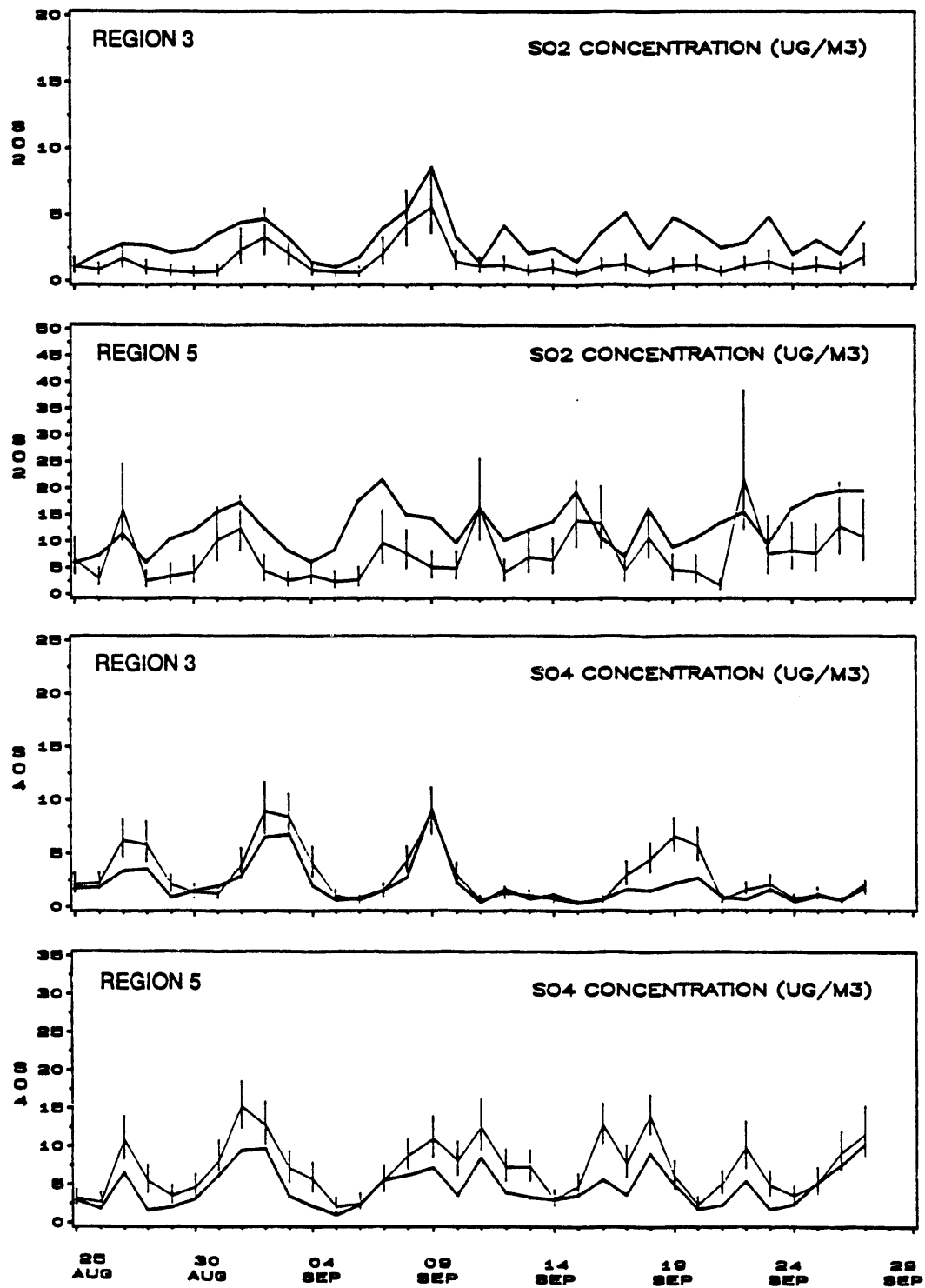


Figure 7. The Daily Variation in the Regional Average ADOM2Bf-Predicted (heavy line) and EMEFS-Observed (thin line) Concentration of SO₂ and SO₄⁼ Aerosol in Regions 3 and 5. Vertical Bars Show the 95% Confidence Interval for the Observations.

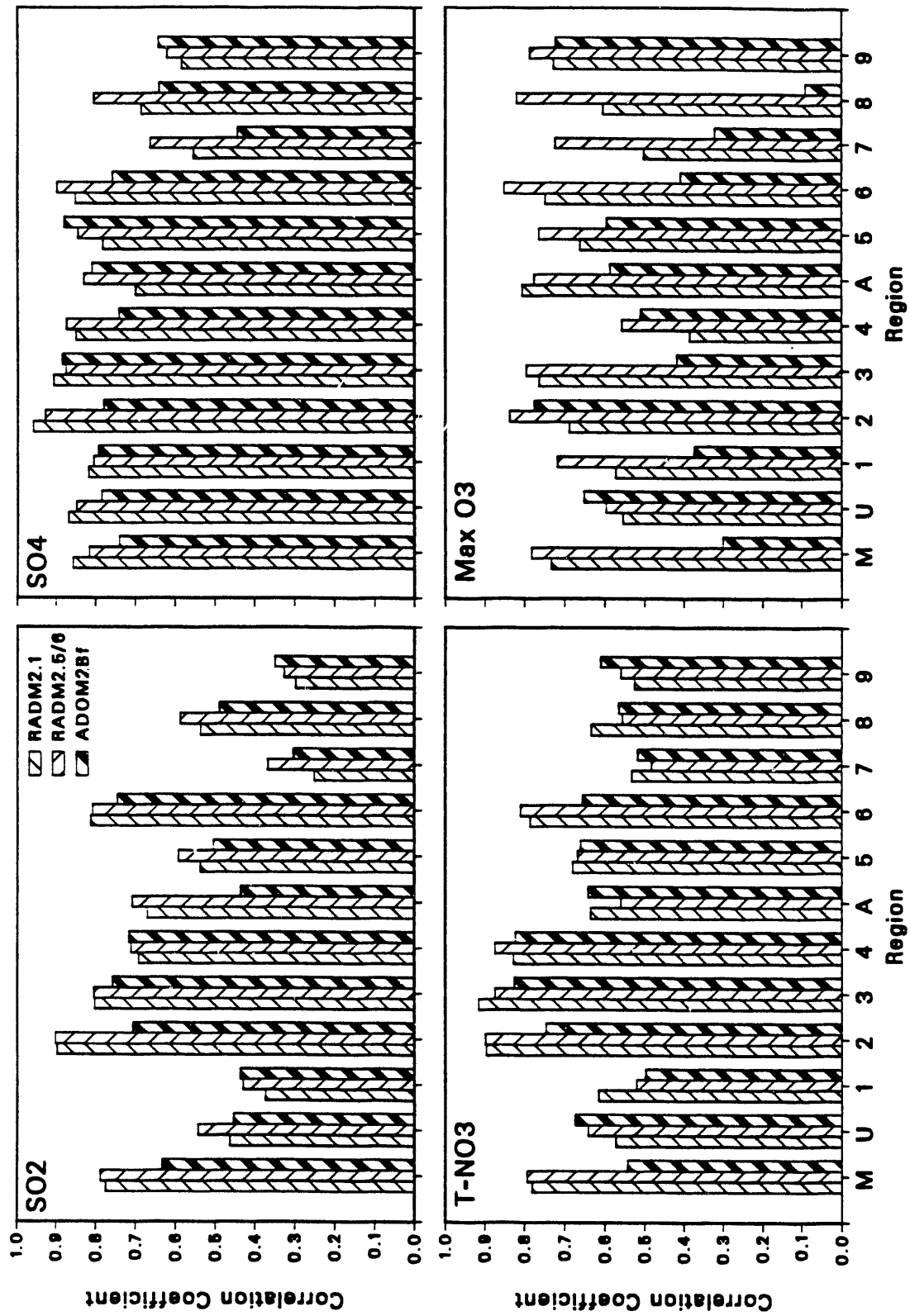


Figure 8. Linear Temporal Correlation Coefficients between the Model-Predicted and EMEFS-Observed Daily Regional Average SO₂, SO₄ = Aerosol, T-NO₃, and Maximum O₃ Concentrations

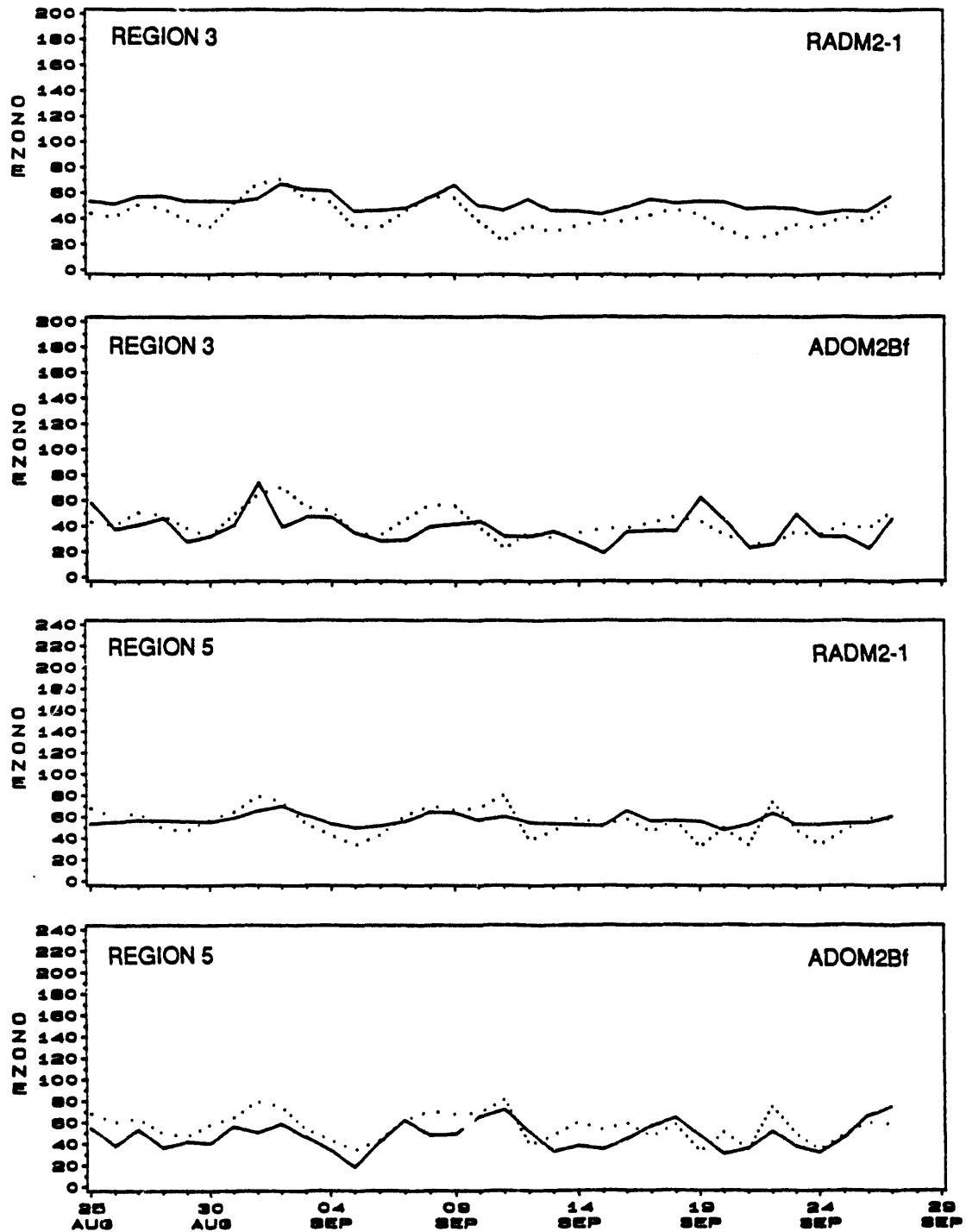


Figure 9. The Daily Variation in the Regional Average RADM2.1- and ADOM2Bf- Predicted (solid line) and EMEFS-Observed (dotted line) Maximum O₃ Concentrations in Regions 3 and 5

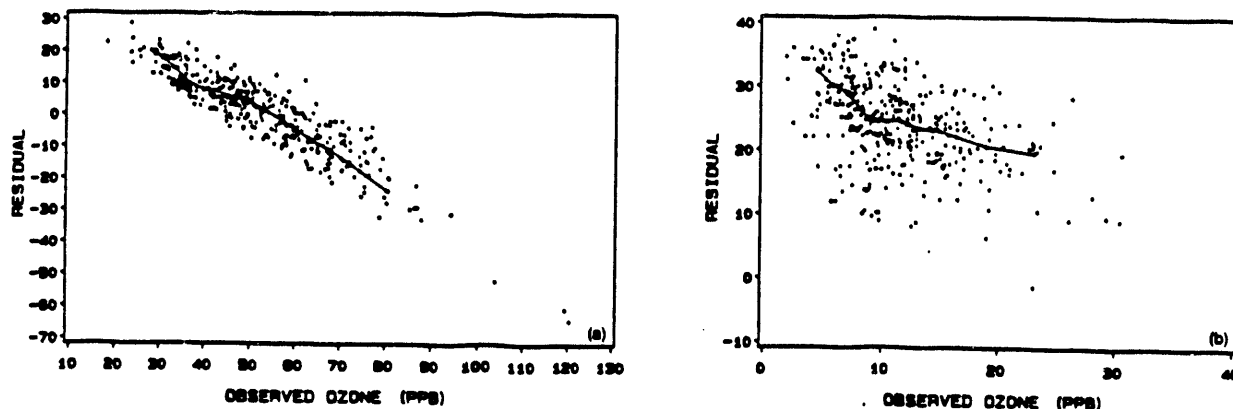


Figure 10. Residual Daily Regionally Averaged Maximum-Hourly and Minimum-Hourly O₃ Concentrations for All Regions and Days in the Model Evaluation Period

are observed. Figure 11 shows three SO₂ concentration contour maps. The upper map is based on all RADM2.1 grid cells for which valid grid-cell observations are available. The center map is based on grid cells with valid observed mean SO₂ concentrations for the evaluation period. If one assumes that those grid cells for which the RADM2.1 prediction exceeds the observation by more than 10 μg/m³ and by a factor of 3 are unrepresentative of the regional pattern and those cells are excluded from the contour map, the resulting predicted regional distribution, as shown in the lower map of Figure 11, becomes much more visually congruent with the map of the observed values.

3.1.4 Surface Gradients

Examination of the variation of observed and predicted concentrations along a transect through the field of grid cells that have valid monthly means allows evaluation of the models' ability to reproduce spatial concentration gradients. Figure 12 shows the EMEFS-observed and the RADM2.1-predicted gradients in SO₂ and SO₄⁼ aerosol along a transect from southwestern Pennsylvania to northeastern New York. Near the source region, the bias for overprediction of SO₂ causes the simulated gradient to be much steeper than that observed. Away from the source region, the observed and predicted gradients are similar. Little difference is seen in the observed and predicted gradients for SO₄⁼ aerosol, even though the predictions are clearly and consistently biased low.

The gradient for ADOM2Bf along approximately the same transect is shown in Figure 13. Because of the grid cell is larger for ADOM, the observed values shown in Figure 13 differ slightly from those shown in Figure 12. However, the results for ADOM2Bf are similar to those obtained with RADM: greater SO₂ overprediction in the SO₂ source areas gives rise to

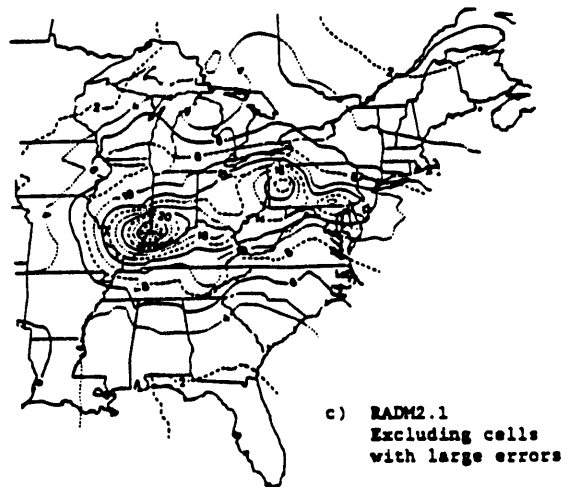
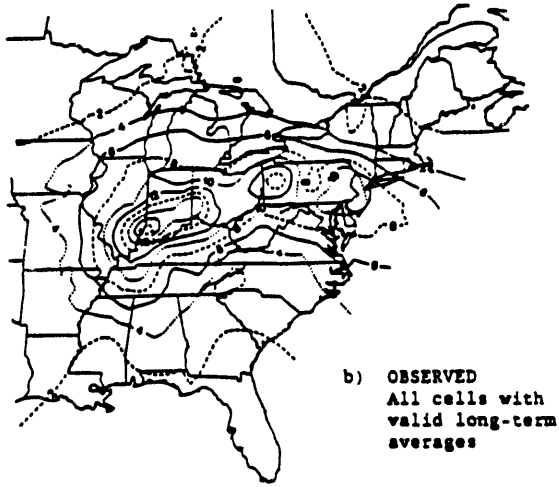
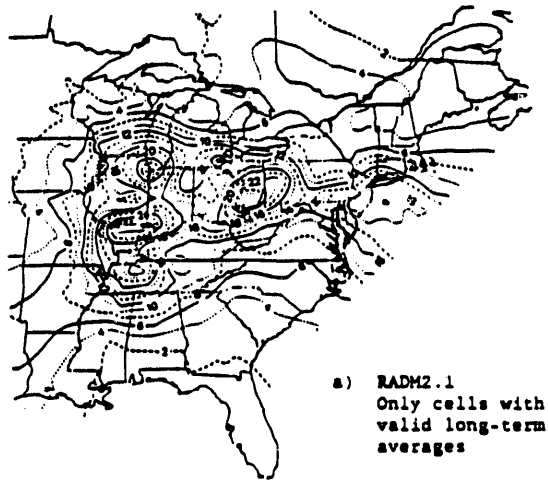
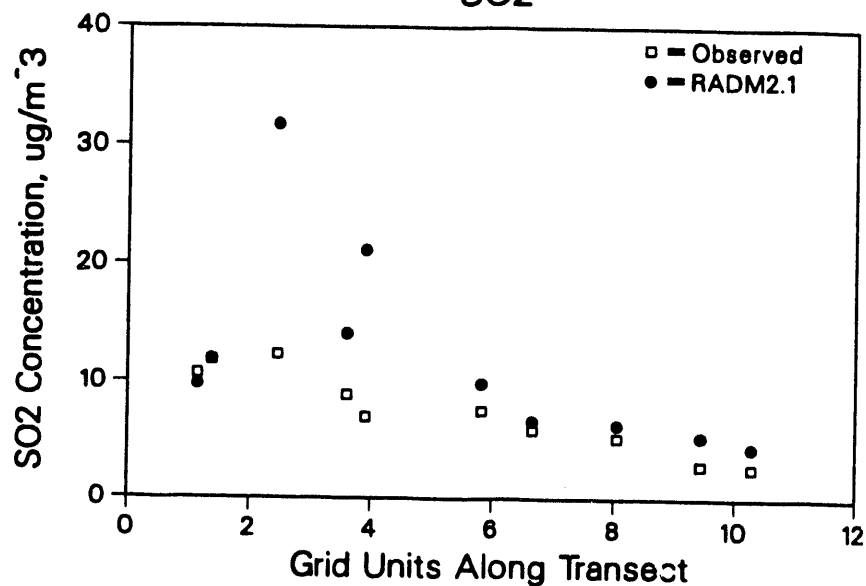


Figure 11. RADM2.1-Predicted and EMEFS-Observed Regional Distribution of the 33-Day Average SO₂ Concentration Based on Grid Cells with Valid Long-Term Averages

Transect from SW PA to NE NY
 (36,22) to (43,33)
 SO₂



Transect from SW PA to NE NY
 (36,22) to (43,33)
 SO₄

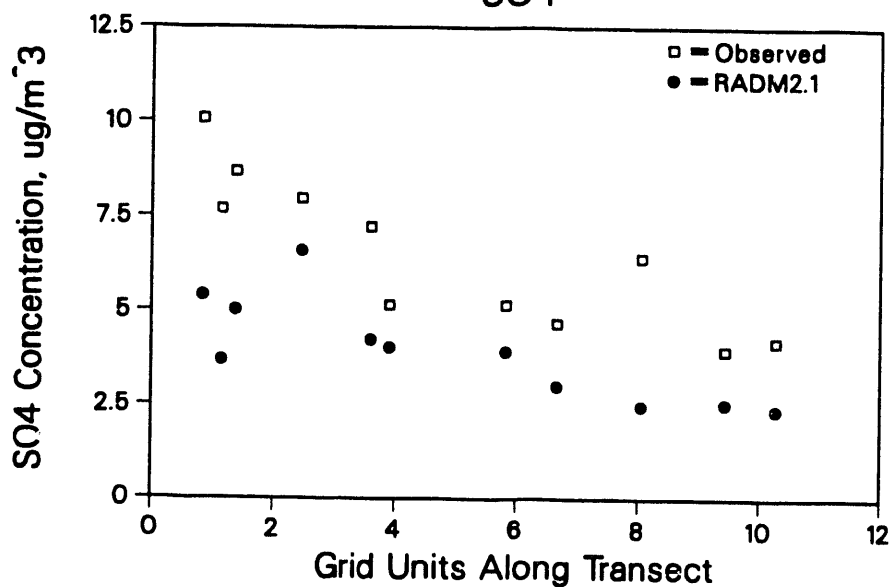
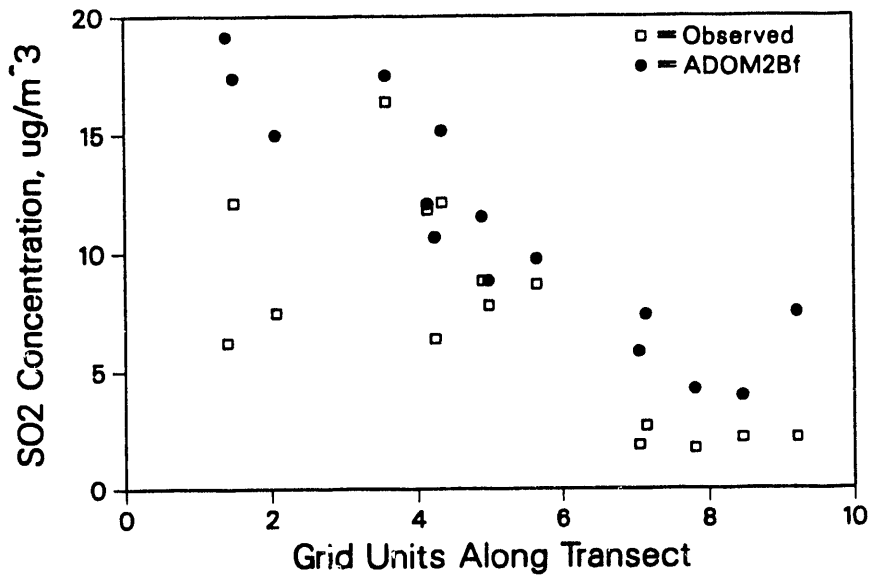


Figure 12. Distribution of EMEFS-Observed and RADM2.1-Predicted 33-Day Average Concentrations of SO₂ and SO₄⁼ Aerosol along a Transect That Extends from the Southwestern Corner of Pennsylvania to the Northeastern Corner of New York

Transect from SW PA to NE NY
(14,12) to (21,20)
SO₂



Transect from SW PA to NE NY
(14,12) to (21,20)
SO₄

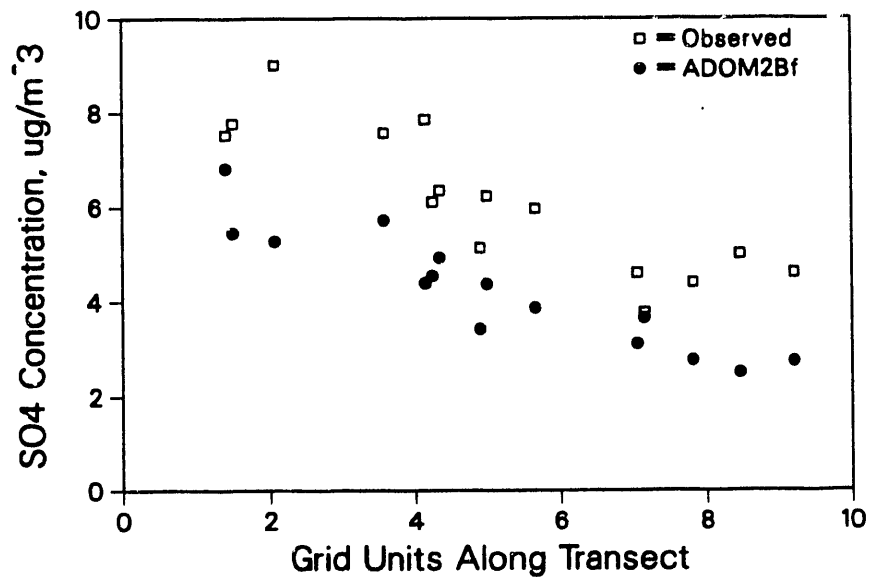


Figure 13. Distribution of EMEFS-Observed and ADOM2Bf-Predicted 33-Day Average Concentrations of SO₂ and SO₄⁼ Aerosol along a Transect That Extends from the Southwestern Corner of Pennsylvania to the Northeastern Corner of New York

a stronger gradient for predicted than for observed SO₂ concentrations and consistent underprediction of SO₄⁼ aerosol concentrations although with approximately the same gradient as was observed.

3.1.5 Daytime and Nighttime Performance

Data obtained from the National Dry Deposition Network (NDDN) were used to examine model performance under daytime and nighttime conditions during the 33-day model evaluation period. During the day, the boundary layer is usually deep and well-mixed. At night, a shallow inversion above the surface produces a boundary layer in which little mixing occurs. Four weeks of weekly daytime and nighttime air concentrations were averaged to form a monthly mean for the model evaluation period. As reported by Dennis *et al.* (1991), there was essentially no bias for SO₂ and T-NO₃ during the daytime. However, at night, RADM2.1 (and the other versions of RADM that have been examined) showed a definite overprediction bias, especially for the lowest concentrations. In contrast, this large difference in daytime and nighttime bias did not occur for SO₄⁼ aerosol, which was underpredicted by about the same amount day or night.

3.1.6 Upper-Air Concentrations

The results of a preliminary analysis of the comparison of RADM2.1 predictions with observations from the first aircraft intensive, reported by Dennis *et al.* (1990), are briefly summarized here. Although the aircraft flight patterns were designed to discern regional patterns in pollutant concentrations aloft, only comparisons of point observations to grid-cell averages have been examined. Such comparisons are a severe test of model performance and, as will be discussed in Section 4, may be unfair if a predicted grid-cell volume-average is incommensurate with an average over a few kilometers of aircraft flight track. Some additional spatial smoothing of the observed field is obtained by comparing the distribution of predictions (the inner and outer quartiles) with the average observed concentration over a narrow range. The scatter plots shown in Figure 14 are but one indication of model performance and do not address the models' ability to predict the regional pattern of pollutant concentrations aloft. In Figure 14, the vertical bars denote the inner quartiles of the predictions, with the median at the small cross bar, the 25th percentile at the bottom, and the 75th percentile at the top. The initial findings from the comparison of RADM2.1 predictions with some of the observations made aloft are that

- SO₂, SO₄⁼ aerosol, NO_y, and T-NO₃ are slightly overpredicted at low concentrations

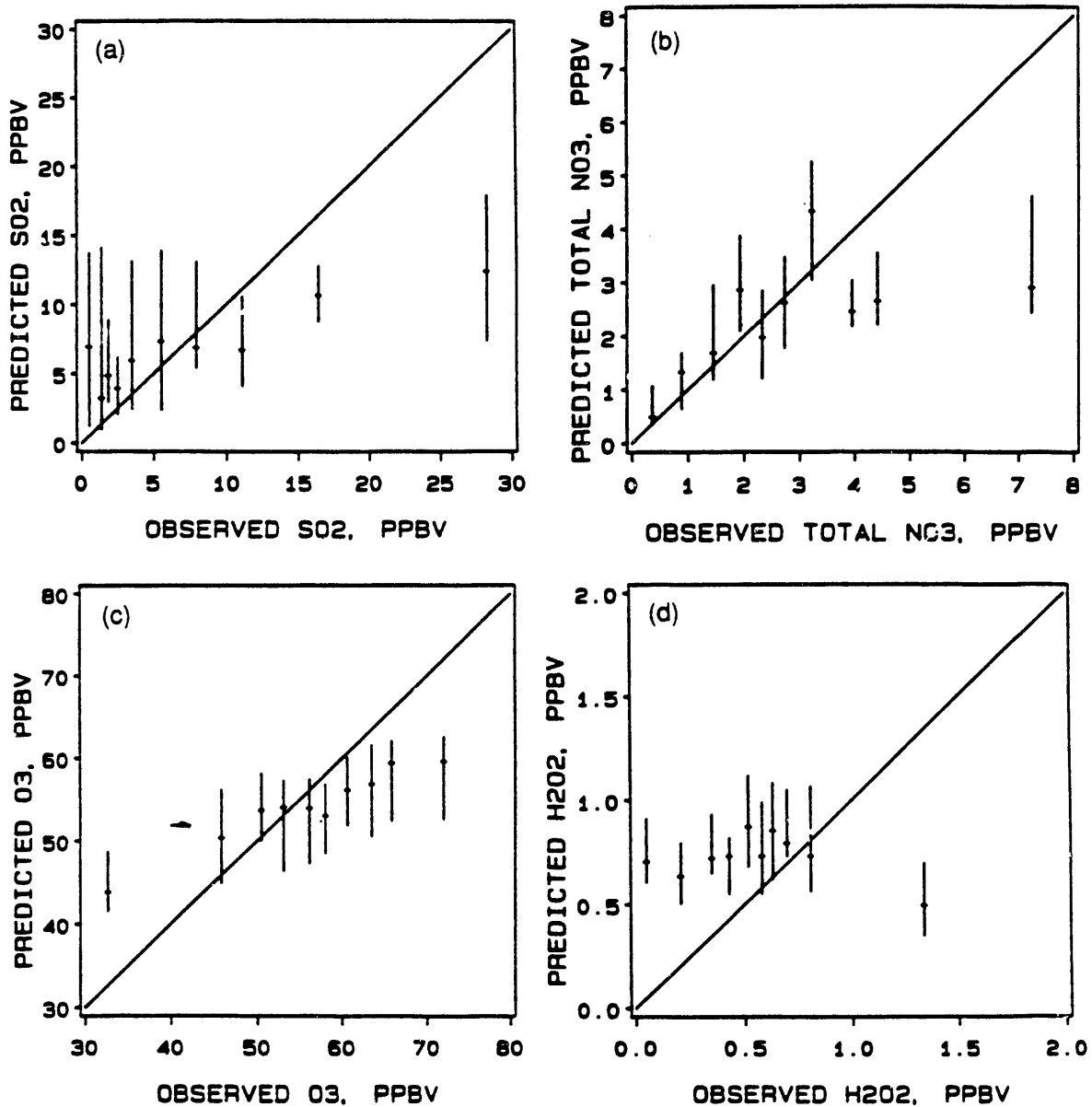


Figure 14. The Relationship between the Median and Inner Quartiles of the RADM2.1-Predicted Concentrations of SO₂, SO₄⁻ Aerosol, O₃, and H₂O₂ and the Concentrations Observed in the Mixed Layer from the Gulfstream-1 Aircraft on Flights Made during the Model Evaluation Period

- high observed concentrations of SO_2 , $\text{SO}_4^{=}$ aerosol, NO_y , O_3 , and H_2O_2 are consistently underpredicted
- predictions of O_3 and H_2O_2 concentrations cover a smaller range than the observations, so that the low concentrations are overpredicted and high concentrations are underpredicted.

The comparisons of RADM2.1 predictions to observations aloft show biases that are consistent with the biases found in the comparisons to surface observations. However, the very large overpredictions of the highest surface concentrations for SO_2 and T- NO_3 are not seen aloft. Additional diagnostic analysis of individual flights is summarized in Section 5.2.

3.2 PRECIPITATION CONCENTRATIONS AND DEPOSITION

A comparison of the precipitation amounts over the 33-day evaluation period provided by the meteorological input to RADM and grid-cell averages obtained from the EMEFS observations is shown in Figure 15. The precipitation amounts used in RADM tend to be higher than those observed at the EMEFS sites. However, grid-cell averages over all available National Weather Service sites also tend to show a similar overestimate of the EMEFS observations. The bias in precipitation amount was less for ADOM (not shown) than for RADM. ADOM's smaller bias may result, in part, from the use of observed precipitation amounts in the meteorological driver for ADOM.

The relationship between the predicted and observed $\text{SO}_4^{=}$ and NO_3^- ion concentrations are shown in Figures 16 to 18 for RADM2.1, RADM2.5/6, and ADOM2Bf. Tables A.4 to A.6 give the average percentage bias for each model as a function of the observed precipitation-weighted concentration and wet deposition of $\text{SO}_4^{=}$ and NO_3^- ions. For all models and both species, there is a tendency to overpredict the smaller values and underpredict the larger values.

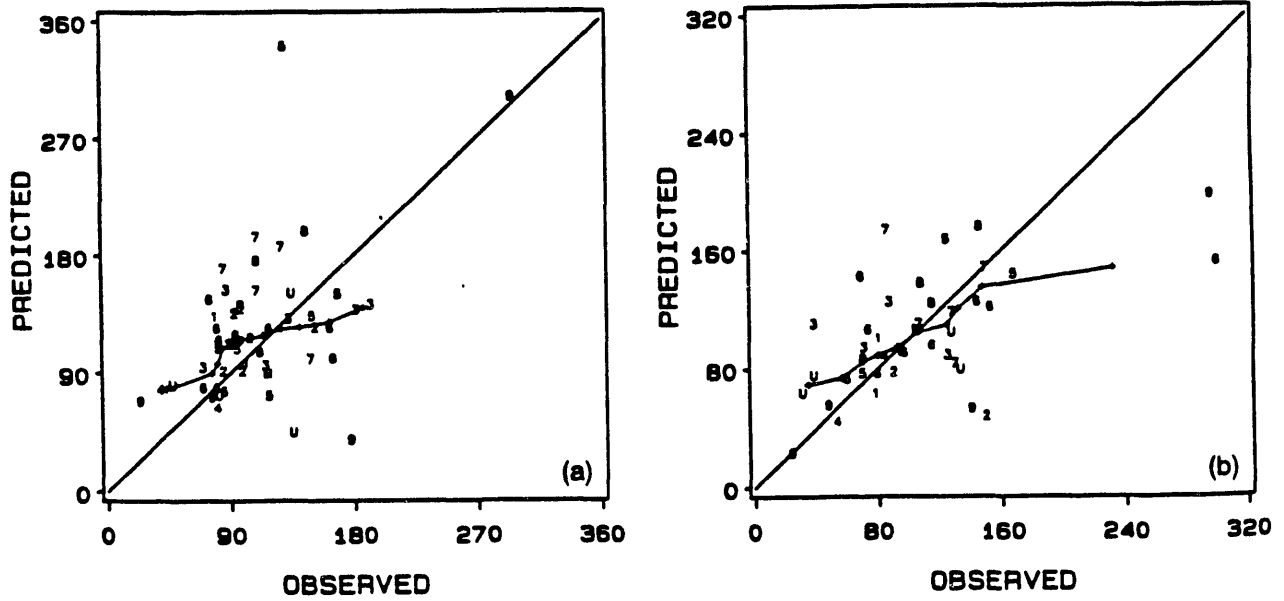


Figure 15. The Relationship between the 33-Day Total Precipitation (mm) Prescribed by the Meteorological Drivers for RADM (left) and the EMEFS-Observed Grid Cell Average (right) for the Evaluation Period

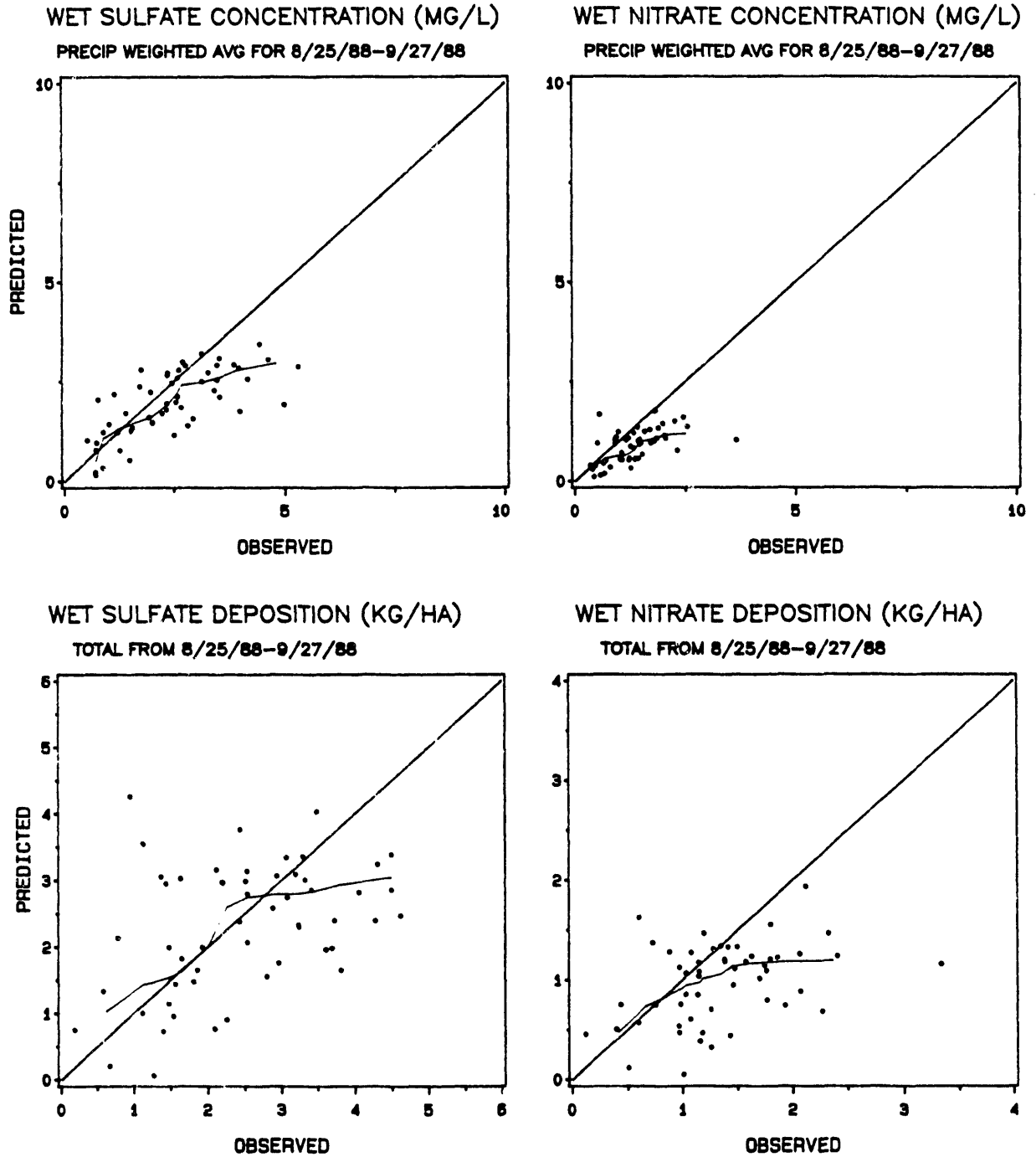


Figure 16. The Relationship between the 33-Day Precipitation-Weighted Average $\text{SO}_4^{=}$ and NO_3^- Ion Concentrations and Their Wet Deposition Predicted by RADM2.1 Versus the EMEFS-Observed Grid Cell Average

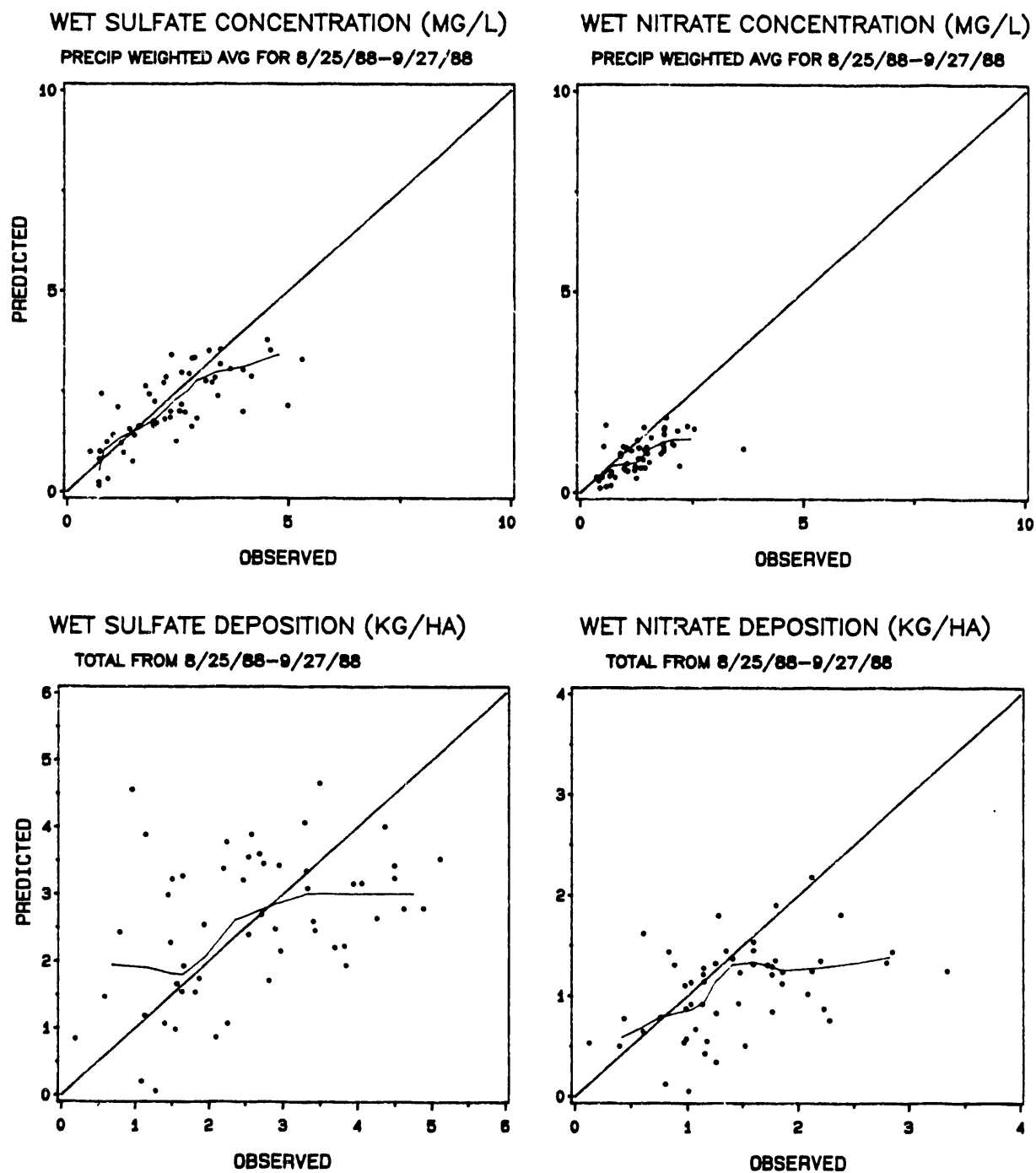


Figure 17. The Relationship between the 33-Day Precipitation-Weighted Average $\text{SO}_4^{=}$ and NO_3^- Ion Concentrations and Their Wet Deposition Predicted by RAD2.5/6 Versus the EMEFS-Observed Grid Cell Average

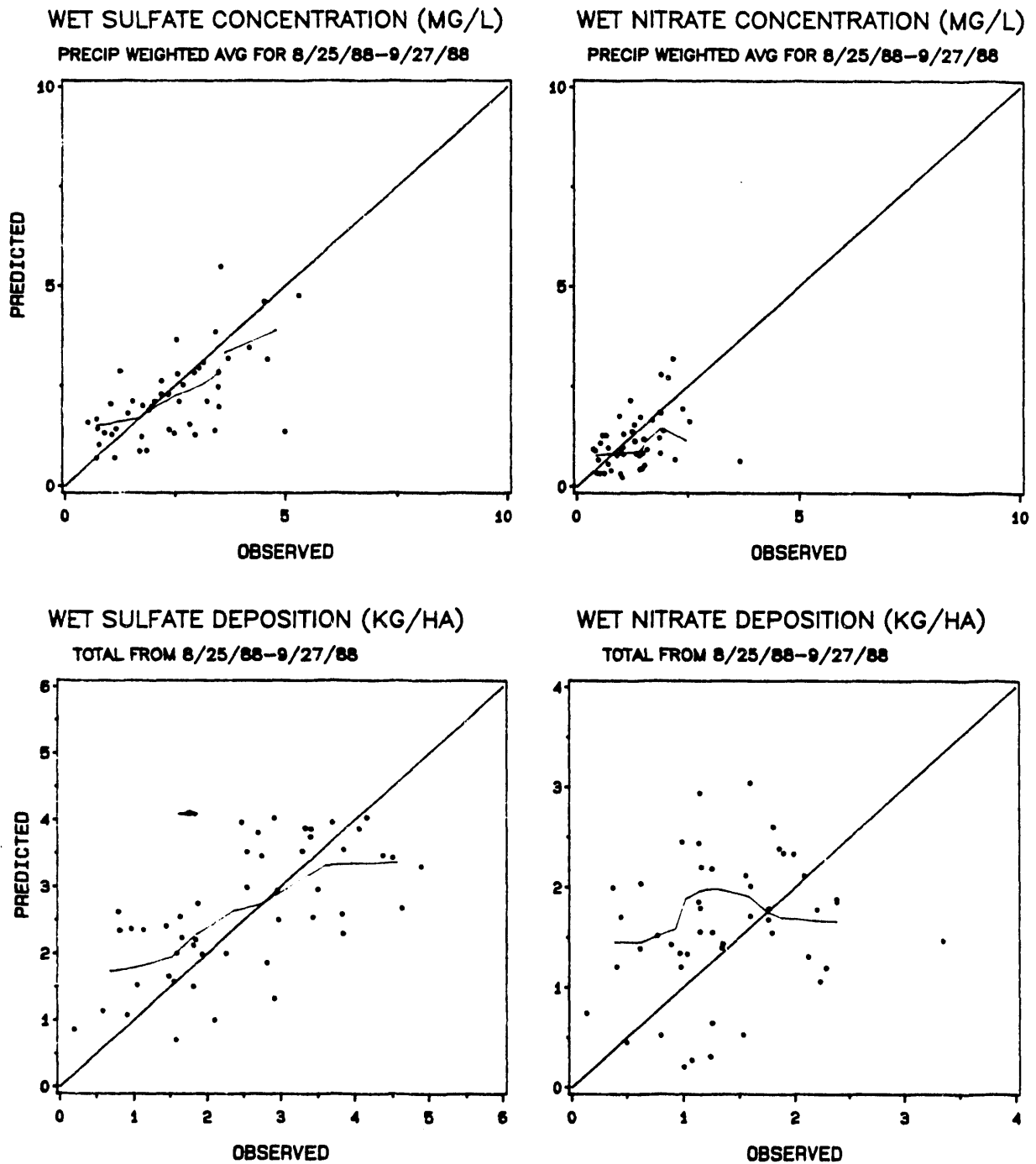


Figure 18. The Relationship between the 33-Day Precipitation-Weighted Average $\text{SO}_4^{=}$ and NO_3^- Ion Concentrations and Their Wet Deposition Predicted by ADOM2Bf Versus the EMEFS-Observed Grid Cell Average

4 MEASUREMENT AND MODEL INCOMMENSURABILITY

An inherent design feature of an Eulerian model, such as RADM or ADOM, is its fixed internal coordinate system or three-dimensional grid. This coordinate system is prescribed by a horizontal grid and one or more vertical layers. Quantities such as the concentrations of pollutants in the air apply to the entire volume of a grid cell. The measurements, on the other hand, actually pertain to a very small volume, in effect points, within the much larger volume of the grid cell. This incommensurability of measured and predicted quantities gives rise to uncertainties in model evaluation (Tesché *et al.*, 1990). Subgrid-scale processes may cause a measurement to be unrepresentative of the volume average for the grid cell in which it is located (Nappo *et al.*, 1982). Such subgrid-scale processes can cause measured concentrations to be lower or higher than the grid-cell average, thereby introducing scatter in the comparison of predictions to observations. Subgrid-scale processes must necessarily be represented by approximations and parameterizations in models so that the model predictions may not precisely reproduce values measured within a grid cell. During periods of persistent weather patterns, certain spatial configurations of sources and measurement sites may cause biases in model performance. A few subgrid-scale processes that can bias measured or modeled concentrations are discussed below.

Most Eulerian models instantaneously disperse emissions by point or area sources throughout the volume of a grid cell. However, measured concentrations are controlled by the spatial relationship between the location of the monitoring site and pollution sources and by the distribution of wind speed and direction. In grid cells wherein a few large sources are located downwind from a monitoring site, model-predicted concentrations might be biased high with respect to the observations because the plume of emissions from the sources will rarely be sampled at the site. On the other hand, if plumes from nearby sources are frequently sampled at a site, the model-predicted concentrations might be biased low relative to observations.

Any aspect of the physical setting of a monitoring site that departs from the "typical" conditions within a grid cell has the potential for causing a bias in the comparison of an observation at that site to the actual average in the grid cell. Key considerations are the proximity of nearby emissions sources, the topographical setting of the monitoring site, and the land use and surface cover near the site. The land use and surface affect the local stability of the atmosphere and hence affect how well an observation made at the surface (actually at 10 m) represents the lowest layer simulated by the model.

In RADM2.1, the lowest layer extends from the surface to a height of approximately 150 m. The vertical profile of concentrations within the depth of this lowest model layer

determines the representativeness of the surface observation. If the boundary layer is well mixed and deeper than the lowest model layer, there will be only a small vertical gradient of concentration (mixing ratio) in that layer, and the surface observations should be representative of the lowest model layer. These conditions are common during the daytime, with normal wind speeds and cloud cover. Under such conditions and at typical monitoring site locations, heterogeneities in topography, land use, and surface cover in the vicinity of a site will generally have little influence on the representativeness of the site.

However, with light winds and a stable atmosphere, the boundary layer may become shallower than the lowest model layer, and strong vertical gradients in pollutants can develop near the surface because of dry deposition and limited mixing. Under those conditions, the concentration measured at the surface will usually be smaller than the average concentration for a layer that is the depth of the lowest model layer. In such conditions, the topographic setting of a site, the surface cover, and the land use in the vicinity of a site can affect the strength and duration of the concentration gradient near the surface. For example, sites in valleys will experience a greater frequency (number of days with) and longer duration (hours in a day) of stable conditions than sites on elevated terrain. Thus, nighttime and daily average surface observations at valley sites may be biased low with respect to the actual average in a layer the depth of the lowest model layer.

The degree to which a vertical gradient in concentration is likely to develop is strongly influenced by the rate at which the substance is dry deposited. That rate is determined by the concentration of the material and its deposition velocity. The deposition velocity in turn is determined by how quickly the atmosphere can bring material to the surface and the rate at which the material can actually be removed at the surface. The rate at which the atmosphere brings materials to the surface is largely a function of wind speed and atmospheric stability, and it is independent of the materials. As long as the boundary layer is well mixed, gradients produced by dry deposition are usually confined to a very shallow layer (much less than 10 m) above the surface and have little effect on the representativeness of an observation made at 10 m.

The rate at which material is actually deposited from the atmosphere is governed by physical and chemical interactions between the material and the surface on which it deposits. Dry deposition should not be a major factor in producing vertical gradients for materials that are inefficiently removed by most surfaces, such as $\text{SO}_4^{=}$ aerosol. However, for materials like HNO_3 that react with most surfaces, removal at the surface can establish a vertical gradient in its concentration. The situation for SO_2 falls somewhere between those extremes. The ability of the surface to remove SO_2 depends on the type and condition of the surface vegetation and especially on the presence of water on the surface. Wet surfaces and vegetation with open stomata take up SO_2 much more readily than dry surfaces and

vegetation with closed stomata. Thus the formation of vertical gradients in SO_2 concentrations under stable conditions depends much more on the condition of the surface than it does for $\text{SO}_4^{=}$ aerosol (usually no gradient) or HNO_3 (usually a gradient).

The incommensurability of model predictions and observations can qualitatively explain many of the large overpredictions of SO_2 and NO_2 that were found at a relatively small number of grid cells. Grid cells assigned to the "Urban" region (Figure 1) represent cases in which monitoring sites are usually upwind of large point and area sources associated with major urban centers. Model-predicted ambient concentrations for these cells are generally biased very high, especially for the primary emitted pollutants.

Comparisons with aircraft data suffer even more from incommensurability because there is so little temporal averaging of the observations. For pollutants with a distribution that is likely to be very heterogeneous, such as SO_2 emitted from point sources, aircraft observations will include concentrations measured both in the relatively clean air between plumes and in the highly polluted air within the plumes. Because the model predicts an average value for a grid cell, the lowest observed concentrations may be overpredicted and the highest observed concentrations may be underpredicted.

5 PRELIMINARY INTERPRETIVE STUDIES AND ANALYSES

Because model developers and evaluators needed to understand the origins of the various biases disclosed by the comparisons of the predicted and observed mean concentrations and time series, several interpretive and diagnostic analyses of the comparison results were conducted. This section summarizes some of that work, which has been more fully reported in several conference presentations and journal articles.

5.1 ADOM-RELATED STUDIES

Most ADOM-related interpretative studies have been carried out by the AES and the OME.

5.1.1 Fog Frequency and ADOM2Bf Underprediction of SO₄⁼ Aerosol

The persistent underprediction of SO₄⁼ aerosols by ADOM2Bf led Fung *et al.* (1991) to examine the relationship between the quality of the daily prediction of SO₄⁼ aerosol and the occurrence of fog. Because ADOM meteorology does not indicate whether fog occurs, ADOM does not simulate a chemical transformation of SO₂ to SO₄⁼ aerosol in fog, as postulated by Ruprecht and Sigg (1990). A weak relationship was found between a greater occurrence of poor daily SO₄⁼ aerosol predictions when fog coverage over the modeling domain was large than when little fog was present. Other factors suggested by Fung *et al.* that could lead to SO₄⁼ aerosol underpredictions included an inaccurate oxidant chemistry that was unable to produce sufficient H₂O₂ and the lack of a means to transform SO₂ to SO₄⁼ aerosol in nonprecipitating clouds.

5.1.2 Dry-Deposition Velocities in ADOM2Bf

Dry deposition is an important mechanism for removing pollutants from the atmosphere. By comparing simulations of the O₃ dry-deposition velocity from the dry-deposition module developed for ADOM (Pleim *et al.*, 1984) to 55 days of eddy-correlation measurements of O₃ deposition to a deciduous forest in central Ontario during July and August 1988, Padro *et al.* (1991) found the module overestimated the deposition velocity because canopy resistance was underestimated (Figure 19). By reducing the leaf area index from 6 to 5 and the mean stomatal opening from 10 to 2.5 μm and increasing the cuticle and ground resistances from 2.5 to 5.0 and 8 to 15 s/cm, respectively, the predictions of the O₃ dry-deposition velocity by the module were improved (Figure 20). Although limited in scope to a brief period (July and August 1988) over one land-use type (deciduous forest), the study suggests that O₃ dry deposition may in general be overestimated by ADOM.

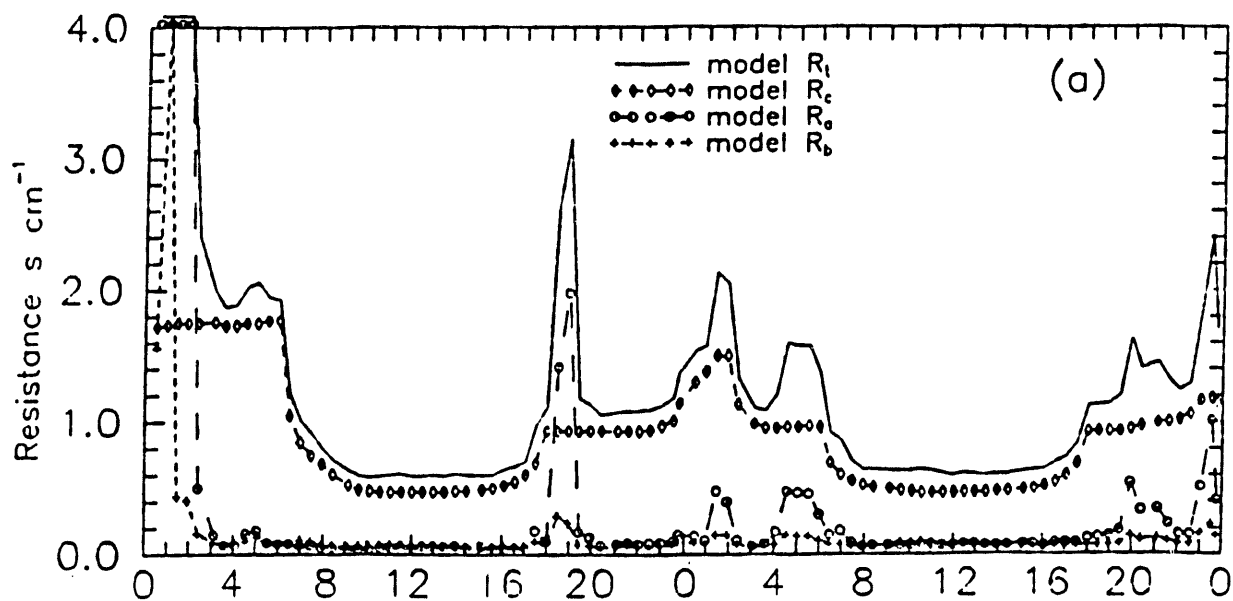


Figure 19. Half-Hourly Variation of Modeled and Observed O_3 Dry-Deposition Velocity for Borden Forest on 3 and 4 August 1988

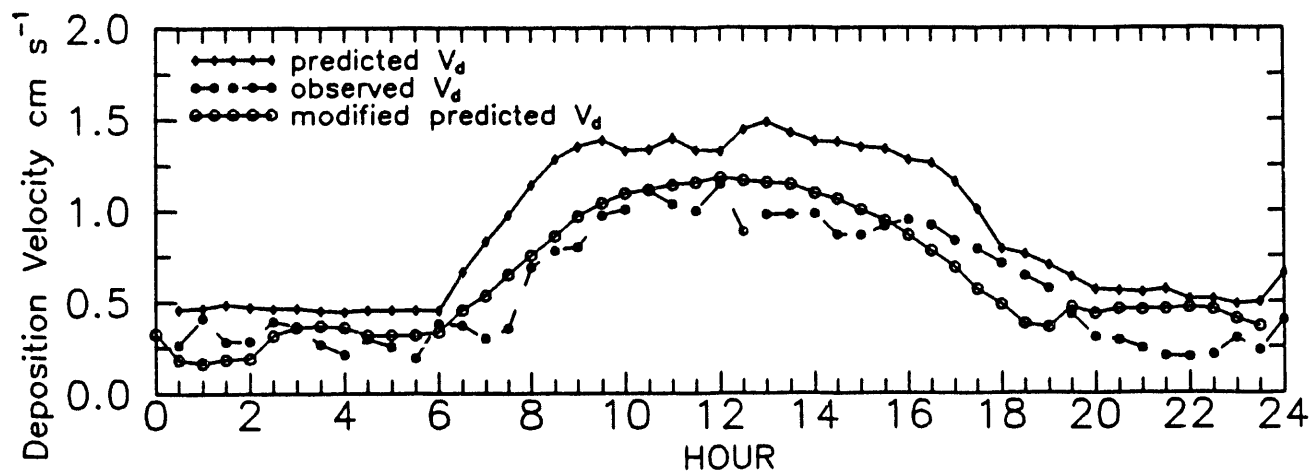


Figure 20. Original and Improved Modeled and Observed Average Diurnal Variation of the O_3 Dry-Deposition Velocity for the Period 7 July through 30 August 1988

5.1.3 Comparison of ADOM2Bf-Predicted and Observed Vertical Profiles of Ozone

One aspect of the design of the EMEFS was the need to collect data in a Eulerian framework. Time-height cross sections of the concentrations of pollutants in the atmosphere would provide a direct comparison with model predictions for one grid column. Hoff *et al.* (1991) describe the measurement of vertical profiles of O₃, meteorology, and aerosols at Egbert, Ontario, and present a comparison of some of those profiles with predictions from ADOM2Bf.

Three periods during the first EMEFS intensive measurement campaign (late summer 1988) were designated as "hyperintensives" during which extensive O₃ profiling measurements were taken. Profiles were obtained with tethered and free-flying ozonesondes, Mie lidar, O₃ DIAL profiler, and profiling aircraft (Hoff *et al.*, 1988). During the six-day hyperintensives, two ozonesondes (Mickle *et al.*, 1991) and two upper-air sondes were released each day, and the DIAL profiler was operated continuously. Tethered ozonesondes were flown mainly at night to profile the lowest part of the boundary layer. Output from the O₃ DIAL system was averaged over each of ADOM layers 4 through 8.

A comparison of the various O₃ profiling measurement systems and output for ADOM2Bf for the Egbert grid cell for 3 August 1988 shows that the profiles obtained by the various measuring systems were of similar shape but that there were some biases between systems (Figure 21). Time-height cross sections of O₃ concentrations for the first and third hyperintensives are shown in Figures 22 and 23.

Comparison of the ADOM2Bf-predicted and measured profiles and time-height cross-sections reveals that

- near-surface O₃ concentrations are severely underpredicted
- the time phasing of predicted near-surface maximum O₃ concentrations is frequently poor
- the time phasing of decreases in O₃ concentration is better than that for maximum O₃ concentrations
- the large underprediction above the mixed layer, possibly caused by the intrusion of stratospheric O₃, indicates that the top boundary condition in ADOM does not account for a stratospheric O₃ source.

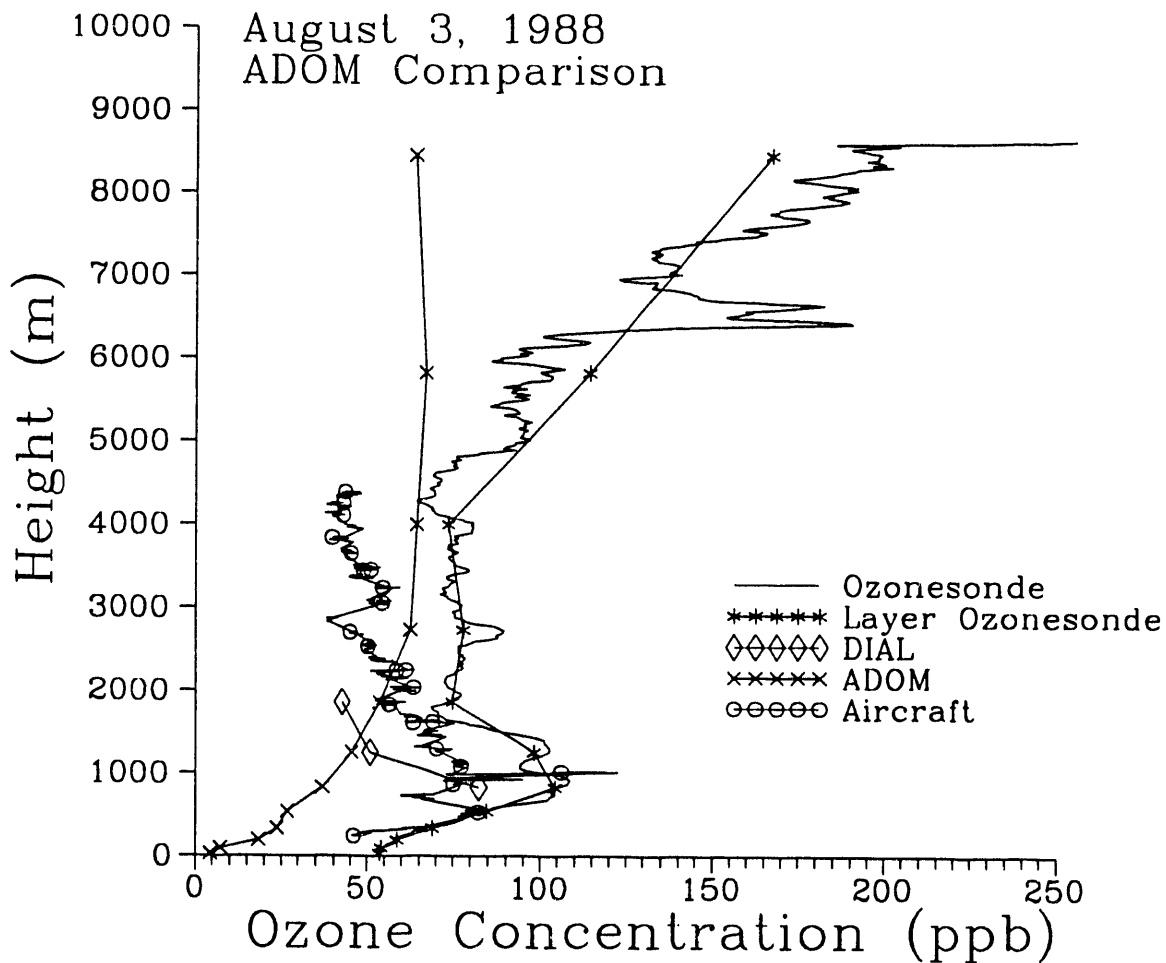


Figure 21. Comparison of DIAL, Aircraft, Ozonesonde, and ADOM2Bf Model Profiles of O₃ Concentrations over Egbert, Ontario, for 31 August 1988

5.1.4 Comparison of ADOM2Bf to Observations at High- and Low-Elevation Sites

Measurements of O₃ concentrations and precipitation chemistry were made as part of the Chemistry of High Elevation Fog (CHEF) program (Schemenauer, 1986) at two high-elevation ridge sites and a neighboring valley site in forested, rural Quebec. Observations from Roundtop (RT) on the border between ADOM grid cells 20,19 and 21,19 and Mont Tremblant (MT) at the center of ADOM grid cell 19,20 were compared by Banic *et al.* (1991) to predictions from ADOM2Bf for the period from 28 July through 8 August 1988.

Wet Deposition

Considering the relatively small number of precipitation events occurring in the simulation period (< 10) and the potentially large contribution to the uncertainty made by local

ADOM Ozone Output - 1st Hyperintensive

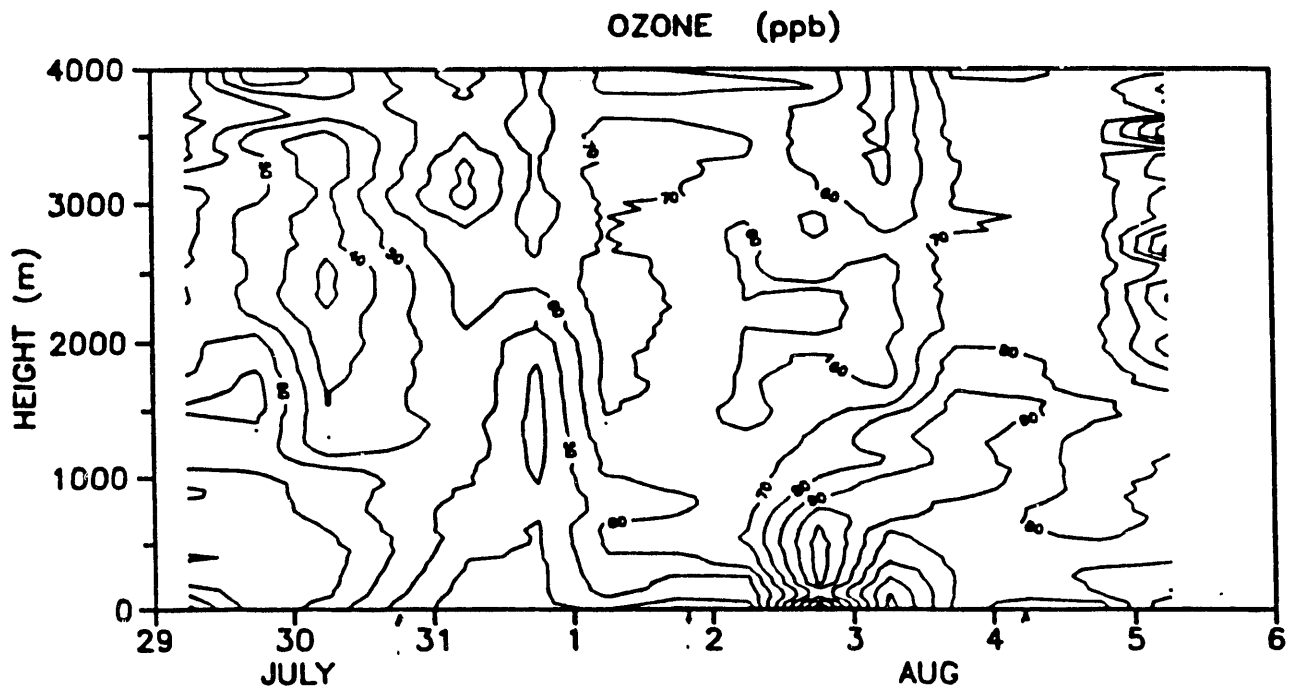
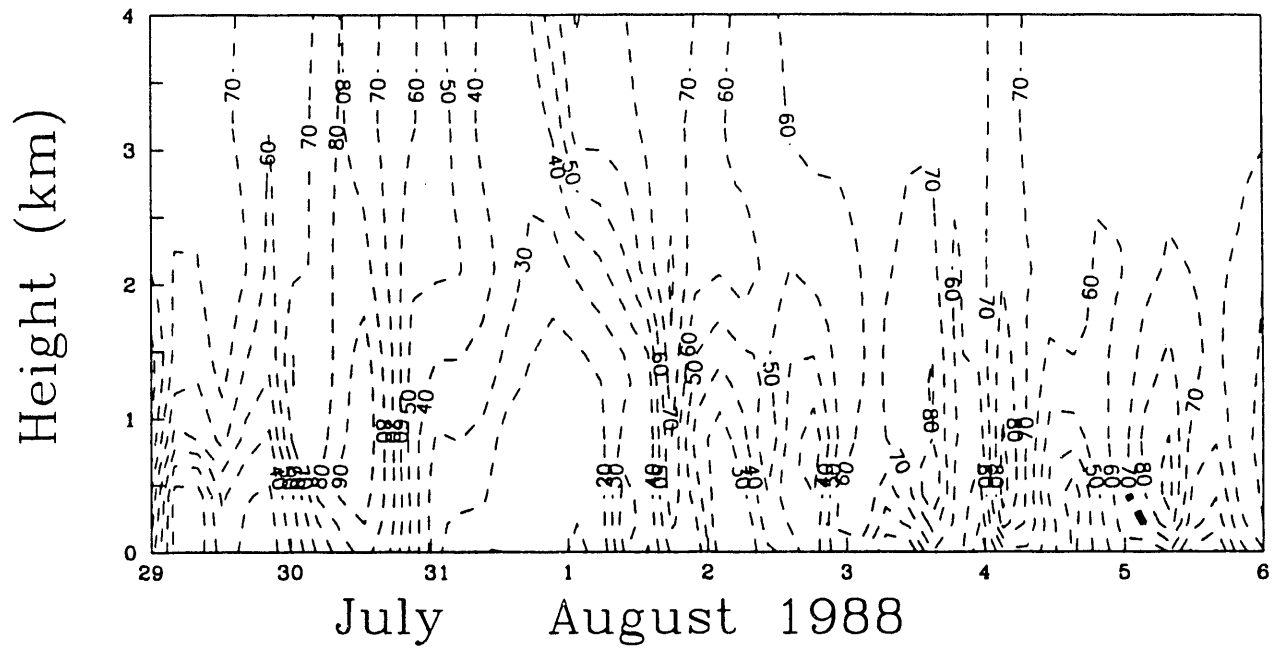


Figure 22. Time-Height Cross Sections of O₃ Concentrations (a) Predicted by ADOM2Bf and (b) Measured by Ozonesondes in the Period 29 July to 6 August 1988

ADOM Ozone Output - 3rd Hyperintensive

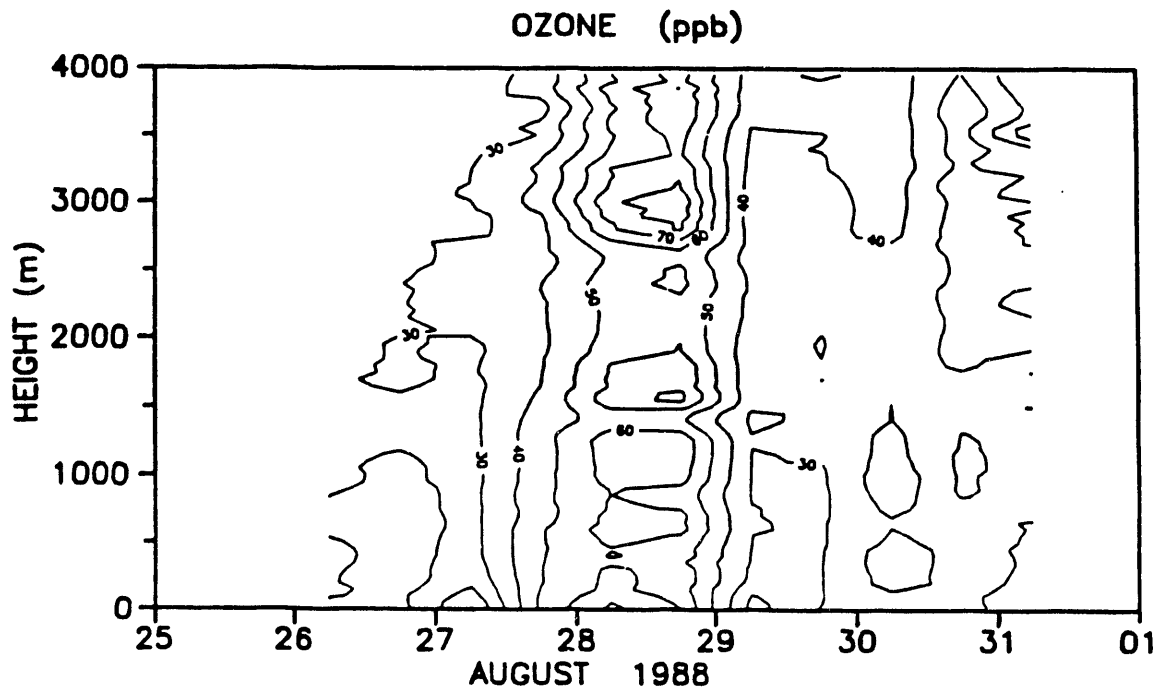
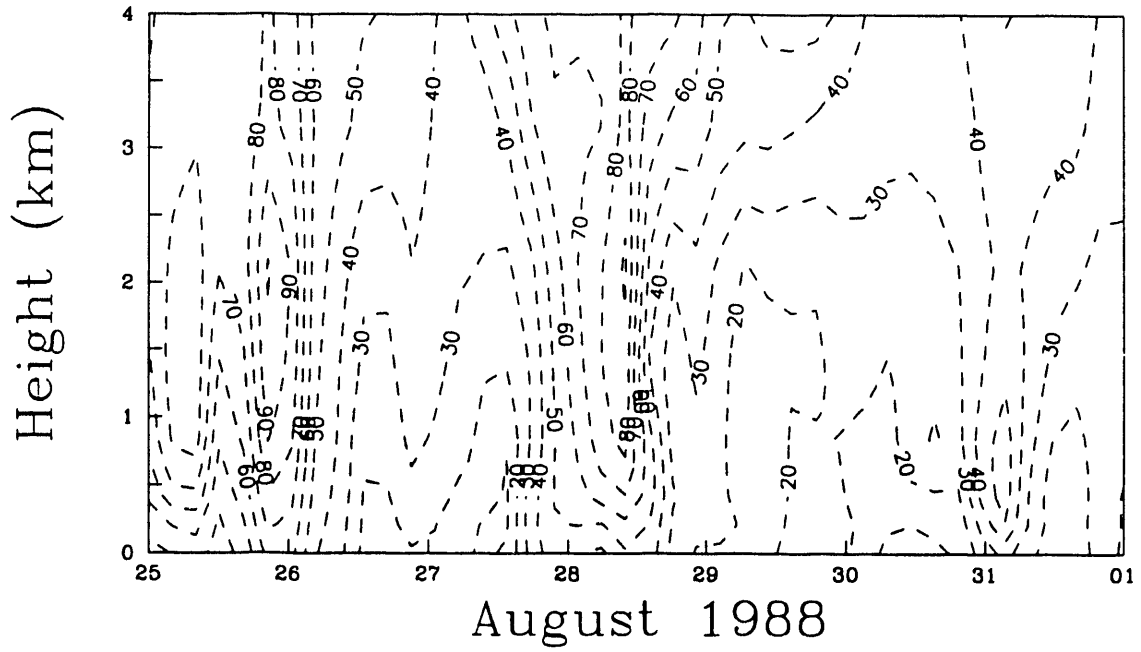


Figure 23. Time-Height Cross Sections of O₃ Concentrations (a) Predicted by ADOM2Bf and (b) Measured by Ozonesondes in the Period 25 August to 1 September 1988

variability in precipitation amount, the modeled and observed $\text{SO}_4^{=}$ and NO_3^- concentrations in precipitation agreed fairly well, but the observed NH_4^+ in precipitation was five to ten times larger than that modeled. Thus it appears that insufficient NH_3 is being incorporated into precipitation by the model.

Unrealistically low modeled pH values led to the discovery of a coding error that produced an incorrect pH whenever small-scale precipitation was indicated. However, because the model calculates pH based on an ion balance that includes ammonium, which is one of the dominant ions in precipitation, the discrepancy in ammonium concentration must be resolved before any meaningful comparison of measured and modeled pH can be made.

Ozone Concentrations

The spatial pattern for 28 July through 8 August was typical of that usually seen in the CHEF data: higher concentrations are seen at the more southerly ridge site (RT) than at the co-located valley site or the ridge site to the north (MT). A comparison of modeled and observed averages for the whole period, given in Table 5, shows that the modeled averages for layers 5 and 6 agree well with the observed averages for both ridge sites. However, for the surface (layer 1), average ozone is underpredicted by about 20 to 30%. Figure 24 shows

Table 5. ADOM2Bf-Predicted and CHEF-Observed Average Ozone Concentration for 28 July through 7 August 1988

Model Layer	Average Ozone Concentration (ppb)		
	Cell (19,20)	Cell (20,19)	Cell (21,19)
1	22.4	31.1	26.3
2	28.9	38.4	31.7
3	33.4	44.2	38.2
4	42.4	51.3	49.0
5	47.5	56.9	56.6
6	51.0	60.5	61.8
<u>Site</u>			
MT-Ridge	48.5		
RT-Ridge	55.8		
RT-Valley	40.5		

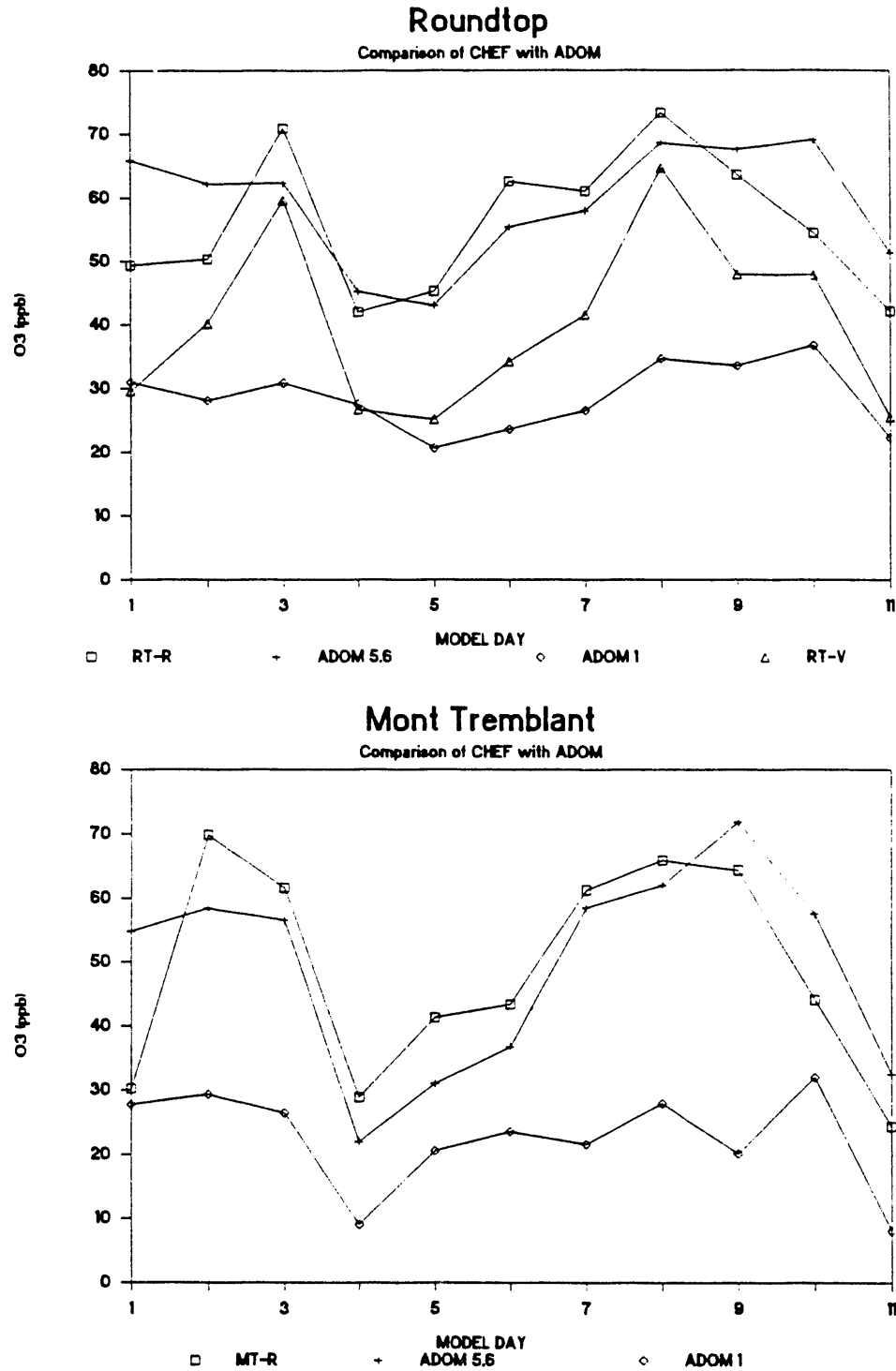


Figure 24. Daily Averages of the ADOM2Bf-Modeled and CHEF-Observed O₃ Concentration for the Period 28 July (day 1) through 7 August (day 11) 1988 at (a) Roundtop and (b) Mont Tremblant

that model predictions averaged for layers 5 and 6 agree well with the daily averages observed at the ridge sites. However, layer 1 of the model underpredicts the peak O₃ concentrations observed at the valley site. Underprediction of ozone at the surface is consistent with the findings at other locations. The overly high modeled dry-deposition velocities are thought to contribute to the lower modeled surface concentrations.

5.1.5 Comparison of ADOM-Predicted and Canadian Aircraft-Measured Profiles

Comparisons were made between O₃, NO₂, H₂O₂, and SO₂ vertical profiles as measured by the Twin Otter aircraft and ADOM2Bf-predicted profiles during the period 3 to 6 August 1988. Table 6 lists the three nighttime and five daytime flights over Dorset, Ontario, that are used for comparison. Profiles were measured during vertical spirals with a radius of 1-2 km and extending from approximately 100 m AGL up to 4 km AGL. During the profile measurement, the aircraft levelled for 1 min approximately every 610 m (2000 ft). Ozone surface data are 15-min average values from an enhanced chemistry site at Dorset. Both H₂O₂ and SO₂ were measured at an enhanced chemistry site at Egbert, 120 km southwest of Dorset (corresponding to about the length of an ADOM grid cell). Aircraft data were

Table 6. Characteristics of the 1988 Twin Otter Flights Used in the Comparison to ADOM2Bf Predictions

Flight Number	Date	Begin (GMT)	End (GMT)	Flight Conditions
16	3 Aug	04:49	07:05	Night, clear, southerly flow
17	3 Aug	18:08	19:22	Mid pm, clear, hot, hazy, post flight thunderstorms
19	4 Aug	17:32	19:41	Early pm, clear
20	4 Aug	21:28	23:54	Late pm, cloud deck 0.5-1.0 km
21	5 Aug	01:32	03:46	Night, clear
23	5 Aug	09:17	11:01	Night, predawn, clear
24	5 Aug	17:30	19:41	Early pm, cloud deck 0.5-1.5 km, post flight cold front passage
25	6 Aug	17:58	18:27	Early pm, cloud deck 2.0-2.4 km

averaged within each ADOM layer. For example, the measured values for layer 4 are the average values between 416 and 655 m AGL.

Model output used in this comparison is from ADOM2Bf for grid 16,19. Dorset is in the northeast corner of this cell. ADOM predictions represent 3-hour averages, including the hours both before and after the hour corresponding to the profile measurement.

The comparison between measured and modeled O₃ concentrations is given in Figure 25; the numbers give the model layer within the profile. Model predictions are within a factor of 0.8 to 1.25 of the measured values, with the exception of the surface values and Flight 19. Measurement uncertainty for O₃ in the observed concentration range is about $\pm 20\%$. Surface concentrations are consistently underpredicted by 10-40 ppbv. The highest ozone concentrations, measured during Flight 19, are consistently underpredicted by 15-45 ppbv. Model predictions agree much better with the lower ozone concentrations measured behind the cold front that passed through on the evening of 5 August (Flight 25). Underprediction of surface O₃ concentrations suggests ADOM may overpredict O₃ dry deposition, consistent with the conclusion of Padro *et al.* (1991).

Figure 26 shows the comparison for H₂O₂. Modeled surface concentrations are widely scattered but equally distributed about the 1:1 line and within 1 ppbv of the measured data (uncertainty ± 0.1 to 0.2 ppbv). Measured concentrations in layers 4 to 8 range from 2 to 4 ppbv greater than model predictions. The persistent underprediction of H₂O₂ appears to be greater at night than during the day. The better agreement for layers 4 and 5 from Flight 20 and for layers 4-7 from Flight 24 may be due to measurements taken within a cloud deck where the measured concentrations are likely to be lower than in clear air. As with O₃, the model-predicted H₂O₂ concentrations agree better with the lower concentrations measured after the passage of the cold front (Flight 25).

The profiles for SO₂ and NO₂ show many similarities. Except for the rather unpolluted case of 6 August, Figures 27 and 28 show that SO₂ and NO₂, respectively, are underpredicted at all levels. The measured SO₂ profiles (uncertainty of about $\pm 10\%$) are characterized by maximum mixing ratios in layers 5-6, whereas the ADOM-predicted maxima are in layers 2-3 of the model domain. All model NO₂ predictions for layers 6-10 are less than 0.25 ppbv, but measurements range up to 1.2 ppbv. However, because the uncertainty in measured NO₂ concentrations in this range is ± 0.2 -0.5 ppbv, these differences are generally not a good indicator of model performance.

In summary, comparisons of ADOM2Bf-predicted vertical profiles against aircraft measurements taken from 3 to 6 August 1988 yielded the following results:

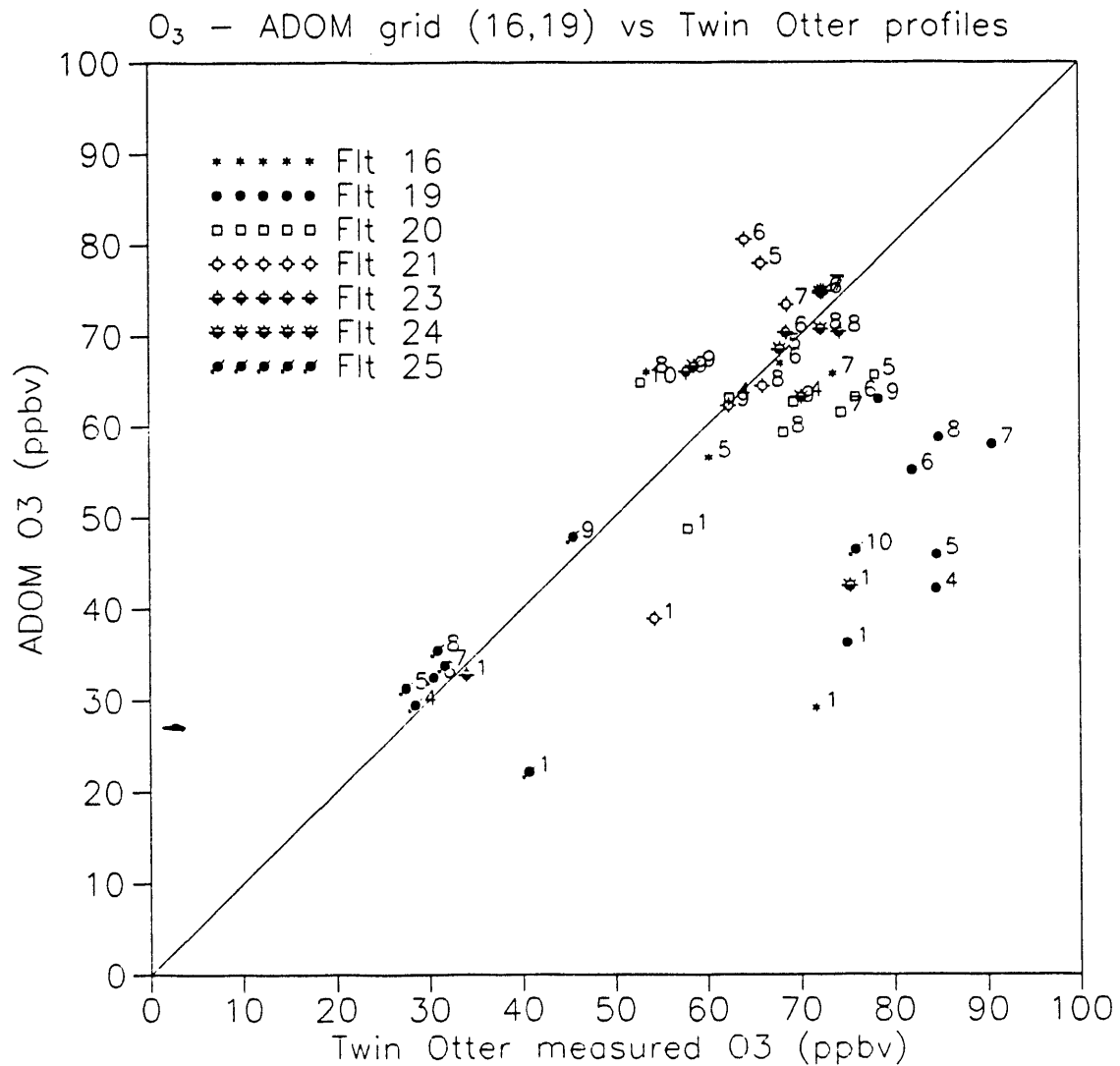


Figure 25. Relationship between ADOM2Bf-Modeled (Cell 16,19) and Twin Otter-Observed O₃ Concentrations. Numbers give the ADOM model layer over which the observed profile is averaged. See Table 6 for the dates and times for each flight.

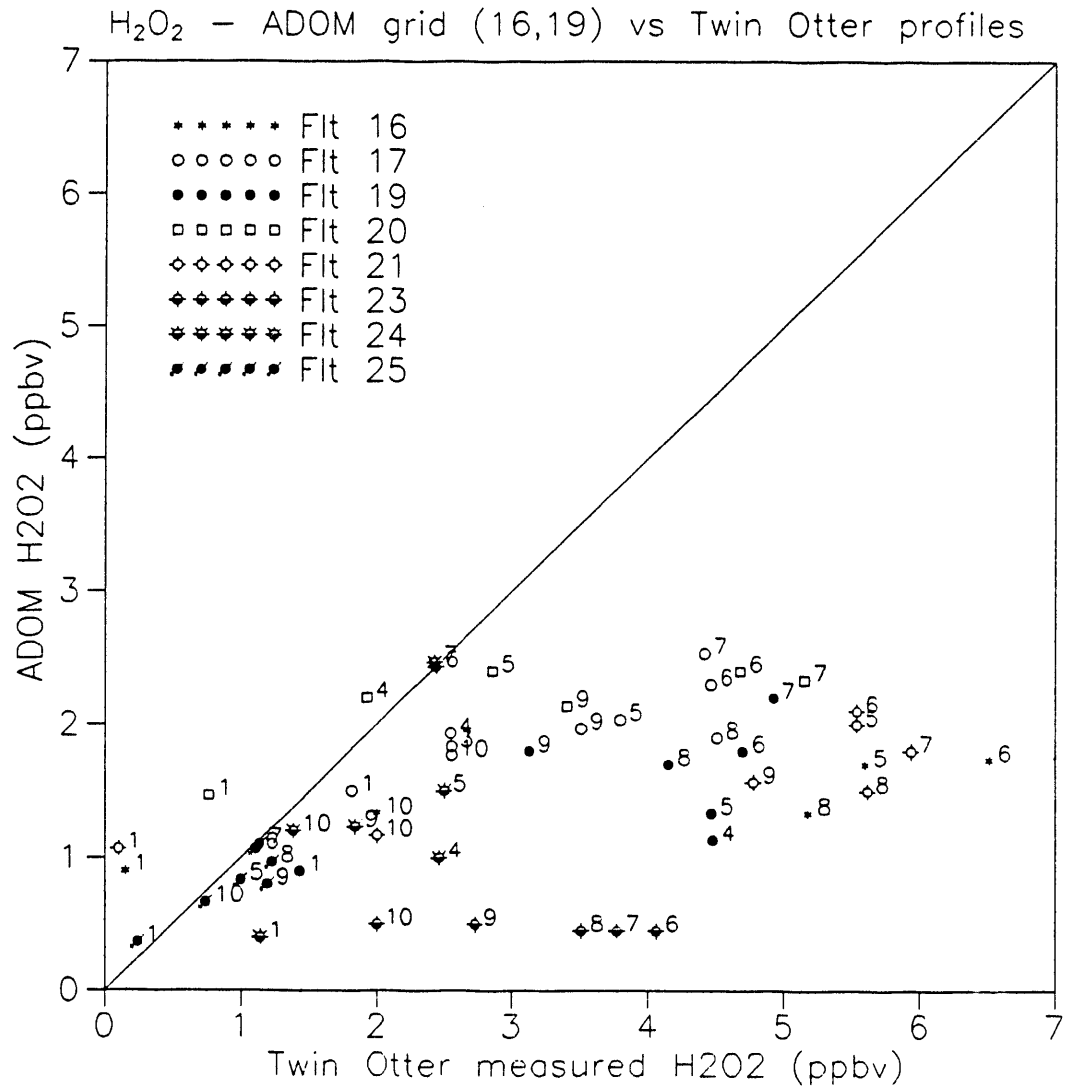


Figure 26. Relationship between ADOM2Bf-Modeled (Cell 16,19) and Twin Otter-Observed H₂O₂ Concentrations. Numbers give the ADOM model layer over which the observed profile is averaged. See Table 6 for the dates and times for each flight.

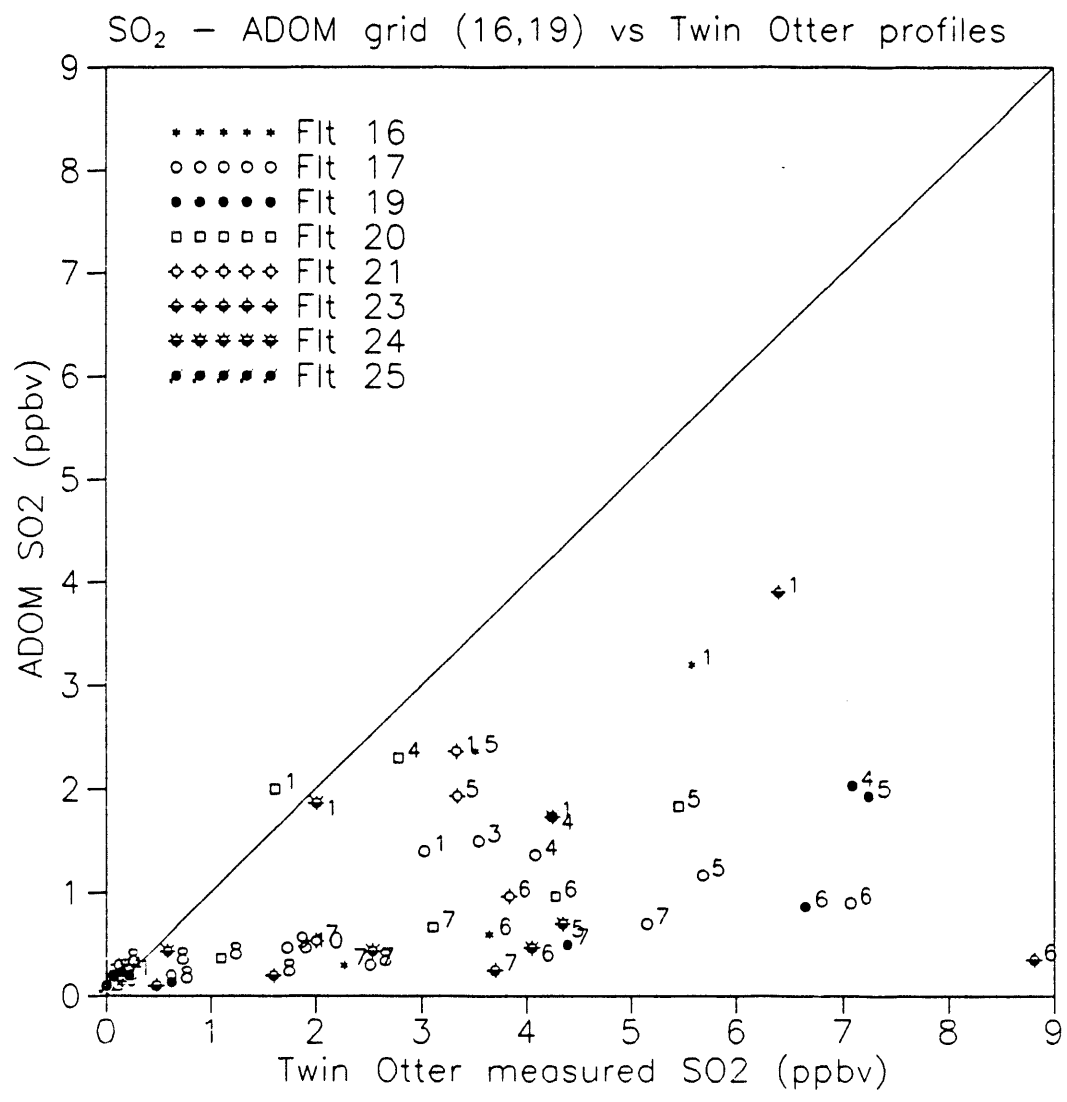


Figure 27. Relationship between ADOM2Bf-Modeled (Cell 16,19) and Twin Otter-Observed SO₂ Concentrations. Numbers give the ADOM model layer over which the observed profile is averaged. See Table 6 for the dates and times for each flight.

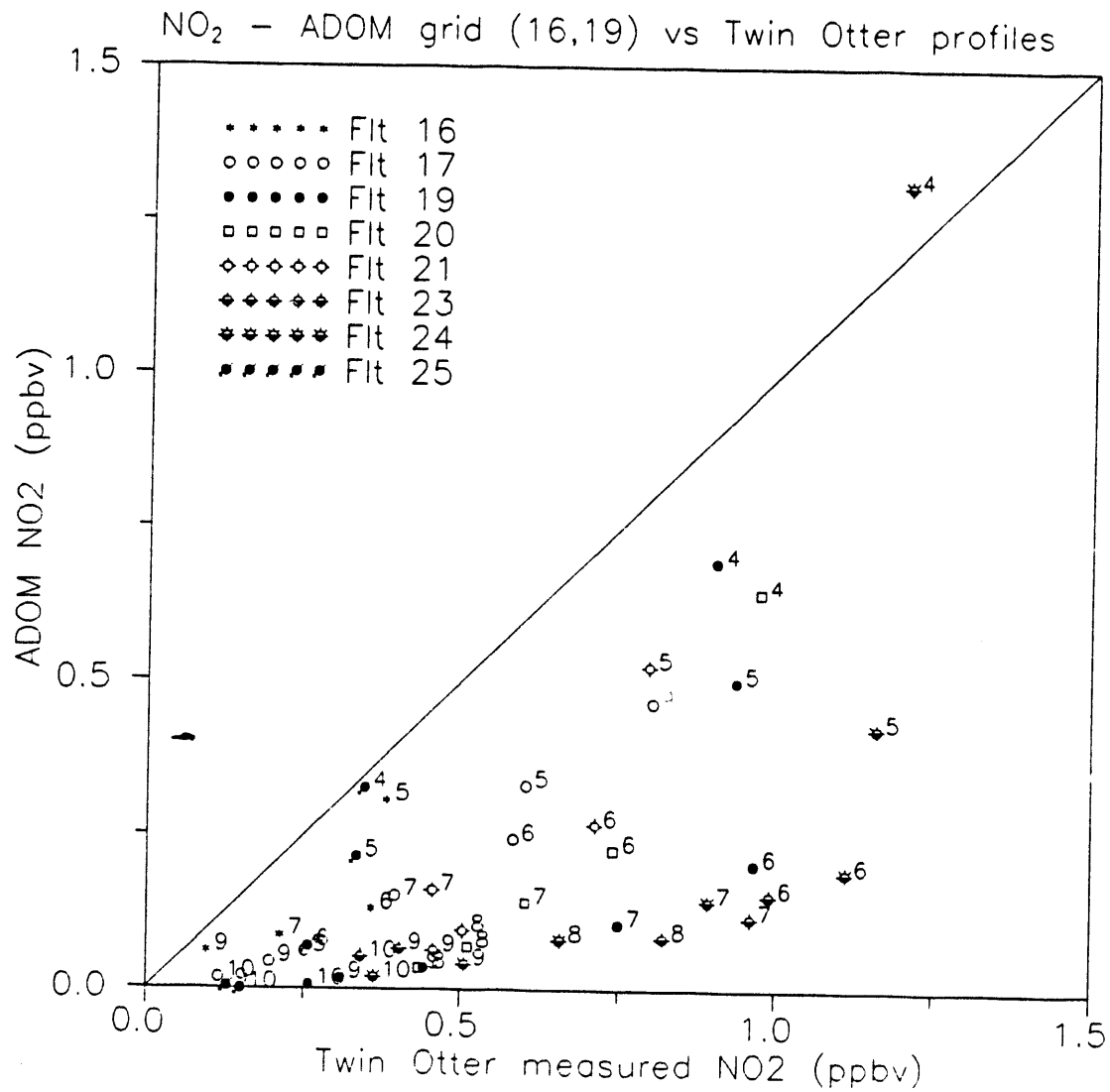


Figure 28. Relationship between ADOM2Bf-Modeled (Cell 16,19) and Twin Otter-Observed NO₂ Concentrations. Numbers give the ADOM model layer over which the observed profile is averaged. See Table 6 for the dates and times for each flight.

- Ozone predictions fall within a factor of 0.8 to 1.25 of measured concentrations except for the concentrations measured at the surface, which are underpredicted by 15-45 ppbv, and for the highest concentrations observed at all levels during Flight 19 on 4 August.
- Underprediction of surface O₃ concentrations is consistent with an overprediction of O₃ dry-deposition velocities.
- Predicted H₂O₂ agrees well with measured H₂O₂ (within 1 ppbv) for the surface and layers 9-10 but is underpredicted in layers 4-8.
- SO₂ and NO₂ are underpredicted at all levels.
- Underprediction of SO₂ and NO₂ aloft suggests that the simulation of upward mixing from the surface layers in ADOM may be too slow.

5.2 RADM-RELATED STUDIES

Investigators participating in the U.S. component of the 1988 EMEFS aircraft intensive have undertaken diagnostic analyses of RADM performance based on several case studies of flights made during the period 25 August through 27 September 1988. These diagnostic studies focus on specific components of the modeling system. The preliminary results summarized here will be discussed in detail in a dedicated volume of the Journal of Atmospheric Chemistry.

5.2.1 Regional Distributions Aloft

Constant altitude, zig-zag flights were flown to determine the skill with which RADM could simulate large-scale regional distributions and gradients of primary and secondary pollutants aloft. Ching *et al.* (1991) report that, for the flight on 31 August 1988, simulations by RADM2.5/15

- identified the region of highest SO₂ concentrations over southeastern Ohio
- matched the south-to-north gradients in SO₂, although the predicted concentrations were generally lower than the observed, especially in the northern section of the flight track

- produced south-to-north gradients in O_3 concentrations that were comparable to those observed
- underpredicted NO and NO_2 concentrations in general, but produced gradients similar to those observed away from the major source region
- predicted a flight-path-averaged NO_y concentration that was comparable to that observed, but underpredicted NO and NO_2 and overpredicted HNO_3 .

5.2.2 Frontal Passage

Spicer *et al.* (1991) concluded that the comparison of model predictions and aircraft observations from sets of three long, approximately constant-altitude flights in the mixed layer would be useful for the diagnostic evaluation of the simulation of pollutant scavenging and pollutant redistribution during a cold front event. In one case study, RADM predictions were compared to aircraft measurements averaged over a long transect from northern Tennessee to western New York for flights made on 2 September (prefrontal), 6 September (first postfrontal) and 8 September (second postfrontal) 1988 (see Figure 29). The following diagnostic information was obtained from this case study:

- For some species, both RADM2.1 and RADM2.5/15 were able to simulate the change from high, prefrontal concentrations to much lower concentrations after passage of the front and the increase in concentration in the days after frontal passage.
- RADM overpredicted SO_2 for the prefrontal and second postfrontal flights but underpredicted SO_2 for the first postfrontal flight.
- Photochemical pollutants (O_3 , PAN, HNO_3) were overpredicted for the flight immediately after frontal passage. Overprediction was largest for the first postfrontal flight. Comparisons to the prefrontal and second postfrontal observations showed less overprediction.

5.2.3 High-Resolution Box

By measuring ambient concentrations in a vertical column over a relatively small geographical domain (about 2x2 80-km grid cells), Schaller *et al.* (1991) were able to study the vertical and daytime diurnal predictive performance of the models. An aircraft (Hawker-Siddeley 125) was used to measure ambient concentrations on the lateral boundary of the box from about 500 to 3000 m AGL, and the data were used to estimate the vertical profiles within the column in late morning, just after local noon, and in late afternoon. Comparison

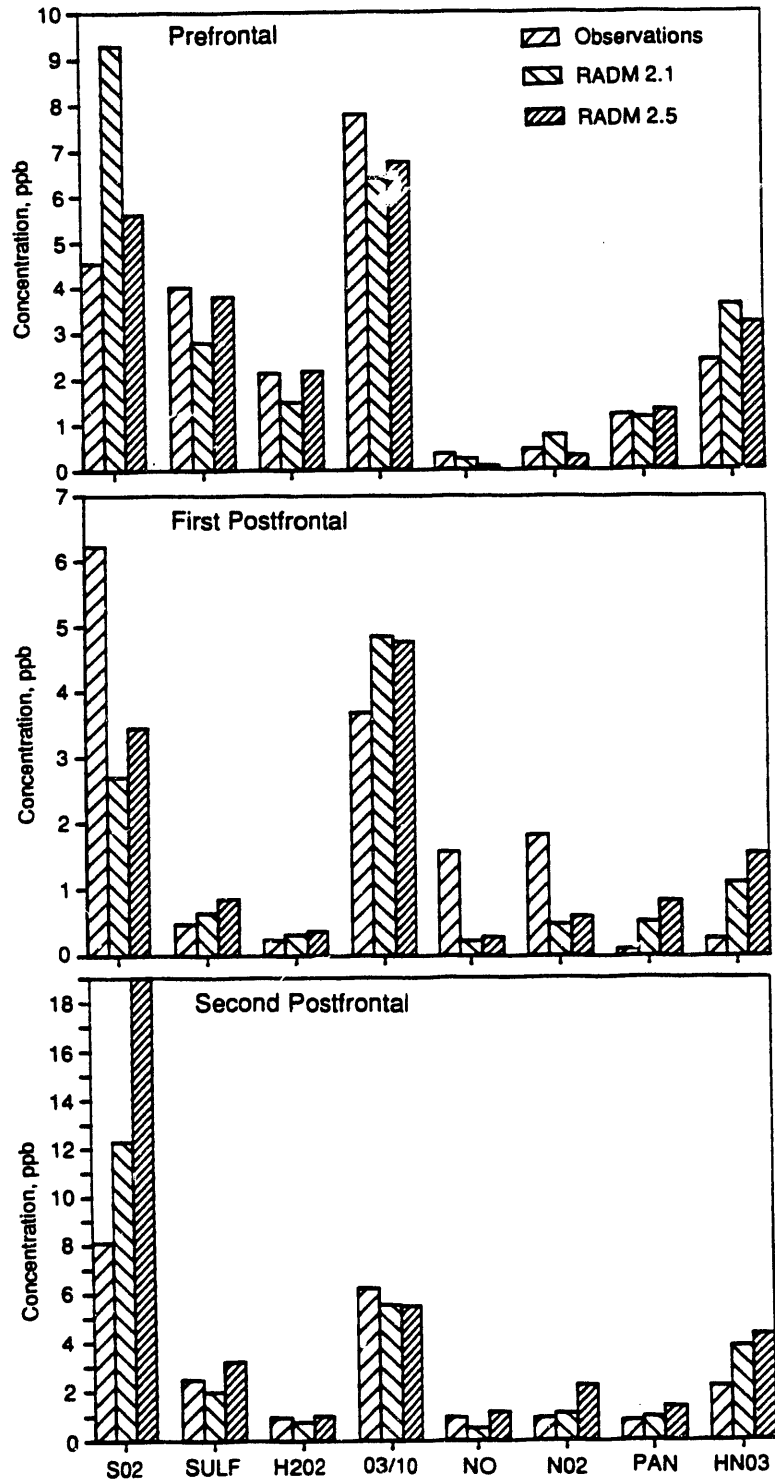


Figure 29. Average Aircraft-Observed and Modeled Pollutant Concentrations within the Mixed Layer along Flight Track for (a) 2 September, (b) 6 September, and (c) 8 September 1988 [source Spicer *et al.* 1991, figure 4c]

with profiles derived from simulations of the 1 September 1988 case study by RADM2.5/15 showed that

- predicted SO_2 , NO , and NO_2 concentrations decreased much more rapidly with height than the observed profiles
- an apparent plume of high SO_2 , NO , and NO_2 concentrations observed during the noon flight peak (around 925 hPa) was not simulated
- vertical variations in predicted O_3 concentrations were less than observed and O_3 concentrations above the boundary layer (top at about 825 hPa) were overpredicted
- predicted profiles for H_2O_2 concentrations differed in shape from those observed and H_2O_2 concentrations were overpredicted within and underpredicted above the boundary layer.

6 MODIFICATIONS TO MODELS ARISING FROM FINDINGS

The schedule for completing major NAPAP state-of-science and integrated assessment documents left little opportunity for fulfilling the ideal of several cycles of model development, evaluation, and refinement before application. Nevertheless, as an integral part of the model evaluation team, model developers could respond immediately to the deficiencies in the models that were indicated by the results of the evaluations. For example, evaluation results not reported here revealed that both RADM and ADOM had assigned the wrong molecular weight to NO in the emissions inventory. This error was corrected before RADM was used for its NAPAP applications. Development of RADM2.5 was based on preliminary evaluation results for RADM2.1. Based on the findings previously summarized, both modeling teams focused on solving the problems of the underprediction of SO_4^{\equiv} aerosol. Additionally, the RADM team addressed the problem of the apparent underprediction of nighttime dry deposition. The following sections describe some of the improvements made to the models that are currently being evaluated.

6.1 ADOM NONPRECIPITATING STRATUS CLOUDS

In contrast to RADM2.1, in which both stratus and cumulus clouds are treated with the same module, ADOM applies separate cloud modules for those two types of clouds (Venkatram *et al.*, 1988). The findings from the EMEFS evaluation stimulated several hypotheses about plausible missing SO_4^{\equiv} aerosol production mechanisms in both RADM and ADOM that could account for the underprediction of ambient SO_4^{\equiv} aerosol. Sensitivity studies with a linearized version of ADOM suggested that aqueous phase production of SO_4^{\equiv} aerosol was a major pathway for SO_4^{\equiv} formation during the EMEFS (Karamchandani and Venkatram, 1991). Since the ADOM convective cloud module handled nonprecipitating clouds but the stratus module did not, Karamchandani and Venkatram analyzed the role of nonprecipitating stratus clouds in producing ambient ground-level SO_4^{\equiv} aerosol concentrations.

For this analysis, the ADOM stratus cloud module was modified by assigning a precipitation rate of 0.005 mm/hr to all grid cells for which stratus clouds but no precipitation were specified by the ADOM meteorological driver. Wet deposition was prevented by switching off rain scavenging and the transfer of pollutants from cloud drops to snow or rain. Cloud scavenging of SO_2 , H_2O_2 , and O_3 allowed aqueous phase reactions in the cloud water to produce SO_4^{\equiv} aerosol. Thus, at the end of the hourly time step when the cloud is evaporated, there is a net loss of SO_2 and H_2O_2 and a net gain in SO_4^{\equiv} within the grid cell.

Because the vertical resolution of the stratus module is not more than 5 layers (in contrast to 12 for the main model), a mass-conserving and profile-conserving scheme is used to go from one vertical grid system to the other at the start and end of a cloud-module time step. Although this ensures that the mass and vertical profiles of inert pollutants do not change, it can result in an artificial vertical mixing of those pollutants for which the stratus cloud layer is a sink (SO_2 and H_2O_2) or a source ($\text{SO}_4^{=}$).

Karamchandani and Venkatram simulated the period 25 August through 6 September 1988 with ADOM2B both with and without the provision for nonprecipitating stratus clouds. Figure 30 shows that the inclusion of nonprecipitating stratus clouds

- reduced the underprediction of ambient surface sulfate concentrations
- reduced the overprediction of SO_2
- left total S essentially unchanged
- left wet $\text{SO}_4^{=}$ concentrations and deposition (not shown) in precipitation essentially unchanged.

Through other sensitivity studies, Karamchandani and Venkatram showed that their results were not sensitive to the prescribed, nominal precipitation rate used by the stratus module in nonprecipitating grid cells.

Regardless of how encouraging these results are, Karamchandani and Venkatram caution that the artificial mixing will increase the supply of SO_2 and H_2O_2 to the stratus cloud and hence enhance $\text{SO}_4^{=}$ production in the cloud as well as bring ambient $\text{SO}_4^{=}$ aerosol to the surface layer. Without some mixing mechanism, which is currently not included in the stratus module, $\text{SO}_4^{=}$ concentrations will be less than those shown in Figure 30. Further improvements in model performance must therefore also provide for vertical mixing in the stratus module.

6.2 RADM BOUNDARY-LAYER PARAMETERIZATIONS

A meteorological preprocessor (hereafter, referred to as just the preprocessor) provides appropriate meteorological inputs to RADM from data files produced by a mesoscale meteorological model, MM4 (Anthes and Warner, 1978; Anthes *et al.*, 1987; Staufer and Seaman, 1990). The preprocessor provides appropriate mean meteorological fields for temperature, horizontal wind components, humidity, pressure, and planetary boundary layer

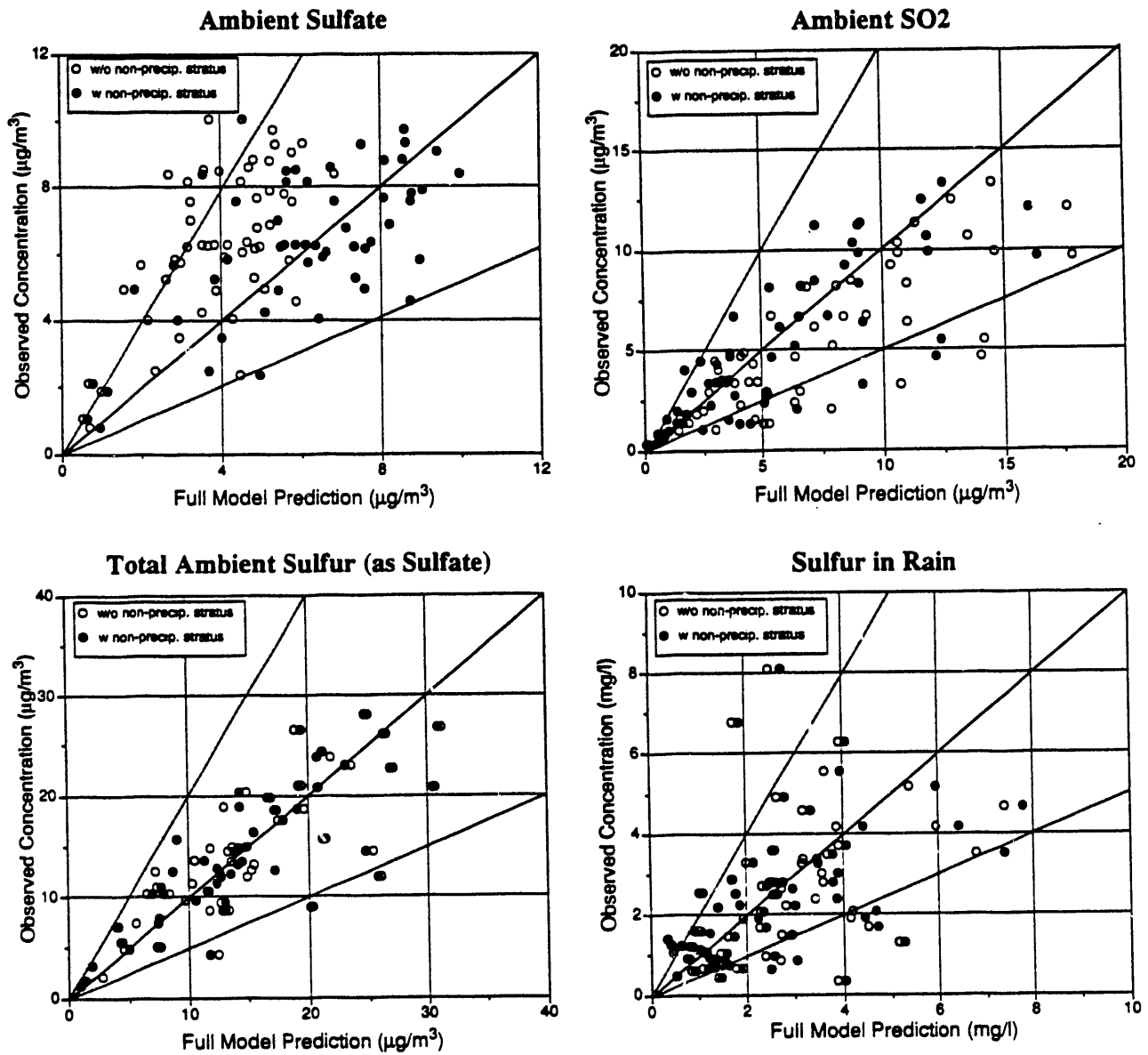


Figure 30. Comparison of Event-Averaged, Layer 1 Sulfur Species Concentrations for ADOM with and without Nonprecipitating Stratus Clouds for the 25 August to 5 September 1988 Event (Karamchandani and Venkatram, 1991)

(PBL) parameters necessary for describing atmospheric turbulence, precipitation rate, cloud fraction, and cloud bottom and top heights. The preprocessor also provides estimated dry-deposition velocities for various chemical species in RADM. For the EMEFS model evaluation discussed above, the preprocessors used were M12 for the 6-layer and M52 for the 15-layer versions of RADM. These preprocessors have been revised to correct problems in the scientific parameterizations used and in code implementation.

Results of the EMEFS evaluation illuminated problems associated with various modules within RADM. However, the severe overprediction of minimum concentrations of certain species during nighttime pointed directly to a problem in the preprocessor. After investigating various possible explanations, the MET concluded that the estimated nighttime dry-deposition velocities were too small. Further study showed that the nighttime friction velocity was predicted to be much less than 1 mm/sec over a large area of the modeling domain. From this, the RADM team concluded that the use of Louis's (1979) formulation to estimate fluxes from the predicted wind and temperature of the lowest layer of MM4 was unreliable at night. Padro *et al.* (1991) discovered a similar problem in an analysis of ADOM dry deposition. More generally, the equations for the surface layer break down for very stable conditions. New PBL profile functions (Byun, 1991) yield surface fluxes that are functions of the wind speed and temperature in the lowest layer of MM4. Byun's method provides a rigorous estimation of PBL parameters from the mean wind and temperature values predicted by a grid model such as MM4 because the range of applicability is extended to the entire PBL, whereas that of the previous method is limited to the surface layer, the lowest one-tenth of the PBL. In addition, a grid-averaged surface roughness that conserves momentum, which is important for the characterization of the atmospheric turbulence in the PBL, is estimated from subgrid-scale land-use data (Byun and Wesley, 1991).

Based on the newly developed PBL parameterization techniques mentioned above, the M14/54 preprocessor has following features:

- The Byun (1991) PBL similarity parameterization replaces the Louis (1979) surface similarity parameterization.
- Grid-averaged surface roughness length is estimated with a new formula that conserves momentum in a cell.
- Surface virtual temperature is estimated using the mixing ratio of the first MM4 layer instead of the saturation assumption.

- The length scale-to-height ratio for a neutral atmosphere is changed from 0.3 to 0.07 to provide a smooth transition of PBL height from stable to unstable conditions. The new coefficient is based on sodar measurements by Koracin and Berkowicz (1988).
- Total cloud cover is used for the actinic flux modulation instead of the precipitating cloud fraction.
- Special treatment of combined aerodynamic and surface resistances over water for SO₂ is removed.

One meteorological period (28 August - 1 September 1988; Case E6) of the EMEFS evaluation has been used for a preliminary analysis of M14 and RADM2.6. Two grid cells, one containing the Pennsylvania State University (PSU) and one containing New York City (NY), were chosen to illustrate the differences between the M12 and M14 preprocessors and RADM2.1 and RADM2.6. Results show that the new technique improved the estimation of the friction velocity and PBL height for stable conditions. Contour plots of grid-averaged surface roughness show good correlation to the surface land-use classification. Consistent estimation of grid-averaged surface roughness and application of PBL similarity to estimate surface fluxes corrected the abnormally low friction velocities at night. Also, as shown in Figure 31, the diurnal variation of PBL parameters is very reasonable. Subsequently, the dynamic range of the diurnal variation of dry-deposition velocities is reduced considerably from the previous version (Figure 32). The preliminary analysis shows that the M14 preprocessor fulfills the development objective of improving PBL parameters and estimations of deposition velocities. Because M14/54 will generate significantly different estimates of the PBL parameters, plume rises of point sources must be re-evaluated. This changes the layered-emission inputs to RADM2.6.

The overall effect of these improvements is shown in Figure 33. For the PSU site, RADM2.6 predicts a smoother and somewhat smaller diurnal variation in O₃ and SO₂ concentrations compared to RADM2.1. For the cell representing New York City and adjacent water surfaces, RADM2.6 produces lower, more realistic daily minimum O₃ concentrations than RADM2.1.

Several other improvements have been made to the RADM modeling system. Modifications to allow the cloud and scavenging module to better handle nonprecipitating clouds are discussed more fully below. Boundary conditions on the concentration of pollutants on the outflow portions of the boundary, which are specified to minimize discontinuities in concentrations and in the advection flux of pollutants through the boundary, as used for the nested RADM (Pleim *et al.*, 1991), have been implemented in the horizontal advection code. Photolysis and reaction rates for several important gas-phase reactions are now saved in a

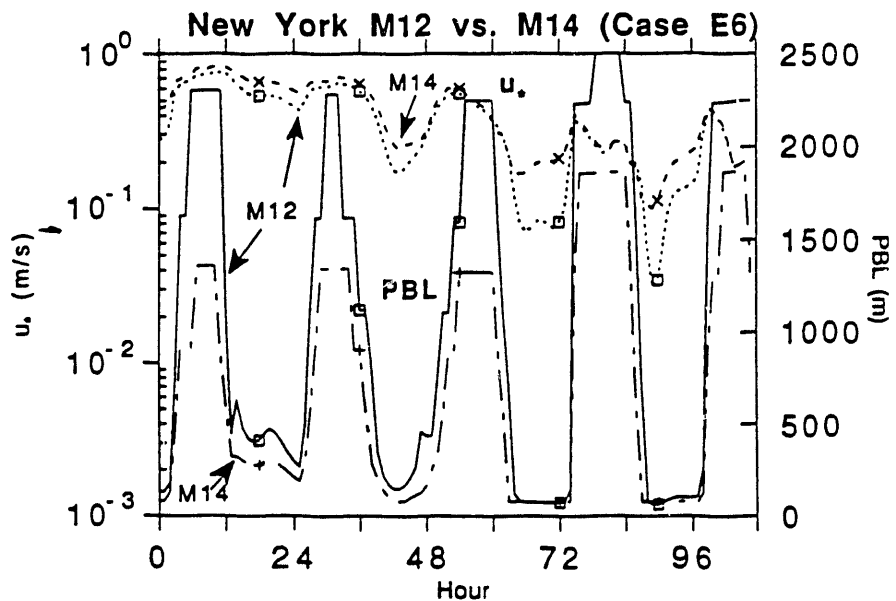
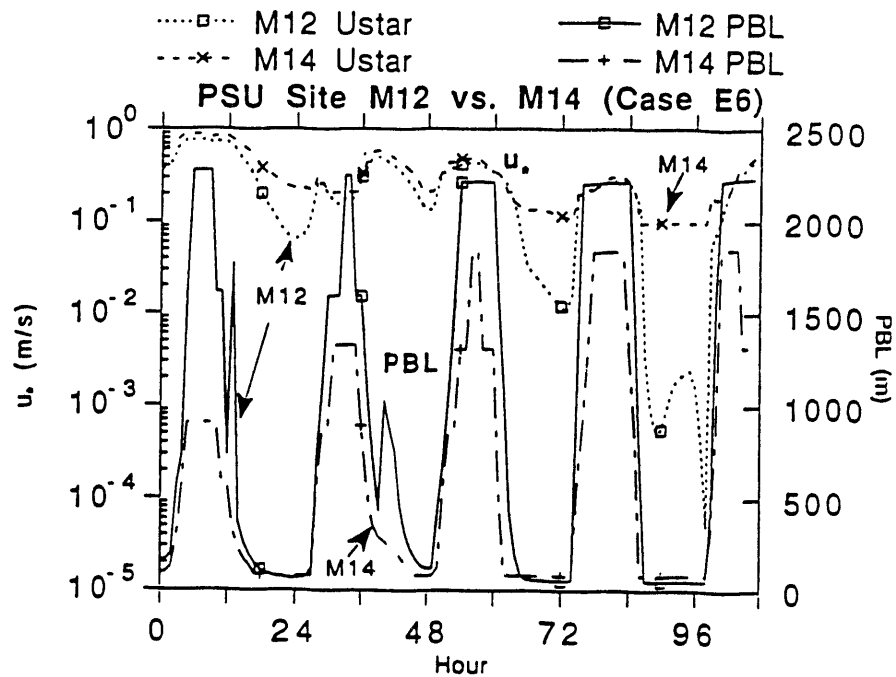


Figure 31. Comparison of Friction Velocity (u_*) and Planetary Boundary Layer (PBL) Height Estimated by M12 and M14 Meteorological Preprocessors for RADM for the Grid Cells Containing (a) Pennsylvania State University and (b) New York City from 28 August to 1 September 1988 (Case E6)

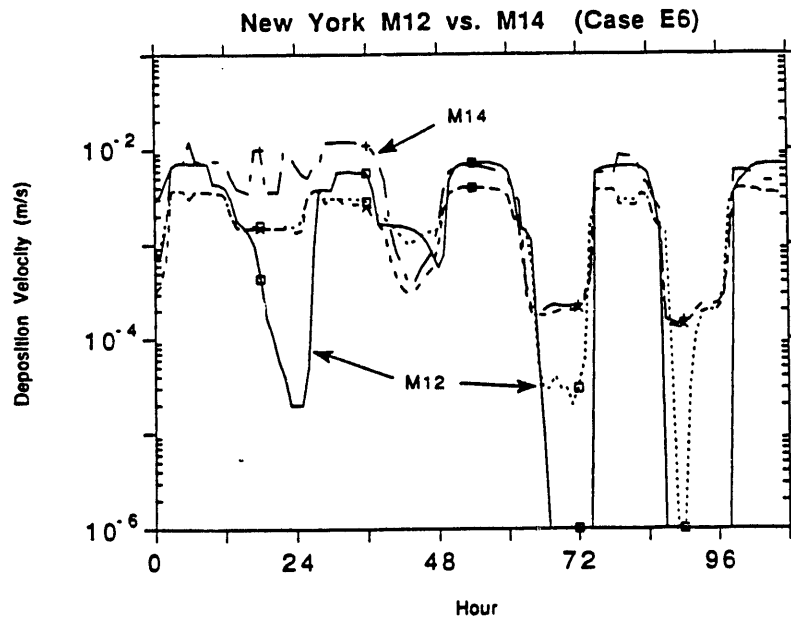
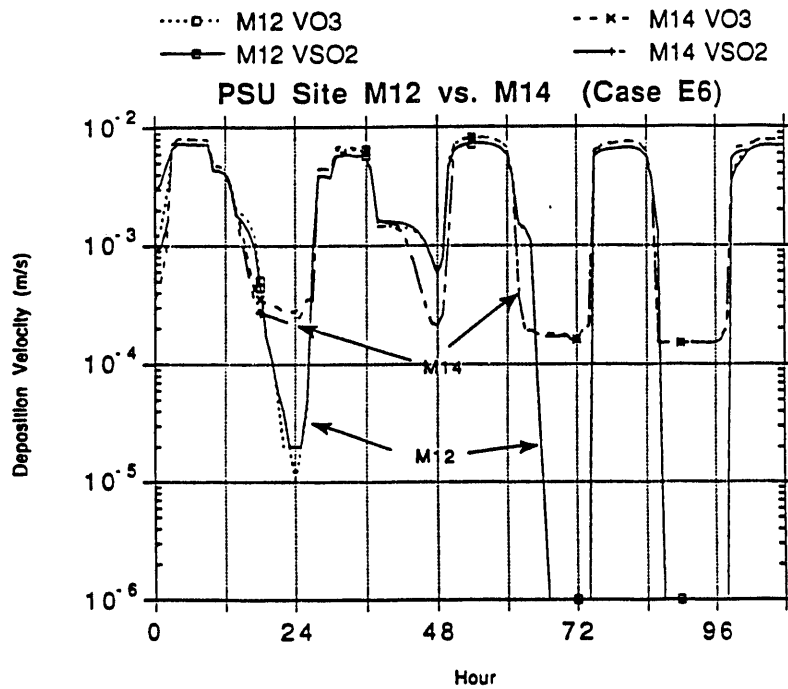


Figure 32. Comparison of Dry-Deposition Velocities of O_3 and SO_2 Calculated by M12 and M14 Meteorological Preprocessors for RADM for the Grid Cells Containing (a) Pennsylvania State University and (b) New York City from 28 August to 1 September 1988 (Case E6)

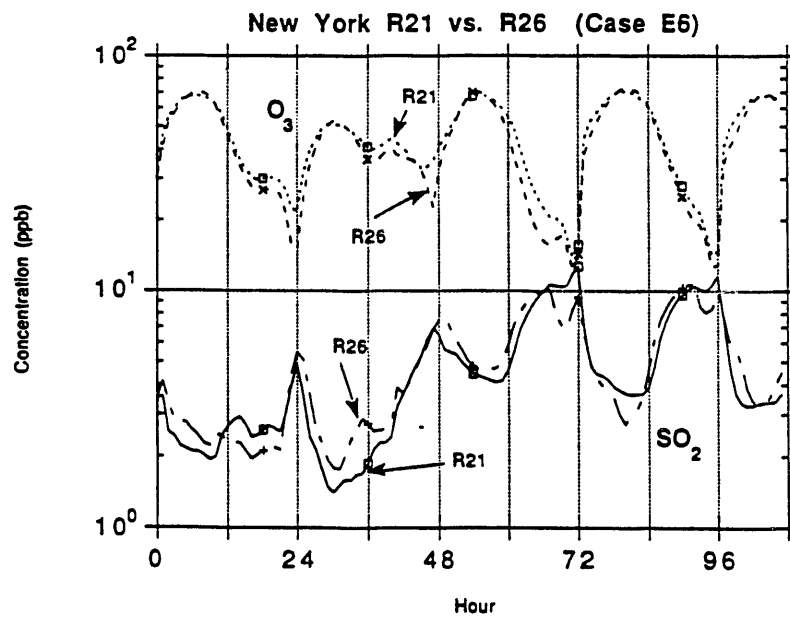
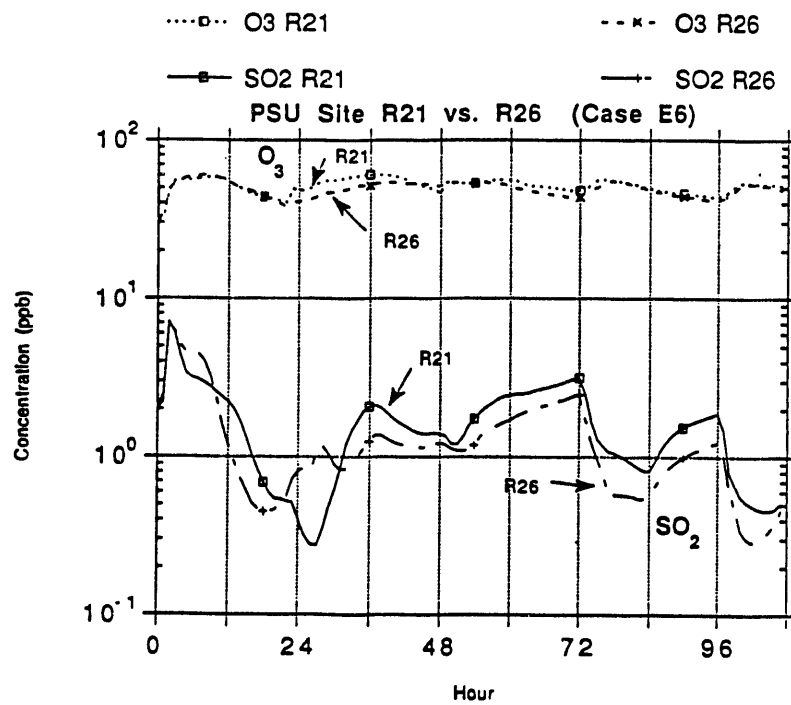


Figure 33. Comparison of O₃ and SO₂ Concentrations for RADM Layer 1 as Calculated by RADM2.1 and RADM2.6 for the Grid Cells Containing (a) Pennsylvania State University and (b) New York City from 28 August to 1 September 1988 (Case E6)

data file to aid diagnostic analyses. With these changes, the latest version of RADM is designated RADM2.6. Evaluation of this version is in progress.

6.3 RADM NONPRECIPITATING CLOUDS

The NAPAP evaluation (Dennis *et al.*, 1990) found that ambient $\text{SO}_4^=$ was systematically underpredicted by significant amounts both in the integrated-diagnostic evaluation of the September 1988 data and in the operational evaluation of annual data. The degree of bias, underprediction by approximately a factor of 0.6, was found to be similar across all seasons and also between day and night. From this, the MET concluded that one or more major processes might be either misrepresented or missing.

Evidence indicates that clouds can produce a substantial amount of $\text{SO}_4^=$ aerosol (Altshuller, 1987; Gillani *et al.*, 1981; Gillani and Wilson, 1983). Also, a budget analysis of RADM predictions showed that a substantial amount of the simulated $\text{SO}_4^=$ from evaporating, precipitating clouds is later scavenged by cloud processes (McHenry and Dennis, 1991a). In addition, comparison of RADM $\text{SO}_4^=$ aerosol predictions with aircraft data, which were taken in clear-air conditions, showed much less underprediction than did surface measurements for the entire September period. It was therefore hypothesized that $\text{SO}_4^=$ production by nonprecipitating clouds was being missed (Dennis *et al.*, 1990).

A detailed examination of how RADM handled nonprecipitating clouds (McHenry and Dennis, 1991) revealed that

- the average fractional cloudiness appeared to be unrealistically low, possibly by a factor of 5 or more
- the upper limits of the vertical extent of those clouds appeared too constrained, possibly by a factor of 2 in many circumstances
- the cloud products were mixed throughout the depth of the model.

The first two findings suggest that there may be a significant underrepresentation of nonprecipitating clouds and their effects in RADM. The excessive mixing depth would significantly dilute and inappropriately redistribute any $\text{SO}_4^=$ aerosol produced by nonprecipitating clouds. Therefore, it appears very promising to correct the identified deficiencies in the RADM cloud and scavenging module and determine the consequence of those corrections on ambient $\text{SO}_4^=$ aerosol production.

Significant improvements in the RADM cloud and scavenging module^(a) have been incorporated into RADM2.6. Information on fractional cloud coverage is now passed between cloud types for co-existing precipitating and nonprecipitating clouds. Maximum fractional coverage for both precipitating and nonprecipitating clouds is determined by imposing a mass-flux constraint. In the new module, nonprecipitating clouds have been broken into two types, nonprecipitating (NP) clouds that accompany precipitating clouds and cumulus humilis (CH) clouds that exist under purely fair-weather conditions. Raising the maximum permissible cloud base height to 3 km and relaxing the cap on maximum cloud top height to 500 hPa increased the frequency and depth of the NP clouds and effectively created bands of nonprecipitating clouds that accompany precipitation systems. Further, sidewall entrainment has been incorporated into all cloud types, and a simple direct-exchange mixing mechanism has been developed for nonprecipitating clouds. The influence of all nonprecipitating clouds on the vertical profile of pollutant concentrations has been capped at the top of the cloud layer, whereas the influence of precipitating clouds has been capped one layer above the cloud top.

A comparative analysis of aggregated annual averages calculated with the new RADM2.6 and the old RADM 2.1 scavenging modules showed that with the new module

- the $\text{SO}_4^{=}$ aerosol underprediction bias is now by a factor of only 0.9 (see Figure 34); that is, the new module explained up to 70% of the original low $\text{SO}_4^{=}$ aerosol concentration bias in RADM2.1
- the overprediction bias in SO_2 has been reduced, especially for the lower concentrations
- the wet $\text{SO}_4^{=}$ deposition is essentially unchanged.

Based on these results, it was concluded that the severe underrepresentation of nonprecipitating clouds is a very likely explanation of the underprediction of $\text{SO}_4^{=}$ aerosol concentrations by RADM2.1.

(a) McHenry J. N. and Dennis R. L. (1991) Improvements to the RADM cloud module and their effect on predictions of ambient sulfate concentrations. *Draft Report*, U. S. Environmental Protection Agency, Atmospheric Research and Exposure Assessment Laboratory, Research Triangle Park, North Carolina.

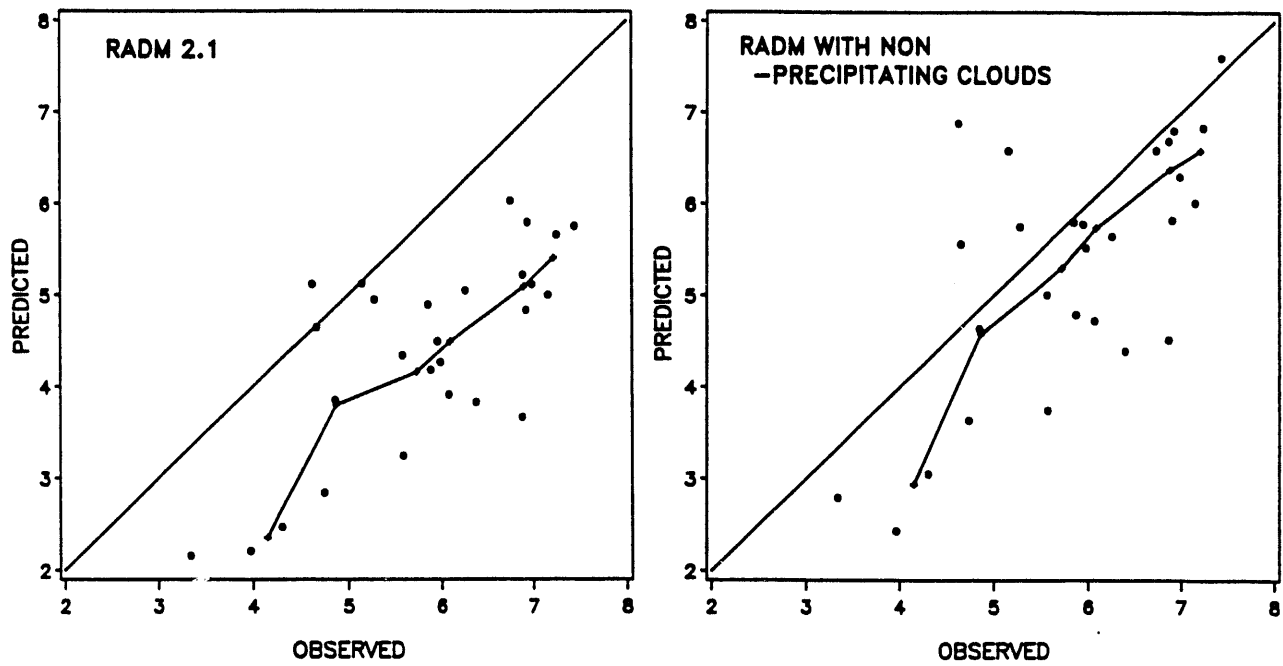


Figure 34. Comparison of Estimated Annual Average Layer 1 $\text{SO}_4^{=}$ Aerosol Concentrations for RADM2.1 with and without Nonprecipitating Clouds. [McHenry and Dennis 1991, Figure 1a & 1b combined on single graph]

7 DISCUSSION AND CONCLUSIONS

The focus of this report is the preliminary evaluation of ADOM and RADM that was conducted to meet demanding NAPAP time constraints. Emphasis has been on evaluating the application of RADM to various NAPAP assessment issues rather than on comparing ADOM and RADM performance. Critical characterizations of model performance are linked to the two primary uses of the models in the assessment: estimation of source attribution and estimation of the change in deposition for a prescribed change in emissions. Neither the operational evaluation nor the integrated-diagnostic evaluation directly tests the models relative to these key applications. Instead, the evaluation seeks to demonstrate that the models are capable of simulating current conditions correctly and that the simulations are correct because the models are based on correct science and numerics.

Source attribution describes how various sources contribute to the air quality or wet or dry deposition at a receptor. With the EMEFS data set, the movement and redistribution of primary and secondary pollutants within the modeling domain could be evaluated. Comparisons of predicted and observed time series, regional spatial patterns, and gradients gave strong indications that the synoptic-scale transport of pollutants around eastern North America was being well simulated.

The EMEFS data set cannot be used directly to test how well the models handle the response to an emissions change. Systematic biases in the simulation of current conditions are of concern, given that a nonlinear response to an emissions change may be affected by the bias. However, sensitivity studies with RADM have shown that changes in S deposition are not highly nonlinear (Dennis *et al.*, 1990). Consequently, although biases in SO₂ and SO₄⁼ aerosol predictions affect the predicted absolute change in ambient air concentrations, they appear to have little effect on relative change. This should also be true for the dry deposition of sulfur (S).

Biases may subtly affect wet deposition change. Because wet deposition is the result of a chain of processes, correct prediction of changes in wet deposition requires that each part of the chain be correctly simulated. Primary and secondary pollutants must be correctly transported and distributed; oxidant production must be correct; scavenging and in-cloud processes must be correct. The transport and distribution component appears to be of little concern. However, it appears that the dynamic range of the key oxidant, H₂O₂, is being underpredicted. This would cause the model predictions of changes in wet S deposition to be too oxidant-limited where H₂O₂ is observed to be abundant and not sufficiently oxidant-limited where H₂O₂ is observed to be scarce. The underprediction of the highest wet deposition amounts during the model evaluation period suggests that RADM2.1 may be too

oxidant-limited. The results of the seasonal operational evaluation further suggest that RADM2.1 may be too oxidant-limited in summer and not sufficiently oxidant-limited in winter.

Through sensitivity tests with RADM, Dennis and McHenry^(a) explored various bounds to oxidant availability and their effect on changes in wet deposition. They concluded that the bounds to RADM2.1 estimates of deposition change are relatively narrow. This means that, although RADM2.1 shows some biases in oxidant concentrations and wet deposition, the uncertainty in the relative change in wet deposition is fairly small for the magnitude of emissions changes analyzed for the NAPAP assessment (Dennis *et al.*, 1990).

The results of the preliminary evaluation of ADOM and RADM have demonstrated the importance of the diagnostic component of the evaluation. The detailed examination of model performance on time scales shorter than long period averages highlighted shortcomings in the evaluation database and in the emissions and meteorological fields used to drive the comprehensive models, as well as in the models. For example, the first interpretation workshop disclosed the severe underprediction of $\text{SO}_4^{=}$ aerosol and overprediction of T- NO_3 . Close examination of how the models used the NO and NO_2 emissions inventory data indicated that both models assigned incorrect values to the NO emissions, thereby increasing the apparent NO_x emissions by almost 30%. Also, a study of the time series of hourly predicted and observed vertical profiles of O_3 concentrations revealed how sensitive the comprehensive models are to mass inconsistencies in the input wind fields.

(a) Dennis R. L. and McHenry J. N. (1991) The spatial and temporal extent of oxidant limitation (nonlinearity) as predicted by the RADM and the engineering model. *Internal Report*, U.S. Environmental Protection Agency, Atmospheric Research and Exposure Assessment Laboratory, Research Triangle Park, North Carolina.

8 DIRECTION OF THE EMEFS EVALUATION

The EMEFS model evaluation is being conducted in several phases. The significant activity that supported the NAPAP assessment process has been completed. That work was part of Phase 1 of the EMEFS evaluation, which is based on data from the summer and fall of 1988. Work remaining in Phase 1 includes

- producing mass-consistent winds for ADOM for the July-September 1988 Phase 1 evaluation period
- simulating the July-September 1988 period with ADOM
- simulating the July-September 1988 period with the latest version of RADM, which uses summer surface characteristics for the whole period and new O₃ boundary conditions aloft
- analysis and interpretation of the new simulations
- documenting the results of phase 1 in a report to be peer-reviewed by the ERP.

Phase 1 of the evaluation includes a complete cycle of model development, evaluation, and modification. Peer review by the ERP of the report on Phase 1 in March 1992 will conclude Phase 1 of the EMEFS model evaluation.

Phase 2 of the evaluation will focus on gaining further diagnostic insight into and operational experience with model performance. In a recent meeting of the MET,^(a) three activities were given the highest priority for Phase 2 of the evaluation:

- Simulation and analysis of the spring 1990 EMEFS U.S. and Canadian intensives
- Simulation and analysis of seasonal contrasts using a period from November-December 1988

(a) MET (1991) *Model Evaluation Team Interpretation Workshop and Meeting*. Prepared for the Model Evaluation Team by the Pacific Northwest Laboratory, Richland, Washington.

- Analysis of the sensitivities of the models to uncertainties in emissions, meteorological fields, and initial and boundary conditions

Phase 2 of the evaluation will conclude in September 1993 when the final MET report on the EMEFS model evaluation will be reviewed by the ERP.

9 REFERENCES

Altshuller A.P. (1987) Potential contribution of sulfate production in cumulus cloud droplets to ground level particle sulfur concentrations. *Atmospheric Environment* **21**, 1097-1105.

Anthes R. A., Kuo Y. -H., Hsei E. -Y., Low-Nam S. and Bettge T. W. (1989) Estimation of skill and uncertainty in regional numerical models. *Q. J. Roy. Met. Soc.* **115**, 763-806.

Anthes R. A., Hsei E.-Y. and Kuo Y.-H. (1987) *Description of the Penn State/NCAR Mesoscale Model Version 4 (MM4)*. NCAR Tech. Note, NCAR/TN-282+STR, National Center for Atmospheric Research, Boulder, CO.

Anthes R. A. and Warner T. T. (1978) Development of hydrodynamic models suitable for air pollution and other mesometeorological studies. *Mon. Wea. Rev.* **106**, 1045-1078.

Banic C. M., Schemenauer R. S. and Anlauf K. G. (1991) Continuous high elevation chemical measurements in Quebec during the 1988 and 1990 EMEFS intensives. *Preprints of the Seventh Joint AMS/AMWA Conference on Applications of Air Pollution Meteorology*, pp. 242-245, American Meteorological Society, Boston, MA.

Barchet W. R. (ed.) (1987) *Evaluation of regional-scale air quality models: Chairman reports from four workshops*. EPRI-EA-5473, Electric Power Research Institute, Palo Alto, CA.

Barchet W. R., Dennis, R. L. and Seilkop S. K. (1991) Evaluation of RADM using surface data from the Eulerian model evaluation field study. *Preprints of the Seventh Joint AMS/AMWA Conference on Applications of Air Pollution Meteorology*, pp. 63-66, American Meteorological Society, Boston, MA.

Barchet W. R. and Dennis R. L. (1990) *The NAPAP model evaluation, Volume 1: Protocol*. U. S. Environmental Protection Agency, Atmospheric Research and Exposure Assessment Laboratory, Research Triangle Park, NC.

Binkowski F. S. (1990) Regional Acid Deposition Modeling. *State of Science and Technology Report No. 3*, National Acid Precipitation Assessment Program, Washington, D.C.

- Blackadar A. K. (1979) High resolution models of the planetary layer. In *Advances in Environmental Science and Engineering*, vol. 1, Pfafflin J. R. and Ziegler E. N. (eds.), pp. 50-85, Gordon and Breach, New York, NY.
- Blackman R. B. and Tukey J. W. (1958) *The Measurement of Power Spectra*. Dover Publications, New York, NY, 190 pp.
- Briggs G. A. (1975) Plume rise predictions. In *Lectures on Air Pollution and Environmental Impact Analysis*, pp. 59-111, American Meteorological Society, Boston, MA.
- Byun D. W. (1991) Determination of similarity functions of the resistance laws for the planetary boundary layer using surface-layer similarity functions. *Boundary Layer Meteorol.* (in press).
- Chang J. S., Brost R. A., Isakson S. A., Madronich S., Middleton P., Stockwell W. R. and Walcek C. J. (1987) A three-dimensional Eulerian acid deposition model: Physical concepts and formulation. *J. Geophys. Res.* **92(D12)**, 14,681-14,700.
- Ching J., Chang J., Spicer C. and Schaller E. (1991) Investigation of RADM performance using aircraft measurements. *Preprints of the Seventh Joint AMS/AMWA Conference on Applications of Air Pollution Meteorology*, pp. 42-45, American Meteorological Society, Boston, MA.
- Clark T., Voldner E. C., Dennis R. L., Seilkop S. K., Alvo M. and Olson M. P. (1989) The evaluation of long-term sulfur deposition models. *Atmospheric Environment* **17**, 2267-2288.
- Dennis R. L., Barchet W. R., Clarke T. L. and Seilkop S. K. (1990) Evaluation of regional acidic deposition models. *State-of-Science/Technology Report No. 5*, National Acid Precipitation Assessment Program, Washington, D.C.
- EPA. See U.S. Environmental Protection Agency.
- Fox D. G. (1981) Judging air quality model performance - Review of the Woods Hole workshop. *Bull. Am. Met. Soc.* **62**, 599-602.
- Fung C., Bloxam R., Misra P. K. and Wong S. (1991) Understanding the performance of a comprehensive model. *Preprints of the Seventh Joint AMS/AMWA Conference on Applications of Air Pollution Meteorology*, pp. 46-49, American Meteorological Society, Boston, MA.

- Gay D. (1987) A national inventory of biogenic hydrocarbon emissions based on a simple forest canopy model. *M.S. Thesis*, Washington State University, Pullman, WA.
- Gillani N. V., Kohli S. and Wilson W. E. (1981) Gas-to-particle conversion of sulfur in power plant plumes - I. Parameterization of the conversion rate for dry, moderately polluted ambient conditions. *Atmospheric Environment* **15**, 2293-2313.
- Gillani N. V. and Wilson W. E. (1983) Gas-to-particle conversion of sulfur in power plant plumes - II. Observations of liquid-phase conversion. *Atmospheric Environment* **17**, 1739-1752.
- Hales J. M. and Pennell W. T. (1988) A computer simulation procedure for designing airborne monitoring programs. In *Proceedings, Lower Tropospheric Profiling: Needs and Technologies*, American Meteorological Society, Boston, MA.
- Hansen D. A. (1989) *Project plan for the acid deposition Eulerian model evaluation and field study*. Electric Power Research Institute, Palo Alto, CA.
- Hansen, D. A., Puckett K. J., Jansen J. J., Lulis M. and Vickery J. S. (1991) The Eulerian Model Evaluation Field Study (EMEFS). *Preprints of the Seventh Joint AMS/AMWA Conference on Applications of Air Pollution Meteorology*, pp. 58-62, American Meteorological Society, Boston, MA.
- Hoff R. M., Mickle R. E., Fanaki F., Froude F. A., Arnold J. and Markes J. (1988) Vertical profiles of ozone and meteorology at CARE, Egbert. *Report ARD-89-009*, Atmospheric Research Directorate, Atmospheric Environment Service, Downsview, Ontario, Canada.
- Hoff R. M., Mickle R. E. and Leitch W. R. (1991) Vertical profiles of ozone using free flying and tethered ozonesondes and DIAL during the 1988 summer and 1990 spring EMEFS intensives. *Preprints of the Seventh Joint AMS/AMWA Conference on Applications of Air Pollution Meteorology*, pp. J223-J225, New Orleans, LA.
- Karamchandani P. and Venkatram A. (1991) The role of nonprecipitating clouds in producing ambient sulfate during summer: Results from simulations with the Acid Deposition and Oxidant Model (ADOM). *Atmospheric Environment* (accepted for publication).
- Karamchandani P., Lurmann F. and Venkatram A. (1985) Numerical experiments with a stratiform cloud/wet chemistry module. *ERT Document No. P-B866-450*, Environmental Research and Technology, Inc., Newbury Park, California.

- Koracin D. and Berkowicz R. (1988) Nocturnal boundary-layer height: Observations and acoustic sounders and predictions in terms of surface-layer parameters. *Boundary Layer Meteorol.* **43**, 65-83.
- Lamb B., Guenther A., Gay D. and Westberg H. (1987) A national inventory of biogenic hydrocarbon emissions. *Atmospheric Environment* **21**, 1695-1705.
- Louis J.-F. (1979) A parametric model of vertical eddy fluxes in the atmosphere. *Boundary Layer Meteorol.* **17**, 187-202.
- Lurmann F. W., Lloyd A. C. and Atkinson R. (1986) A chemical mechanism for use in long-range transport/acid deposition computer modeling. *J. Geophys. Res.* **91**, 10,905-10,936.
- Macdonald A. M., Anlauf K. G., Wiebe H. A., Leitch W. R., Banic C. M., Watt M. F., Puckett K. J. and Bregman B. (1991) Measurement of aqueous and gaseous hydrogen peroxide in central Ontario. *Preprints of the Seventh Joint AMS/AMWA Conference on Applications of Air Pollution Meteorology*, pp. 77-80, American Meteorological Society, Boston, MA.
- McHenry J. N. and Dennis R. L. (1991) Partitioning of the sulfate budget into gas- and aqueous-phase components in the Regional Acid Deposition Model (RADM). *Preprints of the Seventh Joint AMS/AMWA Conference on Applications of Air Pollution Meteorology*, pp. 143-147, American Meteorological Society, Boston, MA.
- Mickle R. E., Hoff R. M., Markes J. and Froude F. A. (1991) Digital ozonesondes: Examples of results from the EMEFS experiments of 1988 and 1990 using aircraft measurements. *Preprints of the Seventh Joint AMS/AMWA Conference on Applications of Air Pollution Meteorology*, pp. J138-J141, New Orleans, LA.
- NAPAP (1989) *Plan and Schedule for NAPAP's Assessment Reports, 1989-1990: State of Science, State of Technology, Integrated Assessment*. National Acid Precipitation Assessment Program, Office of the Director, Washington, DC, 324 pp.
- Nappo C. J., Caneill J. Y., Furman R. W., Gifford F. A., Kaimal J. C., Kramer M. L., Lockhart T. J., Pendergast M. M., Pielke R. A., Randerson D., Shreffler J. H. and Wyngaard J. C. (1982) The workshop on the representativeness of meteorological observations, June 1981, Boulder, Colorado. *Bull. Am. Met. Soc.* **63**, 761-764.

Padro J., den Hartog G. and Neumann H. H. (1991) An investigation of the ADOM dry deposition module using summertime O₃ measurements above a deciduous forest. *Atmospheric Environment* **25(A8)**, 1689-1704.

Pleim J., Venkatram A. and Yamartino R. (1984) ADOM/TADAP development program, Volume 4: The dry deposition module. *ERT Document No. P-B980-520*, Environmental Research and Technology, Inc., Concord, MA.

Pleim J. E., Chang J. S. and Zhang K. (1991) A nested-grid mesoscale atmospheric chemistry model. *J. Geophys. Res.* **96(D2)**, 3065-3084.

Roth P. M. (1988) *Acid Model Operational-Diagnostic Evaluation Study (ACID-MODES). Report of the Workshop held 4-7 August 1987.* U.S. Environmental Protection Agency, Research Triangle Park, North Carolina.

Ruprecht H. and Sigg L. (1990) Interactions of aerosols (ammonium sulfate, ammonium nitrate and ammonium chloride) and of gases (HCl, HNO₃) with fogwater. *Atmospheric Environment* **24(A3)**, 573-584.

Schaller E., Chang J., Boatman J., Ching J. K. S., Meyer-Wyk M., Pleim J. and Spicer C. W. (1991) Evaluation of RADM predictions for a mesoscale- β box volume over northeastern Pennsylvania. *Preprints of the Seventh Joint AMS/AMWA Conference on Applications of Air Pollution Meteorology*, pp. 50-53, American Meteorological Society, Boston, MA.

Schemenauer, R. S. (1986) Acidic deposition to forests: The Chemistry of High Elevation Fog (CHEF) project. *Atmosphere-Ocean* **24**, 303-328.

Scholtz M.T., Weisman B., Mahrt L. and Christie A. D. (1986) Generation of meteorological data fields for the ADOM Eulerian regional model. *Preprints of the Fifth Joint AMS/APCA Conference on Applications of Air Pollution Meteorology*, pp. 145-150, Chapel Hill, NC.

Seilkop S. K. (1988) *Measures and interpretation for regional model evaluation. Report of the workshop held August 19-21, 1988.* U. S. Environmental Protection Agency, Atmospheric Research and Exposure Assessment Laboratory, Research Triangle Park, NC.

Seilkop S. K. and Finkelstein P. L. (1987) Annual precipitation chemistry patterns and trends in eastern North America, 1980-1984. *J. Clim. Appl. Meteor.* **26**, 983-994.

Smolarkiewicz P. K. (1984) A fully multidimensional positive-definite advection scheme with small implicit diffusion. *J. Comput. Phys.* **54**, 325-362.

Spicer C. W., Chang J., Ching J., Dennis R., Schaller E., Kelly T. J., Busness K., Lee R., Lindsey C. and Anderson J. (1991) Diagnostic evaluation of Regional Acid Deposition Model (RADM) during a period of frontal passage using aircraft measurements. *Preprints of the Seventh Joint AMS/AMWA Conference on Applications of Air Pollution Meteorology*, pp. 139-142, American Meteorological Society, Boston, MA.

Staufer D. R. and Seaman N. L. (1990) Use of four-dimensional data assimilation in a limited-area model. Part I: Experiments with synoptic data. *Mon. Wea. Rev.* **118**, 1250-1277.

Stockwell W. R. (1986) A homogeneous gas phase mechanism for use in a regional acid deposition model. *Atmospheric Environment* **20**, 1615-1632.

Stockwell W. R. and Lurmann F. W. (1989) *Intercomparison of the ADOM and RADM gas-phase chemical mechanisms*. Electric Power Research Institute, Palo Alto, CA.

Tesche T. W., Georgopoulos P., Seinfeld J. H., Cass G., Lurmann F. W. and Roth P. M. (1990) Improvement of procedures for evaluating photochemical models. *Final report*, Contract No. A832-103, State of California Air Resources Board, Sacramento, CA.

Tukey J. W. (1977) *Exploratory Data Analysis*. Addison-Wesley Publishing Co., Reading, MA, 688 pp.

U.S. Environmental Protection Agency (EPA) (1989) The 1985 NAPAP emissions inventory (version 2): Development of the annual data and modelers' tapes. *EPA-600/7-89-012a*, U.S. Environmental Protection Agency, Research Triangle Park, NC.

Venkatram A. and Karamchandani P. K. (1989) The ADOMII scavenging module. *ERT Document No. 0780-004-205*, ERT, Inc., Camarillo, California.

Venkatram A., Karamchandani P. K. and Misra P. K. (1988) Testing a comprehensive acid deposition model. *Atmospheric Environment* **24**, 737-747.

Walcek C., Karamchandani P. and Venkatram A. (1991) *Comparison of ADOM and RADM cloud process modules*. Electric Power Research Institute, Palo Alto, CA.

Watson C. R. and Olsen A. R. (1984) Acid Deposition System (ADS) for statistical reporting: System design and user's manual. *EPA 600/8-84/023*, U. S. Environmental Protection Agency, Research Triangle Park, NC.

Weil J. and Brower R. P. (1984) An updated Gaussian plume model for tall stacks. *J. Air Poll. Control Ass.* **34**, 818-827.

Yamartino R. J. and Scire J. S. (1984) ADOM/TADAP model development program, volume 3: The transport and diffusion modules. *ERT Document No. P-B980-210*, Environmental Research and Technology, Inc., Concord, Massachusetts.

Young J. R. and Lurmann F. W. (1984) ADOM/TADAP model development program, volume 7: Aqueous phase chemistry. *ERT Document No. P-B866-535*, Environmental Research and Technology, Inc., Newbury Park, California.

APPENDIX A

DETAILED EVALUATION RESULTS

APPENDIX A

DETAILED EVALUATION RESULTS

PENTILE STATISTICS

Scatter plots of predicted versus observed values, such as those shown in Figures 2 to 4 of the text, show the relationship between the predicted and observed values graphically. To obtain a quantitative measure of this relationship, the ranked observations were divided into five groups, or pentiles, of approximately equal number of observations. For each group the following statistics were calculated:

- range of observed values
- average observed value
- average predicted value
- average percentage deviation of the prediction from the observation where

$$\% \text{ Deviation} = 100 \frac{(\text{Prediction} - \text{Observation})}{\text{Observation}}$$

- standard deviation of the percentage deviation.

Pentile statistics for the SO₂, SO₄⁼ aerosol, NO₂, and T-NO₃ concentrations are given in Tables A.1 to A.3; Tables A.4 to A.6 give the pentile statistics for SO₄⁼ and NO₃⁻ wet concentrations and deposition.

REGIONAL TIME SERIES

Time series of the predicted and observed daily average SO₂, SO₄⁼ aerosol, and T-NO₃ concentrations, and daily maximum O₃ concentration were produced for all regions. Examples of those time series are given in Figures 5 to 7 and 9 of the text. Visual examination of the time series plots gives a qualitative indication of the temporal correspondence between the predicted and observed time series. The linear temporal correlation coefficient quantifies that correspondence. Table A.7 gives the linear temporal correlation coefficient between the RADM2.1-, RADM2.5/6-, and ADOM2Bf-predicted and

observed SO_2 , $\text{SO}_4^=$ aerosol, T- NO_3 , and maximum O_3 concentrations by region. Complete sets of regional time series are given in Figures A.1 to A.4 for RADM2.1, RADM2.5/6, and ADOM2Bf. Time series of predicted and observed SO_2 , $\text{SO}_4^=$ aerosol, T- NO_3 , and maximum O_3 concentrations are shown in these figures. The vertical bar denotes the 95% confidence interval about the regional daily average observed concentration for SO_2 , $\text{SO}_4^=$ aerosol, and T- NO_3 . A dotted line is used to show the observed daily maximum O_3 concentration. A 95% confidence interval has not been developed for the daily maximum O_3 concentration.

Regions have been defined in Figure 1 of the text. Region M consists of a grid cell in Massachusetts. Region U consists of grid cells that contain major metropolitan areas or point sources. Included in Region U are the grid cells in which the cities of New York City, Detroit, and Chicago and a large point source in Indiana near the Illinois state line are located.

Table A.1. Average Bias of RADM2.1 Predictions Classified by EMEFS-Observed Concentrations for Sulfur and Nitrogen Species

SO ₂					
Interval ^(a)	I	II	III	IV	V
Concentration Range ($\mu\text{g}/\text{m}^3$)	0.57-2.06	2.07-3.63	3.74-7.11	7.14-10.70	10.70-23.00
Average Model Prediction ($\mu\text{g}/\text{m}^3$)	2.31	4.41	8.19	11.86	19.93
Average Observation ($\mu\text{g}/\text{m}^3$)	1.35	2.81	5.26	8.49	12.78
Average % Deviation ^(b)	70.7	61.1	51.6	38.3	57.0
Stand. Dev. of % Deviation	131.7	49.3	64.6	66.4	64.0
Sample Size	13	14	14	14	13

SO ₄ aerosol					
Interval	I	II	III	IV	V
Concentration Range ($\mu\text{g}/\text{m}^3$)	0.79-4.20	4.28-5.24	5.24-6.42	6.81-7.75	7.76-10.10
Average Model Prediction ($\mu\text{g}/\text{m}^3$)	1.56	2.85	3.59	4.68	5.49
Average Observation ($\mu\text{g}/\text{m}^3$)	2.66	4.80	5.91	7.36	8.53
Average % Deviation	-44.4	-41.1	-39.4	-36.6	-35.4
Stand. Dev. of % Deviation	17.4	14.5	13.7	11.5	9.5
Sample Size	13	14	13	14	13

NO ₂					
Interval	I	II	III	IV	V
Concentration Range ($\mu\text{g}/\text{m}^3$)	0.95-2.35	2.86-4.34	4.45-5.71	5.96-7.43	8.16-15.10
Average Model Prediction ($\mu\text{g}/\text{m}^3$)	3.04	3.92	5.14	12.31	21.73
Average Observation ($\mu\text{g}/\text{m}^3$)	1.44	3.54	4.92	6.84	10.93
Average % Deviation	121.3	10.8	4.8	81.3	102.3
Stand. Dev. of % Deviation	102.4	31.5	38.5	111.6	164.2
Sample Size	7	8	8	8	7

HNO ₃					
Interval	I	II	III	IV	V
Concentration Range ($\mu\text{g}/\text{m}^3$)	0.77-1.55	1.58-2.29	2.31-2.93	3.00-3.73	3.76-5.64
Average Model Prediction ($\mu\text{g}/\text{m}^3$)	1.75	2.85	3.51	4.61	5.70
Average Observation ($\mu\text{g}/\text{m}^3$)	1.17	1.98	2.65	3.41	4.78
Average % Deviation	53.8	40.0	30.5	35.0	20.3
Stand. Dev. of % Deviation	97.2	47.8	84.2	44.3	27.7
Sample Size	11	12	12	12	12

(a) The ranked observations are placed into five intervals of nearly equal numbers of observations. The statistics apply to the observations and predictions in those intervals.

(b) Percent deviation = 100(prediction-observation)/observation.

Table A.2. Average Bias of RADM2.5/6 Predictions Classified by EMEFS-Observed Concentrations for Sulfur and Nitrogen Species

SO ₂					
Interval ^(a)	I	II	III	IV	V
Concentration Range (µg/m ³)	(0.57,2.06)	(2.07,3.63)	(3.74,7.11)	(7.14,10.7)	(10.7,23)
Average Model Prediction (µg/m ³)	3.05	5.92	11.26	15.46	27.10
Average Observation (µg/m ³)	1.35	2.81	5.26	8.49	12.78
Average % Deviation ^(b)	124.2	117.4	109.2	81.6	113.1
Stand. Dev. of % Deviation	139.6	75.6	71.5	67.2	81.3
Sample Size	13	14	14	13	

SO ₄ aerosol					
Interval	I	II	III	IV	V
Concentration Range (µg/m ³)	(0.79,4.20)	(4.28,5.24)	(5.24,6.42)	(6.81,7.75)	(7.76,10.10)
Average Model Prediction (µg/m ³)	2.32	4.34	5.14	6.86	8.54
Average Observation (µg/m ³)	2.66	4.80	5.91	7.36	8.53
Average % Deviation	-17.5	-10.2	-13.3	7.10	0.30
Stand. Dev. of % Deviation	19.8	18.3	18.2	14.40	14.3
Sample Size	13	14	13	14	13

NO ₂					
Interval	I	II	III	IV	V
Concentration Range (µg/m ³)	(0.95,2.35)	(2.86,4.34)	(4.45,5.71)	(5.96,7.43)	(8.16,15.10)
Average Model Prediction (µg/m ³)	3.77	5.46	7.09	15.28	24.34
Average Observation (µg/m ³)	1.44	3.54	4.92	6.84	10.93
Average % Deviation	168.9	54.3	43.8	124.7	127.9
Stand. Dev. of % Deviation	86.3	61.7	57.2	122.8	173.0
Sample Size	7	8	8	8	7

HNO ₃					
Interval	I	II	III	IV	V
Concentration Range (µg/m ³)	(0.77,1.55)	(1.58,2.29)	(2.31,2.93)	(3,3.73)	(3.76,5.64)
Average Model Prediction (µg/m ³)	2.04	3.20	4.01	4.99	6.09
Average Observation (µg/m ³)	1.16	1.98	2.64	3.41	4.78
Average % Deviation	79.0	57.7	49.1	46.9	27.9
Stand. Dev. of % Deviation	108.2	46.0	97.5	38.6	25.6
Sample Size	11	12	12	12	12

(a) The ranked observations are placed into five intervals of nearly equal numbers of observations.

The statistics apply to the observations and predictions in those intervals.

(b) Percent deviation = 100(prediction-observation)/observation.

Table A.3. Average Bias of ADOM2Bf Predictions Classified by EMEFS-Observed Concentrations for Sulfur and Nitrogen Species

SO ₂					
Interval (a)	I	II	III	IV	V
Concentration Range ($\mu\text{g}/\text{m}^3$)	(0.57,1.88)	(2.06,3.54)	(3.63,6.13)	(6.31,9.77)	(10.20,23.00)
Average Model Prediction ($\mu\text{g}/\text{m}^3$)	2.02	5.36	7.17	12.46	15.45
Average Observation ($\mu\text{g}/\text{m}^3$)	1.26	2.64	4.69	8.00	12.66
Average % Deviation ^(b)	65.9	112.8	52.2	61.1	27.2
Stand. Dev. of % Deviation	140.4	70.8	53.7	66.5	38.1
Sample Size	13	13	13	13	13

SO ₄ aerosol					
Interval	I	II	III	IV	V
Concentration Range ($\mu\text{g}/\text{m}^3$)	(0.79,3.89)	(4.20,5.21)	(5.23,6.81)	(6.98,7.70)	(7.76,10.10)
Average Model Prediction ($\mu\text{g}/\text{m}^3$)	1.75	3.23	3.97	4.49	5.09
Average Observation ($\mu\text{g}/\text{m}^3$)	2.43	4.69	5.91	7.34	8.53
Average % Deviation	-30.7	-31.2	-33.0	-39.1	-40.2
Stand. Dev. of % Deviation	22.1	14.8	10.6	13.1	7.5
Sample Size	12	13	13	13	13

NO ₂					
Interval	I	II	III	IV	V
Concentration Range ($\mu\text{g}/\text{m}^3$)	(0.95,1.72)	(2.35,4.42)	(4.58,5.49)	(5.96,7.85)	(8.16,15.10)
Average Model Prediction ($\mu\text{g}/\text{m}^3$)	3.13	3.17	5.11	7.32	9.86
Average Observation ($\mu\text{g}/\text{m}^3$)	1.29	3.52	4.95	6.88	10.93
Average % Deviation	157.9	-9.3	3.3	6.5	-4.9
Stand. Dev. of % Deviation	108.9	21.2	39.3	56.1	68.6
Sample Size	6	7	7	7	7

HNO ₃					
Interval	I	II	III	IV	V
Concentration Range ($\mu\text{g}/\text{m}^3$)	(0.77,1.55)	(1.55,2.29)	(2.40,2.88)	(3.13,3.86)	(4.27,5.64)
Average Model Prediction ($\mu\text{g}/\text{m}^3$)	2.11	2.59	3.69	4.61	5.15
Average Observation ($\mu\text{g}/\text{m}^3$)	1.16	1.99	2.62	3.51	4.99
Average % Deviation	83.6	28.1	41.0	31.4	4.3
Stand. Dev. of % Deviation	123.8	34.9	48.4	25.2	17.8
Sample Size	11	12	11	12	11

(a) The ranked observations are placed into five intervals of nearly equal numbers of observations. The statistics apply to the observations and predictions in those intervals.

(b) Percent deviation = 100(prediction-observation)/observation.

Table A.4. Average Bias of RADM2.1 Predictions Classified by EMEFS-Observed Monthly Precipitation-Weighted Average Concentrations and Wet Deposition for SO_4^{2-} and NO_3^-

SO_4^{2-} Concentration					
Interval (a)	I	II	III	IV	V
Concentration Range (mg/L)	0.52-1.14	1.22-2.01	2.02-2.59	2.62-3.47	3.48-5.31
Average Prediction (mg/L)	1.03	1.56	2.04	2.45	2.64
Average Observation (mg/L)	0.81	1.63	2.40	2.99	4.17
Average % Deviation (b)	24.3	-5.2	-14.9	-17.6	-35.8
Stand. Dev. of % Deviation	79.1	35.4	20.0	21.5	14.8
Sample Size	10	11	11	11	11

SO_4^{2-} Deposition					
Interval	I	II	III	IV	V
Deposition Range (kg/ha)	0.19-01.40	1.45-2.10	2.12-2.81	2.89-3.42	3.49-4.62
Average Prediction (kg/ha)	1.70	1.75	2.61	2.76	2.65
Average Observation (kg/ha)	0.95	1.68	2.42	3.15	4.05
Average % Deviation	105.5	6.5	8.5	-12.3	-34.2
Stand. Dev. of % Deviation	156.4	50.2	37.1	15.4	19.3
Sample Size	10	11	11	11	11

NO_3^- Concentration					
Interval	I	II	III	IV	V
Concentration Range (mg/L)	0.36-0.69	0.70-1.06	1.15-1.41	1.43-1.81	1.85-3.66
Average Prediction (mg/L)	0.49	0.71	0.79	1.02	1.22
Average Observation (mg/L)	0.53	0.94	1.28	1.59	2.31
Average % Deviation	-7.0	-23.9	-38.2	-36.1	-45.2
Stand. Dev. of % Deviation	85.8	31.8	25.4	16.5	14.8
Sample Size	10	11	11	11	10

NO_3^- Deposition					
Interval	I	II	III	IV	V
Deposition Range (kg/ha)	0.12-0.96	0.97-1.15	1.15-1.41	1.43-1.80	1.80-3.34
Average Prediction (kg/ha)	0.79	0.84	0.98	1.04	1.21
Average Observation (kg/ha)	0.60	1.05	1.27	1.62	2.22
Average % Deviation	53.5	-21.0	-23.8	-35.6	-43.7
Stand. Dev. of % Deviation	102.1	33.3	32.4	15.8	21.0
Sample Size	10	11	11	11	10

(a) The ranked observations are placed into five intervals of nearly equal numbers of observations.

The statistics apply to the observations and predictions in those intervals.

(b) Percent deviation = $100(\text{prediction}-\text{observation})/\text{observation}$.

Table A.5. Average Bias of RADM2.5/6 Predictions Classified by EMEFS-Observed Monthly Precipitation-Weighted Average Concentrations and Wet Deposition for SO_4^{2-} and NO_3^-

SO_4^{2-} Concentration					
Interval ^(a)	I	II	III	IV	V
Concentration Range (mg/L)	(0.52,1.14)	(1.22,1.97)	(2.02,2.59)	(2.67,3.41)	(3.47,5.31)
Average Prediction (mg/L)	1.07	1.65	2.25	2.65	3.04
Average Observation (mg/L)	0.82	1.64	2.35	3.02	4.22
Average % Deviation ^(b)	30.2	-0.2	-4.1	-12.0	-26.6
Stand. Dev. of % Deviation	89.3	26.6	27.7	21.4	18.1
Sample Size	10	11	11	11	10

SO_4^{2-} Deposition					
Interval	I	II	III	IV	V
Deposition Range (kg/ha)	(0.19,1.45)	(1.48,2.1)	(2.2,2.81)	(2.89,3.82)	(3.84,5.11)
Average Prediction (kg/ha)	1.87	1.96	2.98	2.98	3.07
Average Observation (kg/ha)	1.00	1.70	2.52	3.33	4.41
Average % Deviation	124.7	18.2	18.6	-9.8	-30.3
Stand. Dev. of % Deviation	171.1	53.5	38.7	25.7	12.4
Sample Size	10	11	11	11	10

NO_3^- Concentration					
Interval	I	II	III	IV	V
Concentration Range (mg/L)	(0.36,0.69)	(0.7,1.06)	(1.15,1.41)	(1.43,1.87)	(1.88,3.66)
Average Prediction (mg/L)	0.51	0.72	0.86	1.07	1.38
Average Observation (mg/L)	0.53	0.95	1.29	1.65	2.28
Average % Deviation	-2.3	-23.5	-33.5	-35.6	-36.2
Stand. Dev. of % Deviation	91.5	26.7	27.7	14.2	21.7
Sample Size	10	11	11	11	10

NO_3^- Deposition					
Interval	I	II	III	IV	V
Deposition Range (kg/ha)	(0.12,0.96)	(0.98,1.15)	(1.16,1.52)	(1.6,1.86)	(2.08,3.34)
Average Prediction (kg/ha)	0.83	0.90	0.98	1.33	1.33
Average Observation (kg/ha)	0.64	1.06	1.33	1.74	2.44
Average % Deviation	60.0	-15.9	-26.4	-23.2	-44.4
Stand. Dev. of % Deviation	116.9	32.2	36.6	16.5	20.9
Sample Size	10	11	11	11	10

(a) The ranked observations are placed into five intervals of nearly equal numbers of observations.

The statistics apply to the observations and predictions in those intervals.

(b) Percent deviation = 100(prediction-observation)/observation.

Table A.6. Average Bias of ADOM2Bf Predictions Classified by EMEFS-Observed Monthly Precipitation-Weighted Average Concentrations and Wet Deposition for SO_4^{2-} and NO_3^-

SO_4^{2-} Concentration					
Interval (a)	I	II	III	IV	V
Concentration Range (mg/L)	(0.52,1.12)	(1.14,1.97)	(2.04,2.59)	(2.67,3.47)	(3.48,5.31)
Average Prediction (mg/L)	1.30	1.70	2.28	2.43	3.38
Average Observation (mg/L)	0.84	1.62	2.36	3.10	4.20
Average % Deviation (b)	64.9	10.7	-3.1	-21.6	-18.0
Stand. Dev. of % Deviation	74.0	53.9	27.2	25.7	34.9
Sample Size	9	10	10	10	9

SO_4^{2-} Deposition					
Interval	I	II	III	IV	V
Deposition Range (kg/ha)	(0.19,1.45)	(1.48,1.86)	(1.93,2.91)	(2.91,3.69)	(3.82,4.89)
Average Prediction (kg/ha)	0.62	0.64	0.95	1.04	1.08
Average Observation (kg/ha)	0.87	1.68	2.50	3.29	4.23
Average % Deviation	-19.8	-61.9	-62.4	-68.6	-74.3
Stand. Dev. of % Deviation	35.5	10.8	12.0	7.4	5.0
Sample Size	9	10	10	10	9

NO_3^- Concentration					
Interval	I	II	III	IV	V
Concentration Range (mg/L)	(0.36,0.65)	(0.69,1.06)	(1.06,1.43)	(1.45,1.88)	(1.89,3.66)
Average Prediction (mg/L)	0.77	0.75	1.22	1.01	1.85
Average Observation (mg/L)	0.50	0.92	1.30	1.63	2.30
Average % Deviation	58.4	-17.3	-4.2	-39.1	-13.1
Stand. Dev. of % Deviation	78.9	47.1	42.6	24.0	47.7
Sample Size	9	10	10	10	9

NO_3^- Deposition					
Interval	I	II	III	IV	V
Deposition Range (kg/ha)	(0.12,0.79)	(0.88,1.15)	(1.15,1.53)	(1.55,1.89)	(1.99,3.34)
Average Prediction (kg/ha)	0.29	0.35	0.31	0.48	0.38
Average Observation (kg/ha)	0.51	1.03	1.27	1.72	2.34
Average % Deviation	-30.7	-66.4	-75.1	-71.9	-83.3
Stand. Dev. of % Deviation	42.0	18.4	13.1	6.8	5.7
Sample Size	9	10	10	10	9

(a) The ranked observations are placed into five intervals of nearly equal numbers of observations. The statistics apply to the observations and predictions in those intervals.

(b) Percent deviation = $100(\text{prediction} - \text{observation}) / \text{observation}$.

Table A.7. Linear Temporal Correlation Coefficients for the Regression of Model-Predicted and EMEFS-Observed Daily Regionally Averaged Surface Concentrations

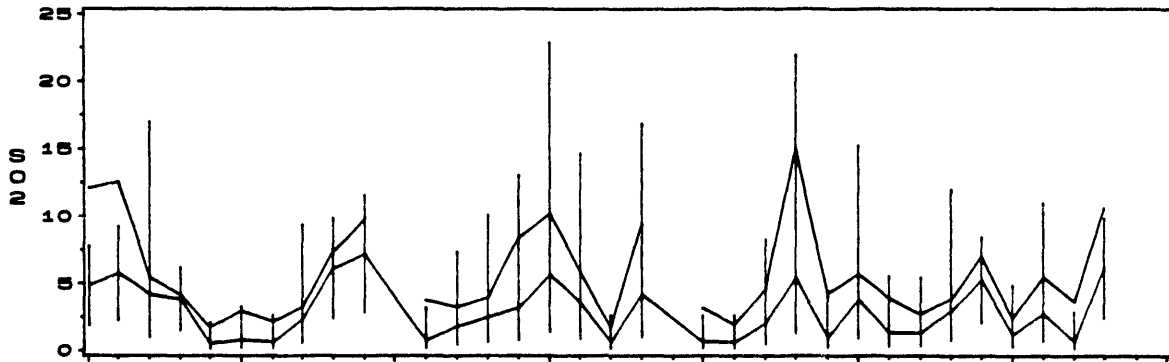
25 August - 28 September 1988

Model	Species	M	U	1	2	3	Region				8	9	
							4	4A	5	6			
RADM2.1	S02	0.775	0.463	0.373	0.897	0.802	0.691	0.670	0.536	0.811	0.250	0.535	0.297
	S04	0.857	0.868	0.817	0.959	0.906	0.850	0.698	0.781	0.851	0.552	0.685	0.583
	T-N03	0.780	0.572	0.615	0.896	0.915	0.828	0.636	0.680	0.785	0.532	0.634	0.525
	03	0.733	0.555	0.572	0.688	0.762	0.385	0.806	0.662	0.747	0.502	0.605	0.728
RADM2.5/6	S02	0.788	0.542	0.429	0.901	0.804	0.710	0.707	0.591	0.807	0.366	0.586	0.325
	S04	0.816	0.848	0.804	0.928	0.875	0.873	0.829	0.844	0.897	0.662	0.804	0.620
	T-N03	0.793	0.642	0.520	0.898	0.875	0.875	0.560	0.668	0.810	0.483	0.556	0.560
	03	0.782	0.597	0.717	0.838	0.795	0.557	0.775	0.763	0.852	0.723	0.821	0.786
ADOM2Bf	S02	0.633	0.453	0.435	0.705	0.758	0.715	0.434	0.504	0.745	0.302	0.488	0.348
	S04	0.740	0.784	0.792	0.779	0.883	0.740	0.808	0.878	0.757	0.442	0.640	0.642
	T-N03	0.543	0.673	0.497	0.745	0.826	0.823	0.642	0.661	0.656	0.517	0.565	0.610
	03	0.300	0.652	0.372	0.774	0.418	0.510	0.587	0.595	0.409	0.321	0.090	0.722

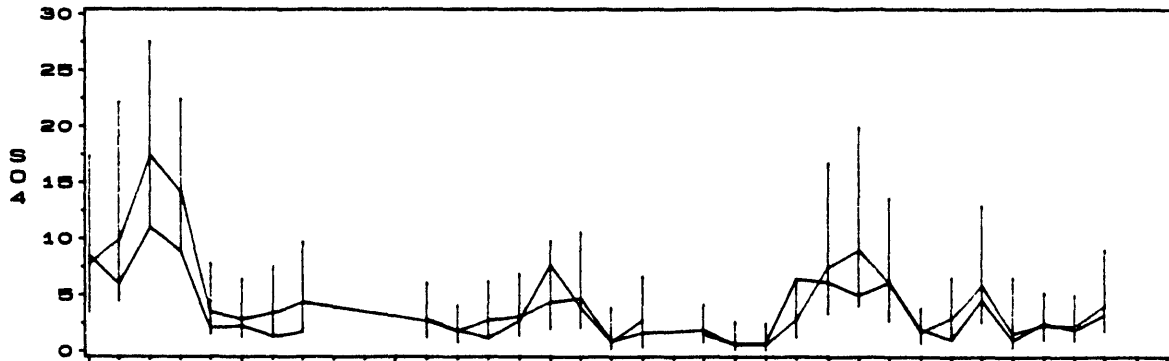
Figure A.1 The Daily Variation in the Regional Average RADM2.1-Predicted and EMEFS-Observed Concentration of SO_2 , $\text{SO}_4^{=}$ Aerosol, T- NO_3 , and Maximum O_3 in All Regions

AVERAGE OF RADM 2.1 PREDICTIONS AND OBSERVATIONS
25AUG88 - 27SEP88
REGION M

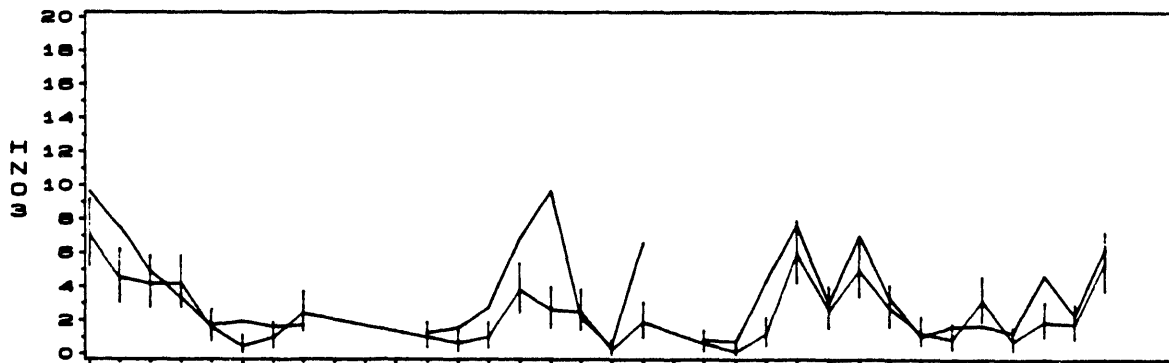
SO2 CONCENTRATION (UG/M3)



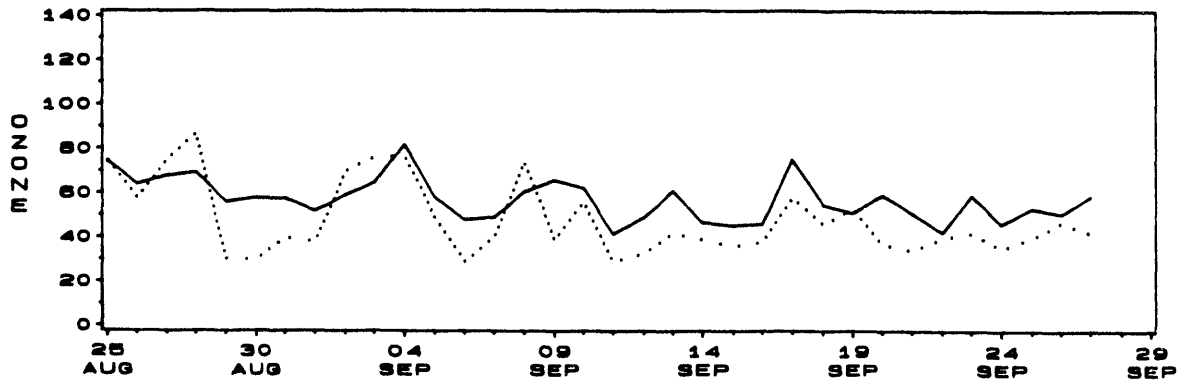
SO4 CONCENTRATION (UG/M3)



HNO3 CONCENTRATION (UG/M3)

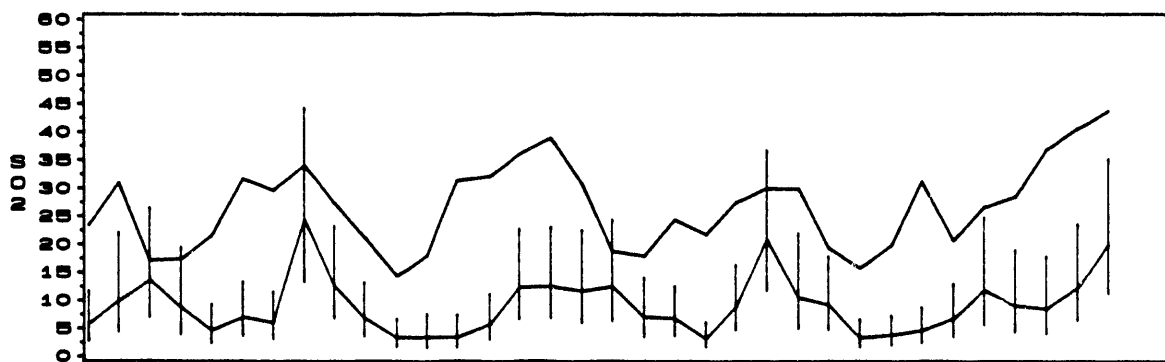


MAXIMUM OZONE 10AM-6PM (PPB)

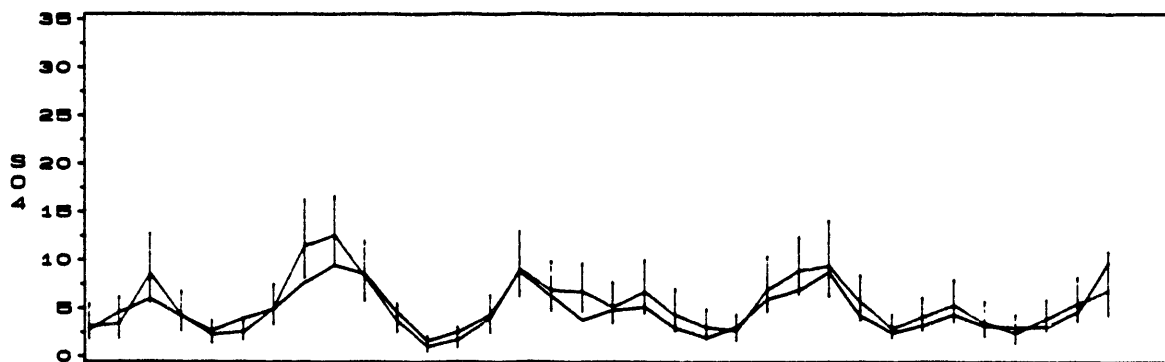


AVERAGE OF RADM 2.1 PREDICTIONS AND OBSERVATIONS
25AUG88 - 27SEP88
REGION U

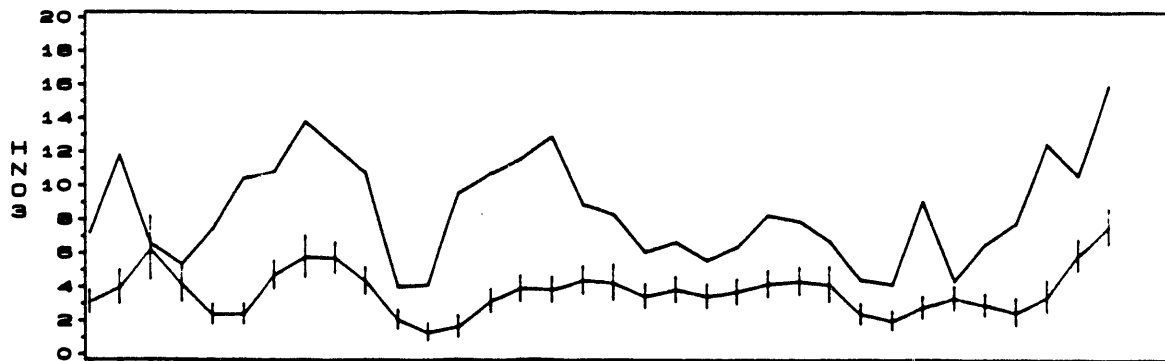
SO2 CONCENTRATION (UG/M3)



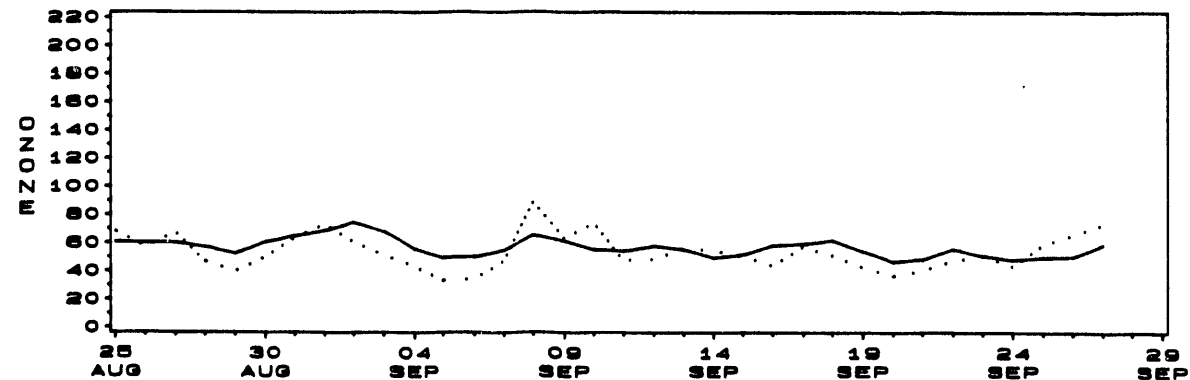
SO4 CONCENTRATION (UG/M3)



HNO3 CONCENTRATION (UG/M3)

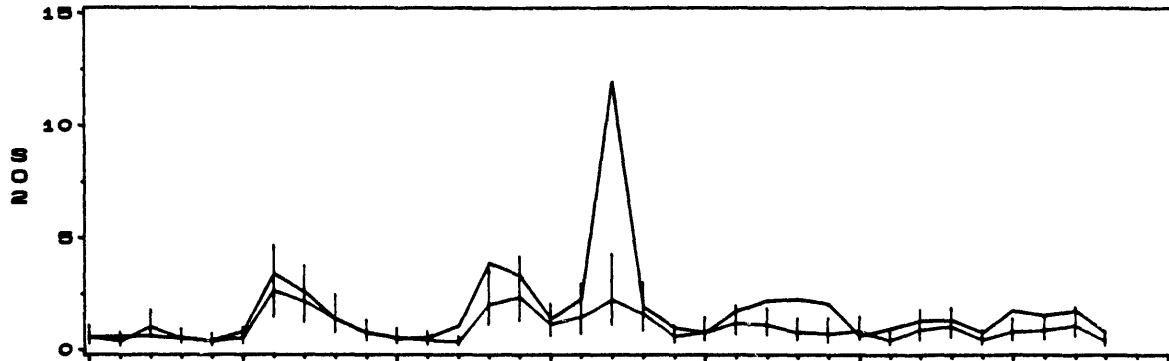


MAXIMUM OZONE 10AM-6PM (PPB)

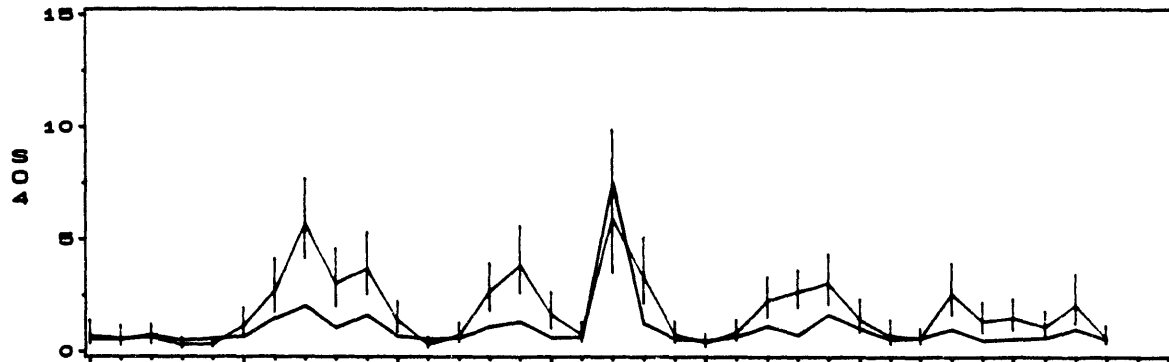


AVERAGE OF RADM 2.1 PREDICTIONS AND OBSERVATIONS
25AUG88 - 27SEP88
REGION 1

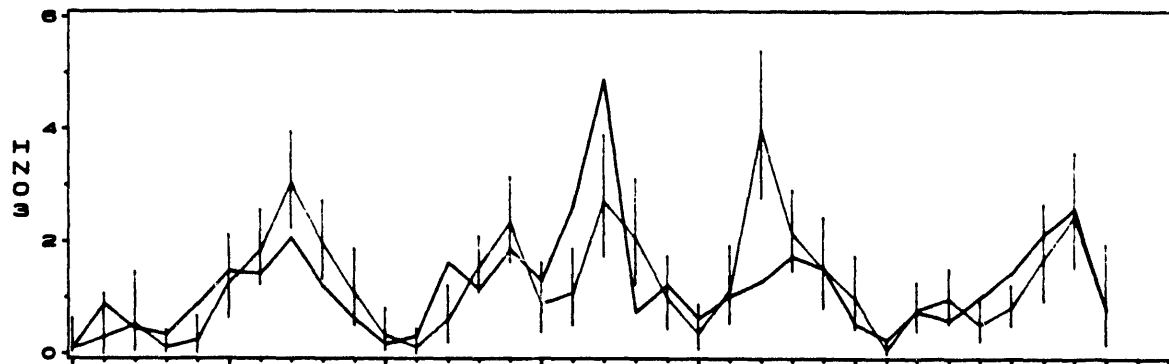
SO2 CONCENTRATION (UG/M3)



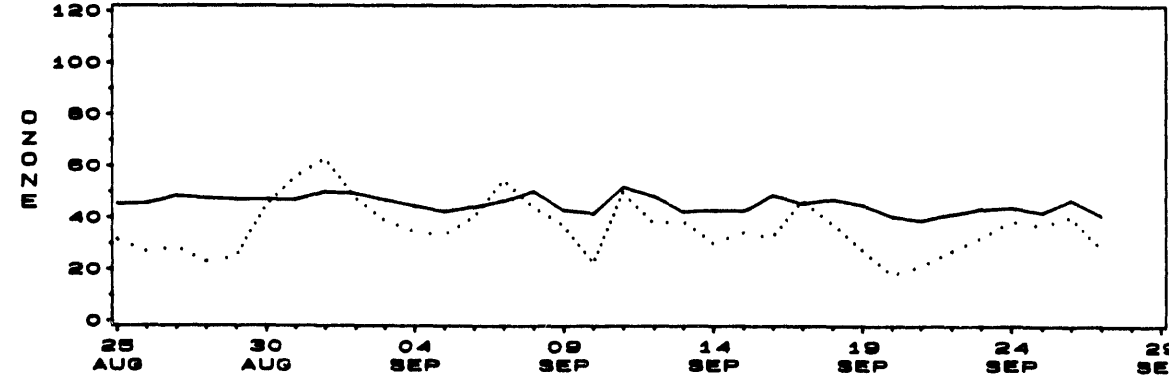
SO4 CONCENTRATION (UG/M3)



HNO3 CONCENTRATION (UG/M3)

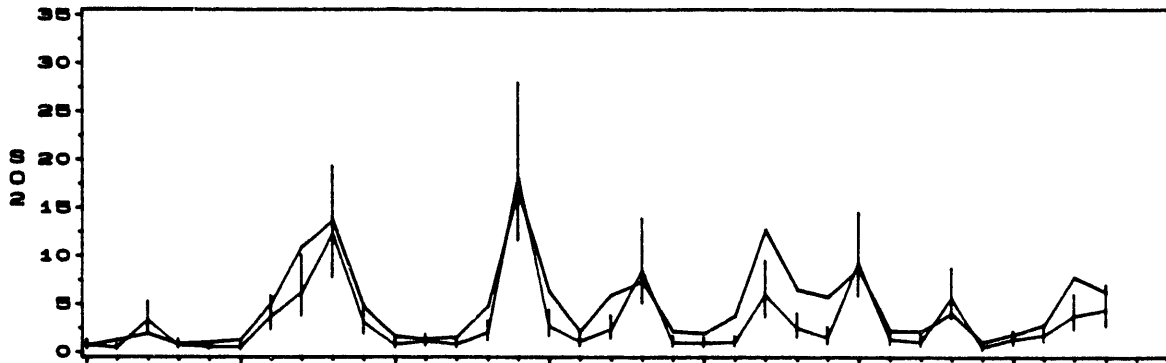


MAXIMUM OZONE 10AM-6PM (PPB)

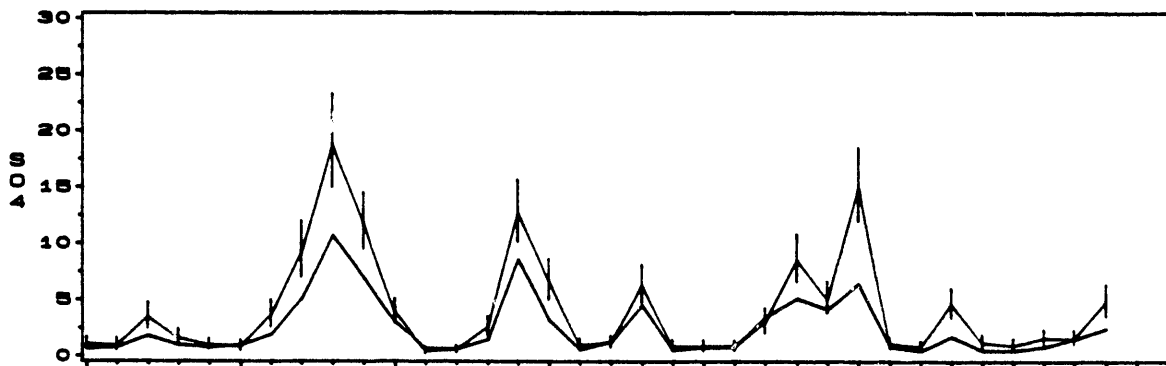


AVERAGE OF RADM 2.1 PREDICTIONS AND OBSERVATIONS
25AUG88 - 27SEP88
REGION 2

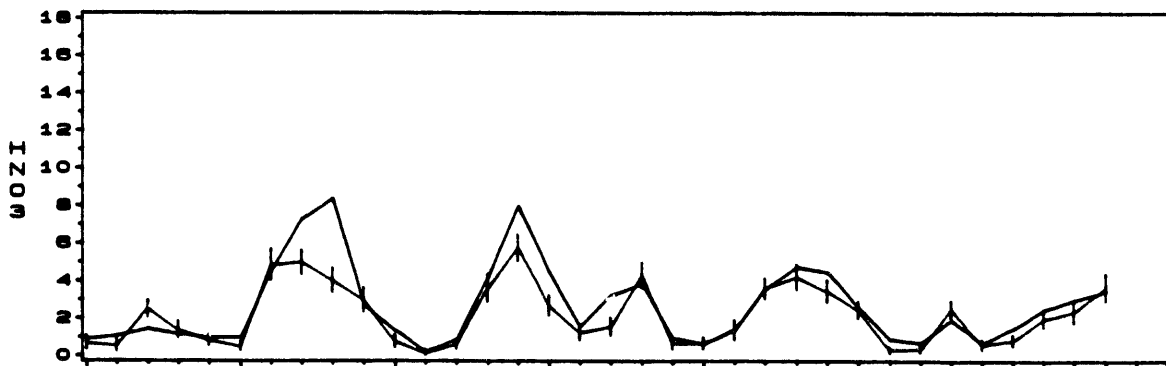
SO2 CONCENTRATION (UG/M3)



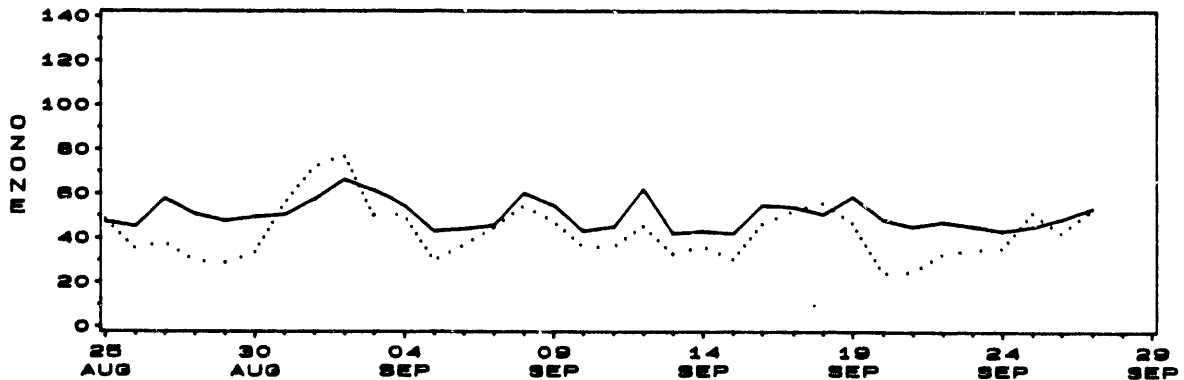
SO4 CONCENTRATION (UG/M3)



HNO3 CONCENTRATION (UG/M3)

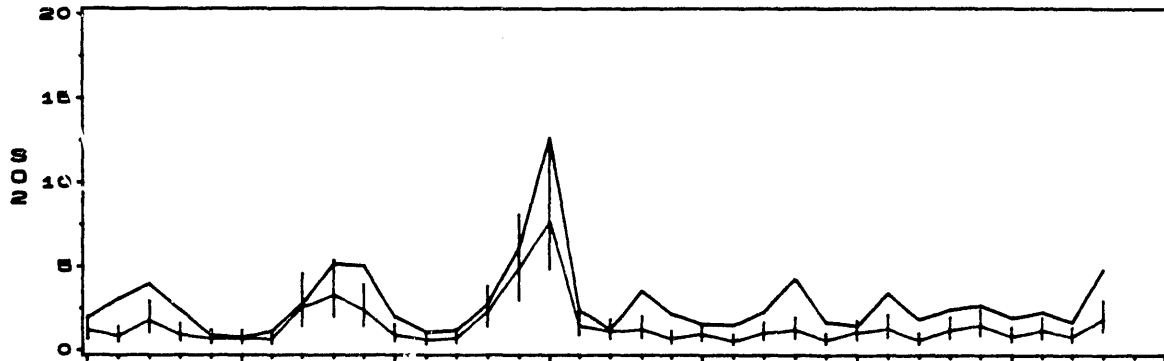


MAXIMUM OZONE 10AM-6PM (PPB)

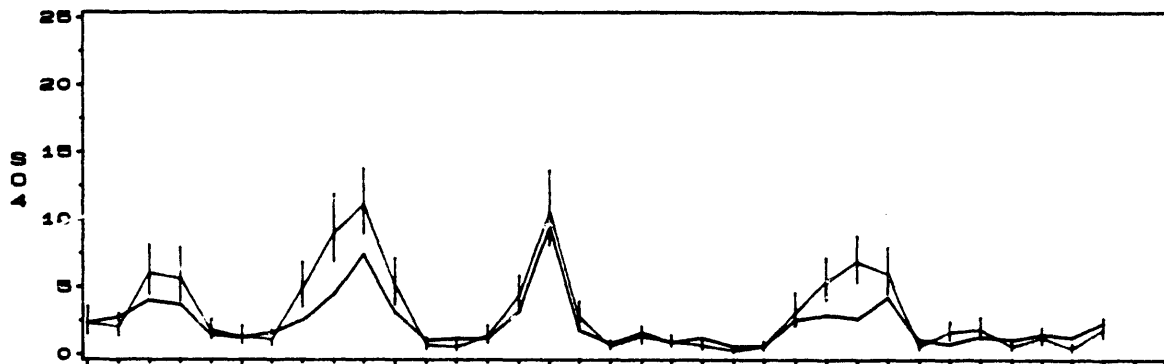


AVERAGE OF RADM 2.1 PREDICTIONS AND OBSERVATIONS
25AUG88 - 27SEP88
REGION 3

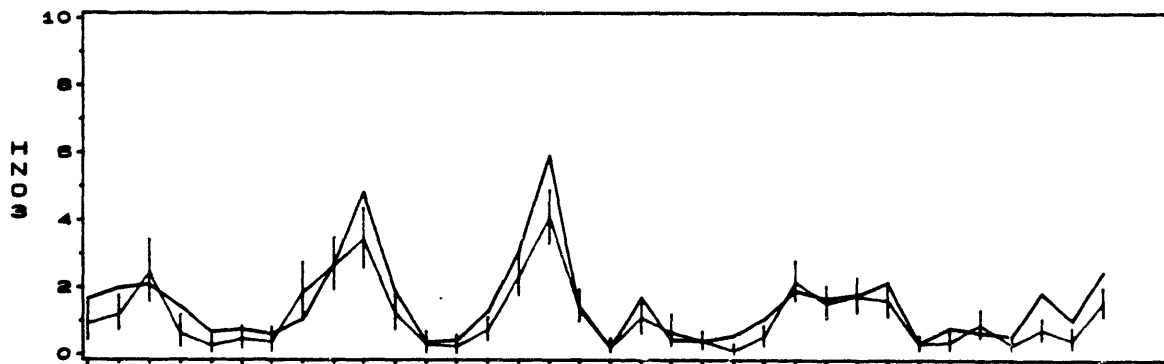
SO2 CONCENTRATION (UG/M3)



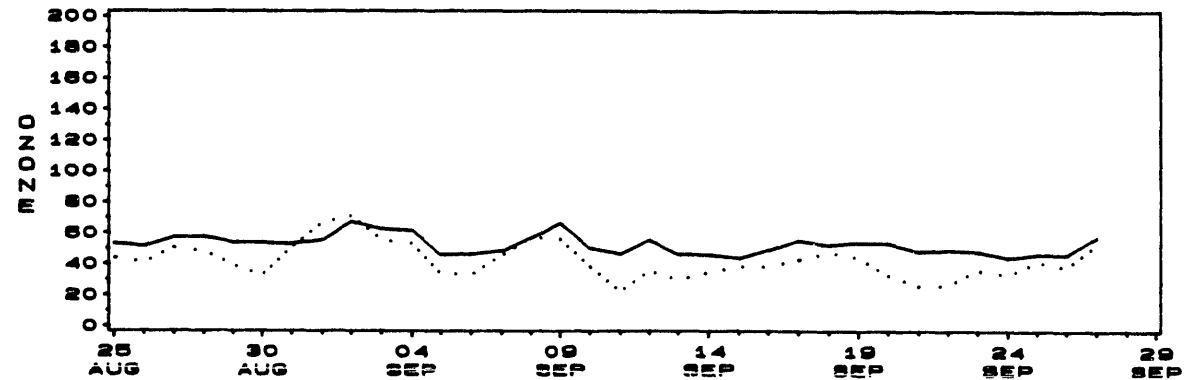
SO4 CONCENTRATION (UG/M3)



HNO3 CONCENTRATION (UG/M3)

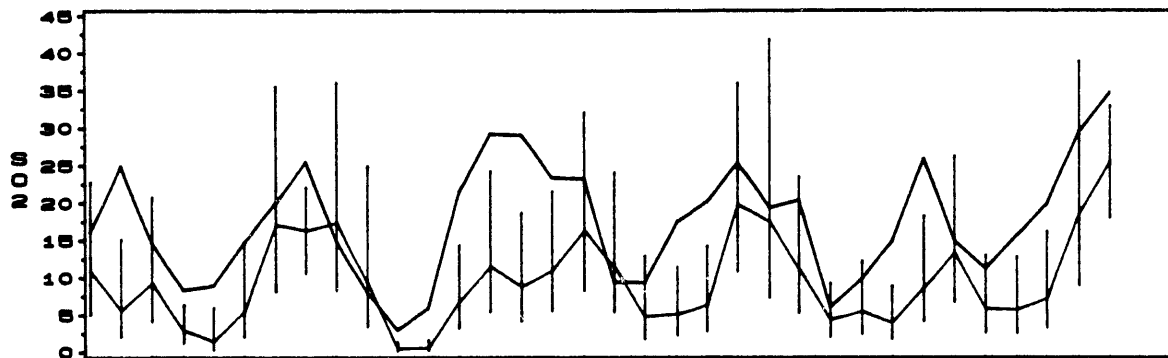


MAXIMUM OZONE 10AM-6PM (PPB)

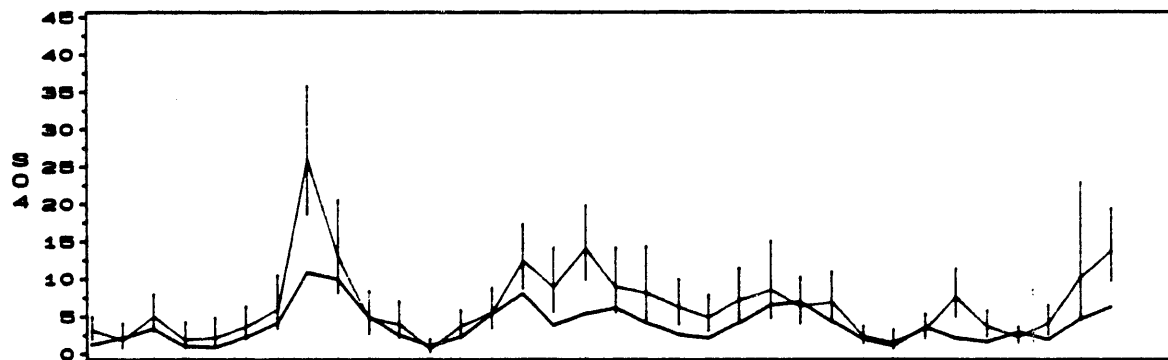


AVERAGE OF RADM 2.1 PREDICTIONS AND OBSERVATIONS
25AUG88 - 27SEP88
REGION 4

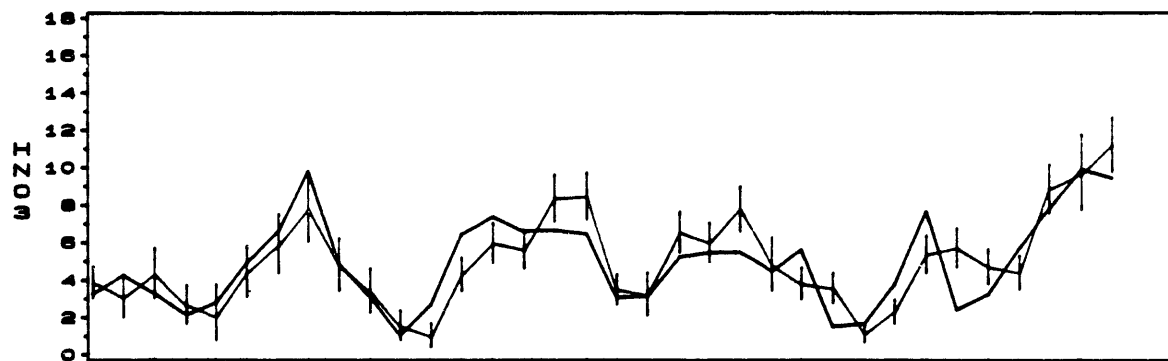
SO2 CONCENTRATION (UG/M3)



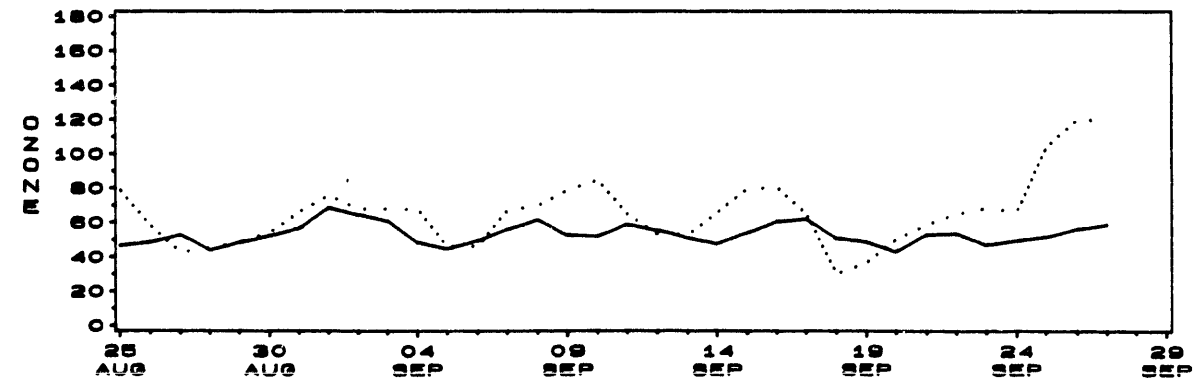
SO4 CONCENTRATION (UG/M3)



HNO3 CONCENTRATION (UG/M3)

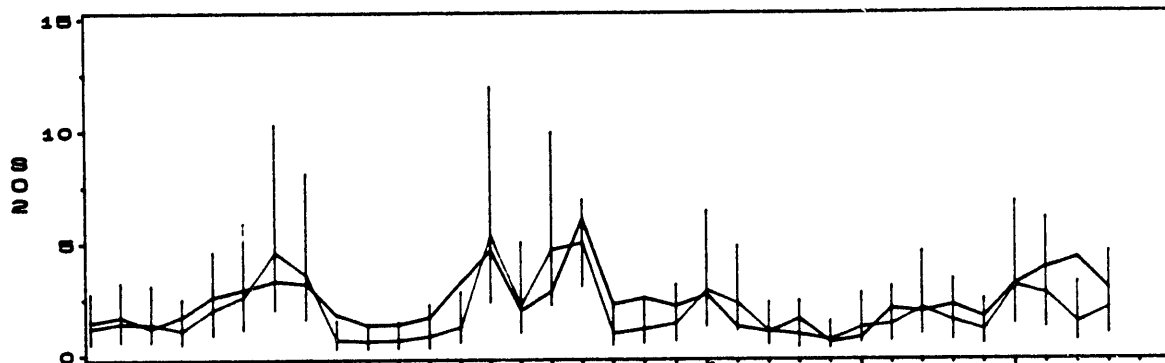


MAXIMUM OZONE 10AM-6PM (PPB)

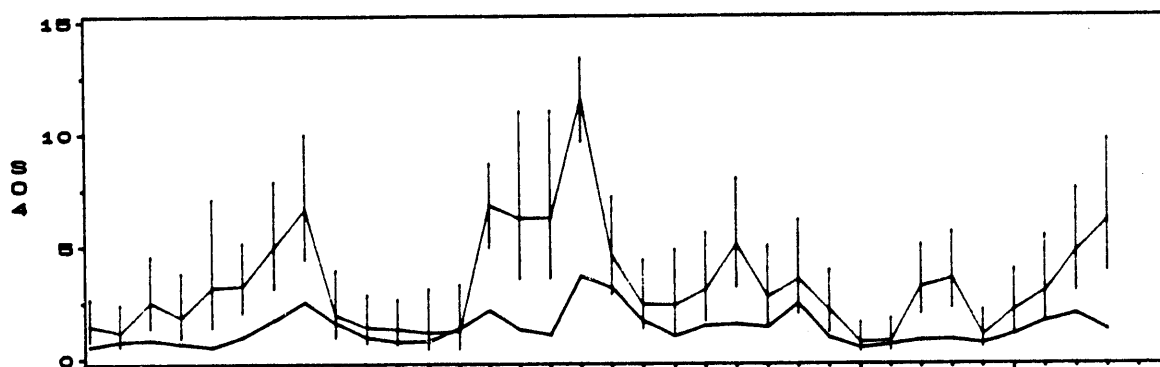


AVERAGE OF RADM 2.1 PREDICTIONS AND OBSERVATIONS
25AUG88 - 27SEP88
REGION 4A

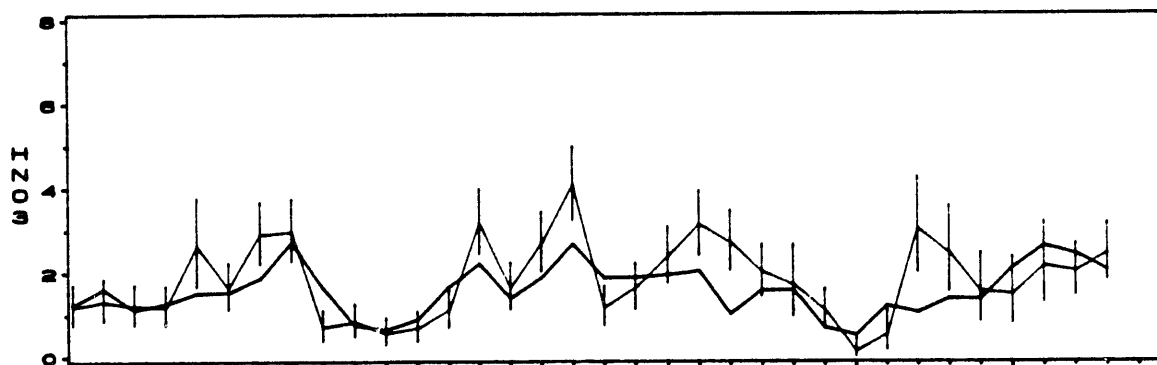
SO2 CONCENTRATION (UG/M3)



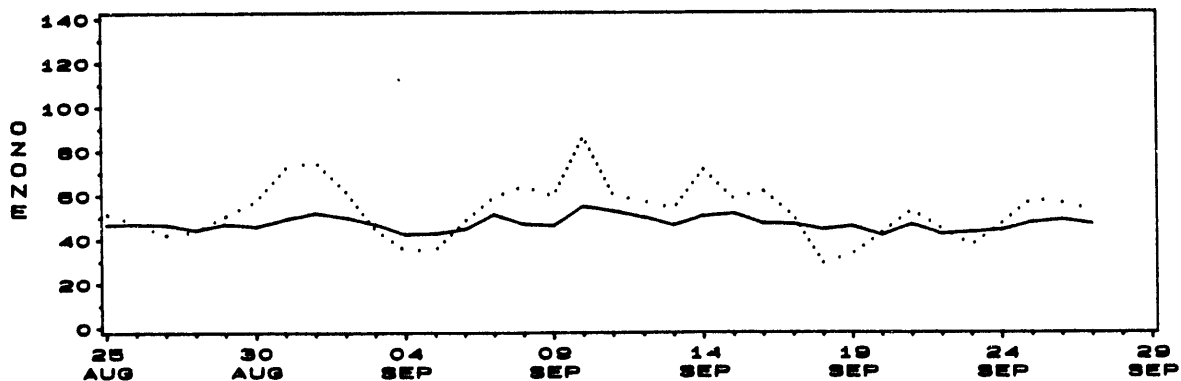
SO4 CONCENTRATION (UG/M3)



HNO3 CONCENTRATION (UG/M3)

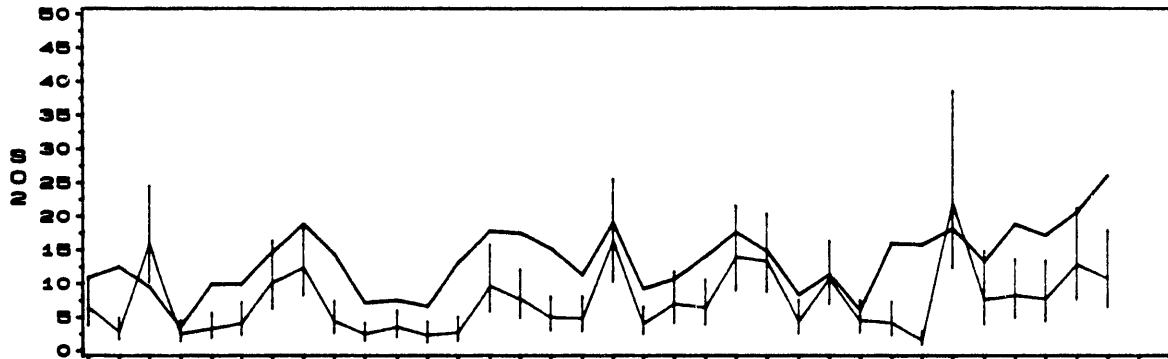


MAXIMUM OZONE 10AM-6PM (PPB)

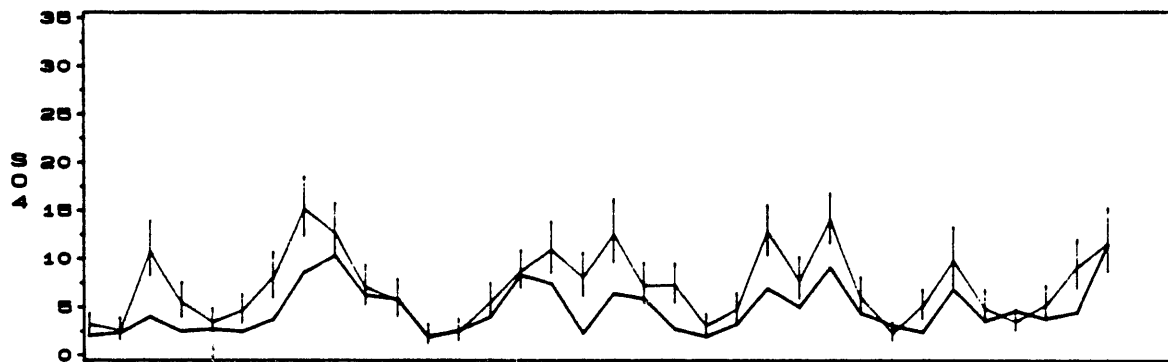


AVERAGE OF RADM 2.1 PREDICTIONS AND OBSERVATIONS
 25AUG88 - 27SEP88
 REGION 5

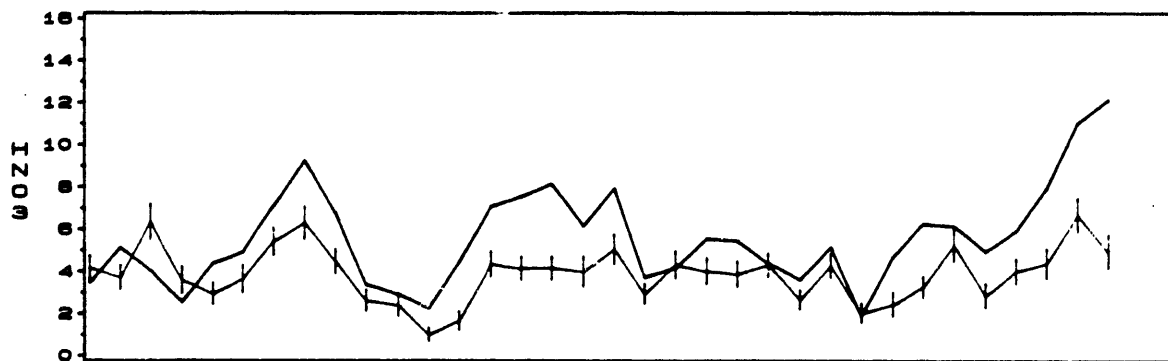
SO2 CONCENTRATION (UG/M3)



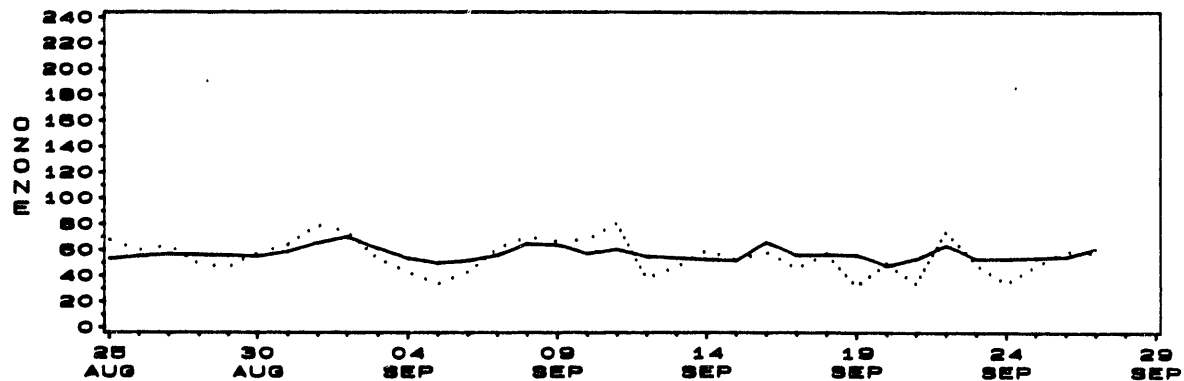
SO4 CONCENTRATION (UG/M3)



HNO3 CONCENTRATION (UG/M3)

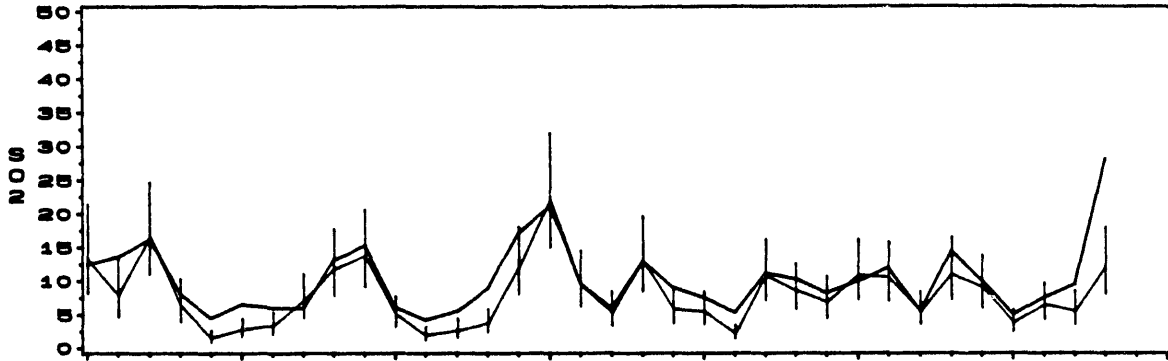


MAXIMUM OZONE 10AM-6PM (PPB)

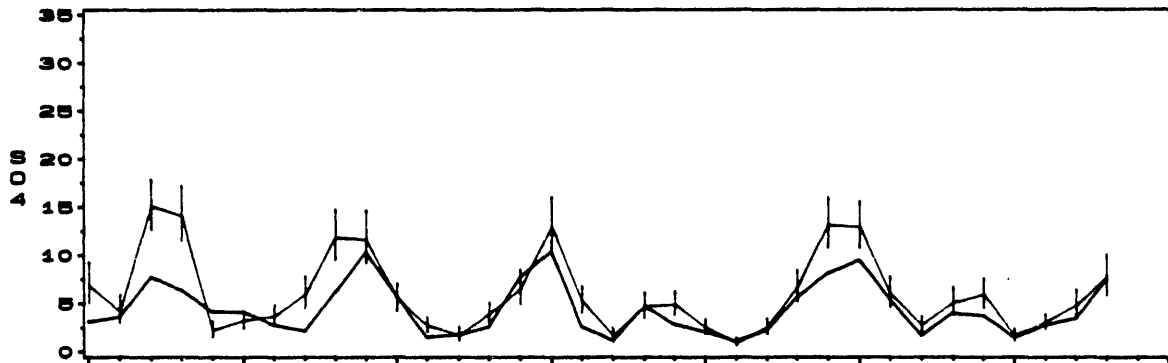


AVERAGE OF RADM 2.1 PREDICTIONS AND OBSERVATIONS
25AUG88 - 27SEP88
REGION 6

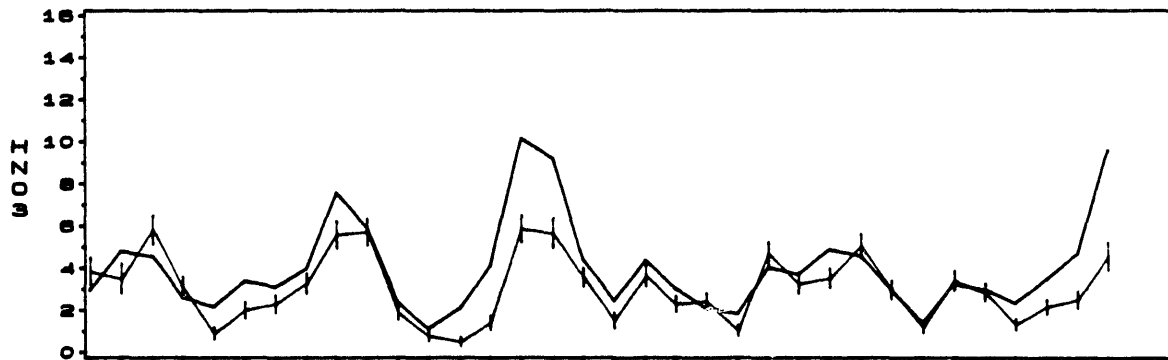
SO2 CONCENTRATION (UG/M3)



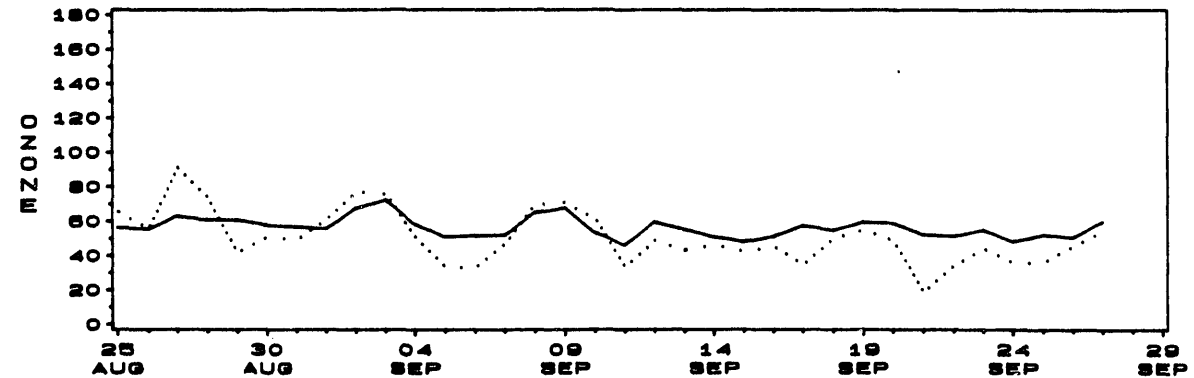
SO4 CONCENTRATION (UG/M3)



HNO3 CONCENTRATION (UG/M3)

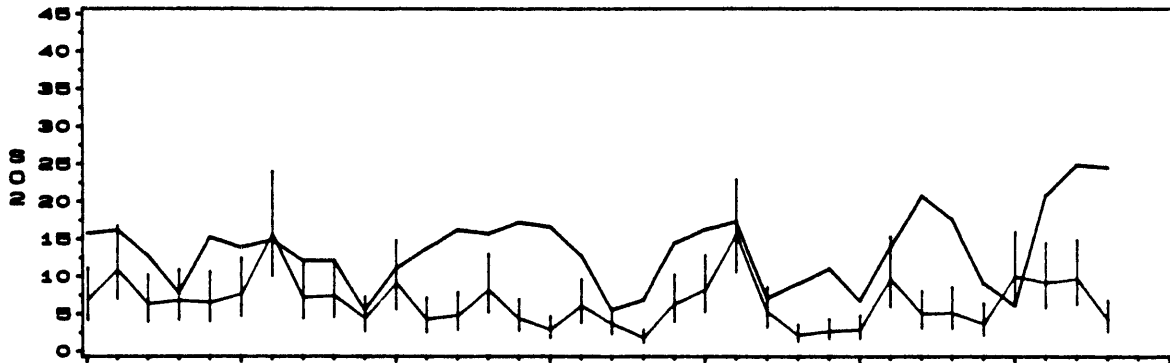


MAXIMUM OZONE 10AM-6PM (PPB)

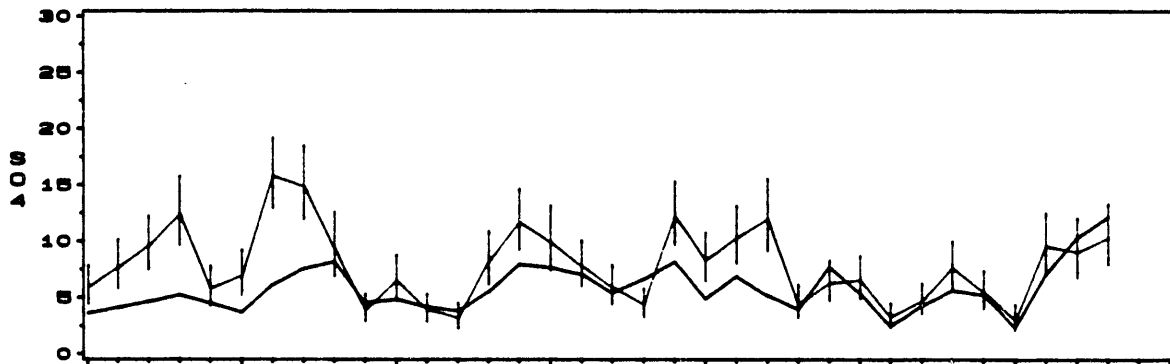


AVERAGE OF RADM 2.1 PREDICTIONS AND OBSERVATIONS
25AUG88 - 27SEP88
REGION 7

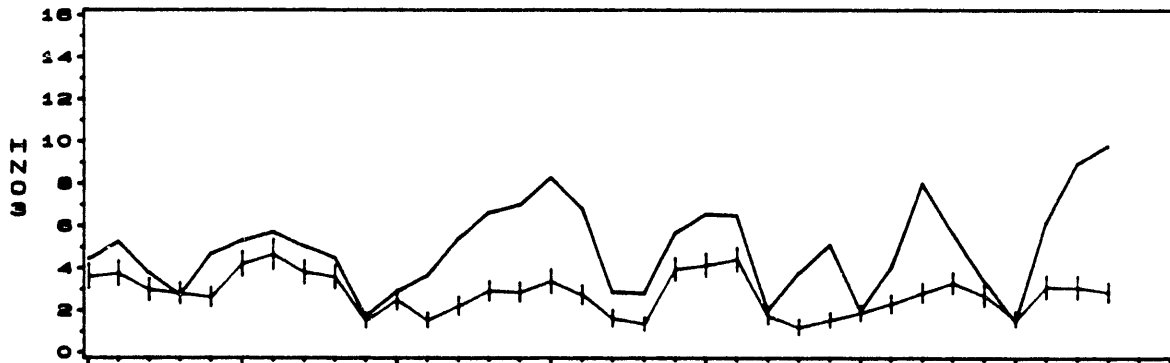
SO2 CONCENTRATION (UG/M3)



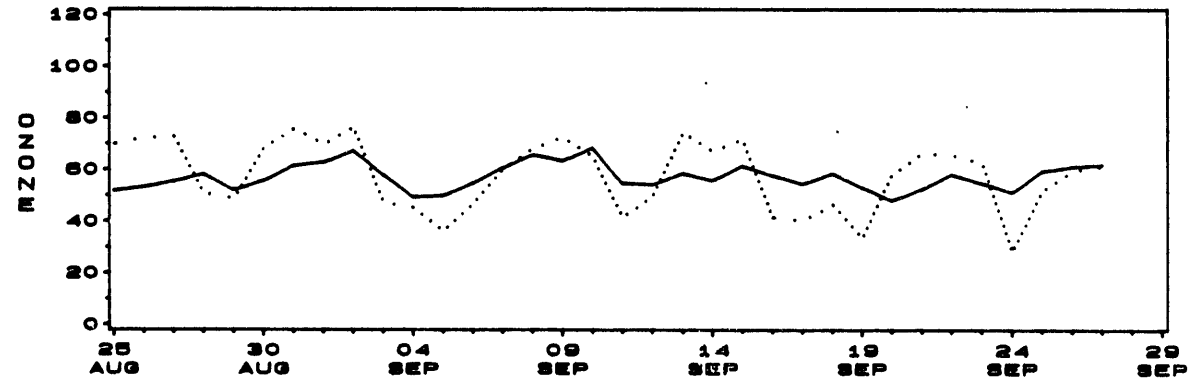
SO4 CONCENTRATION (UG/M3)



HNO3 CONCENTRATION (UG/M3)

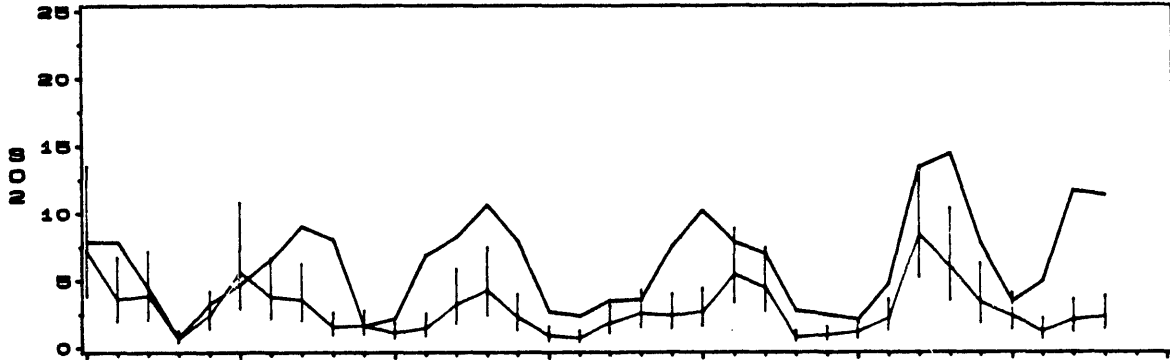


MAXIMUM OZONE 10AM-6PM (PPB)

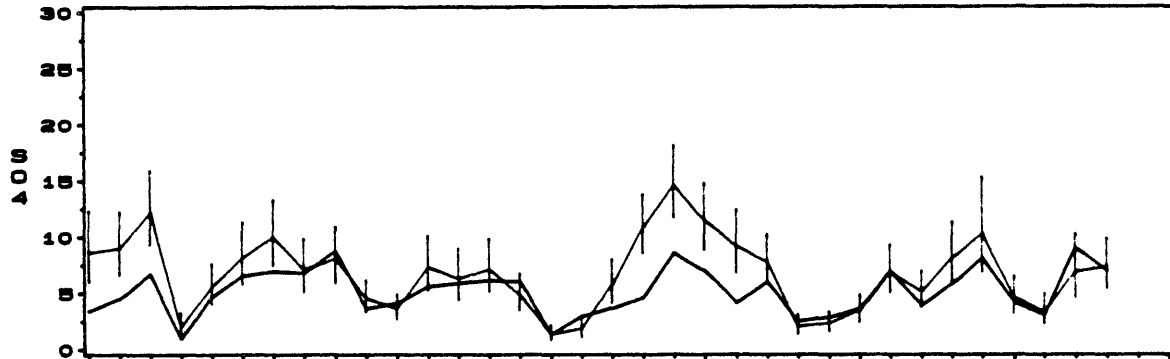


AVERAGE OF RADM 2.1 PREDICTIONS AND OBSERVATIONS
25AUG88 - 27SEP88
REGION 8

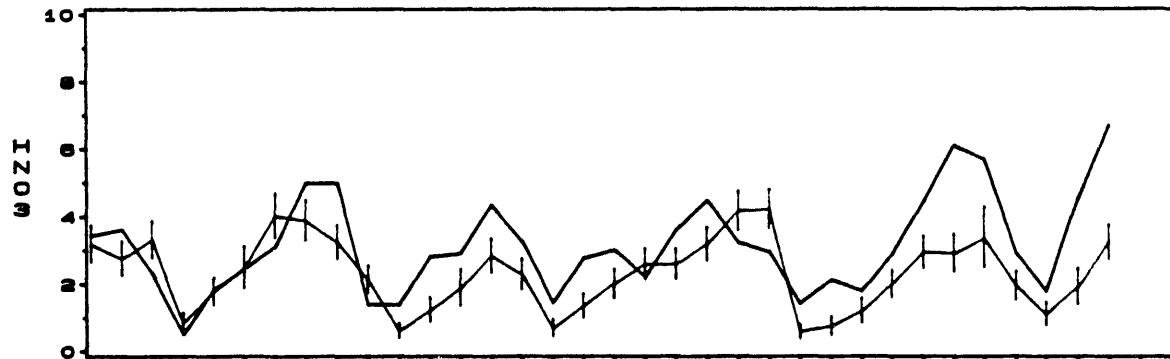
SO2 CONCENTRATION (UG/M3)



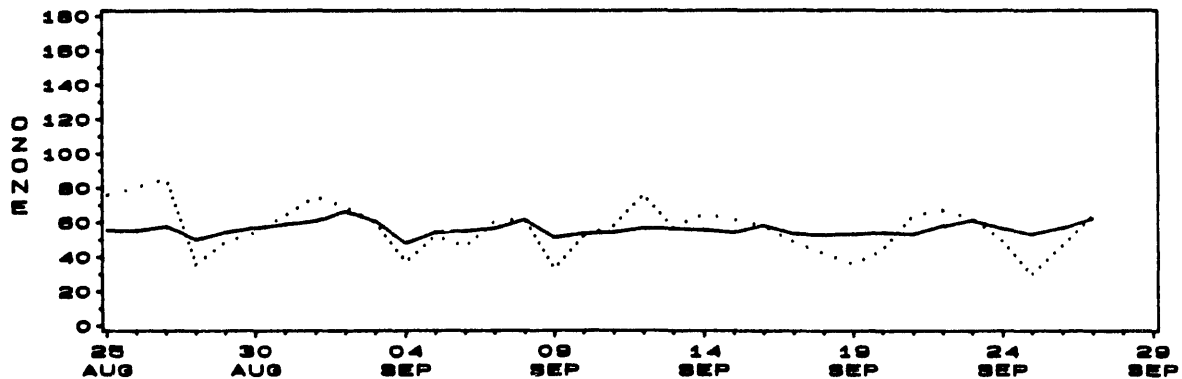
SO4 CONCENTRATION (UG/M3)



HNO3 CONCENTRATION (UG/M3)

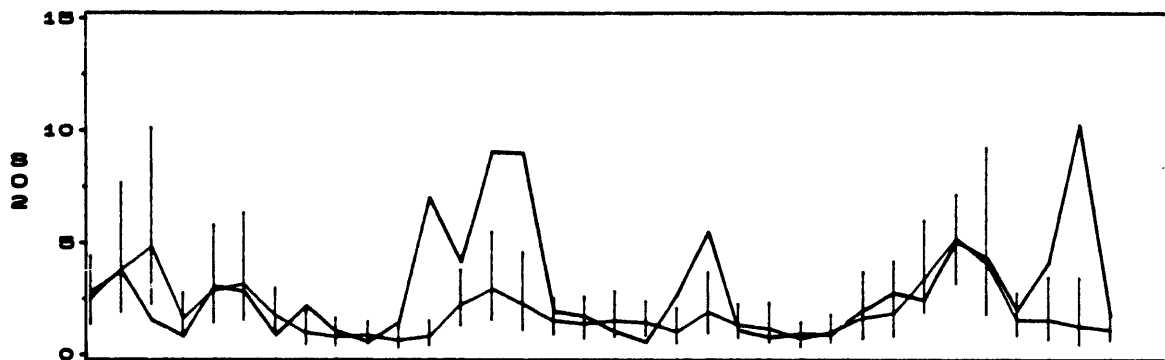


MAXIMUM OZONE 10AM-6PM (PPB)

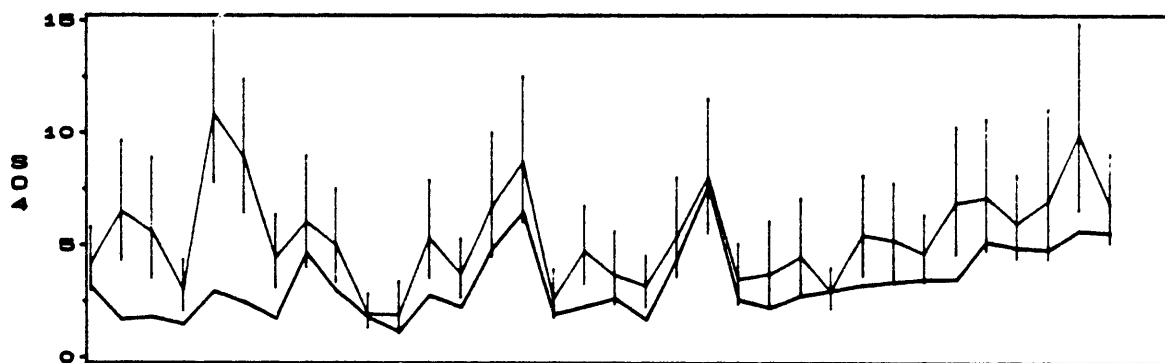


AVERAGE OF RADM 2.1 PREDICTIONS AND OBSERVATIONS
25AUG88 - 27SEP88
REGION 9

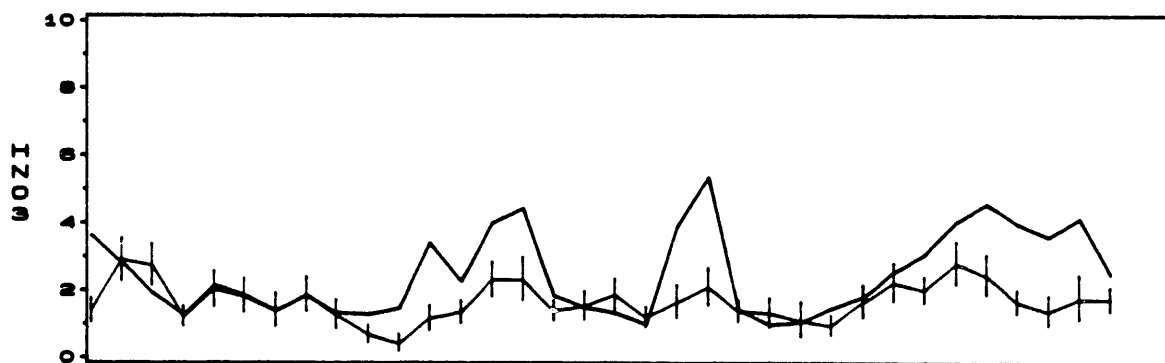
SO2 CONCENTRATION (UG/M3)



SO4 CONCENTRATION (UG/M3)



HNO3 CONCENTRATION (UG/M3)



MAXIMUM OZONE 10AM-6PM (PPB)

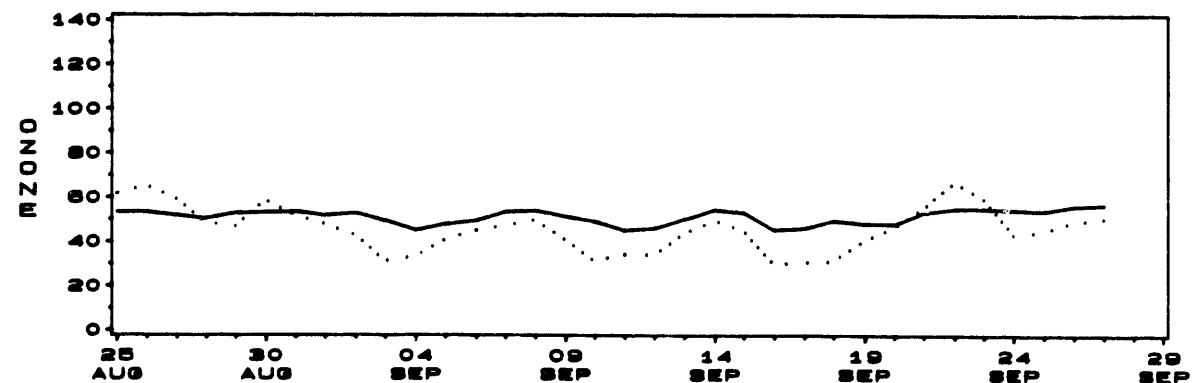
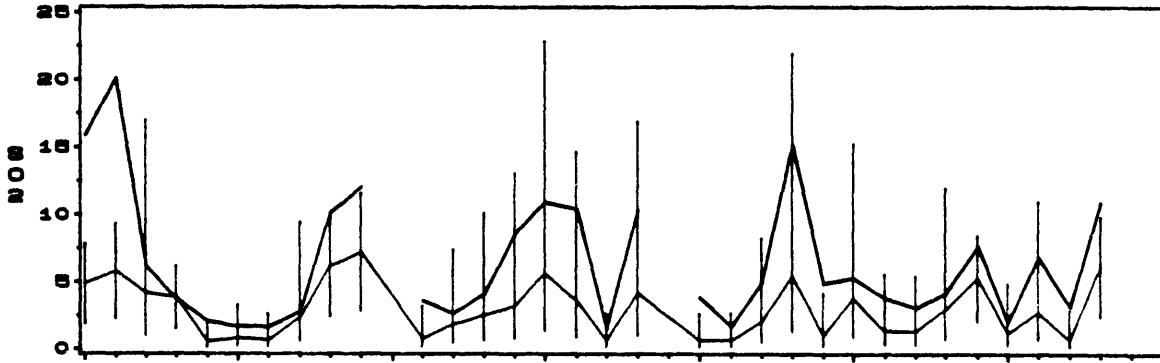


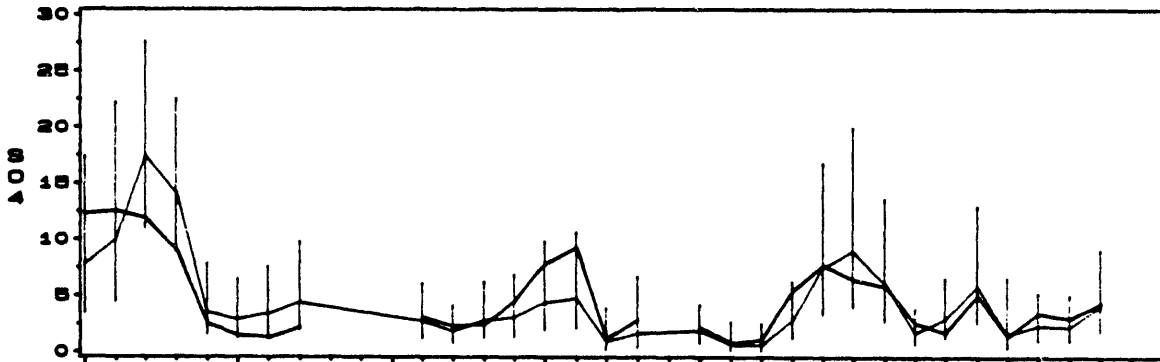
Figure A.2 The Daily Variation in the Regional Average RADM2.5-Predicted and EMEFS-Observed Concentration of SO₂, SO₄⁼ Aerosol, T-NO₃, and Maximum O₃ in All Regions

AVERAGE OF RADM 2.5/6L PREDICTIONS AND OBSERVATIONS
 25AUG88 - 27SEP88
 REGION M

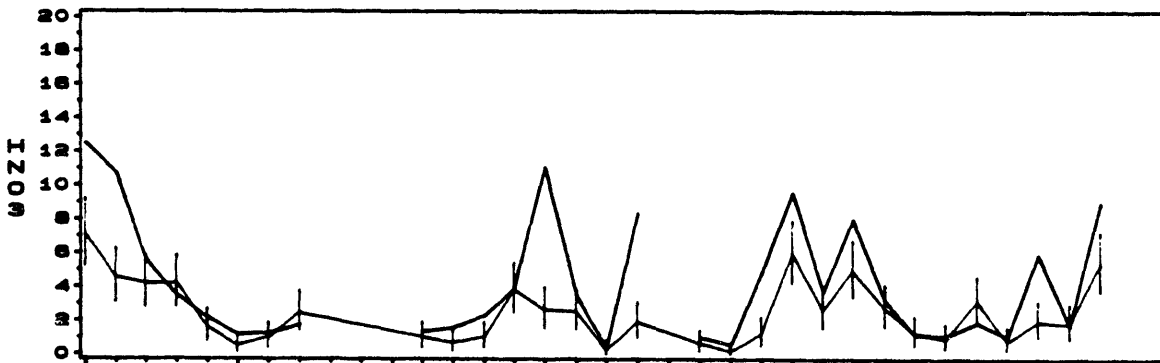
SO2 CONCENTRATION (UG/M3)



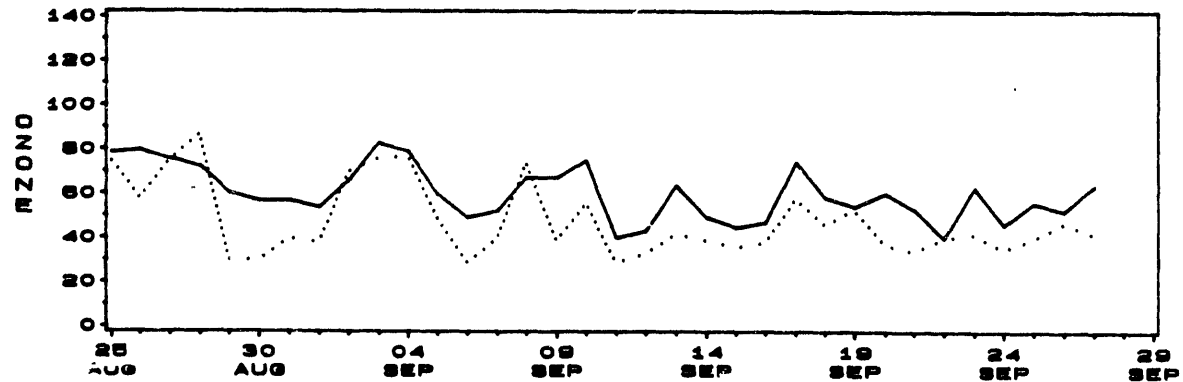
SO4 CONCENTRATION (UG/M3)



HNO3 CONCENTRATION (UG/M3)

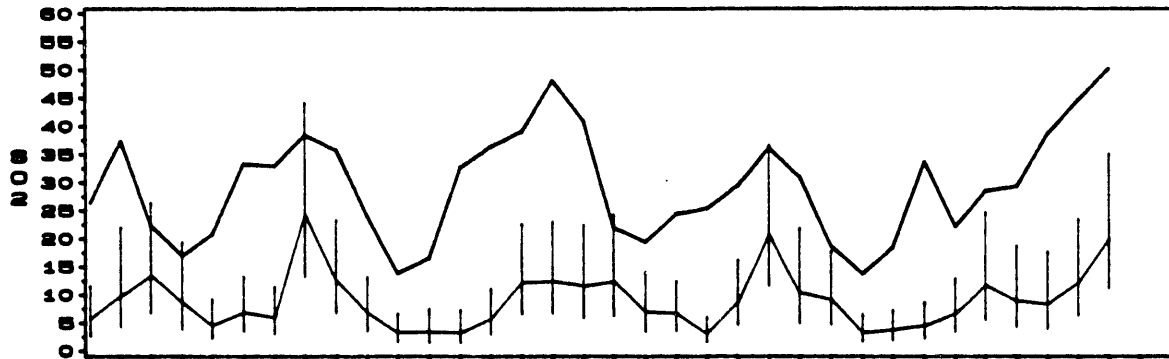


MAXIMUM OZONE 10AM-6PM (PPB)

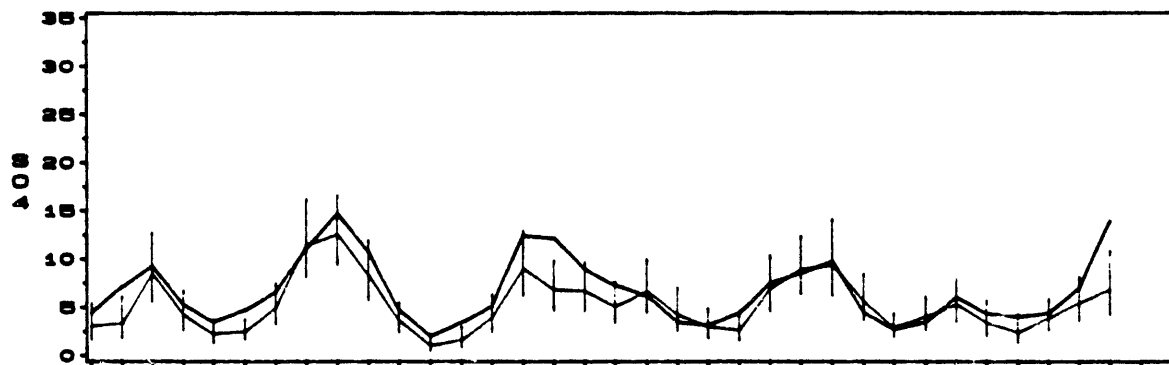


AVERAGE OF RADM 2.5/6L PREDICTIONS AND OBSERVATIONS
 25AUG88 - 27SEP88
 REGION U

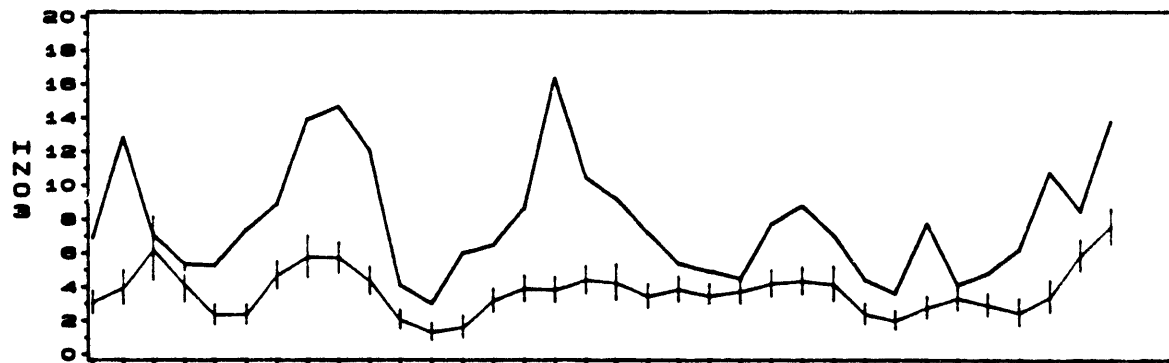
SO2 CONCENTRATION (UG/M3)



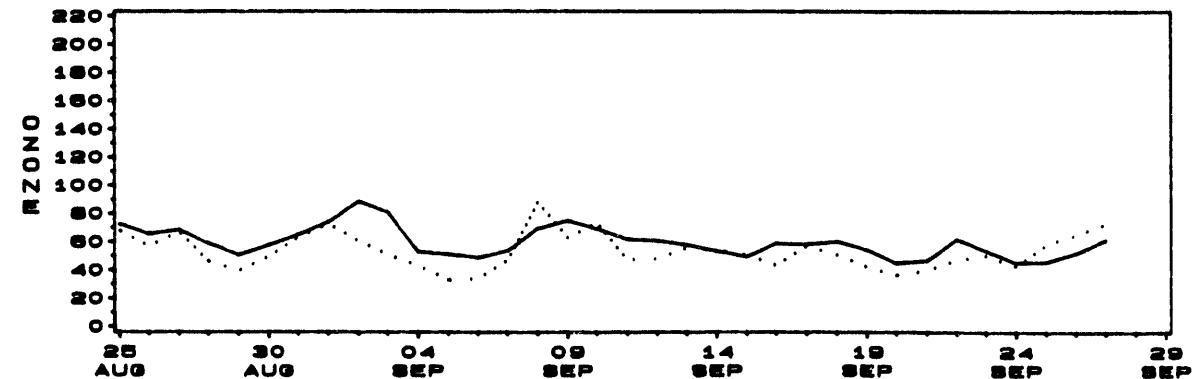
SO4 CONCENTRATION (UG/M3)



HNO3 CONCENTRATION (UG/M3)

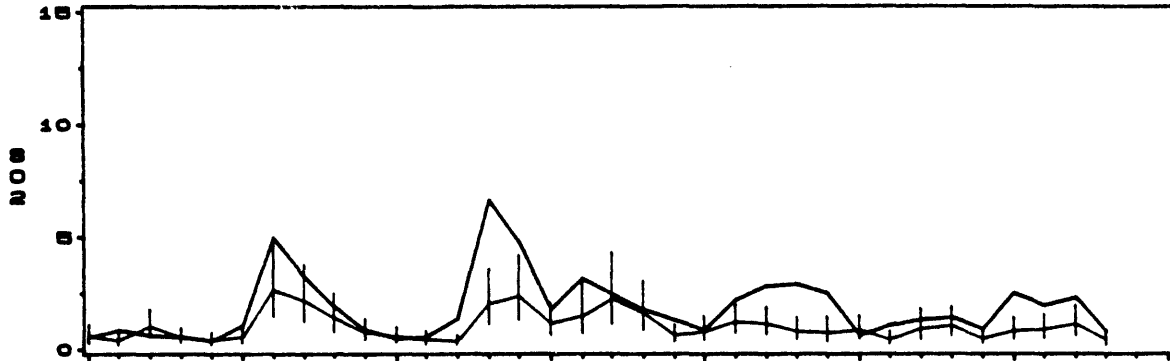


MAXIMUM OZONE 10AM-6PM (PPB)

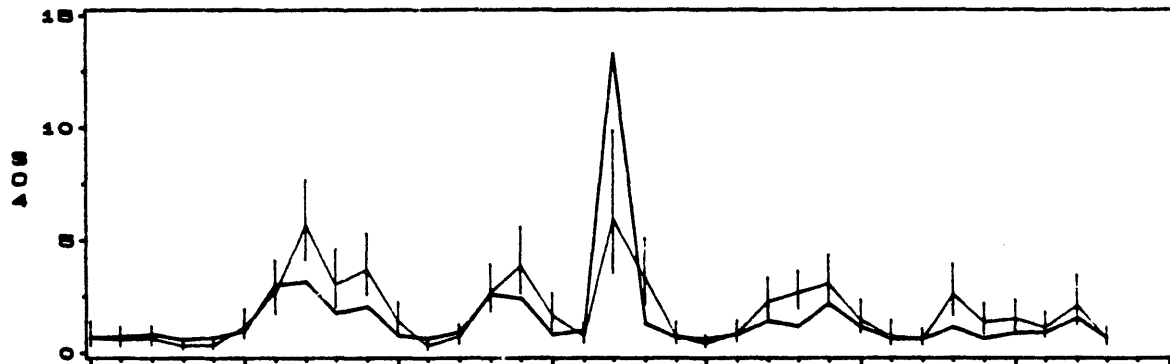


AVERAGE OF RADM 2.5/6L PREDICTIONS AND OBSERVATIONS
25AUG88 - 27SEP88
REGION 1

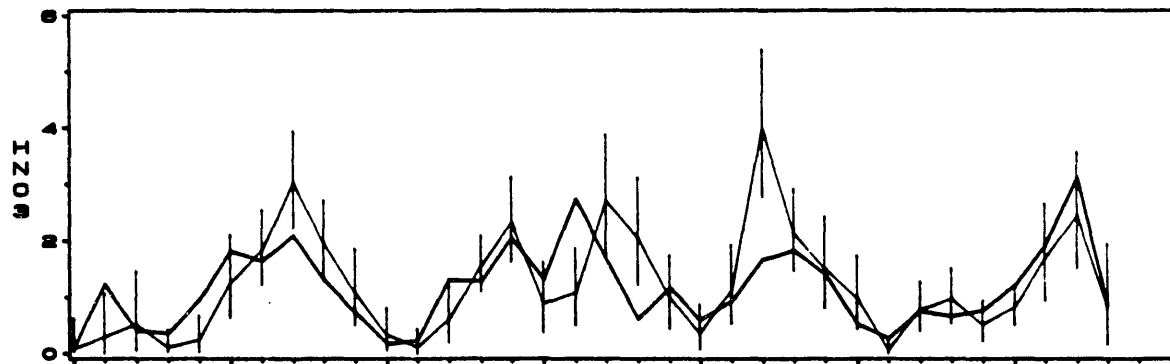
SO2 CONCENTRATION (UG/M3)



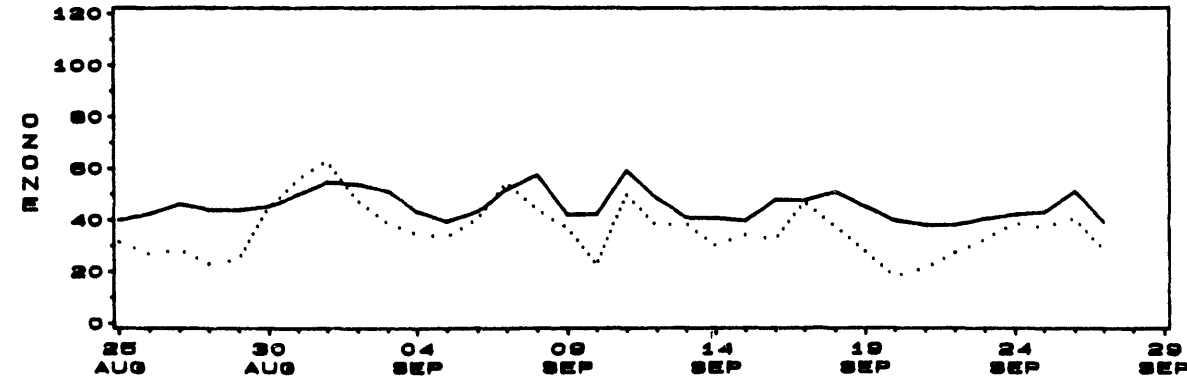
SO4 CONCENTRATION (UG/M3)



HNO3 CONCENTRATION (UG/M3)

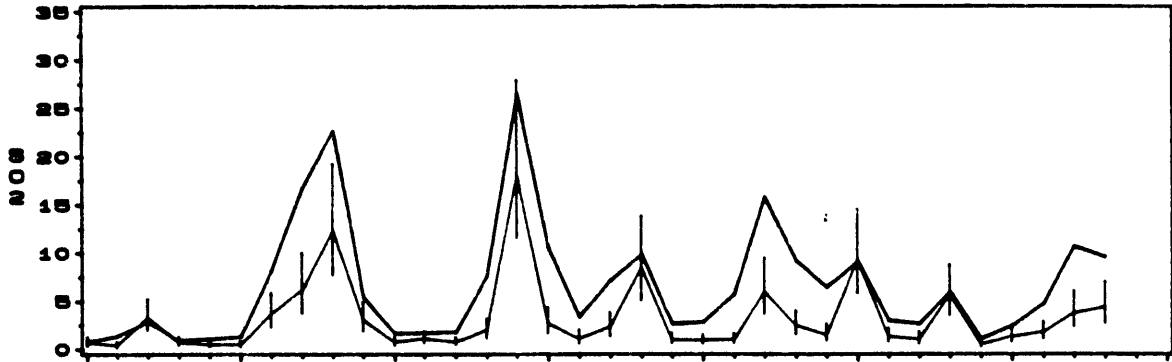


MAXIMUM OZONE 10AM-6PM (PPB)

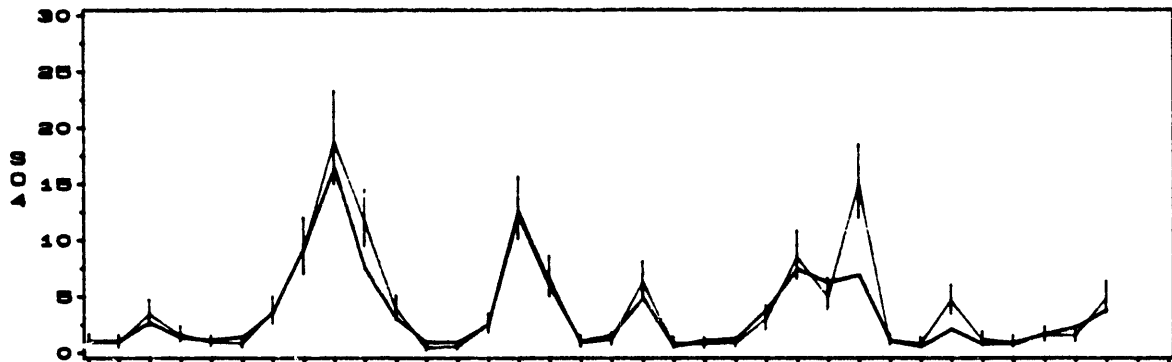


AVERAGE OF RADM 2.5/6L PREDICTIONS AND OBSERVATIONS
 25AUG88 – 27SEP88
 REGION 2

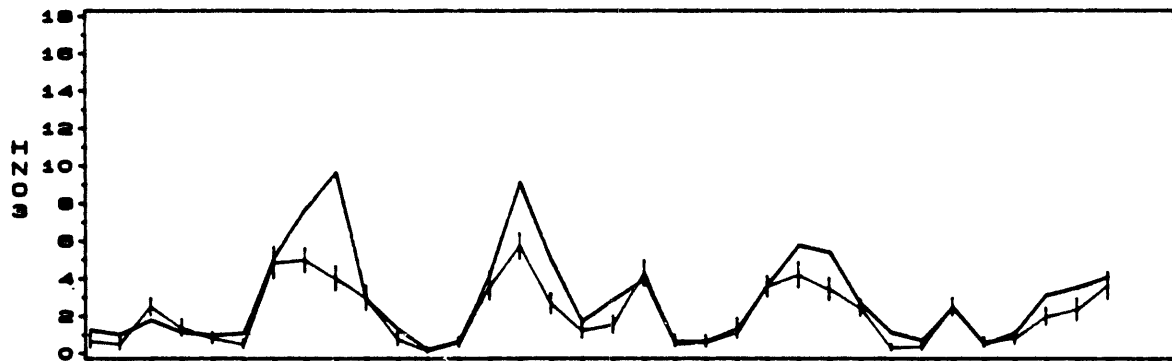
SO2 CONCENTRATION (UG/M3)



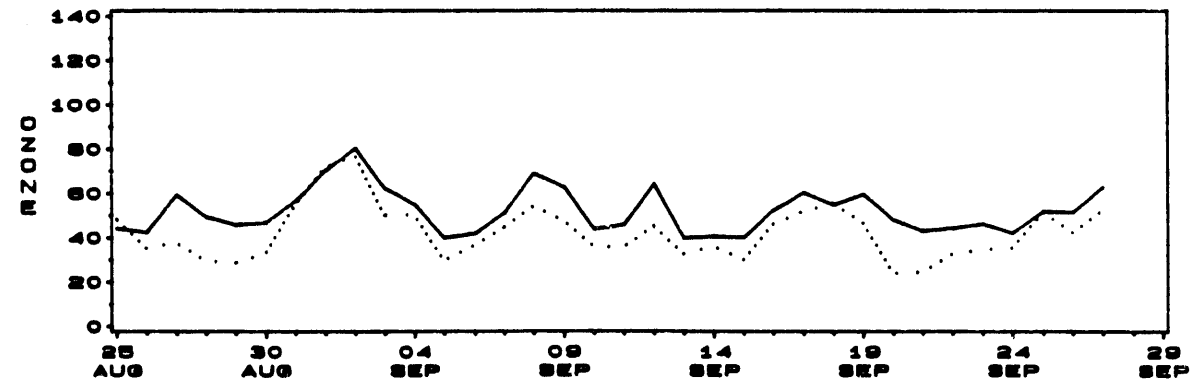
SO4 CONCENTRATION (UG/M3)



HNO3 CONCENTRATION (UG/M3)

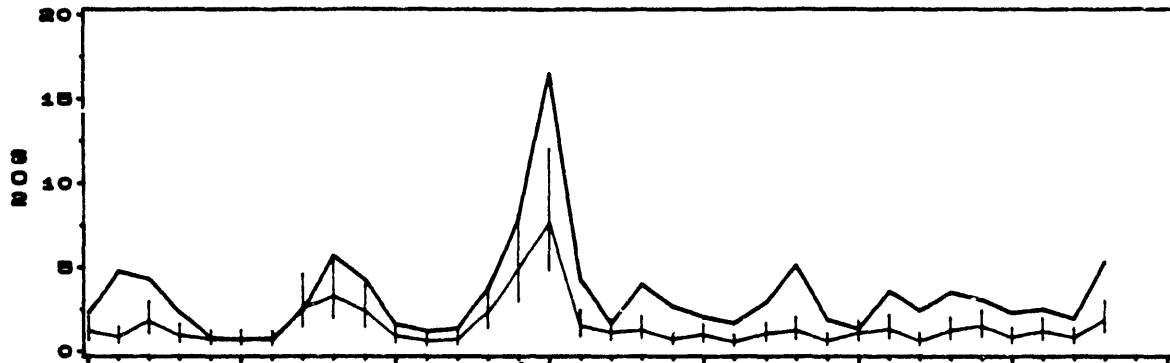


MAXIMUM OZONE 10AM-6PM (PPB)

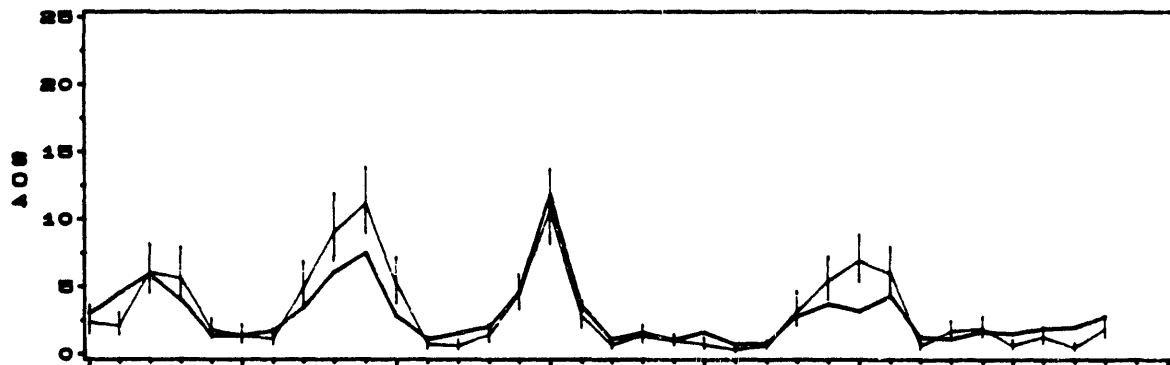


AVERAGE OF RADM 2.5/6L PREDICTIONS AND OBSERVATIONS
25AUG88 - 27SEP88
REGION 3

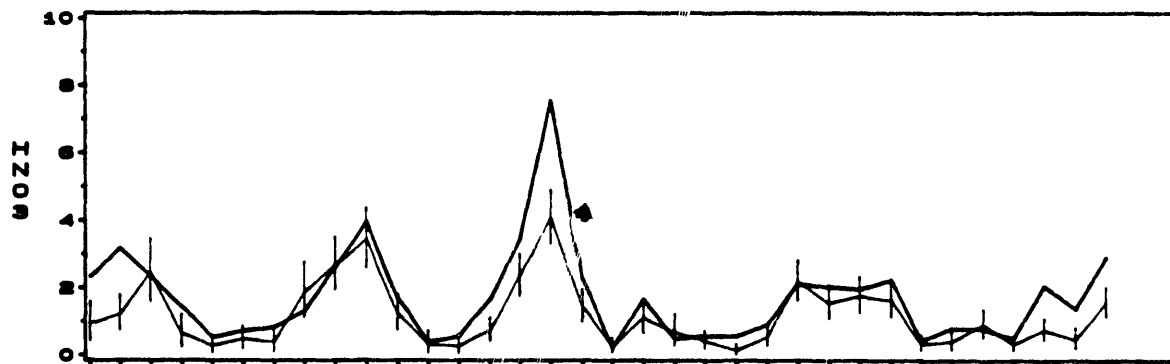
SO2 CONCENTRATION (UG/M3)



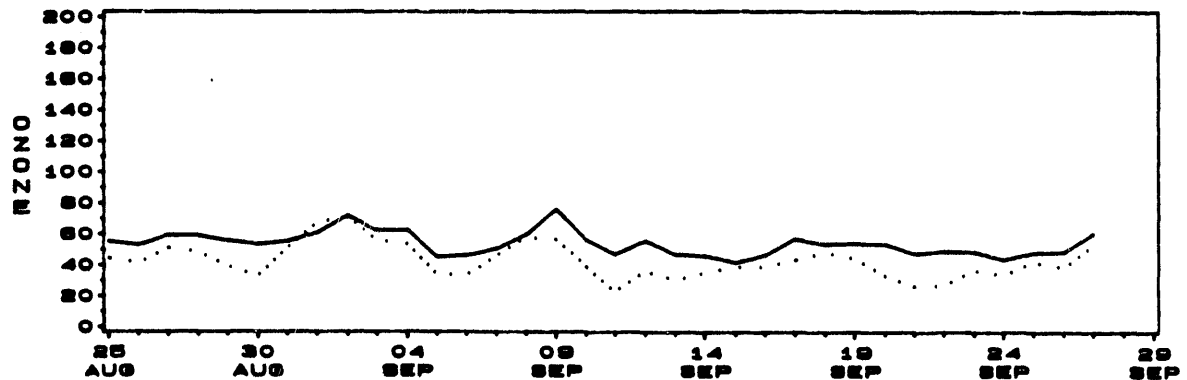
SO4 CONCENTRATION (UG/M3)



HNO3 CONCENTRATION (UG/M3)

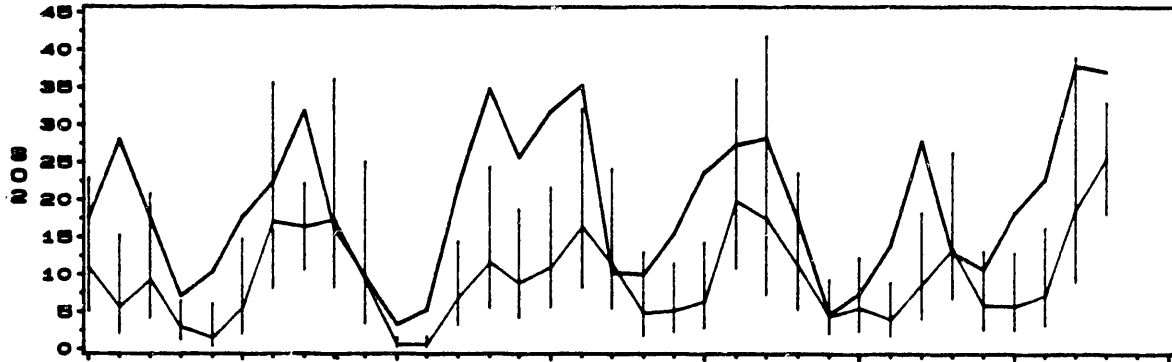


MAXIMUM OZONE 10AM-6PM (PPB)

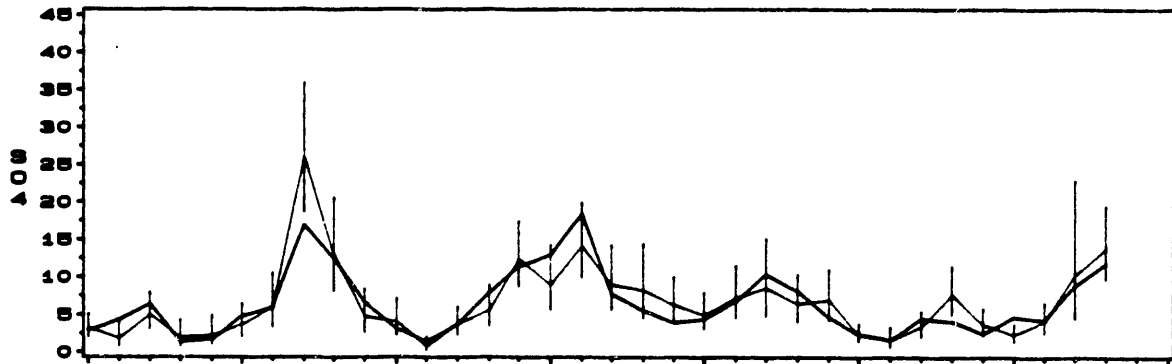


AVERAGE OF RADM 2.5/6L PREDICTIONS AND OBSERVATIONS
 25AUG88 - 27SEP88
 REGION 4

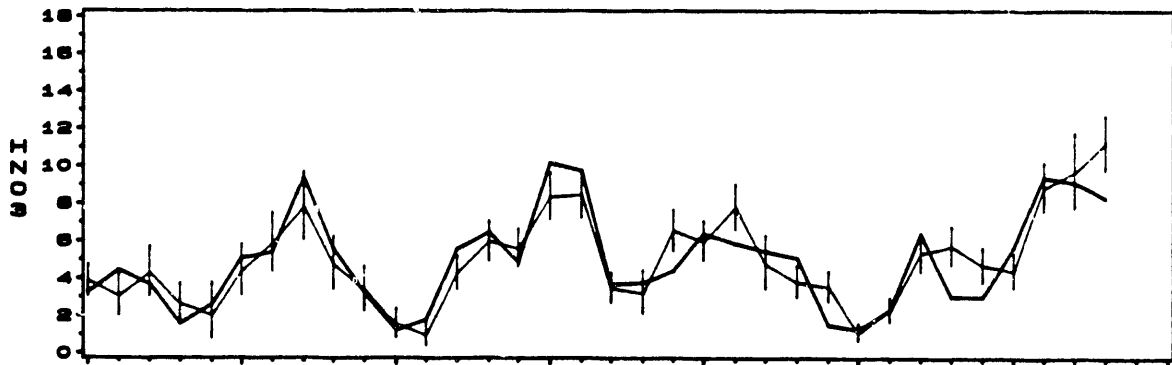
SO2 CONCENTRATION (UG/M3)



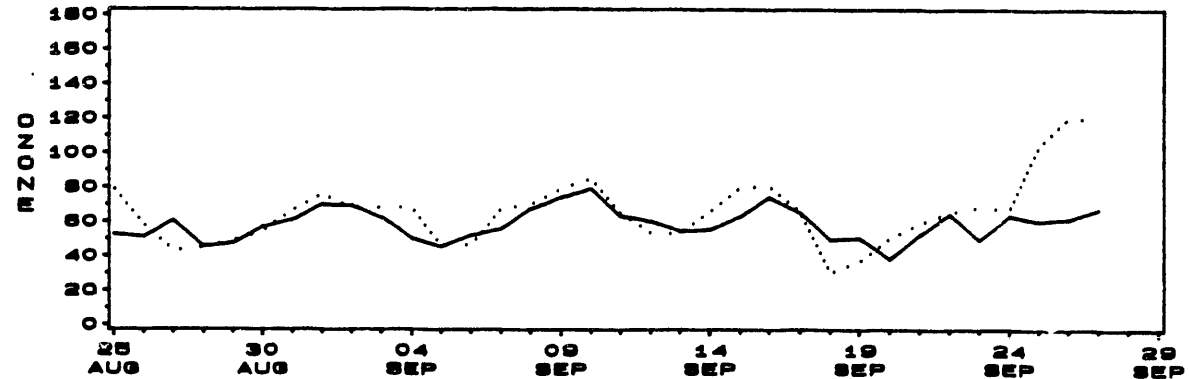
SO4 CONCENTRATION (UG/M3)



HN03 CONCENTRATION (UG/M3)

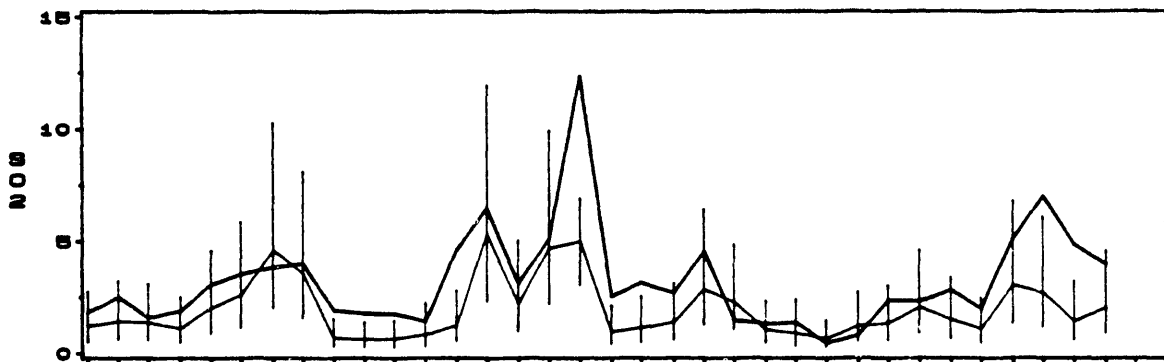


MAXIMUM OZONE 10AM-6PM (PPB)

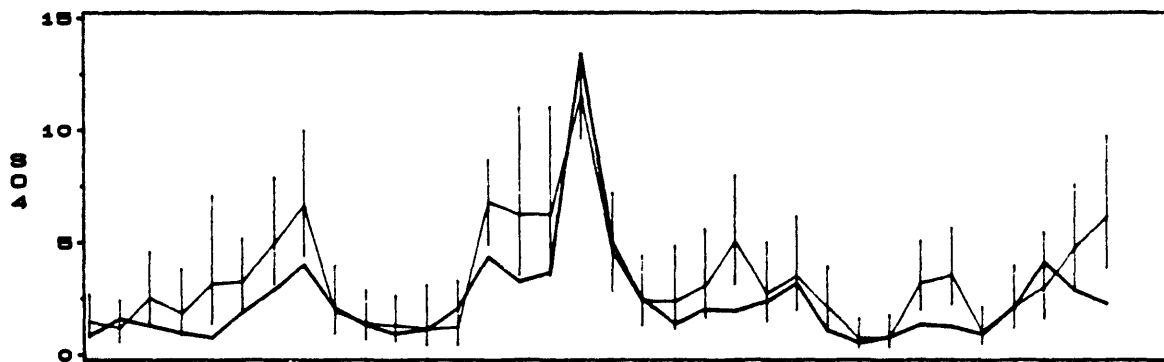


AVERAGE OF RADM 2.5/6L PREDICTIONS AND OBSERVATIONS
25AUG88 - 27SEP88
REGION 4A

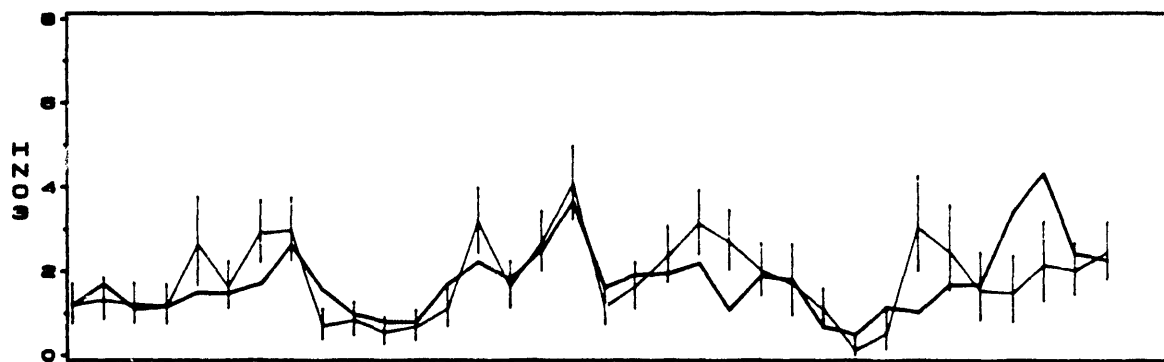
SO2 CONCENTRATION (UG/M3)



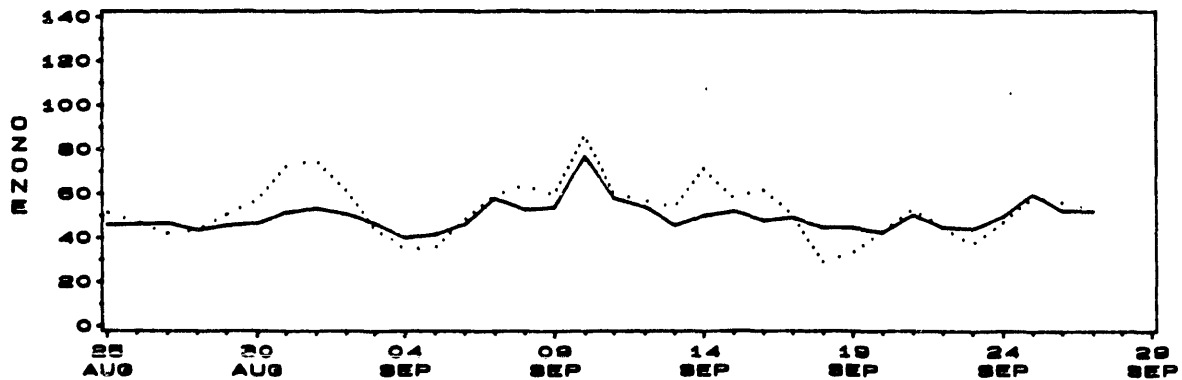
SO4 CONCENTRATION (UG/M3)



HNO3 CONCENTRATION (UG/M3)

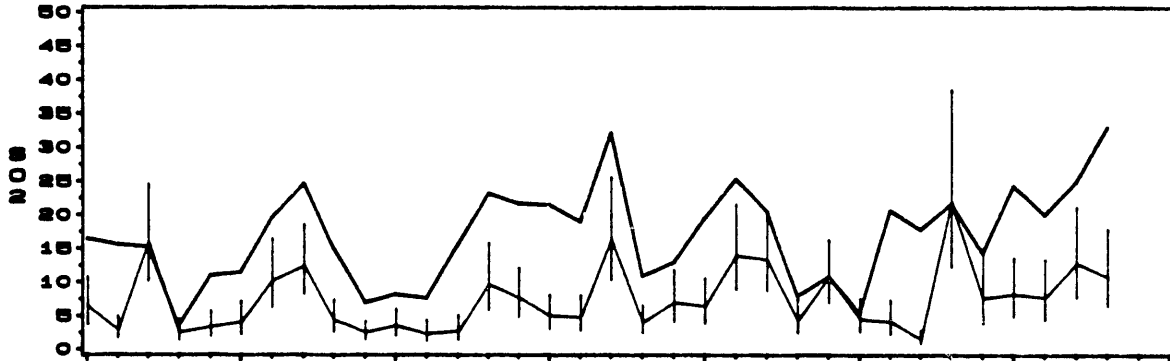


MAXIMUM OZONE 10AM-6PM (PPB)

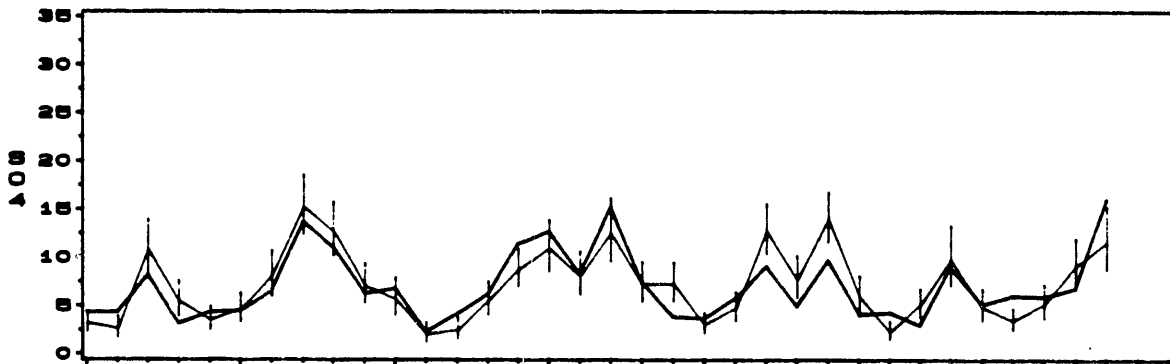


AVERAGE OF RADM 2.5/6L PREDICTIONS AND OBSERVATIONS
 25AUG88 - 27SEP88
 REGION 5

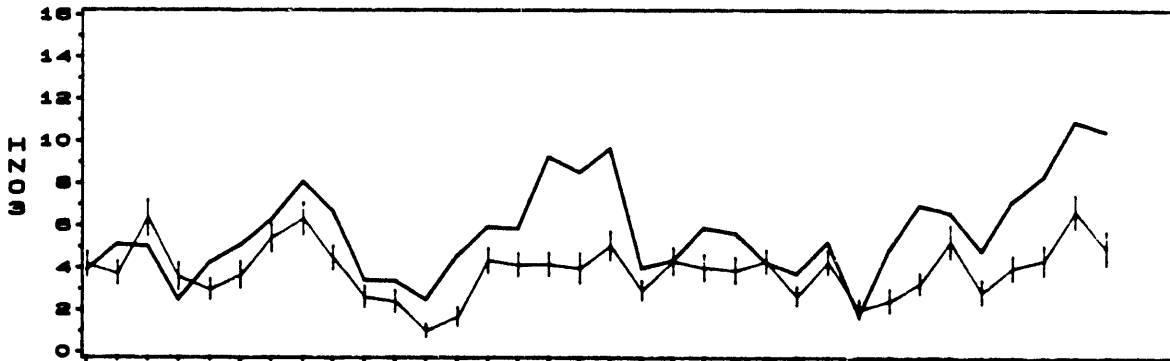
SO2 CONCENTRATION (UG/M3)



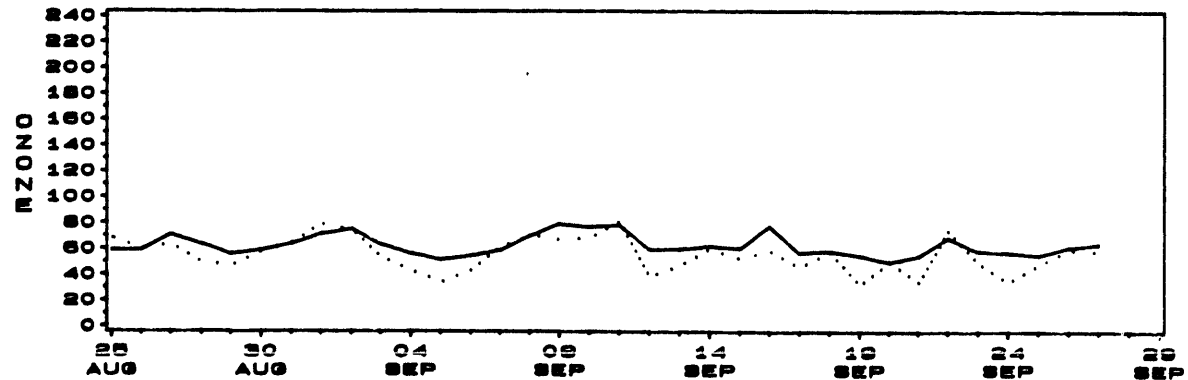
SO4 CONCENTRATION (UG/M3)



HNO3 CONCENTRATION (UG/M3)

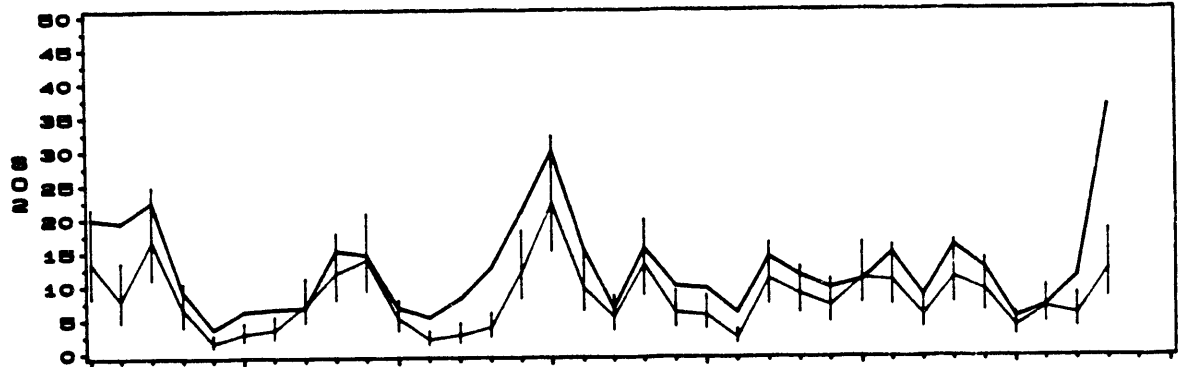


MAXIMUM OZONE 10AM-6PM (PPB)

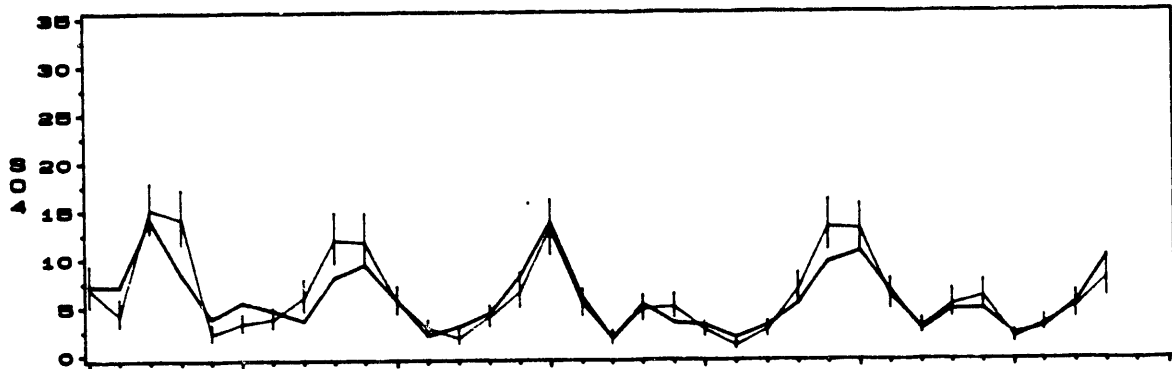


AVERAGE OF RADM 2.5/6L PREDICTIONS AND OBSERVATIONS
 25AUG88 - 27SEP88
 REGION 6

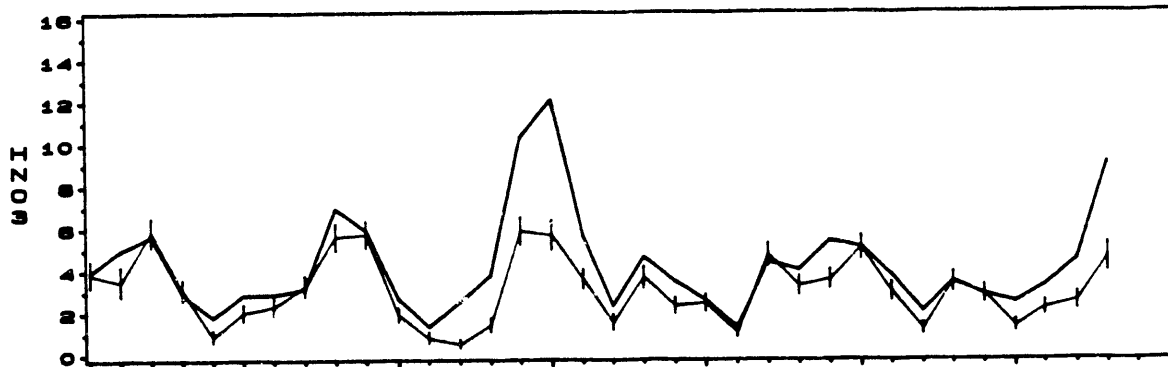
SO2 CONCENTRATION (UG/M3)



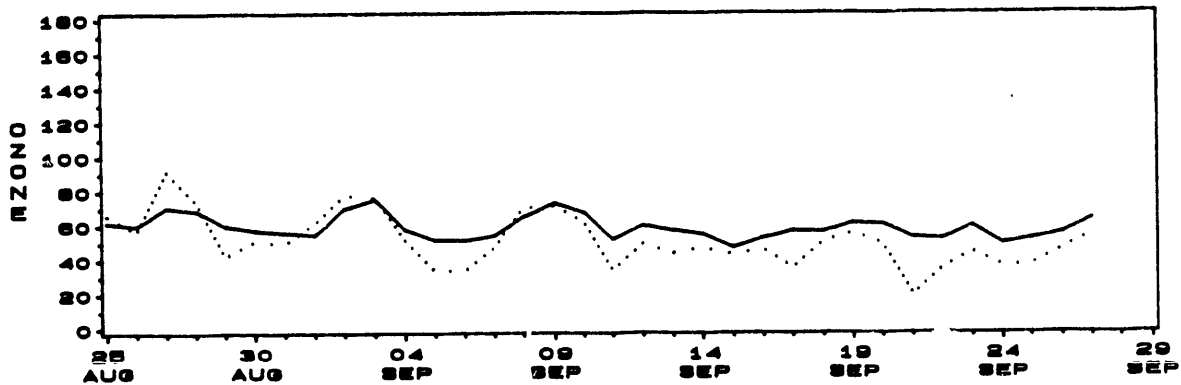
SO4 CONCENTRATION (UG/M3)



HNO3 CONCENTRATION (UG/M3)

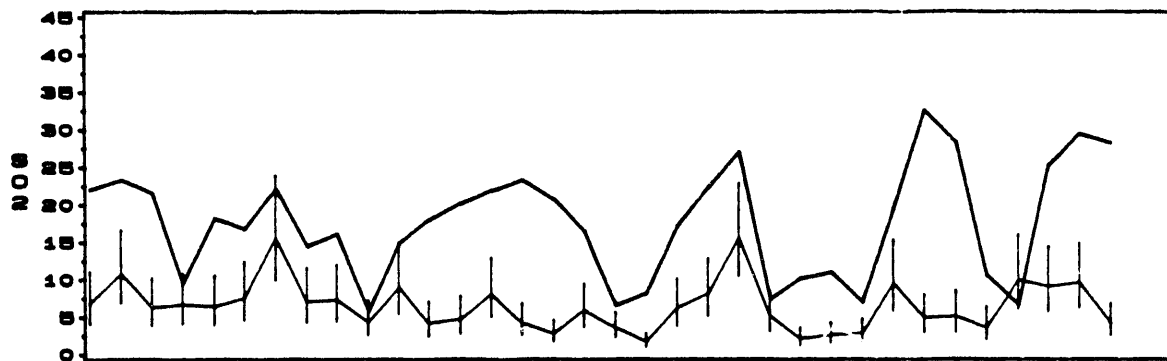


MAXIMUM OZONE 10AM-6PM (PPB)

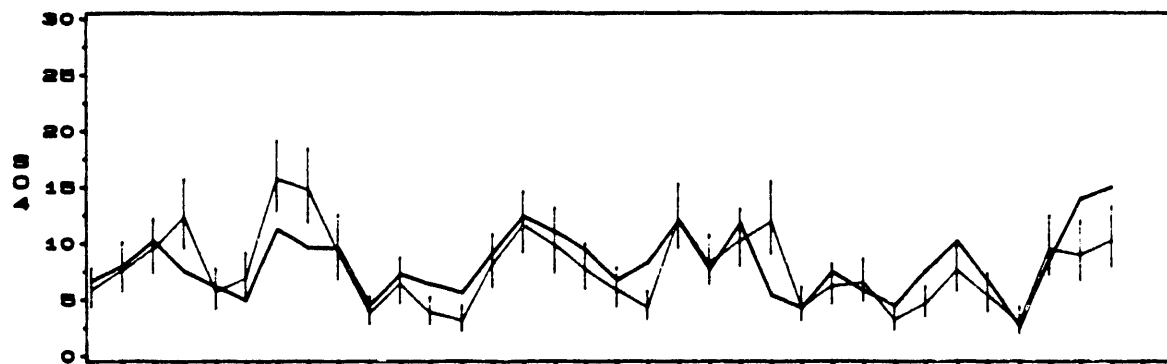


AVERAGE OF RADM 2.5/6L PREDICTIONS AND OBSERVATIONS
 25AUG88 - 27SEP88
 REGION 7

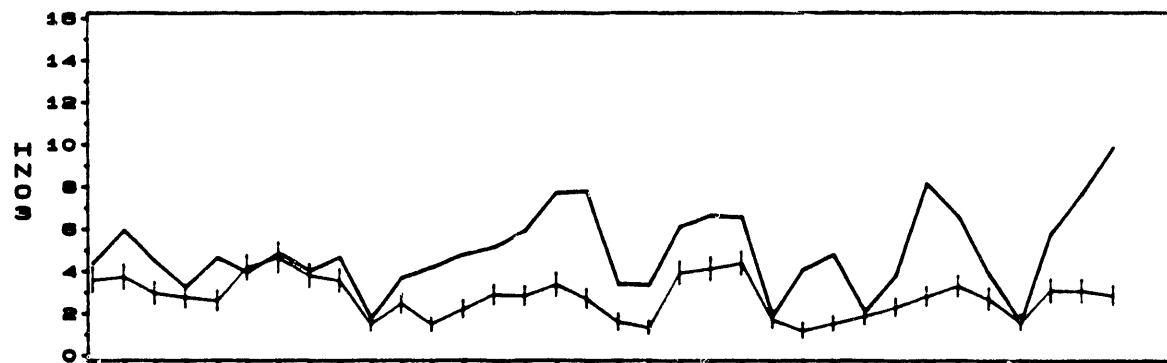
SO2 CONCENTRATION (UG/M3)



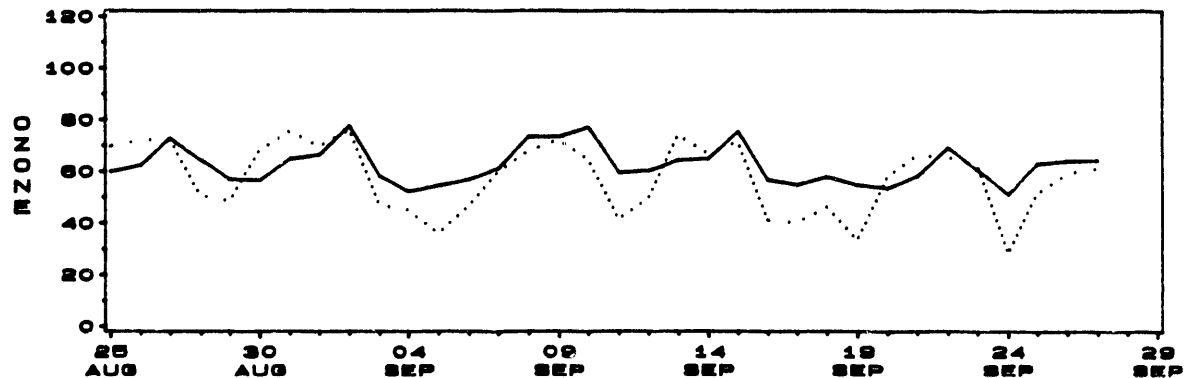
SO4 CONCENTRATION (UG/M3)



HNO3 CONCENTRATION (UG/M3)

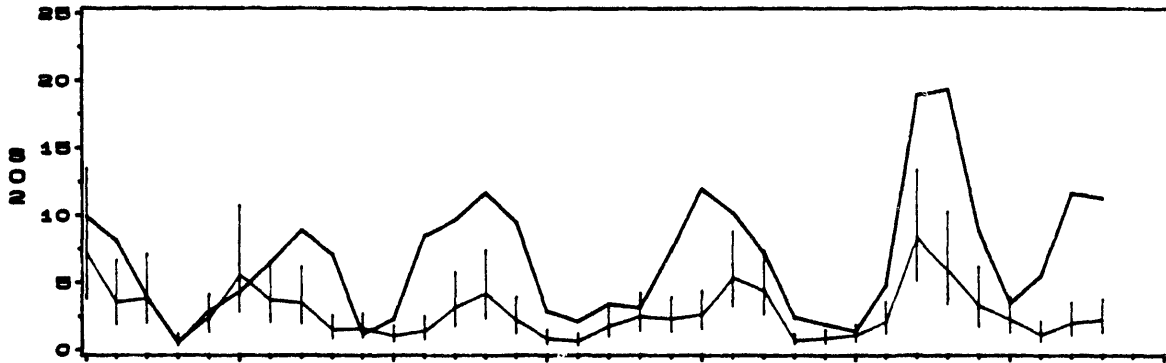


MAXIMUM OZONE 10AM-6PM (PPB)

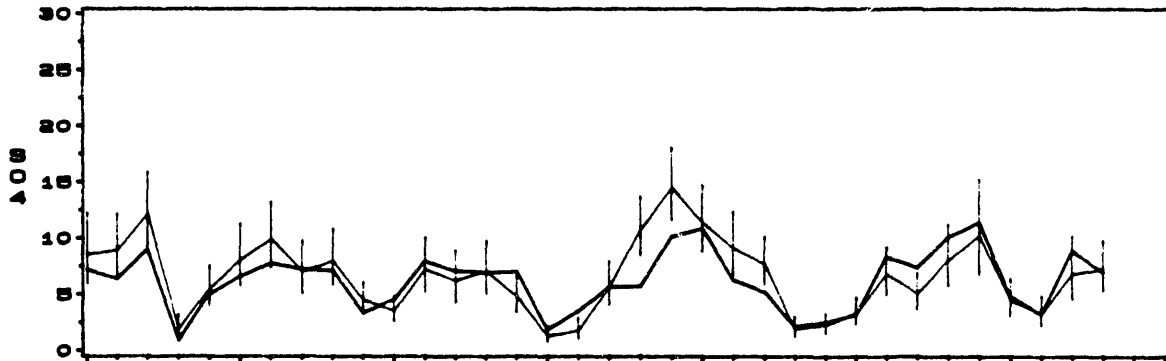


AVERAGE OF RADM 2.5/6L PREDICTIONS AND OBSERVATIONS
25AUG88 - 27SEP88
REGION 8

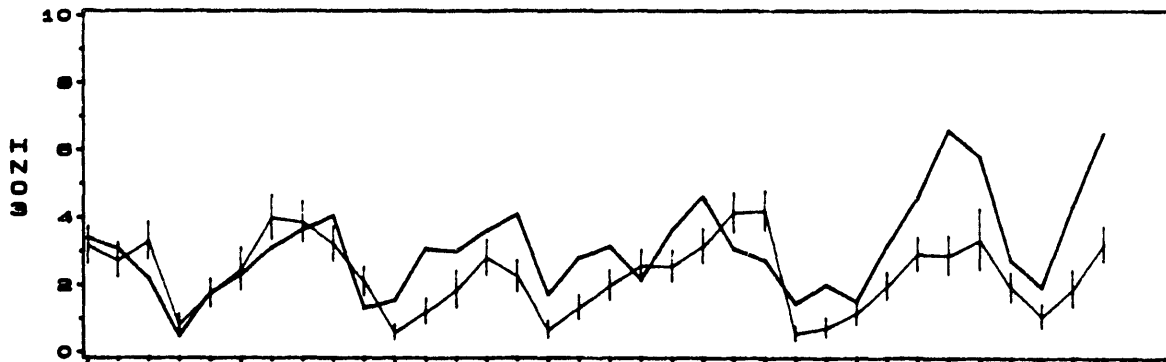
SO2 CONCENTRATION (UG/M3)



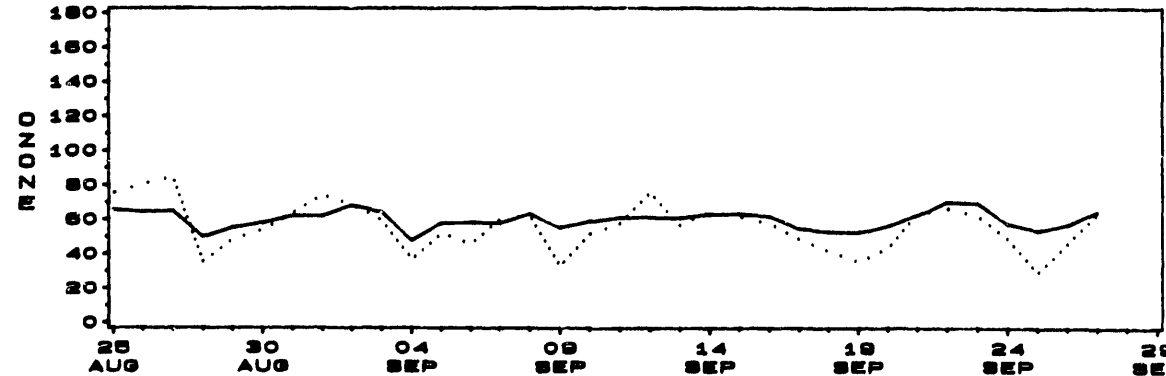
SO4 CONCENTRATION (UG/M3)



HNO3 CONCENTRATION (UG/M3)

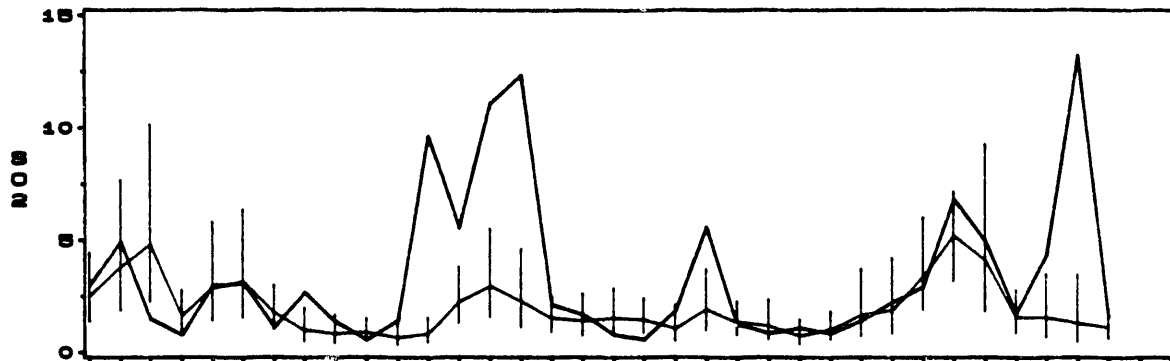


MAXIMUM OZONE 10AM-6PM (PPB)

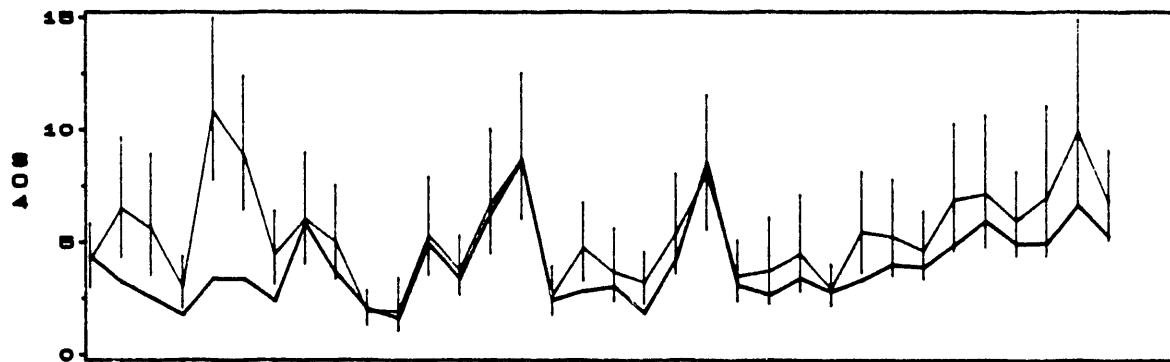


AVERAGE OF RADM 2.5/6L PREDICTIONS AND OBSERVATIONS
 25AUG88 – 27SEP88
 REGION 9

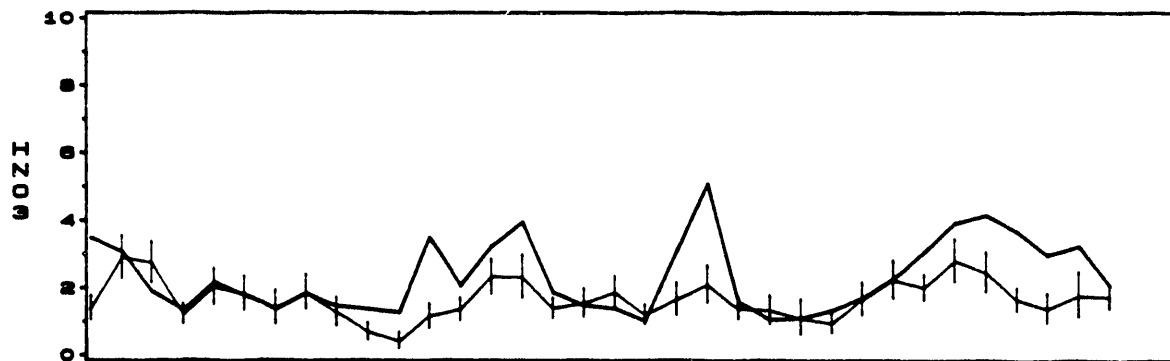
SO2 CONCENTRATION (UG/M3)



SO4 CONCENTRATION (UG/M3)



HNO3 CONCENTRATION (UG/M3)



MAXIMUM OZONE 10AM-6PM (PPB)

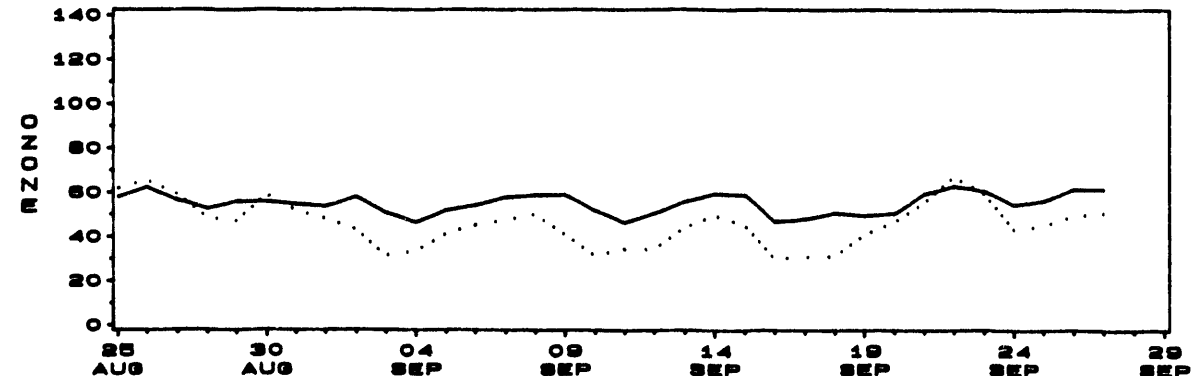
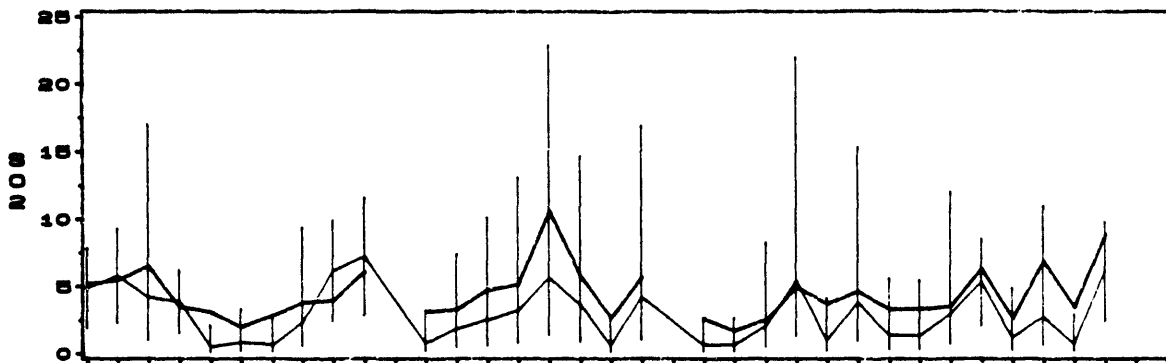


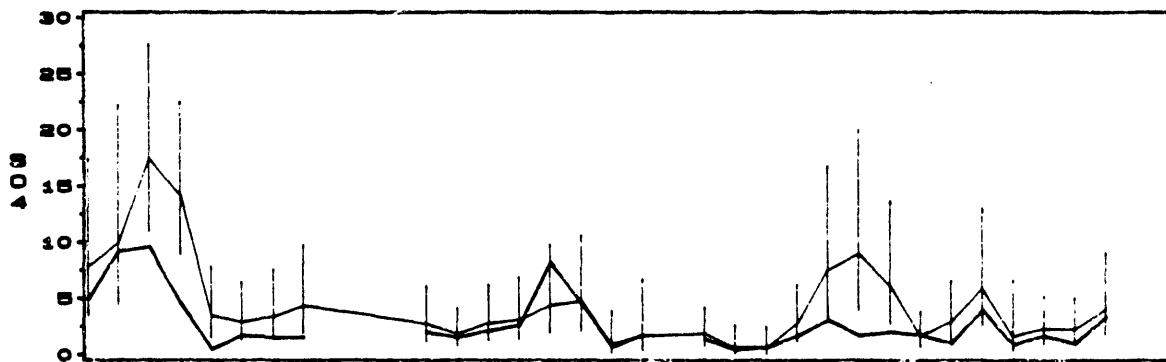
Figure A.3 The Daily Variation in the Regional Average ADOM2Bf-Predicted and EMEFS-Observed Concentration of SO₂, SO₄⁼ Aerosol, T-NO₃, and Maximum O₃ in All Regions

AVERAGE OF ADOM2BF PREDICTIONS AND OBSERVATIONS
25AUG88 - 27SEP88
REGION M

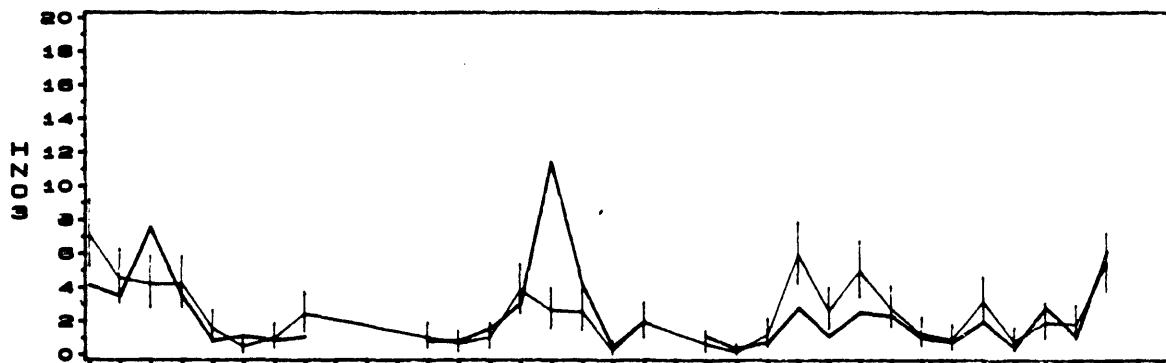
SO2 CONCENTRATION (UG/M3)



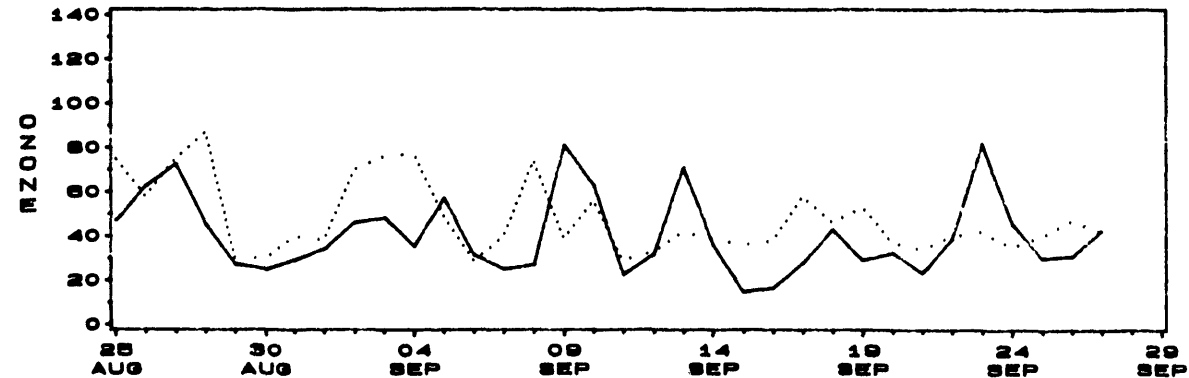
SO4 CONCENTRATION (UG/M3)



HNO3 CONCENTRATION (UG/M3)

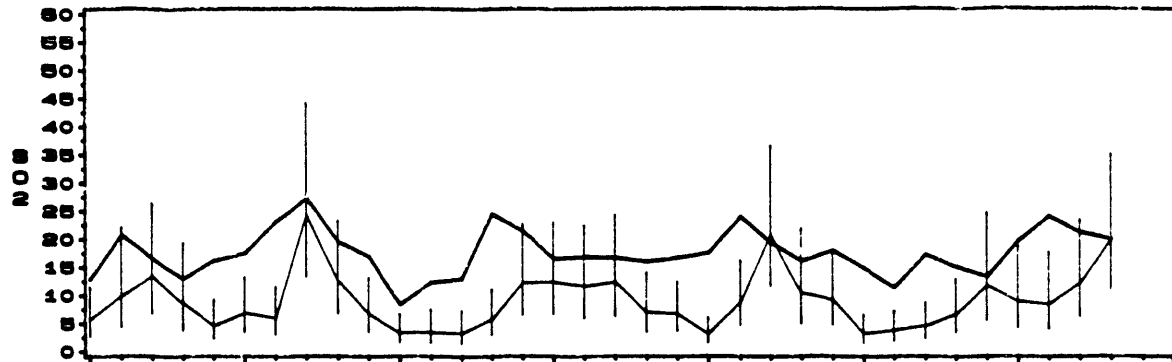


MAXIMUM OZONE 10AM-6PM (PPB)

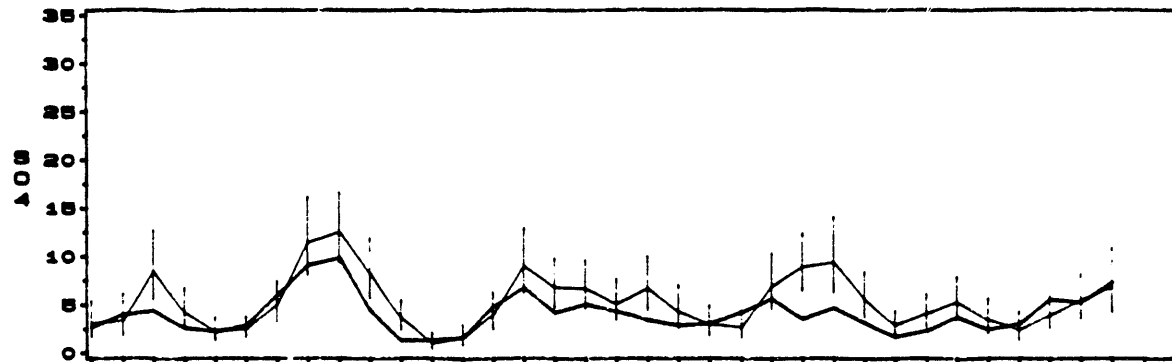


AVERAGE OF ADOM2BF PREDICTIONS AND OBSERVATIONS
 25AUG88 – 27SEP88
 REGION U

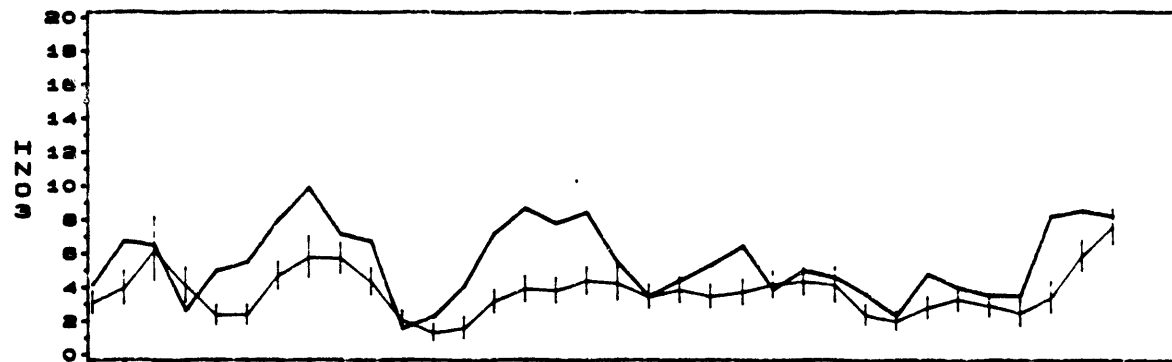
SO2 CONCENTRATION (UG/M3)



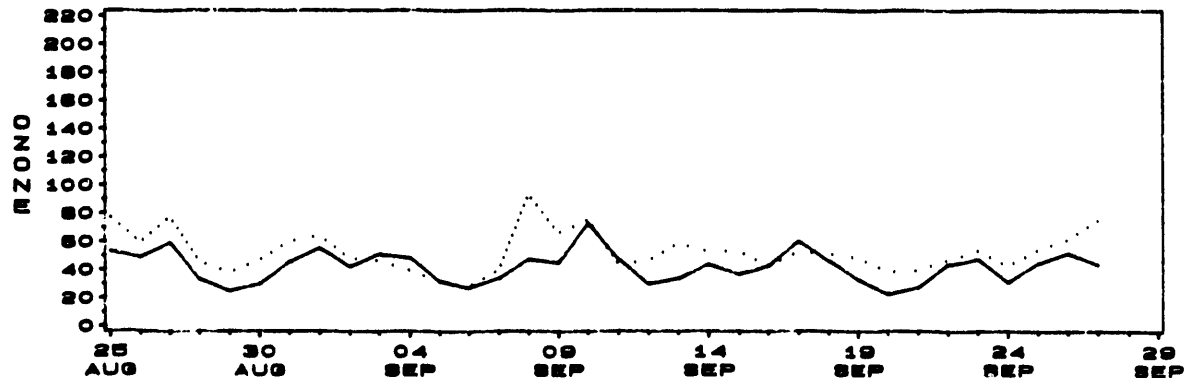
SO4 CONCENTRATION (UG/M3)



HNO3 CONCENTRATION (UG/M3)

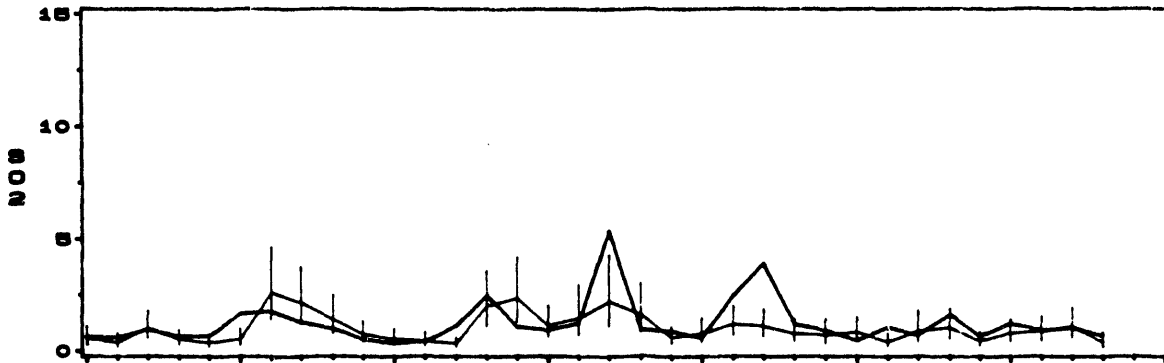


MAXIMUM OZONE 10AM-6PM (PPB)

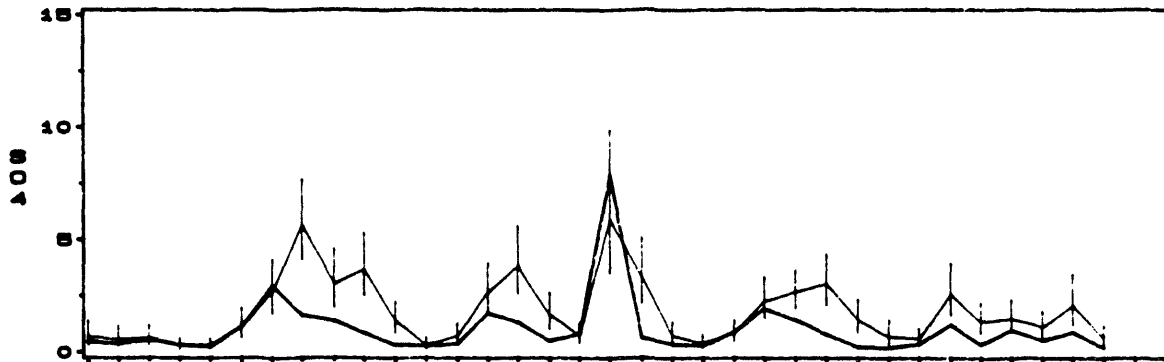


AVERAGE OF ADOM2BF PREDICTIONS AND OBSERVATIONS
25AUG88 - 27SEP88
REGION 1

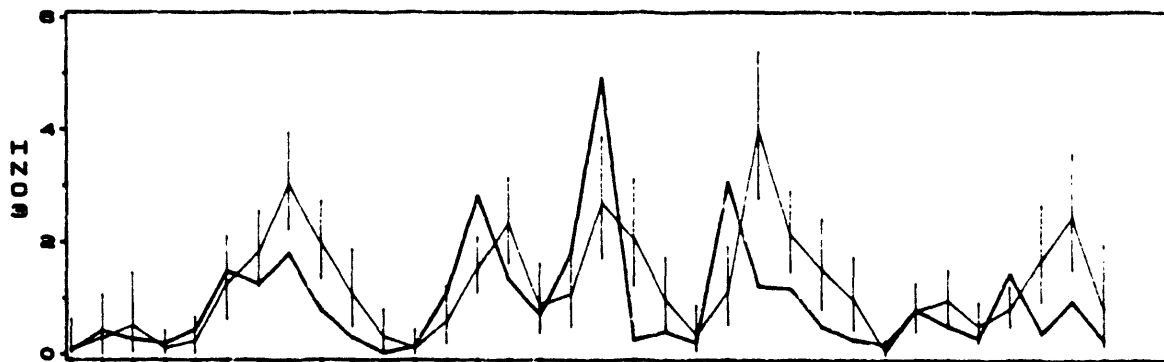
SO2 CONCENTRATION (UG/M3)



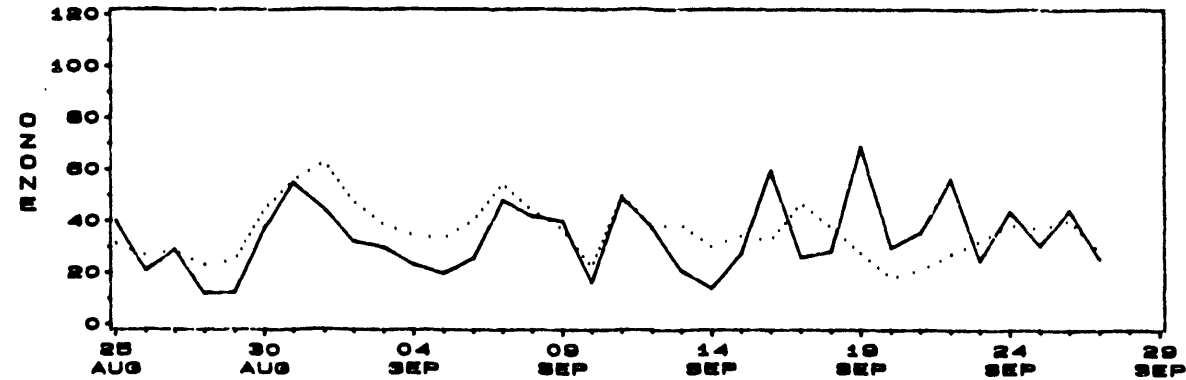
SO4 CONCENTRATION (UG/M3)



HNO3 CONCENTRATION (UG/M3)

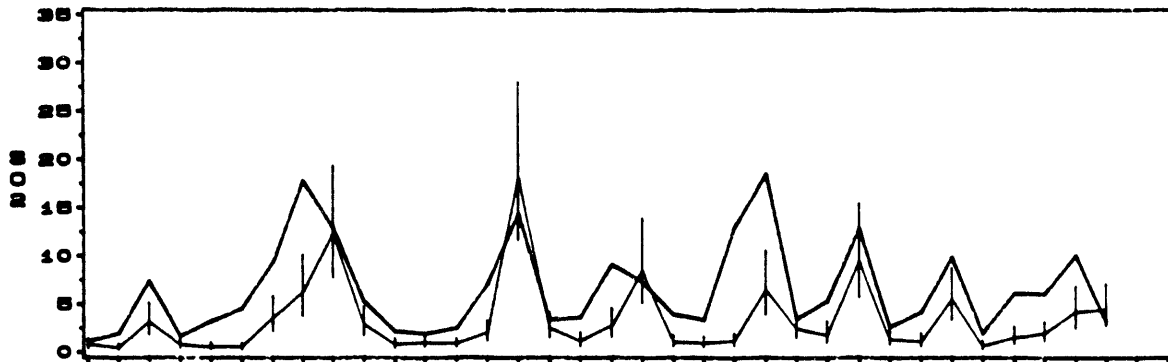


MAXIMUM OZONE 10AM-6PM (PPB)

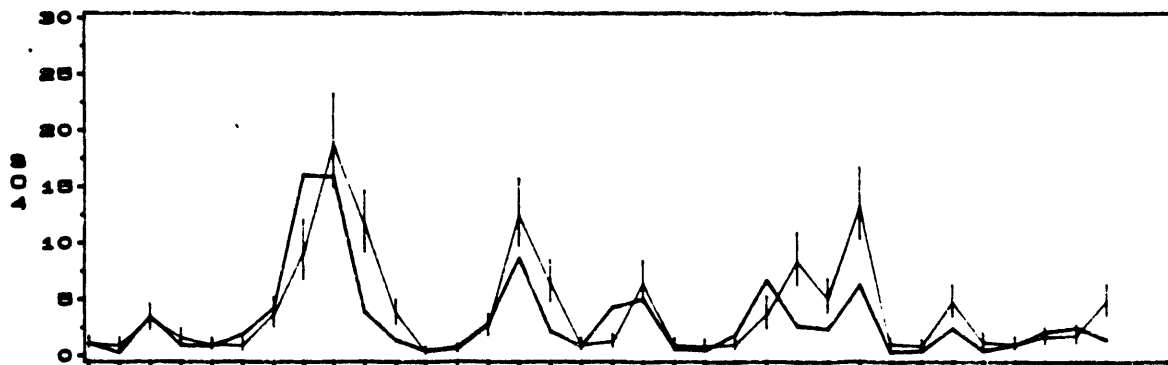


AVERAGE OF ADOM2BF PREDICTIONS AND OBSERVATIONS
25AUG88 - 27SEP88
REGION 2

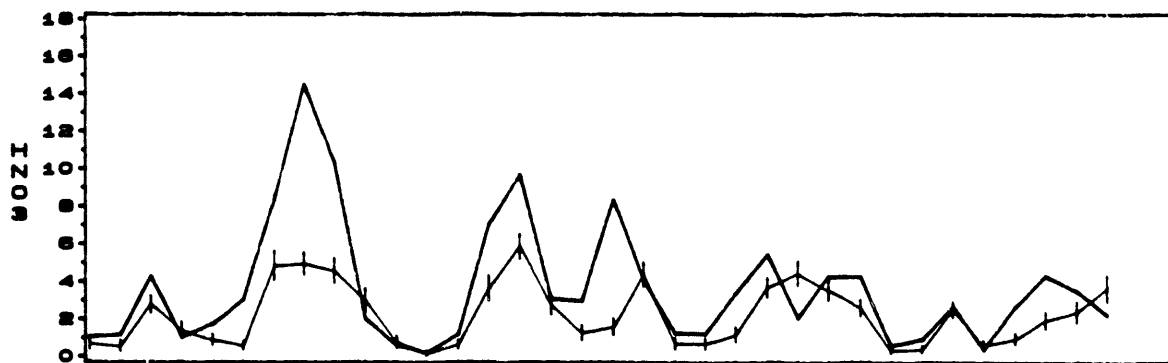
SO2 CONCENTRATION (UG/M3)



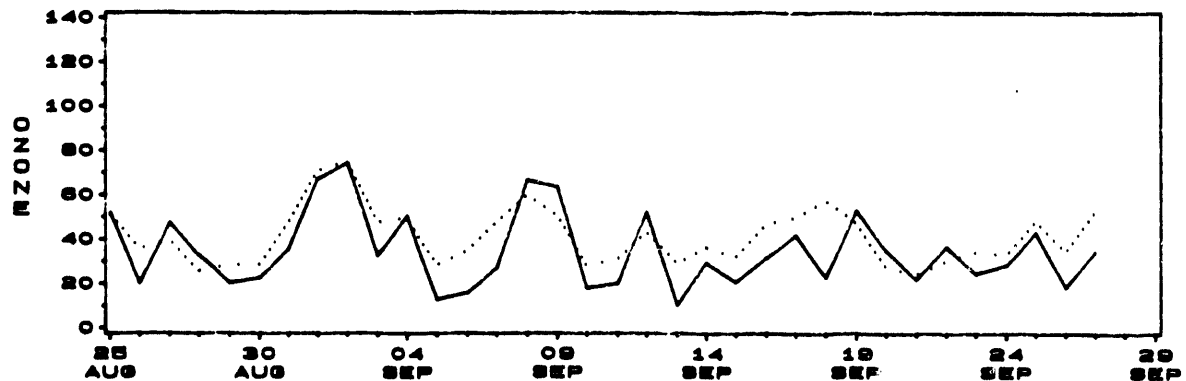
SO4 CONCENTRATION (UG/M3)



HN03 CONCENTRATION (UG/M3)

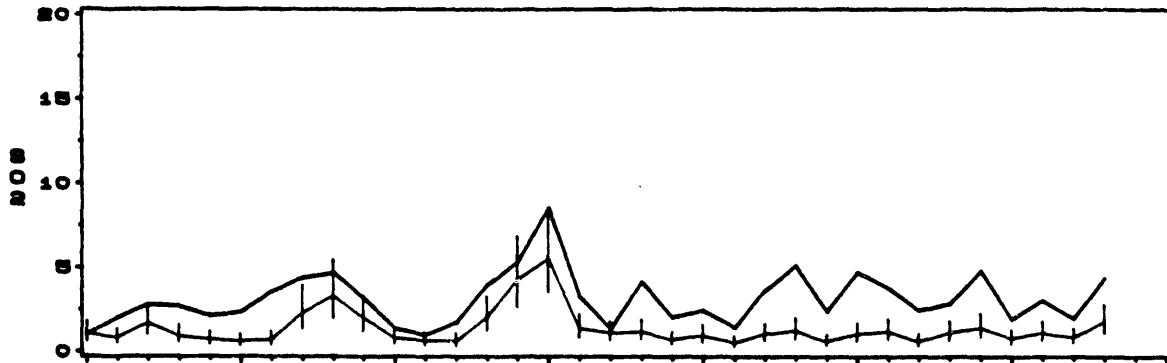


MAXIMUM OZONE 10AM-6PM (PPB)

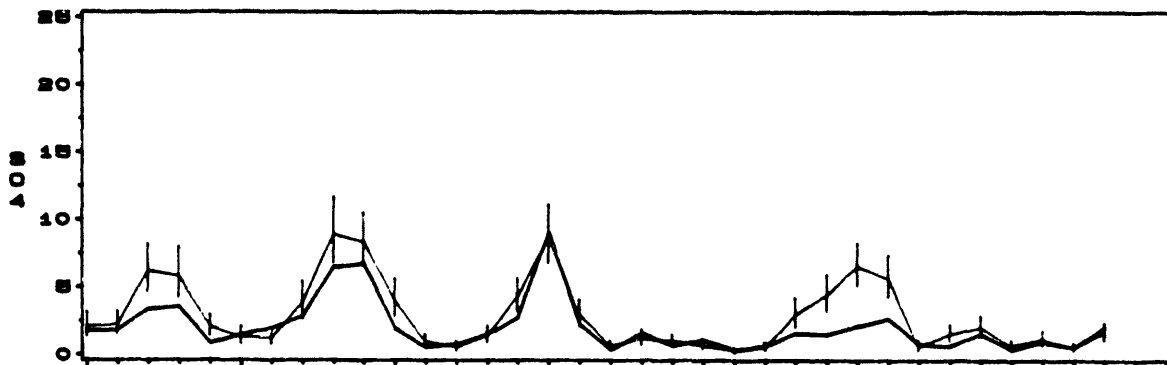


AVERAGE OF ADOM2BF PREDICTIONS AND OBSERVATIONS
25AUG88 - 27SEP88
REGION 3

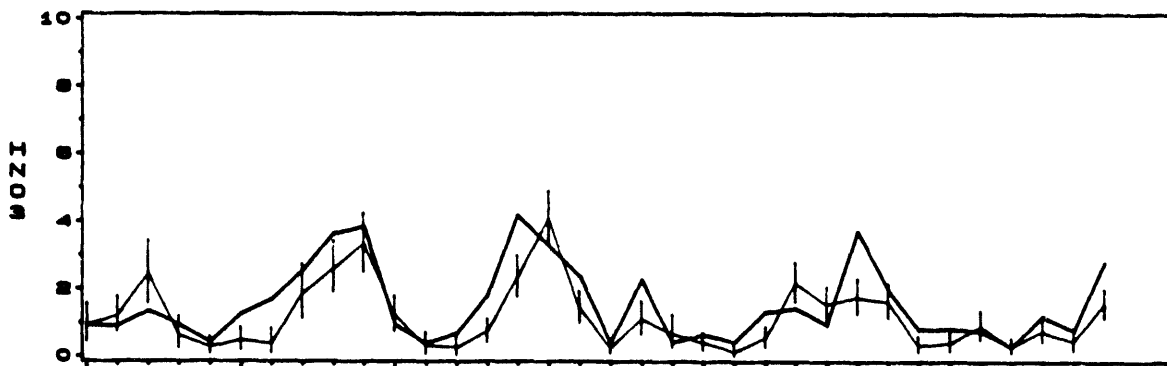
SO2 CONCENTRATION (UG/M3)



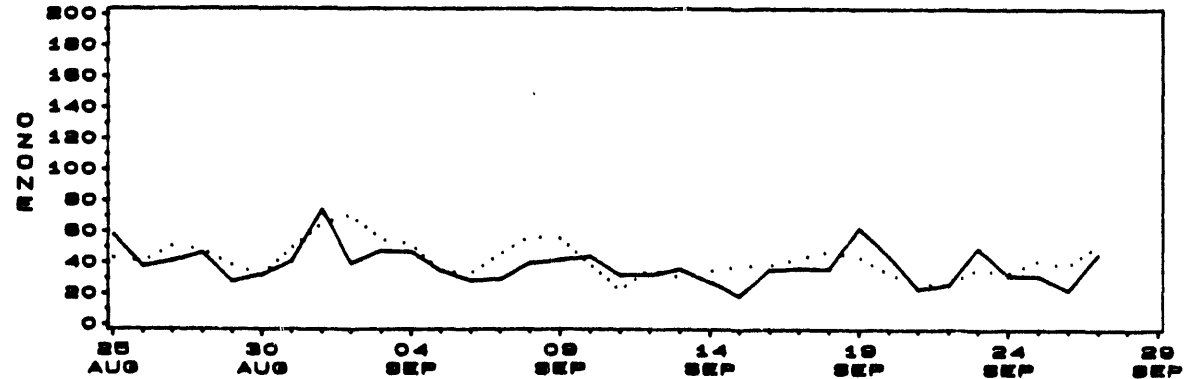
SO4 CONCENTRATION (UG/M3)



HNO3 CONCENTRATION (UG/M3)

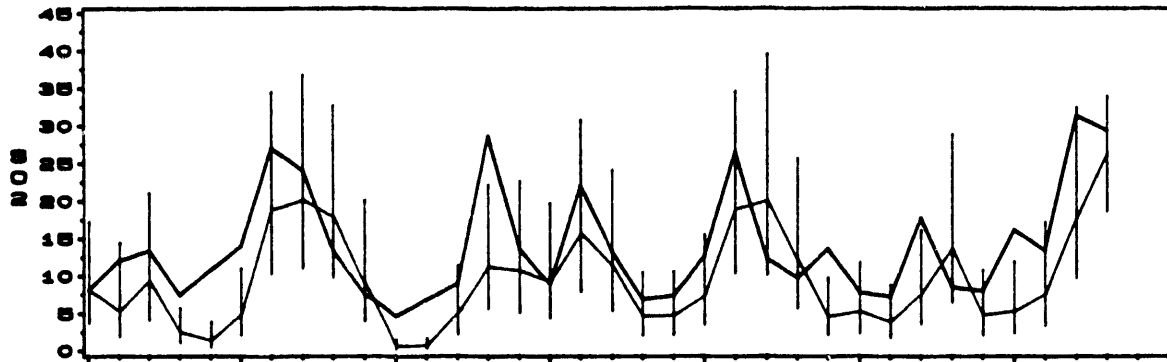


MAXIMUM OZONE 10AM-6PM (PPB)

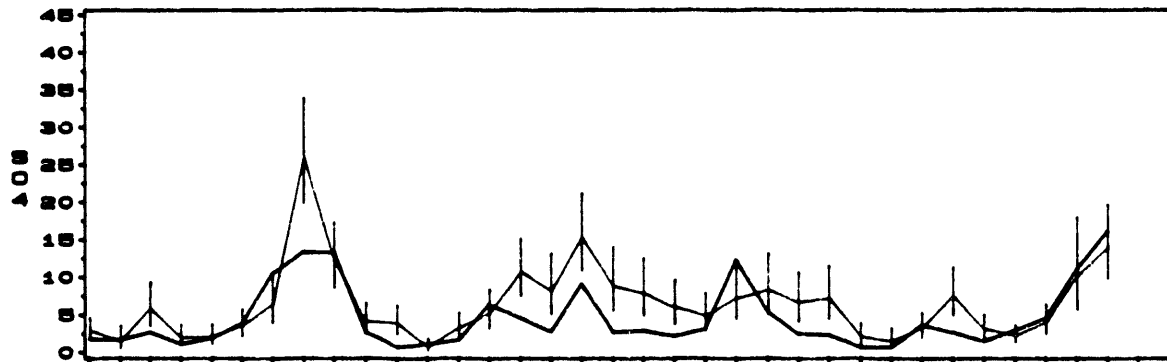


AVERAGE OF ADOM2BF PREDICTIONS AND OBSERVATIONS
25AUG88 - 27SEP88
REGION 4

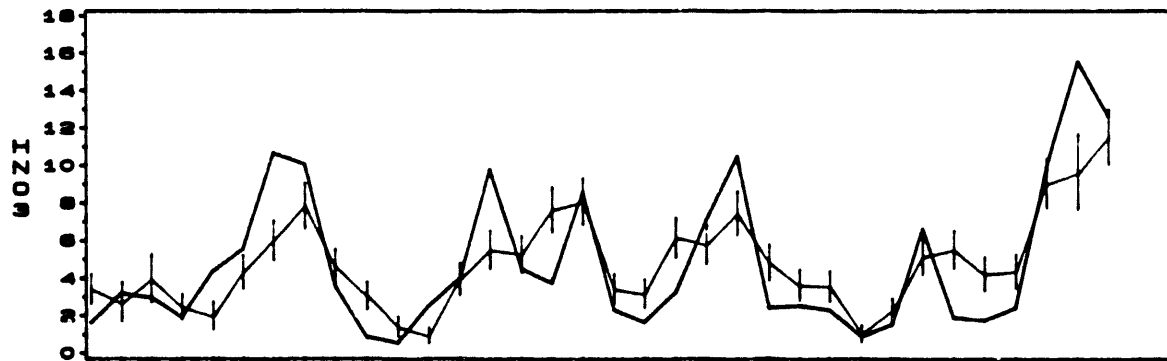
SO2 CONCENTRATION (UG/M3)



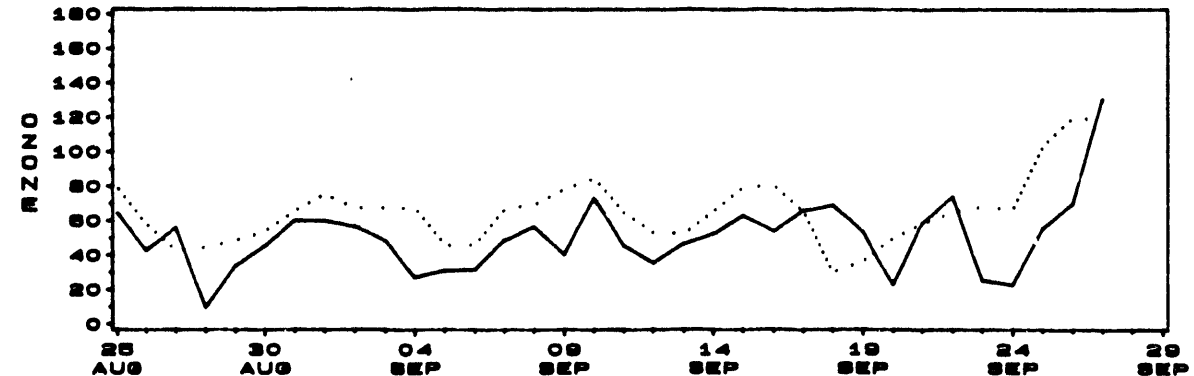
SO4 CONCENTRATION (UG/M3)



HNO3 CONCENTRATION (UG/M3)

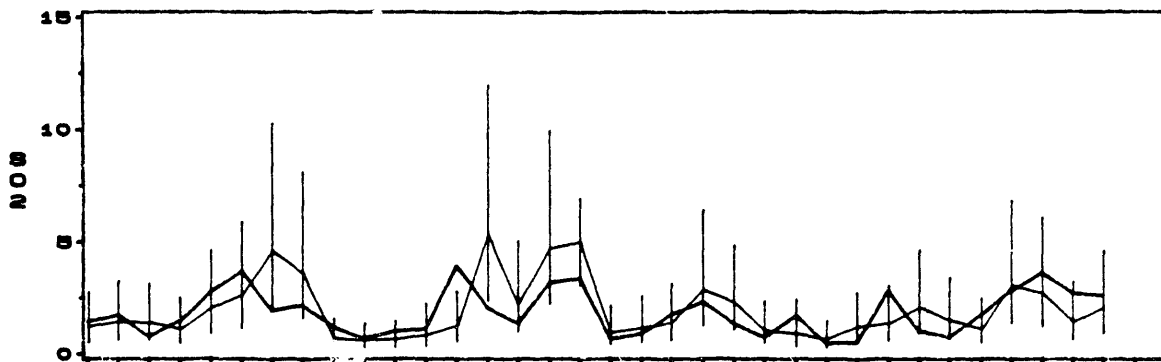


MAXIMUM OZONE 10AM-6PM (PPB)

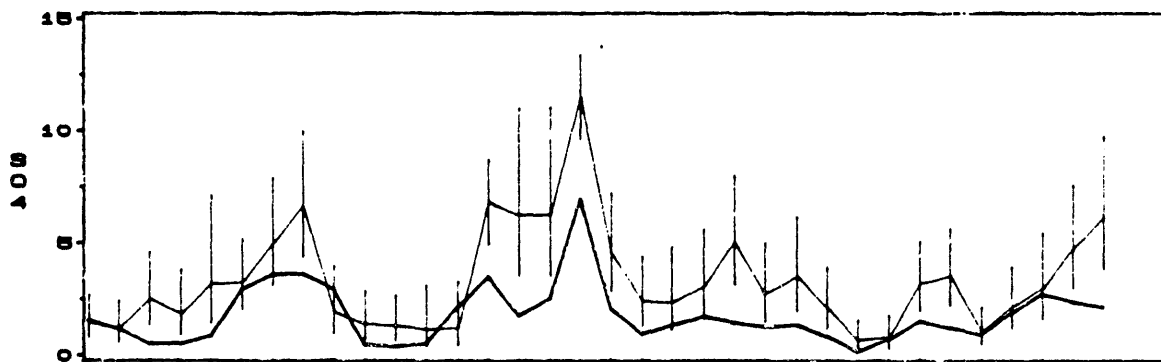


AVERAGE OF ADOM2BF PREDICTIONS AND OBSERVATIONS
25AUG88 - 27SEP88
REGION 4A

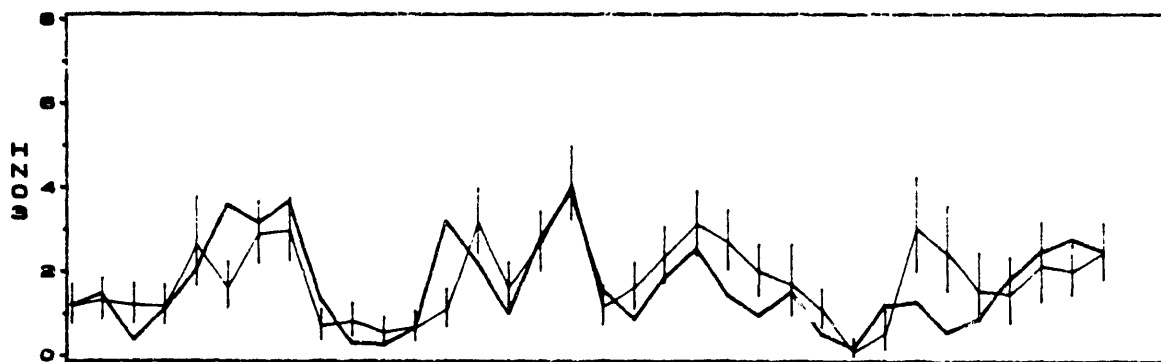
SO2 CONCENTRATION (UG/M3)



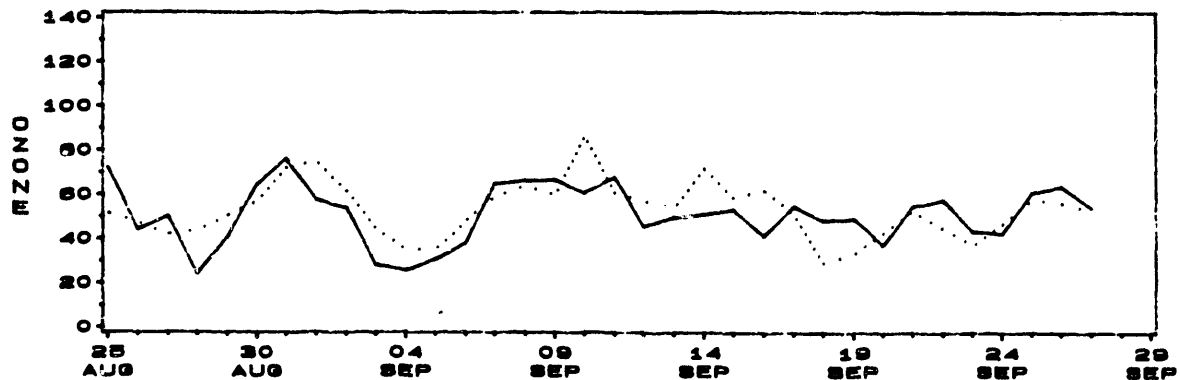
SO4 CONCENTRATION (UG/M3)



HNO3 CONCENTRATION (UG/M3)

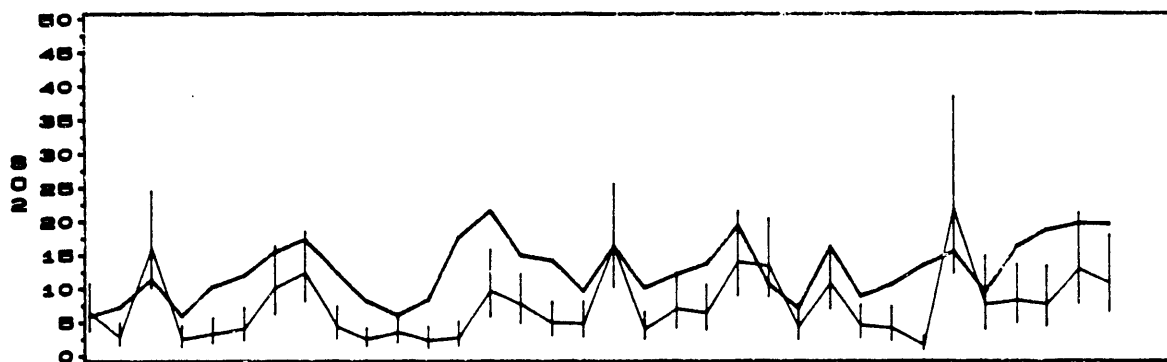


MAXIMUM OZONE 10AM-6PM (PPB)

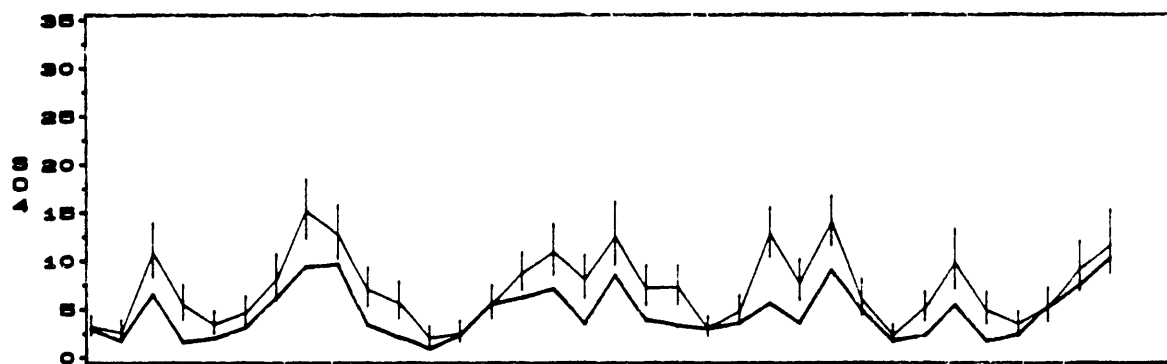


AVERAGE OF ADOM2BF PREDICTIONS AND OBSERVATIONS
25AUG88 - 27SEP88
REGION 5

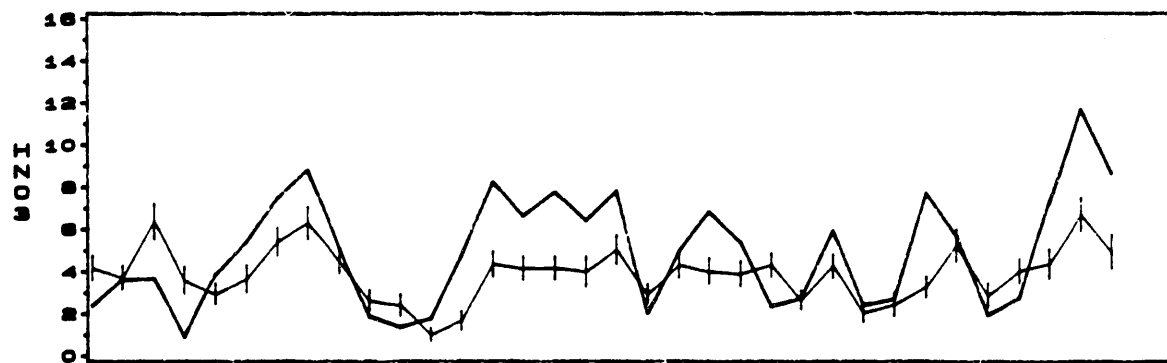
SO2 CONCENTRATION (UG/M3)



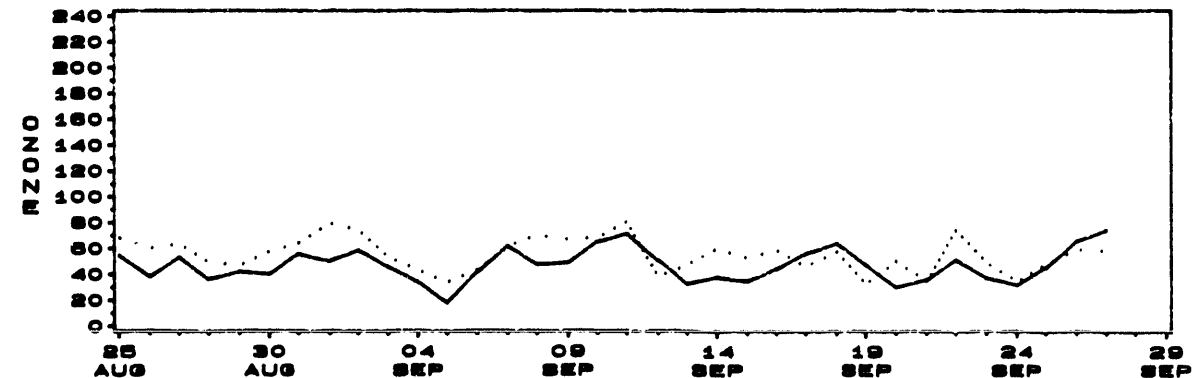
SO4 CONCENTRATION (UG/M3)



HN03 CONCENTRATION (UG/M3)

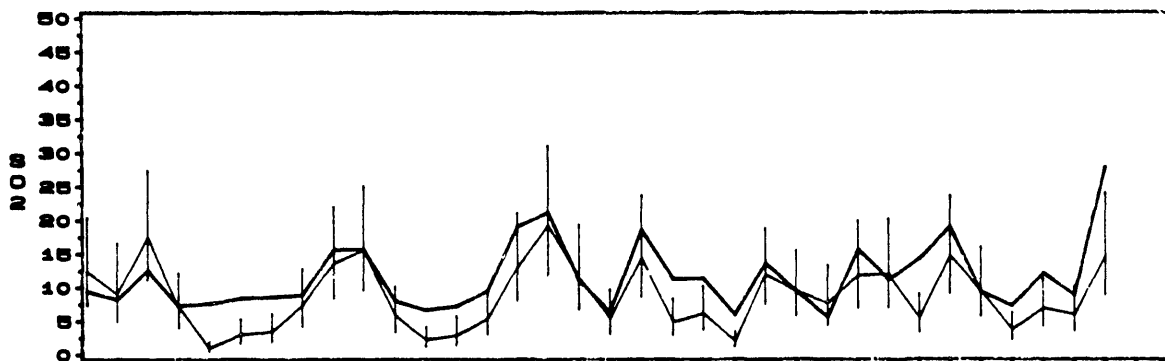


MAXIMUM OZONE 10AM-6PM (PPB)

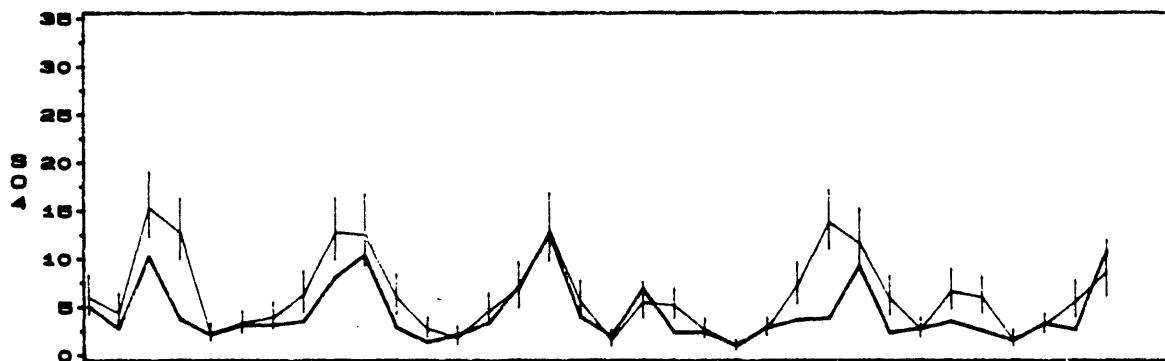


AVERAGE OF ADM2BF PREDICTIONS AND OBSERVATIONS
25AUG88 - 27SEP88
REGION 6

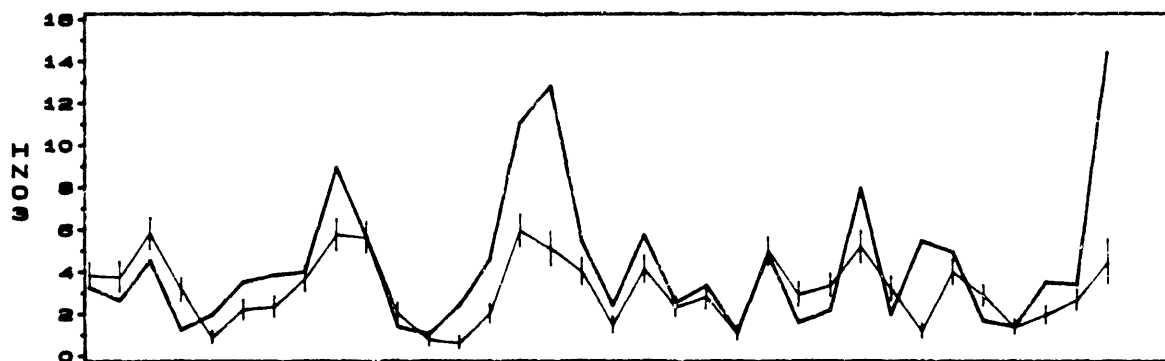
SO2 CONCENTRATION (UG/M3)



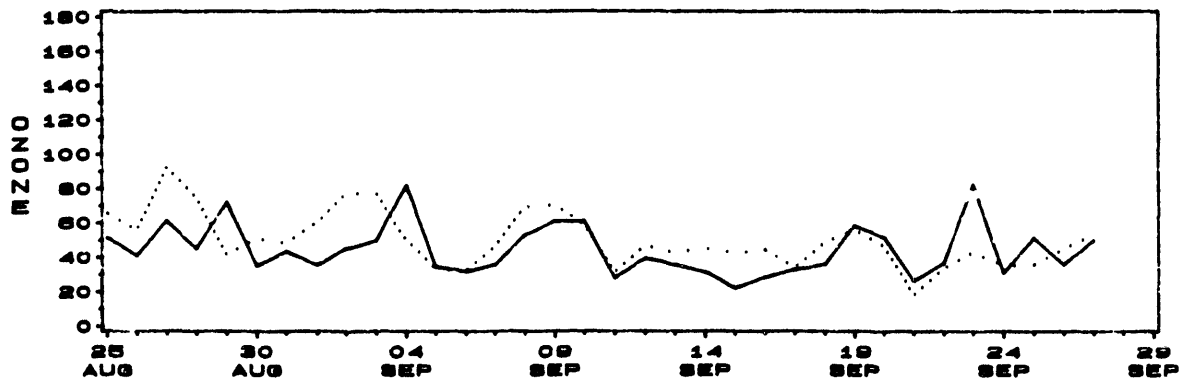
SO4 CONCENTRATION (UG/M3)



HNO3 CONCENTRATION (UG/M3)

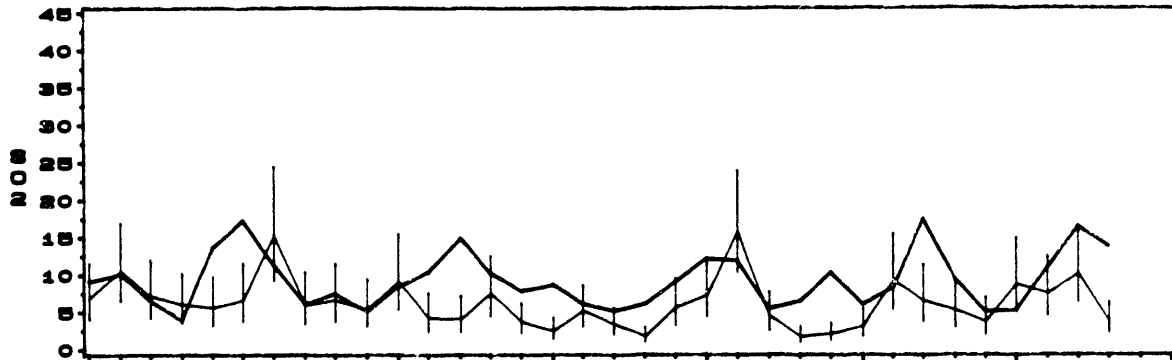


MAXIMUM OZONE 10AM-6PM (PPB)

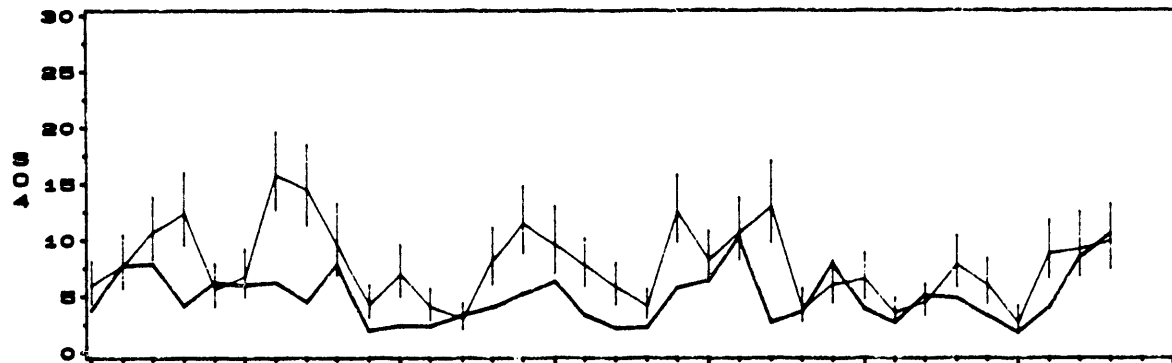


AVERAGE OF ADOM2BF PREDICTIONS AND OBSERVATIONS
25AUG88 - 27SEP88
REGION 7

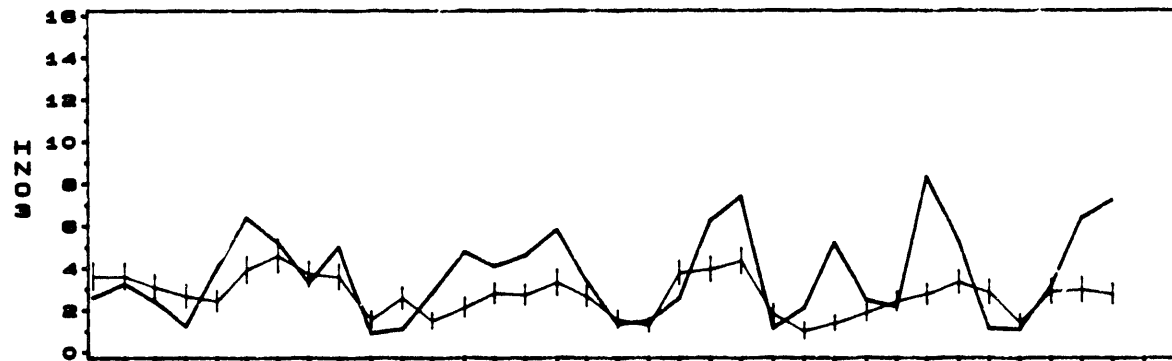
SO2 CONCENTRATION (UG/M3)



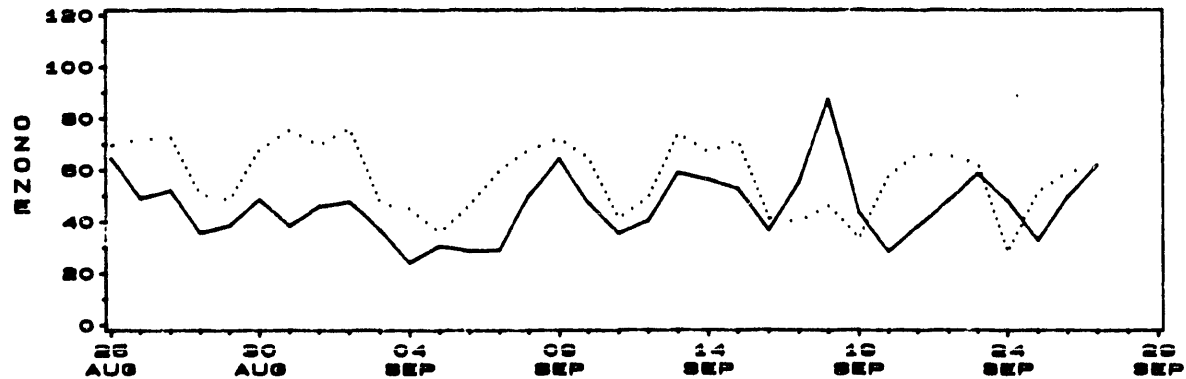
SO4 CONCENTRATION (UG/M3)



HNO3 CONCENTRATION (UG/M3)

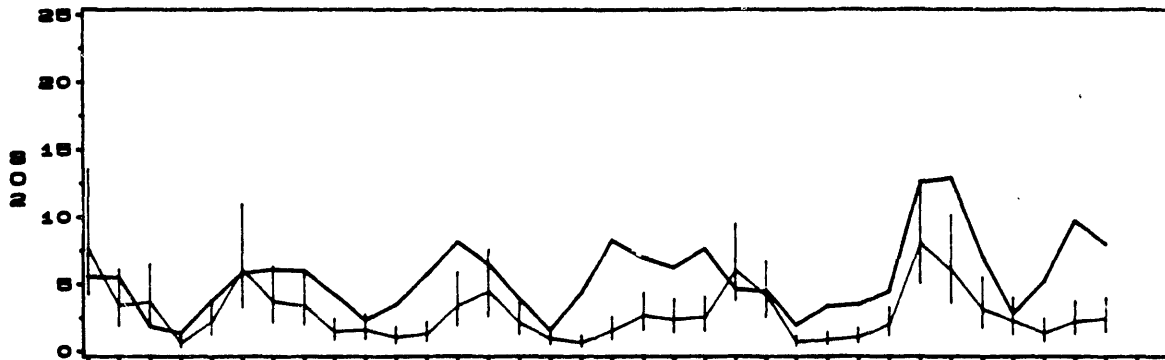


MAXIMUM OZONE 10AM-6PM (PPB)

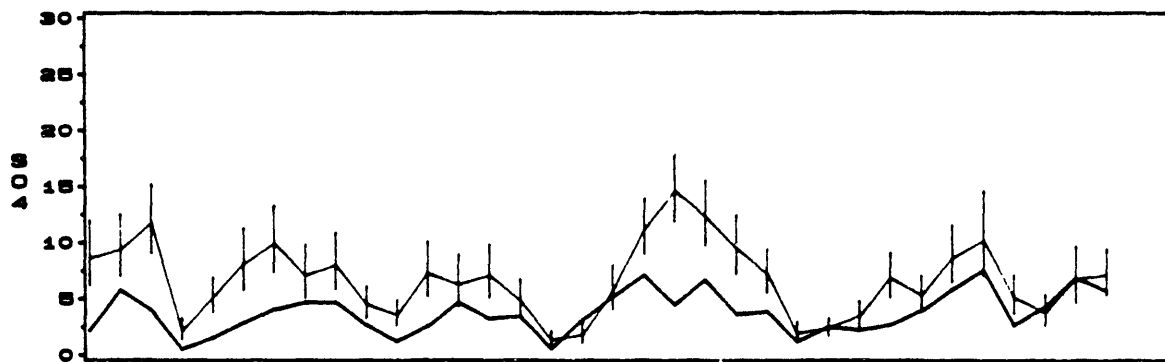


AVERAGE OF ADOM2BF PREDICTIONS AND OBSERVATIONS
25AUG88 - 27SEP88
REGION 8

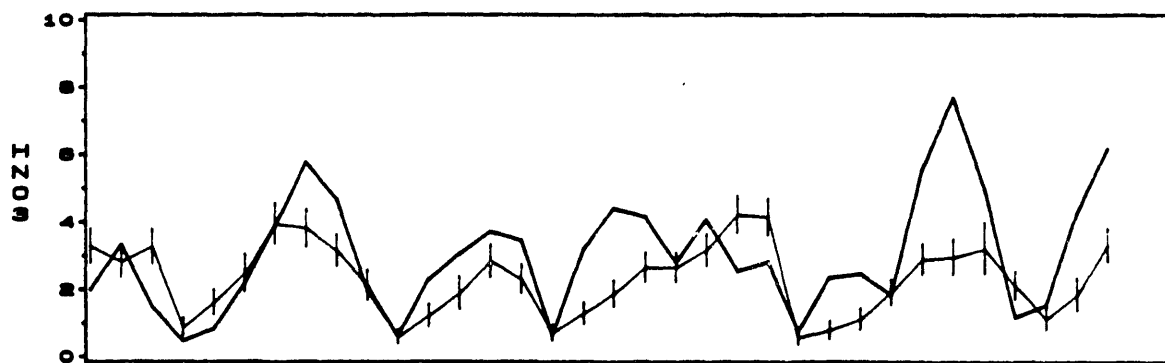
SO2 CONCENTRATION (UG/M3)



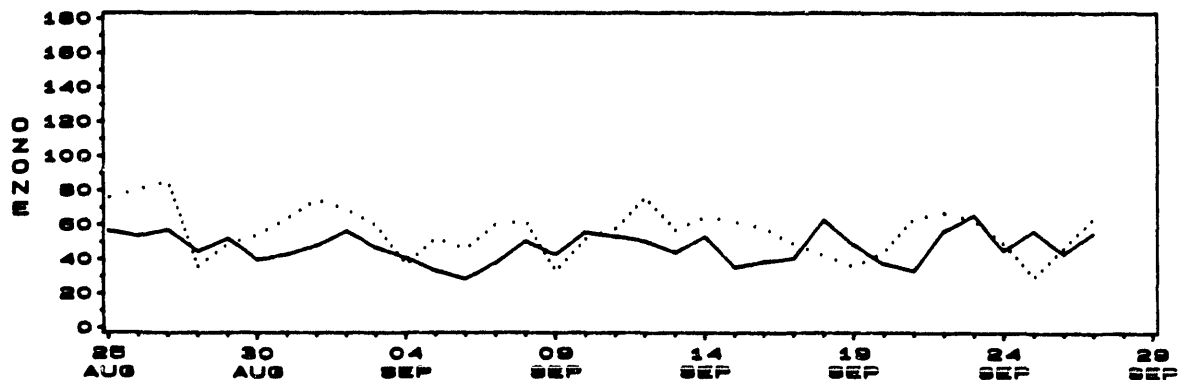
SO4 CONCENTRATION (UG/M3)



HNO3 CONCENTRATION (UG/M3)

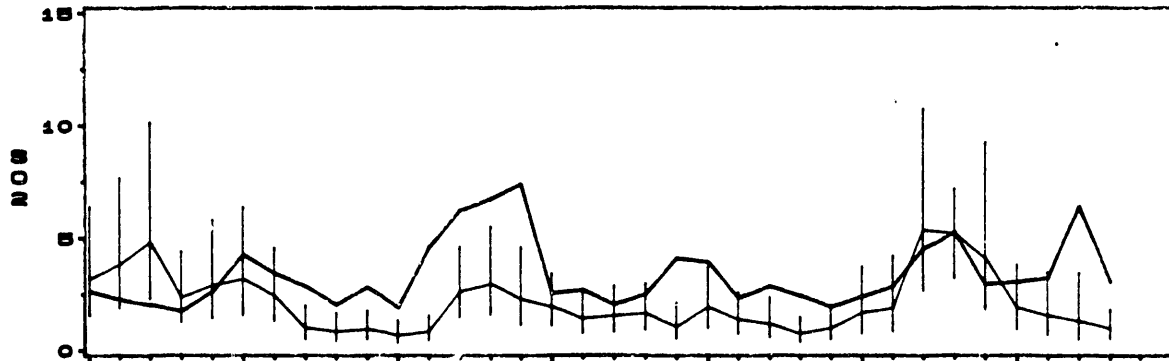


MAXIMUM OZONE 10AM-6PM (PPB)

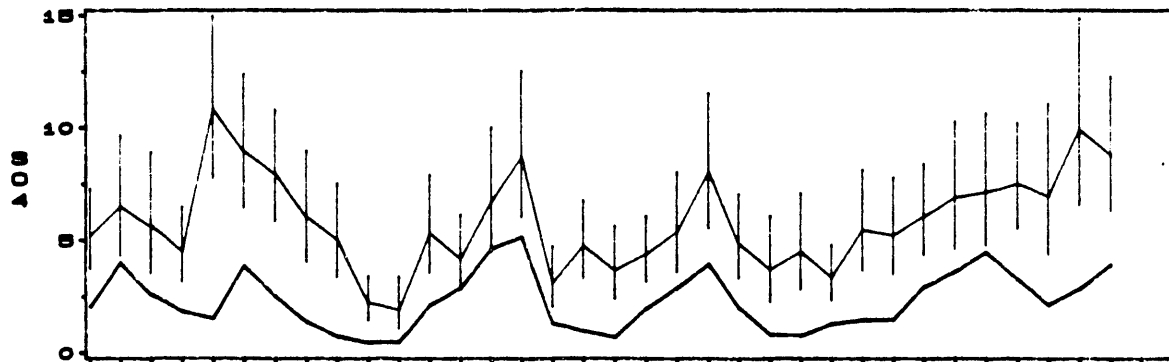


AVERAGE OF ADOM2BF PREDICTIONS AND OBSERVATIONS
 25AUG88 - 27SEP88
 REGION 9

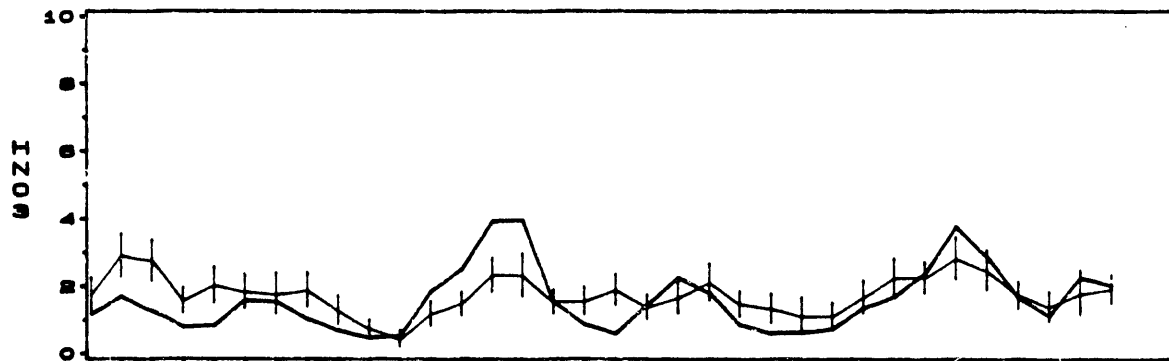
SO2 CONCENTRATION (UG/M3)



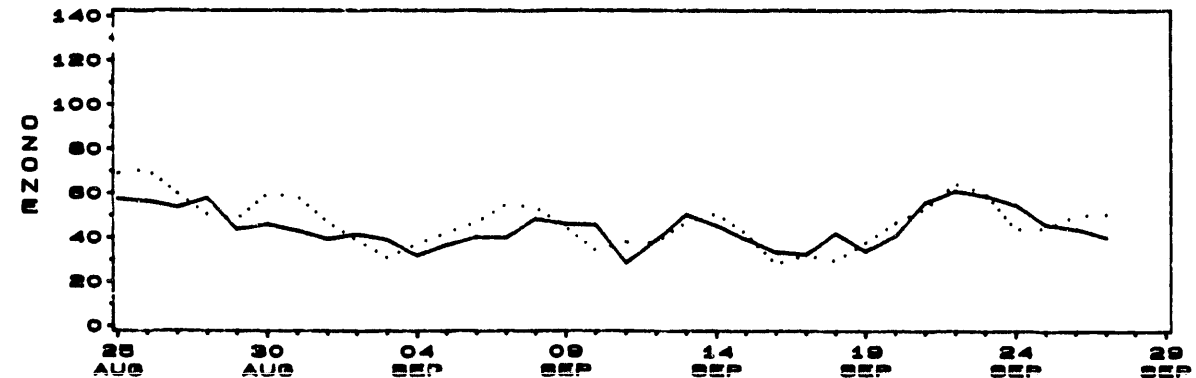
SO4 CONCENTRATION (UG/M3)



HNO3 CONCENTRATION (UG/M3)



MAXIMUM OZONE 10AM-6PM (PPB)



DISTRIBUTION

<u>No. of Copies</u>		<u>No. of Copies</u>
<u>OFFSITE</u>		
12	DOE/Office of Scientific and Technical Information	J. Jansen Southern Company Services P.O. Box 2625 Birmingham, AL 35202
5	R. Dennis U.S. Environmental Protection Agency AREAL, MD-80 Research Triangle Park, NC 27711	N. Kaplan U.S. Environmental Protection Agency AEERL, MD-62 Research Triangle Park, NC 27711
5	D. A. Hansen Environment Division Electric Power Research Institute P.O. Box 10412 Palo Alto, CA 94303	P. Karamchandani ENSR Consulting and Engineering 1220 Avenida Acaso Camarillo, CA 93010
	F. Binkowski U.S. Environmental Protection Agency AREAL, MD-80 Research Triangle Park, NC 27711	T. Lavery Environmental Science and Engineering, Inc. P.O. Box ESE Gainesville, FL 32602
	D. Byun Computer Sciences Corporation P. O. Box 12767 4401 Building, Suite 200 Research Triangle Park, NC 27711	J. McHenry Computer Sciences Corporation P. O. Box 12767 4401 Building, Suite 200 Research Triangle Park, NC 27711
	J. Chang State University of New York Atmospheric Sciences Research Center 100 Fuller Road Albany, NY 12205	P. Mueller Environment Division Electric Power Research Institute P.O. Box 10412 Palo Alto, CA 94303
	J. Ching U.S. Environmental Protection Agency AREAL, MD-80 Research Triangle Park, NC 27711	J. Novak U.S. Environmental Protection Agency AREAL, MD-80 Research Triangle Park, NC 27711

No. of
Copies

No. of
Copies

F. Schiermeier
U.S. Environmental Protection
Agency
AREAL, MD-80
Research Triangle Park, NC
27711

S. Seilkop
Analytical Sciences, Inc.
100 Capitola Drive, Suite 106
Durham, NC 27713

C. Spicer
Battelle, Columbus Division
505 King Avenue
Columbus, OH 43201-2693

A. Venkatram
ENSR Consulting and Engineering
1220 Avenida Acaso
Camarillo, CA 93010

J. Vickery
U.S. Environmental Protection
Agency
AREAL, MD-75
Research Triangle Park, NC
27711

FOREIGN

- 5 P. K. Misra
Ontario Ministry of the
Environment
125 Resources Road, East Wing
Rexdale, Ontario
CANADA M9W 5L1
- 5 K. Puckett
Atmospheric Environment Service
4905 Dufferin Street
Downsview, Ontario
CANADA M3H 5T4
- C. Banic
Atmospheric Environment Service
4905 Dufferin Street
Downsview, Ontario
CANADA M3H 5T4

D. Davies
Recherche en Prevision Numerique
Environment Canada
2121 Trans-Canada Highway,
Room 508
Dorval, Quebec
CANADA H9P 1J3

C. Fung
Ontario Ministry of the
Environment
125 Resources Road, East Wing
Rexdale, Ontario
CANADA M9W 5L1

R. Hoff
Atmospheric Environment Service
4905 Dufferin Street
Downsview, Ontario
CANADA M3H 5T4

M. Lusic
Atmospheric Resources Branch
Ministry of the Environment
880 Bay Street, 4th Floor
Toronto, Ontario
CANADA M5S 1Z8

A. Macdonald
Atmospheric Environment Service
4905 Dufferin Street
Downsview, Ontario
CANADA M3H 5T4

R. Mickle
Atmospheric Environment Service
4905 Dufferin Street
Downsview, Ontario
CANADA M3H 5T4

J. Padro
Atmospheric Environment Service
4905 Dufferin Street
Downsview, Ontario
CANADA M3H 5T4

No. of
Copies

J. Pankrath
Air Pollution Dispersion and
Chemical Reactions
Federal Environmental Agency
Bismarckplatz 1
D-1000 Berlin 33
FEDERAL REPUBLIC OF GERMANY

W. Seiler
Fraunhofer Institute for
Atmospheric Environmental
Research - IFU
Kreuzeckbahnstrasse 19
D-8100 Garmisch-Partenkirchen
FEDERAL REPUBLIC OF GERMANY

R. Vet
Atmospheric Environment Service
4905 Dufferin Street
Downsview, Ontario
CANADA M3H 5T4

E. Voldner
Atmospheric Environment Service
4905 Dufferin Street
Downsview, Ontario
CANADA M3H 5T4

ONSITE

DOE Richland Field Office

P. Kruger

33 Pacific Northwest Laboratory

W. R. Barchet (20)
C. M. Berkowitz
J. W. Falco
J. M. Hales
J. M. Hubbe
N. S. Laulainen
R. L. Skaggs
L. L. Wendell
Publishing Coordination
Technical Report Files (5)

END

**DATE
FILMED**

2 / 19 / 92

